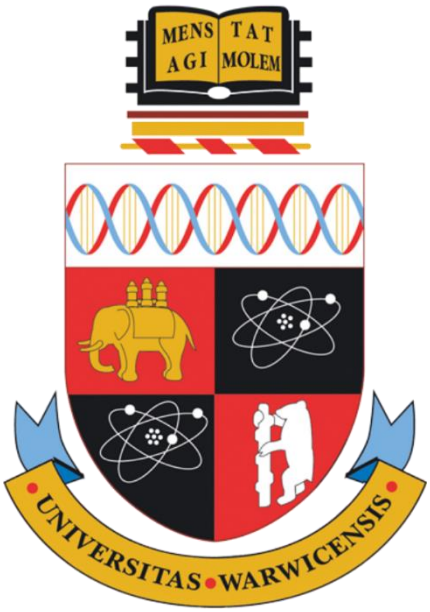

An experimental investigation of ultrasonic assisted milling (UAM) of carbon fibre reinforced polymer (CFRP) and the effect of machining on the BMI 5250-4 matrix resin

By

Nor Farah Huda Binti Abd Halim

A thesis submitted in partial fulfilment of the requirements for the degree of

Doctor of Philosophy

At

WMG, University of Warwick

January 2018

Abstract

Milling of Carbon Fibre Reinforced Polymer (CFRP) is necessary for component accuracy prior to assembly of aircraft. Recently, ultrasonic assisted milling (UAM) which combines conventional machining (CM) with ultrasonic vibration on the cutting tool, has shown beneficial outcomes with respect to the machinability of some metals, however, limited UAM of CFRP has been reported. In this thesis, milling (CM and UAM) of a CFRP incorporating Bismaleimide 5250-4 (BMI 5250-4) resin was carried out in a wide range of cutting parameters and environments (dry, conventional cutting fluid (CCF) and CO_2 cryogenic). Machinability was examined in terms of tool wear, cutting forces and surface roughness. In terms of machinability with conventional cutting tools, machining in a CO_2 had a positive effect on tool life, despite an increase in cutting forces, compared to CCF and dry. UAM was found to reduce cutting forces by up to 10 %, compared with CM, however, this did not yield any benefit in terms of tool wear and/or workpiece surface roughness. When dry machining employing an abrasive diamond tool, CFRP material adhesion was a feature. The application of UAM in this instance yielded, reduced workpiece adhesion on the cutting tool and improved workpiece surface roughness.

Machining of CFRP must be performed below the glass transition temperature (Tg) of the resin to avoid the degradation of the properties of the matrix resin. In this research new findings in the temperature initiated during machining and the consequential effects on the polymer utilised Fourier transform infrared spectroscopy (FTIR) and differential scanning calorimetry (DSC) which is well established in polymer characterization. FTIR and DSC was carried out to investigate the effect of machining on the chemical and material properties of BMI 5250-4 such as Tg and changes to matrix resin chemical bonding, which has been closely associated with degradation of the machined part. Further analysis of the machined surface by DSC indicated that the Tg of the matrix resin had been exceeded during the machining process and led to degradation of the BMI 5250-4 in some cases.

An observed reduction of the maleimide double bond (C=C) at 825 cm^{-1} wavelength by FTIR signified that further post-curing of BMI 5240-4 had occurred which suggested that a higher cutting temperature was developed at the machine tool tip than recorded with the infrared camera. CM dry machining, FTIR analysis also confirmed the formation of isocyanate-derived products (C≡N) at 2250 cm^{-1} wavelength, a bond associated with the point at which BMI 5240-4 is thermally degraded having experienced temperatures in the range 400 to 600 °C. This result suggests that when CM dry machining the actual cutting temperature experienced by the BMI 5240-4 was at least 400 °C. The formation of isocyanate-derived products was not observed for UAM dry machining, suggesting that ultrasonic vibration of the cutting tool may reduce the cutting temperature in the primary shear zone, however this temperature reduction was insufficient to arrest observed post curing effects and shift in the Tg. Other aspects of the FTIR analysis revealed that despite the improvements to workpiece surface roughness when milling with CCF there was an increased presence of moisture (-OH bond) in the BMI 5240-4 resin which may have a detrimental effect on the durability of the material over time.

Machining CFRP has been enhanced by the introduction of the chemical analysis. It suggests that DSC and FTIR exploration of the thermal history of the CFRP can provide more information about the temperature than typical thermal measurement during machining such as thermal cameras and thermocouples. The management of the milling process of CFRP can now be related to the management of the temperature at the tool tip and the effect on polymer characteristics. As a consequence, milling of CFRP in CO_2 exhibited improvement in tool wear, an observed reduction in cutting temperature, and sustenance of the chemical properties of BMI 5250-4. However, there was no significant benefit in additionally employing UAM in a CO_2 environment.

The research has provided a new insight in the milling of polymer composites and could be beneficial in avoiding thermal degradation of the machined part, maintaining the quality of machined part and avoiding scrap parts at the end of machining processes.

Table of Contents

List of Tables

List of Figures

List of Abbreviations and Symbols

BMI	Bismaleimide
BMPM	4,4'- Bismalei-Midi-Phenyl-Methane
CCF	Conventional Cutting Fluid
CFRP	Carbon Fibre Reinforced Polymer
CM	Conventional Machining
CMC	Ceramic Matrix Composite
Co	Cobalt
CO_2	Carbon Dioxide
DBPA	0,0'-Diallyl Bisphenol A
DSC	Differential Scanning Calorimetry
EDS	Energy Dispersive Spectroscopy
f	Feed Rate
FTIR	Fourier Transform Infrared Spectroscopy
f_v	Frequency of Ultrasonic Vibration
Fx	Feed Force
Fy	Normal Force
Fz	Thrust Force
g/cm^3	Gram per Cubic Centimetre
GPa	Giga Pascal
HK	Knoop Hardness
HM	High Modulus
HS	High Strength
HSS	High Speed Steel
HV	Vickers Hardness
Hz	Hertz
ISO	International Organisation for Standardisation
kg/m^3	Kilogram per Cubic Metre
kHz	Kilo Hertz
LN_2	Liquid Nitrogen
m/min	Metre per Minute
mm/rev	Millimetre per Revolution
MMC	Metal Matrix Composite
MPa	Mega Pascal
PAN	Polyacrylonitrile
PCD	Poly Crystalline Diamond
PEEK	Poly Ether Ether Ketone
PET	Polyethylene
PMC	Polymeric Matrix Composite
PP	Polypropylene
RPM	Revolution per Minute

SEM	Scanning Electron Microscopy
Tg	Glass Transition Temperature
TGA	Thermogravimetric Analysis
UAM	Ultrasonic Assisted Machining
VARTM	Vacuum Assisted Resin Transfer Moulding
V_b	Maximum Flank Wear
V_c	Cutting Speed
WC	Tungsten Carbide

Declaration

I declare that this thesis contains an account of my research work carried out at WMG, University of Warwick between January 2014 and October 2017 under the supervision of Prof Stuart Barnes and Dr Helen Ascroft. The research reported here has not been previously submitted, wholly or in part, at this or any other academic institution as consideration for other degree qualification. The investigation on the ultrasonic amplitude measurement technique was carried out by David Ray (WMG's intern). The milling of carbon fibre reinforced polymer (CFRP) employed the uncoated tungsten carbide tooling for Study 1(a) was performed under the author's supervision as a part of Mr Simon Jackson's final year project. The milling of carbon fibre reinforced polymer (CFRP) employing the polycrystalline diamond (PCD) tooling for Study 2 was performed under the author's supervision as a part of Mr Tony Hogan's final year project and the MATLAB simulation on the travelled tool distances (Study 2) was carried out by Aniruddha Gupta. All other experimental work was carried out by the author. The author has carried out all data analysis and interpretation.

Nor Farah Huda Binti Abd Halim

WMG

University of Warwick

2018

Acknowledgement

I would like to express my grateful feelings to God for being very close to me and surrounding me with amazing peoples whilst undertaking this journey. My deepest gratitude goes to my supervisors, Prof Stuart Barnes and Dr Helen Ascroft. Their infinite assistance has lightened the load and kept me calm when facing difficult times. Thank you very much for having trust that I can finish my PhD. Not to forget my yearly progress examiner, Dr Vannessa Goodship for her insights and valuable opinions on the project especially in the thermal analysis of CFRP machined surfaces.

Thank you, Austin Cook and Dave Dawson, from BAE Systems for some technical advice; also, BAE Systems PLC for providing workpiece materials and cutting tools for experimental work. Thank you, Martin Burns, from Exactaform for some technical advice regarding cutting tool selections. DMG Mori is acknowledged for the support of the machine tool. Thank you very much to Mr Darren Grant for helping me doing the machining work and Mr Martin Worrall for training me to use the thermal analysis equipment.

My sincere thanks to my beloved husband, Mohamad Ismail Fahmi for his companionship and sacrifices made, also to my lovely children; Aqil Rizqi and Ayra Nuha Eliza. They brought colour into my life and enlightened this journey with joy and happiness. Special thanks to my parents, Abd Halim Md Hanafiah & Yusma Amin and parents in law, Pathor and Kamaliyah Makrop, to whom I am most in debt. Their encouragement, support, and prayer have motivated me to go beyond my abilities. Not to forget my siblings Hilmi, Liyana ,Haikal, and Iman for trusting me that I can finish my PhD.

Thank you to all my UK friends, especially in Coventry, for making my stay here like a home. Thank you very much for NFarahin, Alifah, Aishah and Ain for always lend their ears to hear my problem and happiness during my PhD journey.

Finally, I would like to gratefully acknowledge the Malaysian Government especially Ministry of Higher Education (MOHE) and the International Islamic University Malaysia (IIUM) sponsoring this study.

Publications

1. **N. F. H. A. Halim**, H. Ascroft, and S. Barnes, "Analysis of Tool Wear, Cutting Force, Surface Roughness and Machining Temperature during Finishing Operation of Ultrasonic Assisted Milling (UAM) of Carbon Fibre Reinforced Plastic (CFRP)," *Procedia Engineering*, Vol. 184, pp. 185-191, 2017.

2. **A.H. N. F. Huda**, H. Ascroft, and S. Barnes, "Machinability Study of Ultrasonic Assisted Machining (UAM) of Carbon Fibre Reinforced Plastic (CFRP) with Multifaceted Tool," *Procedia CIRP*, Vol. 46, pp. 488-491, 2016.

3. H. Ascroft, S. Barnes, A. N. Dahnel, A. Gupta, A. H. **Nor Farah Huda**, and D. Ray, "Ultrasonic Assisted Machining," Presented at the 17th International Conference on Machine Design and Production, Bursa, Turkiye, 2016.

Chapter 1 Introduction

1.1 Research background

Applications of carbon fibre reinforced polymer (CFRP) composite have been significantly increasing in both aerospace and automotive industries. In fact, CFRP has substituted metallic alloys in many aerospace components due to its numerous attractive properties, such as lower weight, higher strength, and resistance against corrosion. For example, a reduced maintenance cost by up to 35 % could be obtained for Boeing 787 when the main components of the aircraft, such as airframe and wing, are 50 % made of CFRP and other composite materials [1]. More recently, the Airbus A350 XWB, which is made of 50 % composite materials, reported a reduction by 50 % for structure maintenance tasks, especially when compared to A380 with a threshold for airframe checks at eight years, while 12 years for A350 XWB [2].

Components that are made from CFRP are usually manufactured to closely resemble the net shape because CFRP materials can be moulded into any desired shape in accordance to the component. Nevertheless, further machining processes, such as milling, are still required for precision joining and finishing. Therefore, milling of CFRP must be performed appropriately to avoid rejection at the end of the manufacturing processes. However, milling of CFRP is difficult due to the nature of CFRP itself, which is non-homogenous and anisotropic, hence challenging to machine. In addition, milling of CFRP is limited to below the glass transition temperature (Tg) of the matrix resin. The Tg of matrix resin refers to the temperature where the properties of matrix change from glassy solid to rubbery and softer state. Nonetheless, milling of CFRP above the Tg can lead to deterioration of both mechanical and chemical properties of the matrix resin [3-5]. In this

research, CFRP comprising a Bismaleimide 5250-4 (BMI 5250-4) matrix was employed as the workpiece material.

Recently, hybrid machining, which reflects an ultrasonic vibration to the cutting tool in combination with conventional machining (CM) parameters, has been widely explored. Moreover, reports have claimed that the ultrasonic vibration of the cutting tool and workpiece during the ultrasonic assisted machining (UAM) improves machinability in terms of the quality of the machined part, longer tool life, and the lower cutting forces [6-12]. It is also claimed that the ultrasonic vibration between the cutting tool and the workpiece may lead to a reduction in cutting temperature due to the existence of an air gap between the cutting tool and the workpiece, which cools down the temperature [13]. Therefore, this leads to the research question if the ultrasonic vibration of the cutting tool during UAM could benefit the machinability of CFRP in terms of tool wear, cutting forces, and surface roughness, apart from reducing the cutting temperature when compared to CM?

Notably, BMI resin within in-service components, typically, is not completely cured primarily because 100 % cured BMI can lead to degradation of CFRP mechanical properties such as tensile and compression strength of CFRP [14-16]. A number of researchers have discovered that the relationship between processing and environmental temperature could eventually result in further post-curing of BMI [14]. Thus, it is important to ensure that during the machining process, the temperature attained by the matrix in the CFRP should be lower than the Tg. Furthermore, a body of research suggests that machining of CFRP should be performed in a dry condition [17]. Nevertheless, as stated earlier, machining at a temperature higher than Tg can deteriorate the properties of the materials. Although the application of cutting fluid can reduce the cutting temperature, machining of CFRP with conventional cutting fluids (CCF) has not

always been recommended, as matrix resin may be susceptible to moisture absorption. Further post-processing to dry the materials after machining is required when machining of CFRP is performed with cutting fluid. However, there is limited knowledge on how the CCF affect the CFRP. More recently, some researchers have investigated machining with cryogenic cooling, i.e. Liquid Nitrogen (LN_2) and Carbon Dioxide (CO_2), which has been reported to offer a significant improvement in the machinability of CFRP and other materials, especially in terms of reducing cutting temperature, extending tool life, lowering cutting forces, and improving workpiece surface roughness [18]. Thus, another research question is raised pertaining to the effect of varying machining environment, such as dry, CCF, and CO_2, upon the machinability (tool wear, cutting force, and surface integrity) of both UAM and CM and what is the effect of machining environment on the machined CFRP surface?

With much attention given to the effect on mechanical properties, i.e. tensile and compressive strength on machining surface [19-23], only a limited of studies have looked into the effect of machining upon shifts in chemical properties within a material that may lead to deterioration of mechanical properties in CFRP. Thus, the effect of cutting temperature on the chemical properties such as changes in Tg and effect on chemical bonding of matrix resin of machined CFRP surface has yet to be established. Techniques such as differential scanning calorimetry (DSC) and Fourier transform infrared (FTIR) are well established polymer chemistry techniques. DSC has been extensively applied to determine thermal transitions, while FTIR has been routinely used to characterise polymer degradation. This leads to another potential research question; 'is it possible to use these techniques on post-machined material samples so as to determine, with sufficient accuracy/certainty, levels of material degradation at varied machining

temperatures, which could ultimately assist in establishing safe machining process windows for temperature-sensitive CFRP materials?'

Therefore, this thesis determined the effects of machining operations and environments on the chemical properties of BMI 5250-4. Throughout this study, dry condition reflects machining without any conventional cutting fluid; CCF machining condition refers to machining with conventional cutting fluid, whereas cryogenic denotes machining with CO_2 coolant. Moreover, the effect of the cutting environment on the machined surface had been investigated by employing both DSC and FTIR analyses to identify the early stages of thermal degradation in CFRP.

1.2 Research aims and objectives

The aim of this research is to develop fundamental knowledge pertaining to the effect of machining on shifts in chemical properties which are the glass transition temperature (Tg) and chemical bonding of BMI 5250-4 resin. This research also aims to develop the knowledge on the machinability of CFRP in terms of tool wear, cutting force, and surface integrity when milling conventionally (CM), along with the assistance of ultrasonic vibration (UAM) in various machining environments.

The research objectives are outlined in the following:

- To perform literature review on machining of CFRP conventionally and with ultrasonic assistance in varied machining conditions (dry, CCF, and CO_2) and thermal analysis of CFRP.
- To explore the thermal behaviour (the glass transition temperature, Tg) and the changes in chemical properties of BMI 5250-4 for the CFRP machined surface of CM and UAM under various machining environments (dry, CCF, and CO_2) by

differential scanning calorimetry (DSC) and Fourier transform infrared (FTIR) spectroscopy.

- To compare the performances of UAM with CM of CFRP and to explain the effect of different machining environments (dry, CCF, and CO_2) in terms of tool wear, cutting forces, and workpiece surface roughness.
- To investigate the effect of tool type on the performance of UAM in terms of tool wear, cutting forces, and workpiece surface roughness.

Chapter 2 Literature review

This chapter reviews the aspects of carbon fibre reinforced polymer (CFRP) and discusses the machinability of CFRP in terms of conventional machining (CM) and ultrasonic assisted machining (UAM). In addition, as the processing of CFRP is limited by glass transition temperature (Tg) of the matrix resin, therefore, this chapter elaborates the method of thermal analysis that has often been employed to study polymeric materials.

2.1 Carbon fibre reinforced polymer (CFRP)

Over the past few years, composite materials have been increasingly selected to replace metallic materials in both aerospace and automotive industries. Composites are made from two or more elements, which are the reinforcement and the matrix resin, so as to gain a new property that possesses both the physical and the mechanical properties of the blend [24]. Several characteristics, such as high strength to weight ratio, low density, high stiffness, and low fatigue resistance, appear to be the benefits of composite over metal. Composites can be classified into three major groups, which are metal matrix composite (MMC), ceramic matrix composite (CMC), and polymer matrix composite (PMC). In this present study, CFRP, which is categorised under PMC, was selected as the main workpiece. The application of PMC is extensive in the present industries since it can be fabricated into broad and complex shapes, apart from being more economical when compared with MMC and CMC [4, 24, 25]. However, there are some limitations of PMC over MMC and CMC, such as the inability to withstand high temperature due to its reliance on the properties of the matrix resin and the reinforcement [4, 26]. In addition, the processing temperature of the PMC must be below the Tg of the matrix resin so as to avoid any damages or changes to the mechanical and physical properties of the composite structure.

Moreover, CFRP is an anisotropic material, where the mechanical properties of the CFRP are determined by the orientation of carbon fibre. Carbon fibre reinforced polymer (CFRP) is usually manufactured to closely resemble the net shape. The carbon fibre is layered with matrix resin and it is stacked at a desired orientation based on the required mechanical properties. Figure 2-1 illustrates the varied orientations of the CFRP that could be unidirectional, multidirectional or quasi-isotropic, which determine the mechanical properties of CFRP.

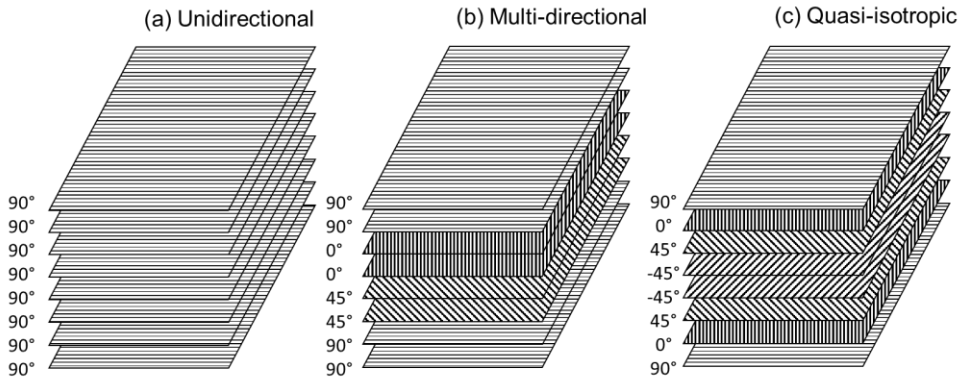

Figure 2-1: Comparison between (a) unidirectional (b) multi-directional and (c) quasi-isotropic fibre orientation of CFRP.

2.1.1 Carbon fibre reinforcement

Carbon fibre serves as reinforcement to provide stiffness and strength to CFRP. Reinforcement is stiffer and stronger when compared to matrix materials. Besides, reinforcement provides mechanical properties to the composite and strengthens the matrix in the preferred direction [5]. Carbon fibre is heat-treated at a lower temperature that is less than 1650 °C and it consists of up to 95 percent of carbon content. The anisotropic properties of the CFRP indicate that the properties strongly depend on fibre orientation. For instance, the strength of carbon fibre in a longitudinal direction can be 30 times higher (100000 MPa) than that of a transverse direction (35000 MPa) [27]. Meanwhile, the tensile strength of CFRP ranges from 1500 to 3500 MPa, which is higher

when compared to steel (750 - 1500 MPa) and aluminium (450 - 600 MPa) [28]. Carbon fibre is often classified into three major groups, which are; high modulus (HM), intermediate modulus (IM), and high strength (HS). HM carbon fibre is made from petroleum pitch, while both IM and HS carbon fibres are made from polyacrylonitrile (PAN). Although the petroleum pitch-based carbon fibre can be processed at a lower cost, the PAN-based carbon fibre has higher tensile strength than the petroleum pitch-based carbon fibre [3]. Although the petroleum pitch precursors can produce high modulus fibres that ranges between 345 and 1000 GPa, they have lower strength in comparison to the carbon fibre provided by PAN [26]. Table 2-1 summarises several typical properties of carbon fibre.

Table 2-1: Typical mechanical properties of carbon fibre for CFRP applications [4, 25, 26].

Properties	Standard Modulus	Intermediate Modulus	High Strength
Density (g/cm^2)	1.80	1.80	1.90
Tensile strength (MPa)	3400-4800	4136-6200	4136-5500
Tensile modulus (GPa)	220-241	276-300	345-450
Coefficient of thermal expansion (10^{-6} °C)	-0.4	-0.6	-0.75

2.1.2 Polymeric matrix resin

The primary function of matrix resin is to support the reinforcement, as well as to maintain the desired shape and orientation. Matrix resin also provides toughness, impact, and abrasive resistance, which serves as a barrier against adverse environments due to elevated temperature and humidity [3, 4]. Furthermore, matrix resin protects the surface of the fibre from composite mechanical degradation, such as compressive stress and interlaminar shear strength [4, 24, 25]. The processing temperature of the matrix resin is determined by the Tg of the matrix resin. Section 2.1.2.1 explains the Tg of matrix resin.

Polymeric matrix resin can be categorised into two major groups, which are: thermosets and thermoplastics. Thermoplastics contain high–viscosity resin that is processed by heating above its melting temperature [26]. Although it melts and flows during the processing, it does not form any crosslinking reaction. Nonetheless, as they have high molecular weight resin, the viscosity of thermoplastic during the processing is greater than that of a thermoset (10^4 to 10^7 poise of thermoplastics vs 10 thermosets) [4]. Compared to thermosets, the crosslinking reaction does not occur in thermoplastics, as shown in Figure 2-2. Hence, less processing time is needed due to absence of chemical reaction while curing. Thermoplastics can be reprocessed as they can be thermoformed into structural shapes by reheating to processing temperatures [4, 24, 25]. Thermoplastics offer advantages in forming and joining applications since they can be reprocessed by just heating until hitting their melting temperature. Some examples of thermoplastics commercially available in the industry are polyethylene (PET), polypropylene (PP), and polyetheretherketone (PEEK). Table 2-2 presents the typical mechanical properties of thermoplastics used as matrix for CFRP.

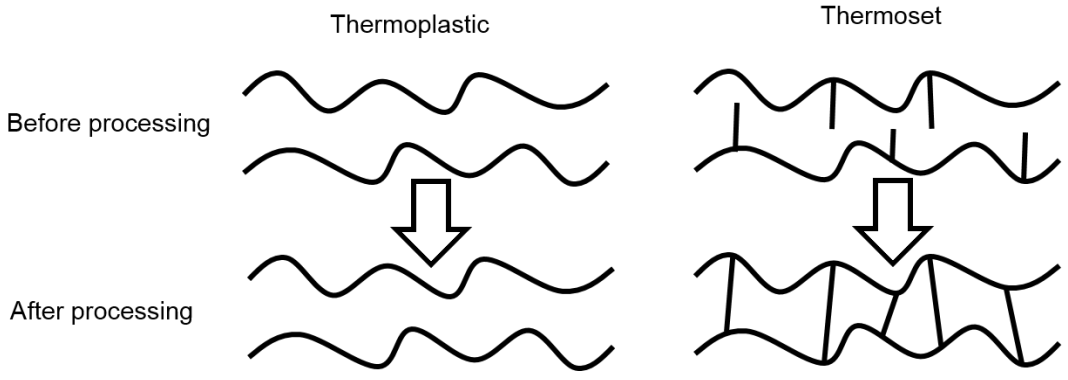

Figure 2-2: Polymer structure of thermoplastic and thermoset before and after processing indicating that the crosslinking occurs in a thermoset [4].

Table 2-2: Typical mechanical properties of thermoplastics used as the matrix for CFRP [25, 27].

Properties	Polyethylene (PET)	Polypropylene (PP)	Polyetherether ketone (PEEK)
Density (g/cm^3)	1.35	0.9	1.32
Tensile modulus (GPa)	2.8-4.1	1.1-1.6	3.24
Tensile strength (MPa)	48-72	31-41	10
Glass transition temperature, T_g (°C)	69	-10	143
Service temperature (°C)	120	150	250

In contrast to thermoplastics, thermoset resin is characterised by low molecular weight and monomer viscosity [3, 4, 25]. Curing thermoset resin involves crosslinking reaction that transforms the molecule into a three-dimensional crosslinked molecule that is infusible and insoluble. Besides, the chemical reaction is driven by heat generated, either from chemical reactions (exothermic heat of reaction) or from externally applied heat that generates the crosslinking effect in a thermoset [4, 24, 25, 29]. As the curing process of thermoset continues, the molecular weight and the viscosity of thermoset resin increase. As a result, the thermoset cannot be re-melted or re-processed upon turning into a rubbery solid [27]. Furthermore, additional crosslinking produces completely cured thermoset resin, especially when further heating is applied to the resin system. Processing thermoset resin requires a longer time due to its complicated process that incorporates both chemical- and thermal-driven reactions, when compared to thermoplastics [24]. During the curing process of thermoset, the effect of crosslinking transforms the thermoset into a rigid and intractable solid form. The thermoset molecules are randomly arranged and they are amorphous in both liquid and stable states [3, 4]. Some commonly used thermoset resins are epoxy, phenolic, Bismaleimide (BMI), and polymerised monomeric reactant-15 (PMR-15) [3]. Table 2-3 compares the properties of the commonly used thermosets used as matrix for CFRP.

Table 2-3: Typical mechanical properties of thermosets used as matrix for CFRP (Adapted from [25, 26]).

Properties	Epoxy	Phenolic	BMI	PMR-15
Density (g/cm^3)	1.2-1.3	1.3	1.4	1.32
Tensile modulus (GPa)	4.5	3.0	4-19	3.9
Tensile strength (MPa)	130	70	70	38.6
Glass transition temperature, Tg (°C)	180	110-220	230-290	340
Service temperature (°C)	90-200	120-200	250-300	315

2.1.2.1 Glass transition temperature (Tg)

The selection of matrix resin determines the maximum temperature use of CFRP as this is influenced by the glass transition temperature (Tg) of the matrix resin. The Tg refers to the temperature at which a material changes from a rigid glassy solid into a softer and semi-flexible material. Consequently, the use of CFRP is limited to temperatures that range below the Tg of the matrix materials, mainly because heat application that exceeds the Tg can significantly reduce the mechanical properties of polymeric composite [4, 30, 31]. For example, a study reported that typically, the matrix material exhibits low surface hardness, low modulus, and high ductility at temperatures exceeding the Tg [25].

2.1.3 Bismaleimide (BMI) 5250-4 resin

The main workpiece selected for this research was CFRP that comprised of BMI resin type 5250-4. Hence, the term 'BMI 5250-4' is used throughout this thesis hereafter. Sections 2.1.3.1 to 2.1.3.3 elaborate the properties, curing mechanism and degradation of BMI.

2.1.3.1 Properties and applications

The selection of thermoset resin is based on both industrial preferences and applications. For instance, polyimides are suitable for high-temperature applications ranging between 290 and 315 °C, while BMI can be used for medium range temperature (135 - 175 °C) applications, and epoxy resin is usually used for low and moderate temperatures (up to 135 °C) [4]. As the properties of epoxy resin are combined of high strength and adhesion, low shrinkage, as well as easy to process; such resins are often chosen as matrix for high-performance composite and adhesive. Nevertheless, when higher temperature application is required, BMI appears to be a potential matrix resin because it possesses similar characteristics and manufacturing process as epoxy resin. Table 2-4 compares the mechanical properties of the CFRP types 5250-4/IM7 BMI with medium-high toughened carbon fibre reinforced epoxies.

Table 2-4: Comparison between 5250-4 BMI with leading epoxies, Medium and High toughness carbon fibre reinforced epoxies [32].

Properties	BMI 5250-4	Medium-High toughened epoxies
Tensile strength (MPa)	2827	2758-2827
Tensile modulus (GPa)	161	163-164
Compression strength at 80 °C (MPa)	1586	1310-1448
Glass transition temperature, Tg (°C)	280	180-210

Furthermore, certain BMI resins match the performance exerted by PMR-15 polyamides resin due to its high processing temperature, which may as well exceed 290 °C. Besides, BMI resin is increasingly being accepted in the industry due to its excellent retention of physical properties at elevated temperature and wet conditions, apart from possessing almost stable electrical properties over a broad range of temperature and non-flammability properties [33-35]. Furthermore, BMI exhibits excellent mechanical properties over epoxy resins at temperature that ranges between 150 and 230 °C. With

such exceptional characteristics, BMI has been widely used as the main resin component in aerospace applications. Additionally, processing BMI resin is less intricate when compared to thermoplastic polyimide matrix, given that the BMI can be processed like an epoxy matrix. Nonetheless, BMI matrices demonstrate a more brittle mechanical response due to its high crosslinking nature within the cured network [36-38]. As such, extensive researches have addressed these drawbacks by introducing several versions of modified BMIs so as to improve their mechanical properties [15].

2.1.3.2 Curing mechanism

Carbon fibre reinforced polymer (CFRP) with BMI 5250-4 had been selected as the main workpiece material employed in this research and it consisted of three main components, which are: 4,4'- bismaleimidiphenylmethane (BMPM), 0,0'-diallyl bisphenol A (DABPA), and BMI-1,3, tolyl. Figure 2-3 illustrates the main chemical compositions of the BMI 5250-4 network system.

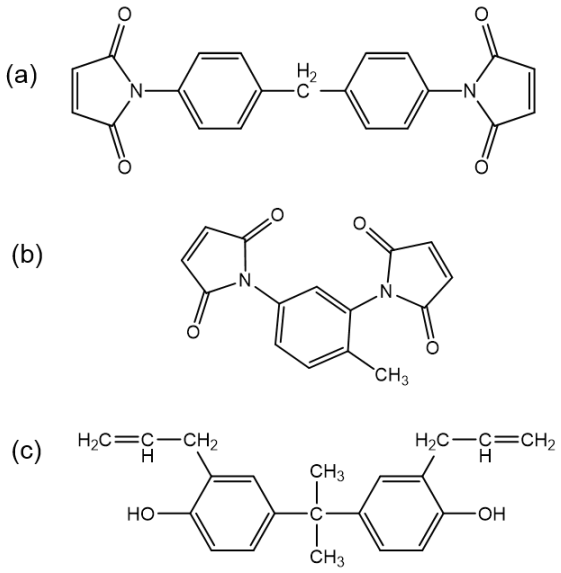

Figure 2-3: Chemical structure of 5250-4 BMI consist of three major component a) 4,4'-bismaleimidiphenylmethane (BMPM), b) BMI-1, 3-tolyl and c) 0,0'-diallyl bisphenol A (DABPA) (Adapted from [14, 15]).

Polymerisation and crosslinking of maleimide double bonds (C=C) take place in the BMI 5250-4 resin curing mechanism [14, 15]. Several factors, such as maximum curing temperature, curing time, and post-curing cycle during the curing mechanism, determine both the mechanical and the chemical properties of the matrix resin, as well as its composite [14, 15, 33]. Furthermore, the chemical components of BMPM and BMI-1,3-tolyl appear to be similar from the three components of BMI employed in this study. Thus, the curing mechanism for two and three components of BMI is similar [14, 33, 35]. The curing mechanism for two components of BMI (BMPM and DABPA) is discussed extensively in the literature [14, 15, 35, 39]. At lower curing temperature (100 - 200 °C), the 'ene' reaction occurs between BMPM and DABPA monomers. The curing mechanism of BMI involves five-functional groups, which includes three carbon-carbon double bonds (C=C) and two hydroxyl groups (–OH). Hydroxyl dehydration can be attained via etherification of hydroxyl group, while crosslinking and chain extension can be completed by C=C that consists of ally, propenyl, and maleimide, as portrayed in Figure 2-4.

The principal cure reaction of BMI that involves C=C occurs when the temperature ranges from 200 to 300 °C. Curing of BMI, however, is incomplete due to restriction of glassy-state diffusion at 250 °C curing and post-curing at 300 °C for an hour [14]. The crosslinking of C=C improves the mechanical properties of BMI and its composite [35, 40]. On the contrary, dehydration of the hydroxyl group deteriorates the mechanical properties. The effect of hydroxyl bond dehydration is dominated, in comparison to crosslinking of C=C as the maximum curing temperature increases [34, 38, 41].

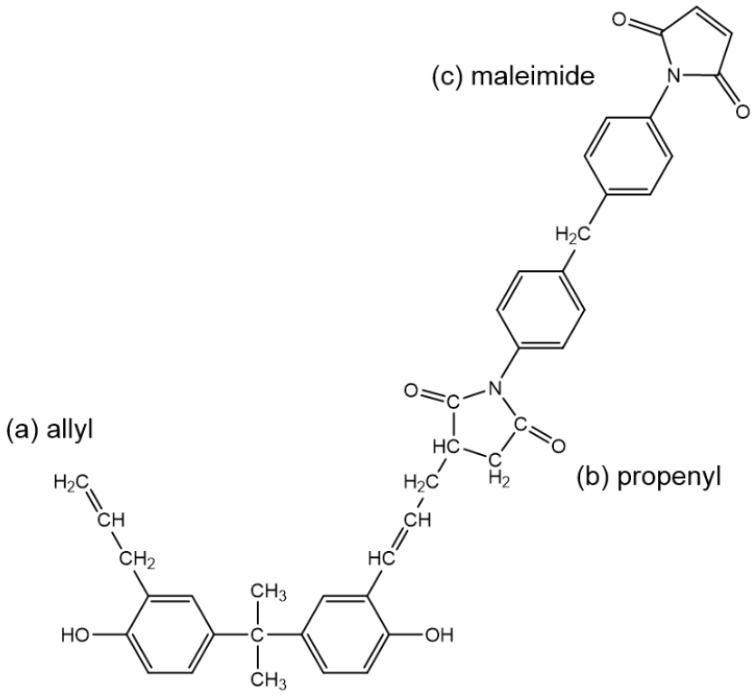

Figure 2-4: The chemical structure of BMPM/DABPA 'ene' addict pre-polymer where a) allyl, b) propenyl and c) maleimide are capable of polymerisation (Adapted from [14]).

However, CFRP is not 100 % cured after the standard composite fabrication or post-cure procedures [14, 33, 35]. This is because; the complete curing of BMI and its composite can deteriorate the mechanical properties of the composite [16, 42]. Consequently, further post-cure of BMI resin system can be accomplished by the service environment exposure, which leads to increment in Tg, hence deteriorating the mechanical properties in service over time [14, 33, 43].

Furthermore, some studies have investigated the correlation between Tg of BMI and changes in chemical properties [43-47]. In order to do so, the Differential Scanning Calorimetry (DSC) and the Fourier Transform Infrared (FTIR) analyses were combined, especially to determine the curing reaction of BMI. Morgan et al. [14] explained that BMI curing can be evaluated thoroughly by using DSC and FTIR. Both techniques was employed to investigate the effects of curing time and temperature mechanism upon both chemical structure and Tg of the resin system. Figure 2-5 presents the changes in

absorbance of the chemical structure over curing temperature and curing time. The reduction of the peak at a wavelength of 825 cm^{-1} indicated that increment in curing temperature increases the consumption of C=C [14, 39]. Meanwhile, Li et al. [40] claimed that the intensities of C=C peak are inversely proportional to the degree of crosslinking. Thus, increment in curing temperature leads to an increase in Tg of BMI composite. Nonetheless, the increased Tg may deteriorate the mechanical properties of the composite [43].

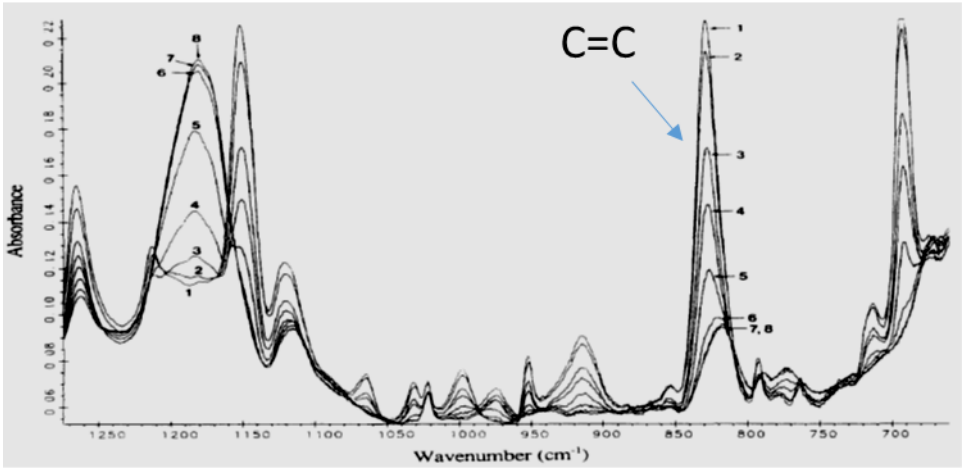

Figure 2-5: FTIR spectra of BMI as a function of sequential cure condition 1,2 (0.5 and 1 hours at 130 °C), 3, 4, 5, 6 (150 °C, 175 °C, 200 °C, 225 °C at 3 hours, respectively) and 7, 8 (250 °C at 1 hour and 3 hours respectively). (Adapted from [14])

Notably, curing temperature [14, 43], curing time [33], post curing time [14], and additional blends [39, 48] can affect both chemical and mechanical properties of the composites. Several studies have looked into the effect of curing mechanism upon mechanical properties and performances of composites. As for the curing mechanism discussed by [14, 39], curing temperature used during the curing reaction of BMI resin displayed a significant effect on the mechanical properties of the carbon fibre reinforced plastic with BMI 5250-4 resin [43]. For example, Khattab et al. [43] discovered that the tensile strength (817 MPa) of CFRP was reduced by 7.6 % when cured with the maximum curing temperature (205 °C). The highest tensile strength of 884 MPa exhibited the lowest

maximum curing temperature at 183 °C. The composite resin was cured with various maximum curing temperatures (183, 194, and 205 °C) and constant post-cure at 227 °C for 2 hours by using a vacuum-assisted resin transfer moulding (VARTM). At higher curing temperatures, water molecule is diffused from the polymer and may lead to more defects. Thus, they concluded that increasing curing temperature could significantly reduce the mechanical properties of the composite.

Research conducted by Tsotsis et al. [44] revealed that the matrix-dependent properties were enhanced during the post-cure stage, while matrix degradation from densification or increased chain scission in the thermosetting matrix polymers. Other studies showed that post-cure reactions enhanced the dominant fibre properties, such as tensile strength and tensile modulus [45, 46], apart from decreasing the matrix-dominated properties, such as toughness [39]. Thus, the curing cycle of BMI resin and its composite significantly affect the properties of the composite. Therefore, curing temperature has a significant effect upon the chemical properties of CFRP. The processing temperature of CFRP, consequently, affects the properties of the CFRP. Machining of the CFRP that has often been carried out at the end of the manufacturing process must be performed with some limitation to the Tg.

2.1.3.3 Degradation of Bismaleimide (BMI)

Extensive researches have investigated the effect of machining on the mechanical properties of the machined surface, however, only a handful of studies have determined the effect of machining on chemical properties. Although no consensus in literature has mentioned about the degradation product after machining for CFRP, it has been assumed that high machining temperature during machining could possibly lead to similar degradation with the typical BMI degradation. Similarly, although it has been mentioned

in literature that machining of CFRP must be done in dry condition due to the nature of the matrix resin that is susceptible towards absorption, no study has been carried out on the effect of cutting fluid (moisture) on chemical properties (changes in Tg and chemical bonding) of the machined surface after machining. Therefore, knowledge pertaining to the effects of thermal and moisture effect on BMI, which have already been established in polymer-related researches, could be beneficial in understanding the degradation product of BMI after machining. This section mainly discusses the degradation of BMI determined by chemical techniques to identify the functional shifts via FTIR and the changes of Tg via DSC. The working mechanisms of DSC and FTIR are elaborated in Sections 2.6.2 and 2.6.3, respectively.

As mentioned earlier, the processing temperature of BMI is limited to Tg, where, a processing temperature higher than the Tg could lead to degradation of both chemical and physical properties of the matrix resin. Moreover, BMI resin is susceptible to moisture absorption when exposed to humid environment [35]. Chemical degradation, cracking, and debonding of CFRP may occur due to absorption of moisture by BMI. Hence, some aspects could lead to degradation of BMI resin, such as thermal degradation, hygrothermal, pyrolysis, hydrolysis, oxidation, and chemical degradation of BMI resin. In this research, CFRP 5250-4 was machined dry and with the presence of cutting fluid, therefore, this section depicts the degradation of BMI in terms of the effects of temperature and moisture absorption upon BMI product. Degradation of polymeric materials can be assessed from four main aspects, which are physical properties, mechanical properties, chemical properties, and percentage degradation. Table 2-5 shows several established techniques employed in determining polymer degradation.

Table 2-5: Different analytical techniques to analyse the polymer degradation [49]

Properties	Aspect	Techniques
Physical	Crystallinity	XRD (X-Ray Diffraction) *DSC (Differential Scanning Calorimetry)* TGA (Thermogravimetric Analysis)
	Morphology	SEM (Scanning Electron Microscopy) TEM (Transmission Electron Microscopy)
Mechanical		Tensile DMA (Dynamic Mechanical Analysis)
Chemical	Surface analysis	ESCA (Electron Spectroscopy for Chemical Analysis)
	Radical	Chemiluminescence
	Functional changes	*FTIR (Fourier Transform Infrared Spectroscopy)* UV Spectroscopy Photophosphoresence Chemiluminescence
	Molecular changes	Viscosity
Percentage degradation		Weight loss LSC (Liquid Scintillation counting) Biodegradation

As mentioned earlier, the processing temperature of CFRP is limited to the Tg of matrix resin. Increased processing temperature may lead to degradation of matrix resin, which is also known as thermal-oxidative degradation. Also, some studies have determined the hygrothermal effect of BMI. Hygrothermal effect can be observed when the BMI is tested under certain temperature with the presence of water. The presence of water/humidity can significantly change the hydroxyl group (-OH). For example, Musto et al. [50] found that the –OH groups at 3500 cm^{-1} decreased to 3360 cm^{-1}, indicating the formation of new species absorbing the lower side of the -OH range when epoxy-BMI was exposed to 200 °C under continuous airflow. In hygrothermal degradation, absorption of moisture is higher when the BMI sample is exposed to higher temperature. For example, Li et al. [40] discovered that the diffusivity of water was higher at 100 °C when compared to 70 °C. Result from FTIR analysis showed that hydrogen bonding took place between water and polymer matrix when the peak shifting occurred at 3000-3700 cm^{-1} suggesting

that the moisture absorption significantly changed the chemical property of BMI resin. In addition, Bao et al. [35] found that the intensity of peak near 1600 cm^{-1} noticeably increased, thus suggesting the occurrence of chemical reaction. The hydrolytic degradation is the most likely mechanism. Figure 2-6 illustrates the FTIR spectra of BMI after water absorption at 70 °C and 90 °C. It was observed that the peak at 3460 cm^{-1} moved to 3375 cm^{-1} with increased intensity after prolonged water absorption at 90 °C. He also compared the Tg of BMI after the water absorption DSC analysis of CFRP BMI 5250-4 indicated: (a) Tg for as-moulded sample was at 270 °C, and (b) disappearance of Tg at 90 °C signified significant depolymerisation and chemical degradation. The chemical degradation most likely involved hydrolysis of imide units, hence resulting in depolymerisation and chain scission. Therefore, the presence of moisture can significantly change the intensity and the wavelength of –OH formation.

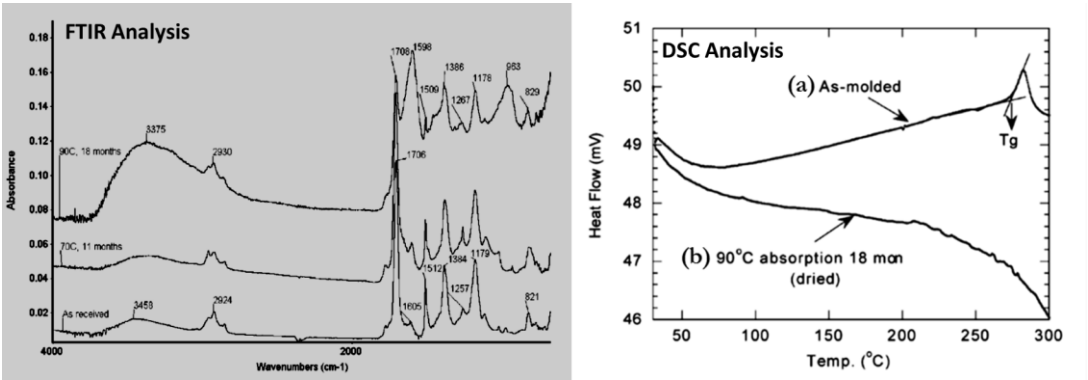

Figure 2-6: FTIR analysis of CFRP BMI 5250-4 specimen after water absorption at temperature of 90 °C and 70 °C indicates that the broad spectra of –OH was observed on 90 °C sample [35] and DSC analysis of CFRP BMI 5250-4 indicates that (a) Tg for as-moulded sample was at 270 °C and (b) the disappearance of the Tg for 90 °C sample indicates that significant depolymerisation and chemical degradation

When exposed to high temperature (thermal degradation), Lv et al. [51] reported that the IR absorption peak at 3444 cm^{-1} assigned to –OH group and the peak at 1507 cm^{-1} assigned to phenyl C=C decreased after the BMI was exposed to 150 °C for 144 hours. However, the intensity of the peak at 1605 cm^{-1} assigned to CO displayed increment.

Hence, the mechanism when BMI is exposed to high temperature is in inverse direction with the mechanism when BMI is exposed to water. Figure 2-8 shows the comparison between thermal degradation and hygrothermal, which indicates the degradation of both products. Lv et al. [38] found that the –OH intensities increased when the sample was exposed to water under certain temperature, while the intensity of –OH decreased after exposing BMI to a constant temperature of 150 °C for 144 hours. Additionally, when BMI was exposed to high temperature, Regnier et al. [41] reported that the BMI thermally degraded at 400, 500, and 600 °C, whereby formation of isocyanate-based product was observed due to chain scission that occurred in the imide ring.

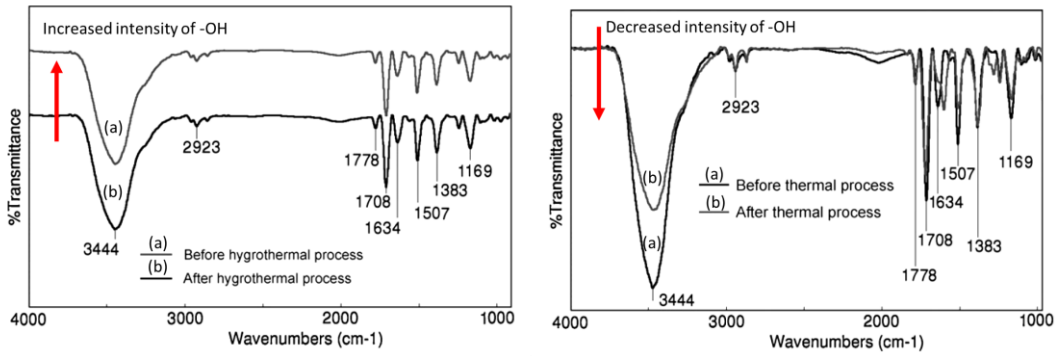

Figure 2-7: Comparison between the effect of hygrothermal and thermal degradation of the BMI indicates that for hygrothermal process the –OH intensity increase whereas for thermal the –OH intensity decrease.

Therefore, from the literature survey, it can be concluded that the effects of moisture absorption and temperature may be detrimental to the chemical reaction of BMI. Hence, this suggests an idea on how machining could affect BMI when varied cutting environment are applied on machining CFRP BMI 5250-4.

2.2 Principles of conventional machining (CM)

2.2.1 Chip formation

Chip formation in metal cutting can be explained by the orthogonal cutting model, as illustrated in Figure 2-8. Chip is formed in metal cutting mainly due to plastic deformation and shearing of material along the shear plane (AB), which occurs at primary deformation zone (i). At secondary deformation zone (ii), the formed chip moves along the rake face of the cutting tool, whilst the tertiary deformation zone (iii) refers to the area where the cutting tool is in contact with the newly machined surface. The shear angle (Φ) is the angle between shear plane (AB) and the direction of movement of workpiece BC, from the tool edge to the position where the chip leaves the worksurface , whereas, the rake angle (α) is the angle between the rake face of the cutting tool and the formed chip (normal to the machined surface) and the flank angle (γ) is the angle between the cutting tool flank face and the machined surface.

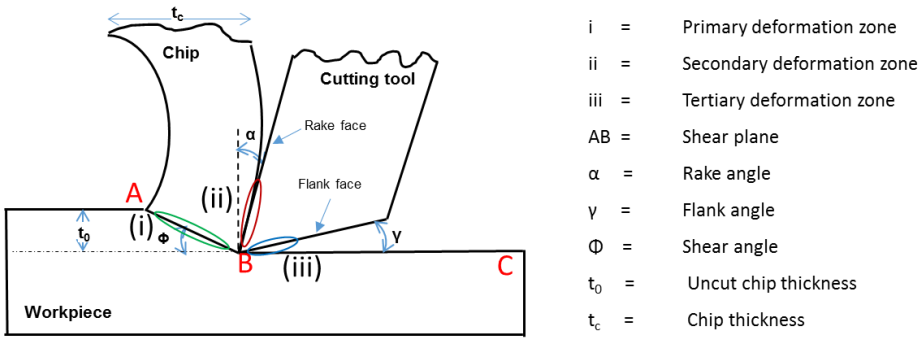

Figure 2-8: Basic principle of metal cutting [52]

Chip formation in metal cutting relies on the material being cut and the cutting conditions, i.e. cutting speed and feed rate. Generally, four types of chip can be observed in metal cutting, which are continuous chip, discontinuous chip, continuous chip with built-up edge, and serrated chip [52]. When machining a ductile material, such as aluminium, mild

steel and bronze with high cutting speed and/or at high rake angle, continuous chips are usually formed. Continuous chips are generated when the continuous plastic deformation of metallic material is produced without fracture in front of the cutting edge. Although continuous chip could have good surface finish, they are not desirable because the chip tend to tangle between the cutting tool and the workpieces. Therefore, the application of a chip breaker is proposed to break the chip into smaller segments and adjustment of cutting parameters is necessary when dealing with continuous chip [52, 53]. In contrast with continuous chip, discontinuous chip, which are formed in a small segment, are attached either firmly or loosely to each other. Such chip are produced by brittle workpiece materials such as cast iron because they do not have the capacity to undergo high shear strains encountered in machining [53]. Besides, the cutting parameters, such as very low/high cutting speed, large depth of cut, and low rake angle, may contribute to the formation of discontinuous chip [53].

A built-up edge (BUE) is formed when layers of material from the workpiece are gradually deposited on the tool tip. The formation of BUE affects the geometry of the cutting tool, aside from deteriorating surface roughness. Therefore, in order to avoid the formation of BUE, it is recommended to use cutting tool with lower chemical affinity for the workpiece materials and applications of cutting fluid. Lastly, serrated or segmented chip are produced when machining metal suggests low thermal conductivity and has strength that decreases with the increase in temperature, such as titanium and its alloy.

The chip formation for metal are mainly due to plastic deformation at the primary shear zone, while chip formation in composite materials, especially CFRP, has less occurrence of plastic deformation. Although some similarities are present in machining composite and metal, CFRP chip formation occurs mostly due to brittle fracture of carbon fibre and matrix resin. The next subsection explains CFRP chip formation in detail.

2.2.1.1 CFRP chip formation

The study of chip formation enables researchers to comprehend the mechanism of material removal. Thus, basic understanding of chip formation when machining CFRP is indeed necessary. The nature of composite materials, which is heterogeneous and abrasive, makes chip formation mechanism in composite both complex and intricate [4, 5]. In contrast to metal cutting, where chip formation is mainly due to plastic deformation and shearing of materials, in CFRP machining, less plastic deformation occurs [3, 5]. Due to the inherently brittle nature of carbon fibre, chip formation in CFRP machining is primarily due to fracture, bending, and buckling; depending on the CFRP fibre orientation [54-56].

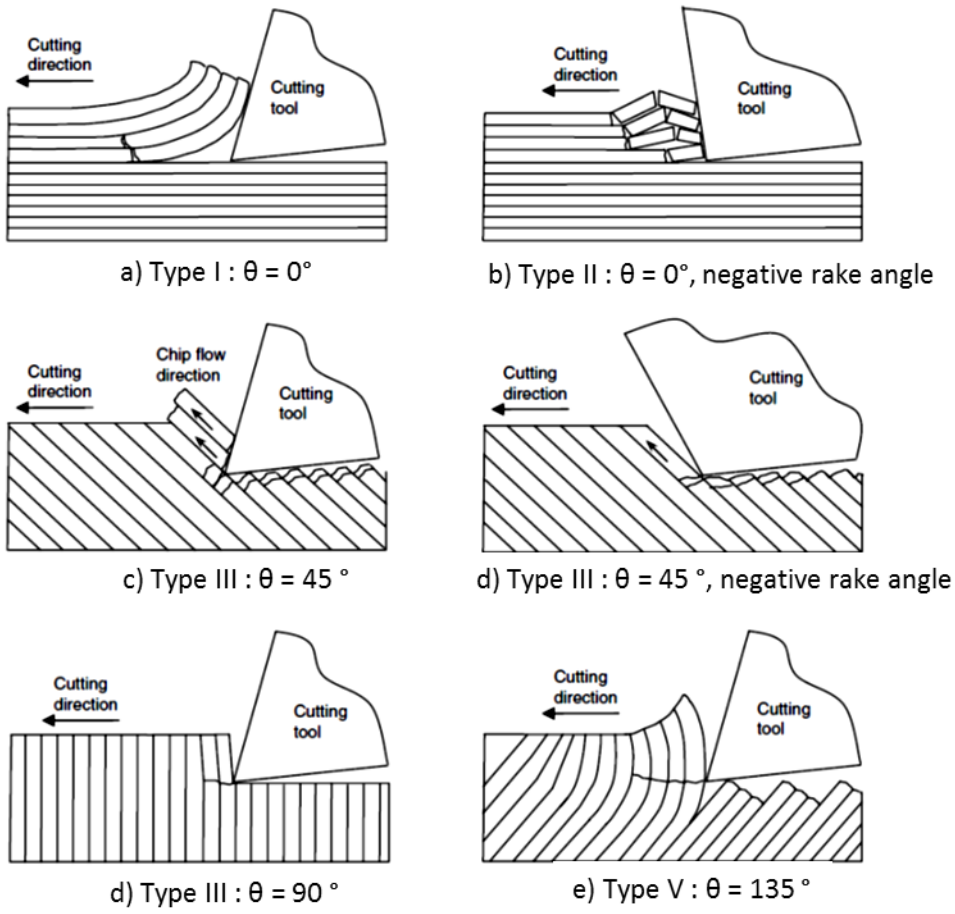

Figure 2-9: Cutting mechanisms in the orthogonal machining of CFRP with a sharp edge [55, 57, 58].

Although the quasi-isotropic CFRP is more practical for application, understanding the mechanism of chip formation in a unidirectional composite is vital. Chip formation is initiated by crack propagation in the primary shear zone [56, 57, 59]. Chip formation when machining unidirectional CFRP can be divided into five different types depending on the fibre orientation and cutting edge rake angle summarised by Wang et al. [58] as in Figure 2-9.

- Type I (Figure 2-9 (a)): Type I chip formation which is delamination occurs when machining 0 ° fibre orientation with positive rake angle. When the tool advances into the workpiece materials, a crack initiates and propagates along the fibre-matrix interface. The peeled layer slides up the rake face as the tool advances into the workpieces and causing it to bend like a cantilever beam.
- Type II (Figure 2-9 (b)): Type II chip formation occurs when machining 0 ° fibre orientation with negative rake angle. The chip formation occurred by buckling. The fibres are subjected to compressive loading along their direction, which cause them to fail by buckling. In-plane shearing and fracture at the fibre matrix interface caused by continuous advancement of cutting tools. The fibres fracture in a direction perpendicular to their length by successive buckling.
- Type III and IV (Figure 2-9 (c-e)): When machining CFRP with fibre orientation greater than 0 and less than 90 °, fibre cutting type of chip formation occurs for all cutting edge rake angle.
- Type V (Figure 2-9 (f)): Macro-fracture type of chip formation occurs when machining 105 to 150 ° fibre orientation. Severe deformation of the fibres that lead to delamination, intra-laminar shear along fibre- matrix interface and severe out-of-plane displacement occur when machining 105 to 150 ° fibre orientation. Extensive elastic bonding is caused by the cutting edge compression against the

fibres. The compressive stress ahead of the tool point causes the fibres and matrix to crack and a long but discontinuous chip is formed.

2.2.2 Cutting temperature

Understanding and monitoring cutting temperature in machining is crucial since the heat generated during machining can significantly affect both cutting tool and workpiece. As mentioned earlier in Section 2.1.2, the processing temperature of CFRP is limited to the Tg of matrix resin. Cutting temperatures that exceed the Tg of the matrix resin may result in thermal damages for CFRP and could significantly modify the chemical properties of matrix resin. Cutting temperatures higher than the Tg induced further post-curing, which then degrades both chemical and mechanical features of the matrix resin [14]. Thermal damage induced by the heat generated during machining can lead to several problems, such as matrix burn-out and thermally degraded resin, which deteriorate the quality of the machined surface. Also, a cutting temperature higher than the Tg of matrix resin can lead to rubbery texture and it is capable of significant extension without any brittle fracture. Moreover, the difference between thermal expansion and conductivity for fibre and resin can cause damage, such as cracks and delamination [60, 61]. Therefore, measuring the cutting temperature during CFRP machining is definitely essential.

2.2.2.1 Heat in machining processes

Properties of metallic materials, such as homogeneity and high conductivity, have made the study of temperature distribution during metal cutting relatively easy, especially when comparing with CFRP machining. Hence, investigations of heat generation in metal cutting are indeed well-established, in comparison to CFRP machining. In CFRP material,

nonetheless, the varying properties of fibre and reinforcement have made understanding temperature distribution a difficult task, hence less consensus in the body of literature.

Therefore, to present an idea pertaining to heat distribution during machining, Figure 2-10 shows the main zone of heat distribution in the metal cutting theory. The heat generated can be divided into three main zones; primary, secondary, and tertiary, as shown in Figure 2-10.

- The highest (80-85 %) heat is generated at the primary deformation zone due to the main shearing of the workpiece material that occurs in this zone (Figure 2-10 (a)). The chip and the new-machined surface produced by shearing of materials occur in the primary shear zone.
- Second, the heat generated at the secondary deformation zone (Figure 2-10 (b)) is between 15 and 20 %.
- Lastly, heat (1-3 %) generated in the tertiary deformation zone is produced by the rubbing action between the new-machined surface and the tool flank face, as shown in Figure 2-10(c). The amount of heat is strongly influenced by the tool flank condition in this zone.

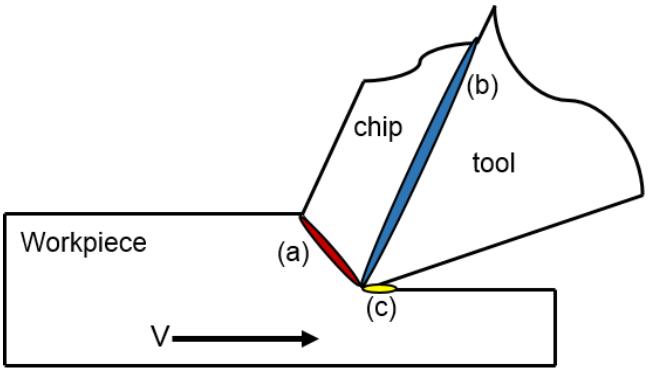

Figure 2-10: Heat generation in machining process indicates that (a) primary, (b) secondary and (c) tertiary deformation zone.

2.2.2.2 Cutting temperature measuring technique

Measuring cutting temperature in CFRP machining is challenging due to the low thermal conductivity of matrix resin, non-homogenous, as well as the different thermal properties of carbon fibre reinforcement and matrix resin. As such, several techniques have been introduced to measure cutting temperature, such as thermocouple [62-65], infrared (IR) thermal camera [22, 64, 66, 67], and pyrometer, which are rather common in CFRP machining.

The most common technique used to measure cutting temperature is the K-type thermocouple. The thermocouple working mechanism is based on the 'Seebeck' effect, where the difference of voltage between hot junction and cold junction in the thermocouple generates the thermoelectric force (thermal e.m.f). In this technique, the thermocouple is embedded inside the cutting tool or the workpiece material. In order to install the thermocouple inside the workpiece, a hole is made before conducting the machining. Another approach is to locate the thermocouple in the CFRP machining by implanting the thermocouple during the fabrication process of CFRP laminate [62, 68]. Nevertheless, this method is intricate due to the ability of the thermocouple to move about during the curing process. To date, there is no consensus in the optimum distance between the thermocouple and the cutting edge to identify the actual cutting temperature. For example, Yashiro et al. [62] suggested that the thermocouple should be implanted 0.3 mm from the cutting edge, while Sorrentino et al. [63] located the thermocouple 1 to 3 mm from the cutting edges to obtain the maximum temperature. However, due to the low thermal conductivity of CFRP, both researchers [62, 63] agreed that the thermocouple should be located as close as possible to the cutting edges in determining the actual cutting temperature. Additionally, to measure the cutting temperature using thermocouple, the thermocouple should be embedded inside the cutting tool through

coolant channel. However, when employing this method, the cutting tool is often stationary while the workpiece rotates. Since this method is not recommended for milling operation, some studies have suggested the K-type thermocouple to be located at the cutting edges while milling CFRP [65, 69-71].

Other than thermocouple, several non-contact methods of measuring cutting temperatures, such as pyrometer [69, 72] and IR thermal camera, can also be applied when milling CFRP [22, 66, 67, 73]. The IR energy/heat produced by the radiating body is detected by the IR thermal camera, which is then converted into an electronic signal for temperature measurement. The effectiveness of IR thermal camera depends on the emissivity of a radiating body, where higher emissivity value of the body results in better temperature measurement. For instance, heat from the blackbody object has an emissivity value of 1.0, while heat from a shiny and reflective surface, such as brass, has an emissivity of 0.3, which is difficult for detection by IR thermal camera. As such, Haddad et al. [22, 66] suggested fixing the IR thermal camera by using a tripod 100 cm from the workpiece to avoid the vibration generated during the machining, which enables the device to capture stable images. Meanwhile, Nor et al. [67] compared cutting temperatures when milling CFRP at room temperature and in chilled air (-10 °C) conditions. The temperature recorded for the room temperature was higher (90 to 130 °C) than the chilled air condition (50 - 107 °C). Although the cutting temperature measured was less than the Tg, thermal damage was found on the machined surface, suggesting that the actual cutting temperature was higher than the Tg. On top of that, Yashiro et al. [62] and Merino-Perez et al. [64] reported that cutting temperature measurements determined via thermocouple and IR thermal camera are comparable for CFRP milling and drilling, respectively. Figure 2-11 (a) and (b) show the comparison between the tool temperatures measured by using thermocouple and IR thermal camera.

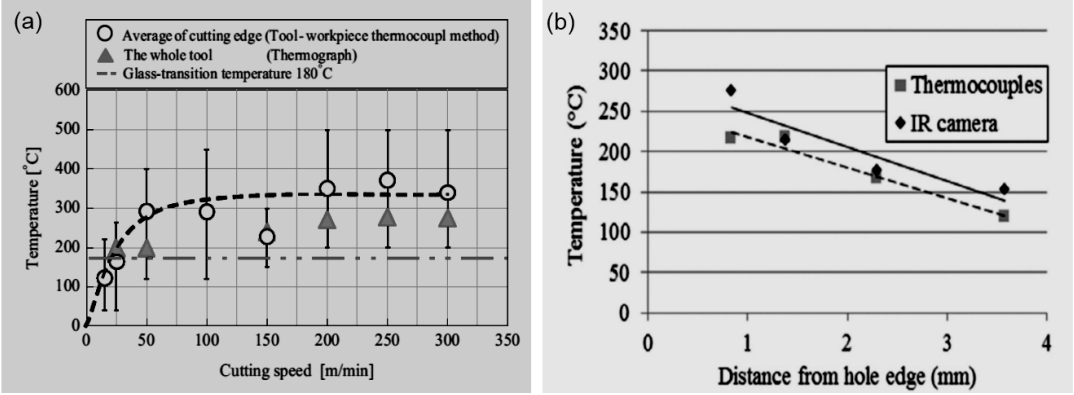

Figure 2-11: The difference in cutting temperature measured using the thermocouple and the IR thermal camera indicates that both work by (a) Yashiro et al. [62] when milling of CFRP with uncoated tungsten carbide and (b) Merino-Perez et al.[64] when drilling CFRP with uncoated tungsten carbide that the cutting temperature measured by both method are comparable.

Although many studies have measured the temperature during machining of CFRP, none has stated the actual machining temperature for CFRP. As mentioned earlier, the processing temperature when machining CFRP should be lower than the Tg. Hence, it is necessary to monitor the cutting temperature to avoid the temperature from exceeding the Tg, which could degrade CFRP properties.

2.2.3 Cutting forces in milling

Fracturing, buckling, and bending of carbon fibre by the cutting tool at the primary shear zone generate cutting forces. Typically, these cutting forces can be denoted as Fx (feed force), which acts in the direction of feed; Fy (normal forces), which acts at a normal direction to the feed; and Fz (thrust force), which acts in the direction of the cutting tool rotation. Figure 2-12 shows the cutting forces in milling, which indicates that the cutting forces are in x- and y-directions.

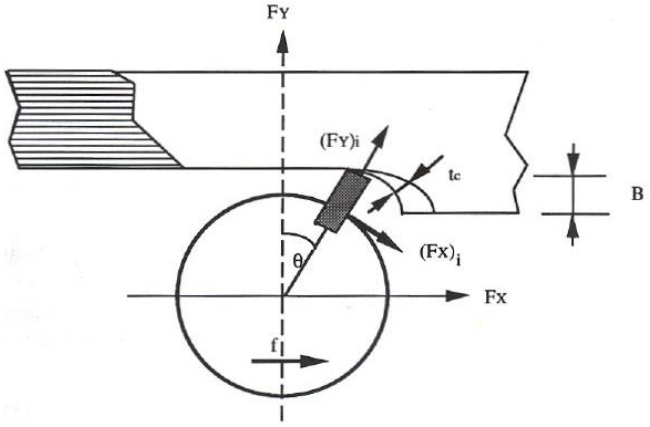

Figure 2-12: Cutting forces in milling [59].

In machining of CFRP, the effect of heat generated by the cutting tool and the CFRP workpieces can significantly affect the cutting forces. Researchers have reported that the cutting temperature generated can substantially affect the cutting force while CFRP machining [68, 71, 74]. In addition, Ghafarizadeh et al. [71] reported that the cutting forces when milling CFRP increases from 60 to 100 N as the cutting speed increases from 200 to 300 m/min. However, when the cutting speed is increases to 375 m/min, it was observed that the cutting forces started to decrease from 100 to 80 N. Thus, the reduction of cutting force at higher cutting speed can be attributed to the cutting temperature generated. It is claimed that the epoxy matrix materials are softened as the cutting speed is increased, thus resulting in reduced cutting forces [71]. A similar observation has been reported by Jia et al. [68] when milling CFRP with temperature that ranged between -25 and 135 °C. The cutting forces increased as the temperature decreased from 135 to -25 °C. Hence, it is proposed that the hardness of matrix resin increases when the temperature decreases, thus resulting in increment for the cutting forces.

The assessment of cutting force during the milling of CFRP is critical because the progress of cutting force may affect the tool life, the heat generated during machining, and the quality of the machined surface. In addition, understanding the mechanism of

cutting forces in CFRP machining is vital, especially in determining the cutting tool life and causes of possible damage, such as delamination and surface roughness.

2.3 Cutting environment

2.3.1 Conventional cutting fluid

The application of cutting fluid during machining is vital for many difficult-to-cut materials. This is because; the heat generated during the machining process can damage the tools, hence increasing surface roughness and force on the workpiece material. The application of cutting fluid is highly recommended to reduce any possible problems, such as rapid tool wear and poor surface condition. Also, some problems that occur frequently at the cutting zone during machining process are friction and heat generation, which may affect tool life, cutting forces, and surface finish [75, 76]. Therefore, the presence of cutting fluid during the machining process can increase tool life and dimensional accuracy, apart from decreasing cutting temperature, surface roughness, and power consumption [18, 77-79]. Additionally, in CFRP machining, the presence of cutting fluid aids the removal of hazardous carbon chip. However, it is not recommended to machine CFRP with the presence of cutting fluid [17]. Post-processing after machining CFRP with the presence of cutting fluid is required so as to ensure that the moisture is not absorbed into the matrix resin, which may deteriorate the mechanical properties and modify the chemical properties of the composite materials [35].

2.3.2 Dry

Although machining with cutting fluid has several advantages, such as reducing heat between cutting tool and workpiece, improving the quality of machined surface and tool life, as well as aiding chip removal during machining [52, 80]; dry condition is

recommended for CFRP [17]. However, if CFRP machining exceeds its Tg, thermal and subsurface damages may occur on the CFRP [67, 81]. Increment in cutting temperature can cause CFRP thermal softening and reduction in material strength. This strength reduction is beneficial for tool wear and cutting force reduction, but the quality of machined surface may be compromised due to high cutting temperature. Furthermore, the fibre pull-out, due to matrix cracking induced by high cutting temperature, produces poorly machined surface in dry machining [62, 81, 82]. Thus, it is important to closely monitor the cutting temperature during CFRP dry machining to avoid degradation of matrix resin, which deteriorates the mechanical properties of CFRP. Moreover, due to the abrasive nature of carbon fibre, the carbon chip/dust is hazardous to human health; thus demanding proper dust extraction during CFRP dry machining.

2.3.3 Cryogenic cutting media

Due to the potential sensitivity of matrix resin towards heat and moisture, machining in a cryogenic cutting environment may be beneficial. Machining CFRP in a cryogenic environment can be considered as similar to dry machining. Hence, post-processing after machining is unnecessary. In addition, cryogenic cooling may reduce the effect of thermal softening and enhance the efficiency of heat removal during machining [77, 78, 83].

Liquid nitrogen (LN_2) and carbon dioxide (CO_2) are the most common media applied for cryogenic machining. Figure 2-13 shows the typical phase diagram relationship between pressure and temperature of both carbon dioxide and nitrogen. Nitrogen accounts for four-fifths (78.03 %) by volume of the atmosphere, which has a melting point at -210 °C and a boiling point at -196 °C. Meanwhile, LN_2 offers better cooling medium (as low as -196 °C) when compared to CO_2 as it improves the machinability of the machined product [79, 84].

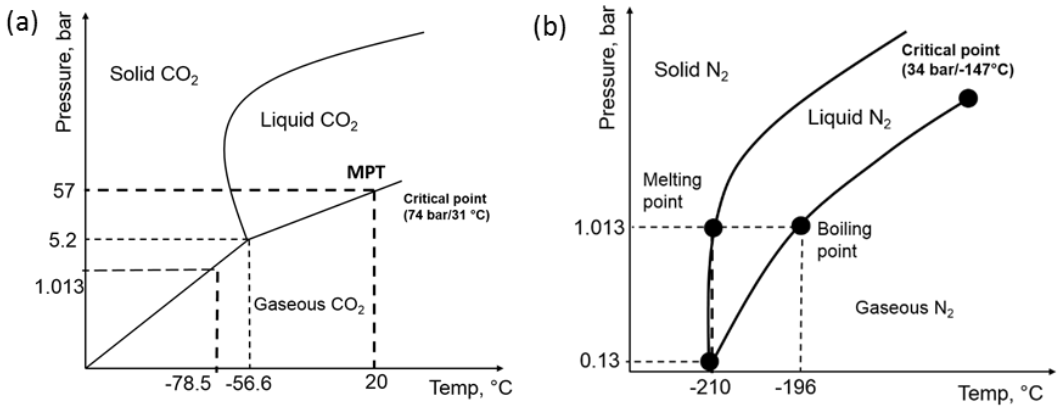

Figure 2-13: Typical phase diagram of a) CO_2 and b) LN_2 (Adapted from [79]).

In addition to the application of LN_2 as a cryogen, several studies have explored the application of CO_2 as a cryogen. Although the temperature achieved by CO_2 fails to reach as low as the temperature in LN_2, some potential outcomes, such as improved tool wear, cutting forces, and quality machined surface in machining with LN_2, could be accomplished with CO_2. CO_2 is stored in a medium pressure tank (MPT) in liquid form. Referring to Figure 2-13, at pressure of 57 bar, the temperature for CO_2 is 20 °C. In order for the liquid CO_2 to transform into ice crystal, the pressure must drop to 1.013 bars to achieve as low as -78.5 °C. Although CO_2 crystal ice could not achieve the low temperatures as LN_2, the effect of cooling is definitely comparable. Besides, CO_2 offers several advantages over LN_2, such as clean work environment due to near-dry cutting condition, less thermal shock on cutting tool, and no secondary cleaning is required after machining [85].

2.3.3.1 Cryogenic cooling technique

The effectiveness of cooling the cutting edges during machining operation can be achieved by modifying the tool to apply the cryogenic cooling where the coolant is supplied continuously and directly to the tool holder, hence, increasing the tool life and maintaining the workpieces ductility [18, 86]. It is suggested that the cryogenic cooling

reduces the heat accumulated at the cutting zone [18] and retained the hardness of the cutting tool [87].

Several techniques have been employed when applying the cryogenic cooling during machining. Yildiz et al. [79] listed four common techniques in cryogenic cooling, which are cryogenic pre-cooling workpiece, indirect cryogenic cooling, cryogenic spraying and jet cooling, as well as cryogenic treatment, which is frequently employed. Hong et al. [88], on the other hand, proposed a dual nozzle system for LN_2 supply for turning operations, where LN_2 can be provided through a well-controlled and focused jet to the tool rake face, flank face or both. Next, Aurich et al. [89] suggested three different cooling methods using two nozzles, which are: (i) cooling the contact zone from the flank face and the rake face direction, (ii) pre-cooling the workpiece and the flank face direction, as well as (iii) both nozzle pre-cooling the workpiece when turning the stainless steel. Nonetheless, only marginal variances are noted for each method. The main aim for cryogenic machining is to reduce heat accumulation during machining. Therefore, longer tool life, lower cutting forces, as well as improved surface roughness and integrity, could be achieved.

The effectiveness of cooling the cutting edges during machining operation can be achieved by modifying the tool to apply the cryogenic cooling, where the coolant is supplied continuously and directly to the tool holder, thus increasing the tool life and maintaining the workpieces ductility [18, 86]. Thus, it is suggested that the cryogenic cooling reduces the heat accumulated at the cutting zone [18], aside from retaining the hardness of the cutting tool [87]. Sections 2.3.3.2 to 2.3.3.4 further elaborate cryogenic machining for both metal and composite due to the limited literature available for composite machining in a cryogenic cutting environment.

2.3.3.2 Tool wear/tool life

The heat generated due to plastic deformation of metal at shear zone during the machining process could be removed when applying the cryogenic coolant [86]. The effectiveness of cryogenic cooling also depends on how the coolant is applied during machining. The presence of cryogenic media can sometimes affect the property of the machined materials and as a result, affect the progression of tool wear when machining with the presence of cryogenic coolant. Khan et al. [18] modified the cutting tool by supplying the LN_2 directly towards the cutting insert. They found that when machining stainless steel using the tungsten carbide inserts coated with titanium carbonitride (TiCN) at a cutting speed of 100 m/min and feed rate of 0.05 mm/rev the tool life improved more than four times compared to conventional cutting fluid. They proposed that machining at lower cutting speed with presence of cryogenic coolant could increase tool life whereas, when machining at high cutting speed the cutting tool suffered from microcrack and flank wear.

However, Barnes et al. [90] reported that tool wear for solid carbide coated with titanium aluminium nitride (TiAlN) drill was higher when the cutting tool was cooled by LN_2 as compared with dry machining when drilling CFRP at a cutting speed of 96 m/min and feed rate of 0.065 mm/rev. They claimed that when drilling with pre-cooled tool the tool wear progressed at a faster rate due to the more brittle fracture and lower localised plastic deformation at the crack initiation zone in the epoxy matrix when compared with dry drilling. When drilling in dry condition, the epoxy matrix softened and resulted in lower tool wear.

In contrast with Barnes et al. [90], Xia et al. [91] reported that when drilling of CFRP using uncoated carbide drill with cutting speed of 60 m/min and feed rate of

0.025-0.05 mm/rev, the outer corner wear of the drill used for dry drilling was 496 μm, whereas for cryogenic machining the wear was only 196 μm after producing 50 holes. They claimed that continuous cooling of the cutting tool during cryogenic drilling aided in heat removal between the cutting tool and the workpiece thus reducing the cutting temperature as well as retaining the sharpness of the cutting tool. The difference in this result might be due to the method of how the cutting tool was cooled during machining. Barnes et al. [90] cooled the cutting tool by submerging the cutting tool inside LN_2 for 30 seconds before drilling was performed, whereas, Xia et al. [91] supplied the LN_2 continuously through the coolant channel inside the cutting tool.

In order to have a clear view of the temperature distribution when applying cryogenic cooling, Dix et al. [92] performed a modelling study to investigate the efficiency of drilling assisted by cryogenic cooling. The maximum temperature at the contact area between the stainless steel workpiece and the rake face of tungsten carbide tool when drilling with the presence of cryogenic coolant can be reduced to 450 °C, whereas the maximum temperature for the dry machining was 820 °C. Figure 2-14 shows the temperature distribution of the conventional cutting fluid and cryogenic cooling when drilling ten holes of steel using tungsten carbide tool with constant parameters (speed, V=105 m/min, feed rate, f=0.21 mm/rev). However, it was suggested that the cooling effect is strongly related to the position of the cooling channel for the temperature distribution during the machining process.

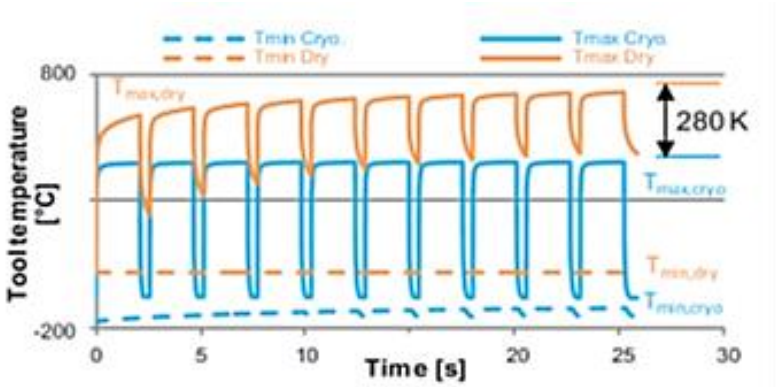

Figure 2-14: Cutting tool temperature between dry and cryogenic machining when drilling ten holes of steel using tungsten carbide tool with constant parameter (*V*= 105m/min, *f*=0.21mm/rev) [92].

2.3.3.3 Cutting forces

Some researches claimed that reduction of cutting forces could be established when employing the cryogenic cooling because the cutting tool can retain it sharpness [93, 94]. Kumar et al. [93] observed that reduction of cutting force by 15 % was obtained when machining with the presence of cryogenic coolant when machining stainless steels using tungsten carbide tool with constant cutting parameters. However, Xia et al. [91] reported that the thrust force for cryogenic drilling was higher by 20 % as compared to the dry drilling of CFRP. The LN_2 was supplied through the cutting tool during the drilling operation. Drilling of CFRP was performed using uncoated carbide drill with a constant speed of 60 m/min and feed rate of 0.025-0.05 mm/min with the dry and cryogenic condition as shown in Figure 2-15. When dry drilling CFRP, the heat generated soften the matrix materials, thus reduce the cutting forces. However, when drilling CFRP with the presence of cryogenic condition, the heat generated was removed more efficiently and the strength of the matrix material was retained.

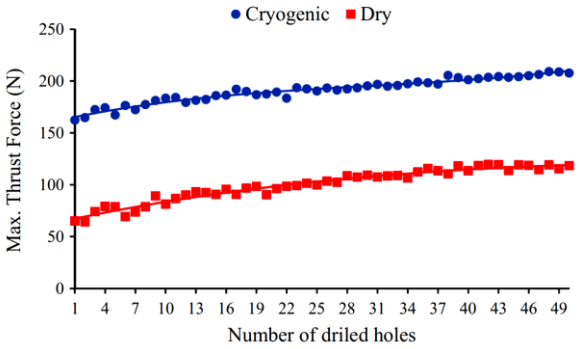

Figure 2-15: Maximum thrust force when drilling of CFRP in dry and cryogenic conditions indicate that the thrust force in cryogenic condition was higher 20 % than dry condition [91].

Bhattacharya et al. [95] and Ahmed et al. [86] also discovered that thrust force and torque were higher when machining Kevlar composite with the presence of cryogenic cooling. Findings obtained by Xia et al. [91], Bhattacharya and Horrigan [96], and Ahmed et al. [86] are in line with several other studies that reported the presence of cryogenic cooling during the machining process leading to increased hardness and reduction in resistance of the composite to deform [90, 97, 98]. Additionally, some properties of CFRP, such as tensile and Young's modulus, could increase when the temperature is reduced. Moreover, in dry machining, high temperature may lead to the softening of matrix composite, apart from minimising the strength of resin to hold the carbon fibre [61, 81, 99, 100]. Thus, the cutting forces when machining of CFRP in cryogenic environment are generally higher when compared to that generated in dry machining.

2.3.3.4 Surface roughness and integrity

With regard to surface roughness and surface quality when machining with the presence of cryogenic cooling, reduction in cutting temperature via cryogenic cooling improved the machined surface [91, 101-103]. This can be attributed to the low cutting temperature that retained the sharpness of the cutting tool. Additionally, low cutting temperature reduces adhesion and chemical interactions between the cutting tool and the workpiece. Moreover, high cutting temperature in dry machining softens the matrix of the materials,

which may lead to fibre pull-out and rougher surface, as well as deformed matrix on the machined surface [91, 95]. In contrast, less fibre pull-out, less surface cracks, and clean surface were observed when machining CFRP in cryogenic condition. Rivera-Moreno et al. [101] reported that surface roughness was reduced by 75 % when CO_2 cooling was applied during the grooving operation of elastomer. It was further observed that the grooved dimension when machining with cryogenic cooling approached the nominal dimension (≈ 4 mm) whereas, when machining in room temperature condition the grooved dimension reduce to ≈3 mm due to the material expandability.

Improvement in surface roughness and damage with cryogenic machining can be attributed to the reduction in the cutting temperature during machining [102, 104]. Less heat generated between the cutting tool and the workpiece reduces deformation via chip formation mechanism, thus enhancing the quality of machined surface. This can be attributed to the reduction of cutting temperature and tool wear in cryogenic cooling condition [97]. The same finding was also reported by Kumaran et al. [102] when drilling woven CFRP in cryogenic cooling, where the surface roughness and the quality of the machined surface improved with cryogenic machining, although the thrust force was higher. Furthermore, it was reported that increment in temperature reduced the mechanical strength of the composite [105]. Meanwhile, adhesion between the matrix resin and the fibre is dependent on the processing temperature due to the varying coefficient of thermal expansion of both matrix and fibre [60]. This notion is in agreement with the findings from Hojo et al. [104], who claimed that CFRP damage, such as delamination and fracture toughness, are strongly related to the processing temperature. Such processing temperature significantly influences the impact of damage in CFRP [104, 106].

Therefore, machining with the presence of cryogenic cooling can reduce the machining temperature, apart from improving tool wear, cutting forces, as well as surface roughness and integrity. The cooling techniques employed when performing the cryogenic machining are necessary to determine the effectiveness of the machining operation.

2.4 Machining of CFRP

As discussed in Section 2.1, CFRP composite has been increasingly replacing metal in both aerospace and automotive applications. Machining of CFRP, nonetheless, is more complicated and challenging than machining metallic materials [3, 5, 17]. The different mechanical and physical properties of both fibre and matrix complicate the machining operation of CFRP. Although many studies have focused on drilling of CFRP, milling appears to be essential in some applications so as to achieve the final dimensional accuracy and perfect finishing of CFRP parts [5]. Milling of CFRP can be performed by using either abrasive cutting tools or conventional cutters. Section 2.4.1 presents the available literature that depicts conventional CFRP milling, while Section 2.4.2 explains abrasive machining of CFRP.

2.4.1 Conventional milling (CM)

Milling of CFRP has often been required to remove excess materials and for a perfect finishing of the final part. Milling is often carried out at the end of the manufacturing process before assembly. Nonetheless, milling of CFRP must be carried out in such a way to avoid rejection of any part. Typically, in a milling operation, the rotating cutting tool is moved, while the workpieces are secured on the machined bed to remove the material. The cutting tool employed for milling is usually comprised of multiple cutting points. These processes are required to meet the final product tolerance, dimensional accuracy, and quality of the produced parts [3]. The following sections discuss the cutting tool, the

tool wear mechanism, and the machinability (tool wear, cutting forces, as well as surface roughness and integrity) of the conventional milling (CM) of CFRP.

2.4.1.1 Cutting tool

Rapid tool wear and reduced tool life are the major problems reported when machining CFRP due to its highly abrasive and inhomogeneous properties. Therefore, selection of cutting tool for machining CFRP is crucial and critical [5, 107-109]. Material toughness and wear resistance are the main criteria in selecting the cutting tool [52, 80, 110]. The aspect of high toughness in cutting tool materials is crucial to avoid catastrophic failure during machining, such as fracture and chipping of the tool materials [5, 111, 112]. Figure 2-16 shows the correlation between hardness and toughness in cutting tool materials. Table 2-6 shows the properties of several cutting tool materials. Furthermore, some studies have performed CFRP milling with varied cutting tools, such as diamond abrasive tool [23, 113-117], polycrystalline diamond (PCD) tool [73, 118, 119], and cemented carbide tool [67, 109, 120, 121].

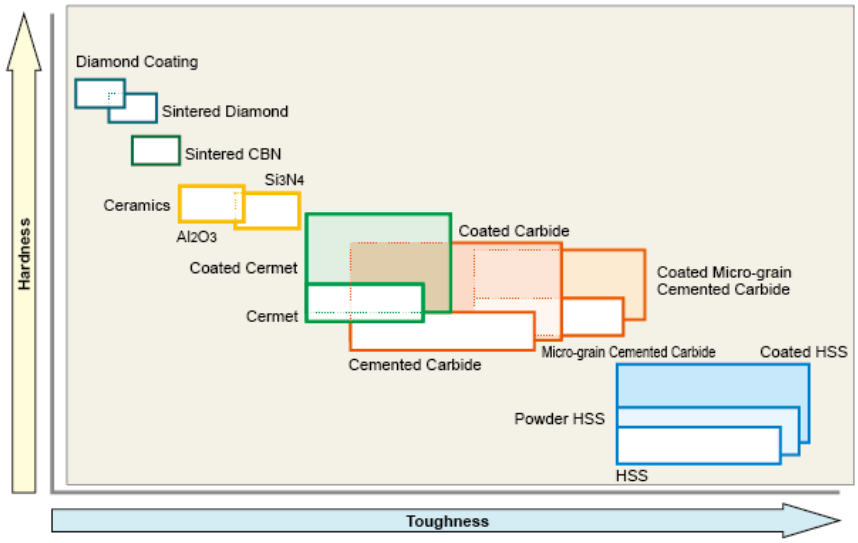

Figure 2-16: Relationship between hardness and toughness of cutting tool material (Adapted from [122]).

Table 2-6: Properties of the cutting tool materials (Adapted from [80, 122]).

Tool materials	Hardness, HV	Thermal conductivity, W/m*k	Thermal expansion, x10^{-6}/k
Diamond	>9000	2100	3.1
CBN	>4500	1300	4.7
Ceramic	2500	100	7.8
Cemented carbide	2100	121	5.2

A polycrystalline diamond (PCD) tool has been widely applied for CFRP machining. PCD offers longer tool life and improved surface roughness due to its properties, such as high hardness and high abrasion resistance [123-125]. However, the intricacy of manufacturing and the cost of PCD tool are 7 to 10 times higher when compared to other types of cutting tool materials, such as tungsten carbide and high speed steel. Besides, only a limited geometry that can be offered by PCD tool [126]. A PCD tool is comprised of synthetic diamond, where graphite and nickel are mixed at a high temperature (up to 1800 °C) and high pressure (up to 700 MPa) to manufacture the PCD tool insert. A PCD tool consists of a layer of fine diamond powder that is sintered together to form a dense and uniform mass, approximately 0.5 to 0.7 mm thick and supported on a substrate of cemented carbide [80, 110, 112]. The carbide also plays an important role in determining the mechanical properties, such as PCD toughness [110, 126]. Moreover, a PCD tool possesses the highest thermal conductivity of any material at room temperature and low-friction surface [127]. Additionally, a PCD also has high thermal conductivity, in which they can machine up to 350 °C before the tool starts to reduce its mechanical and physical strength [111, 126].

Alternatively, the frequent material selected for cutting tool in machining CFRP is cemented carbide. Tungsten carbide and titanium carbide are two groups of cemented carbide that have been commonly used for machining. In order to manufacture cutting tool, tungsten carbide particles, which are usually sized between 1 and 5 μm, are bonded

together in a cobalt matrix using powder metallurgy [80]. At times, other elements, such as titanium and niobium carbides, are incorporated to impart a particular property, such as hot hardness and resistance to oxidation, as well as diffusion of cutting tool. In addition, based on various applications, a wide range of grades of carbide cutting tools are available. Cemented carbide cutting tool can be classified into three major groups, which are: P, M, and K-types based on their applications. Also, they possess high hardness over a wide range of temperatures, high thermal conductivity, and high Young's modulus, thus making them an effective tool and die materials for a range of applications [3].

In contrast to cemented carbide cutting tool, PCD can offer abrasion resistance up to 500 times greater than cemented carbide [80]. However, cemented carbide can be manufactured in complex shapes, when compared to PCD, thus making them to be often chosen as cutting tool to machine CFRP.

2.4.1.2 End mill geometry

The cutting tool geometry has a significant influence on cutting force, chip formation, and machined surface quality. Figure 2-17 displays the standard geometry of a three flutes end mill. Helix angle for milling tool refers to the angle between the helix (flute) and the axis, as shown in Figure 2-17, which usually ranges from 0 to 30 °. Figure 2-18 illustrates the typical milling cutter used for milling CFRP. The straight flute cutter (helix angle= 0°) reflects the simplest geometry that offers good surface finish, but unfortunately, it has poor chip disposal, as exhibited in Figure 2-18 (a). Next, Figure 2-18 (b) shows the helical milling cutter that offers better chip disposal during milling, when compared to straight flute and burr milling cutters. As for helical milling cutter, the cutting force is generated depending on the spiral direction. As a result, surface ply that is not supported in the force direction is prone to delamination and fuzzing of carbon fibre. Meanwhile, burr

milling cutter, as shown in Figure 2-18 (c), is comprised of opposing spirals that ground on the body of the cutting tool to generate many cutting points [3]. This cutting tool is recommended for high cutting speed and feed rate application, however, the disadvantages of this cutting tool are premature fracture of the cutting points and poor chip disposal [117]. Poor chip disposal when machining CFRP is detrimental due to the clogging of chip on the cutting tool, which may increase the heat generated between the cutting tool and the workpiece. Therefore, selection of the most suitable cutting tool geometry is crucial when machining of CFRP. The geometry of PCD tool is limited to the straight flute cutter, whereas the tungsten carbide end mill can be manufactured into a variety of tool geometries based on the application.

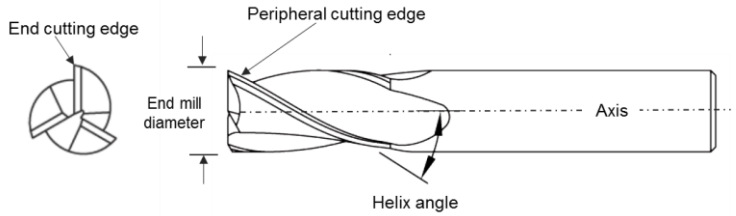

Figure 2-17: Major geometry of standard three-flute end mill (Adapted from [128]).

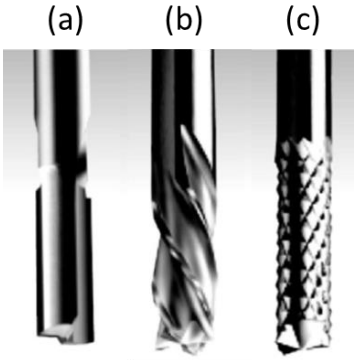

Figure 2-18: Typical available geometry for milling CFRP a) straight flute cutter, b) helical milling cutter and c)burr milling cutter (Images not in scale, adapted from [3]).

2.4.1.3 Tool wear mechanism

The wear mechanism in PCD is similar to that of cemented carbide tool [3]. Several aspects can lead to the progression of PCD tool wear, such as particle size, content of

cobalt binder, diamond types, and impurities [124, 125, 129]. The PCD consists of diamond particles with Co binder. Hence, the wear mechanism in PCD tool is mainly due to abrasion by the dislodged diamond particles, cracking, and fracturing caused by brittle fracture and microchipping [118, 124]. Similar to the wear mechanism of tungsten carbide cutting tool, abrasion that occurs between PCD and workpiece may result in removal of Co binder. Although the high hardness of PCD tool could improve tool life, removal of Co binder results in dislodging of diamond particles. Figure 2-19 compares the tool life of several cutting tool materials, where it indicates PCD possesses less than 0.2 mm flank wear with a cutting length of 1400 m.

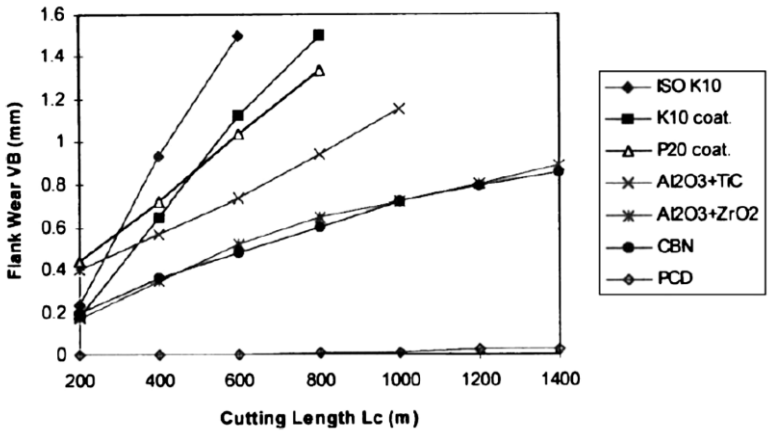

Figure 2-19: Progression of flank wears in machining of CFRP when employed different cutting tools [123].

Other typical wear mechanisms observed in the PCD tool are edge rounding, cracking, and chipping, which could lead to the catastrophic failure of the cutting tool [3, 118]. Sheikh-Ahmad [3] explained that the wear mechanism of the PCD tool when machining the composite materials at a lower feed rate is abrasive wear, which is dominant wear. Microchipping initiates the abrasive wear at the cutting edges of the PCD tool, which is due to the removal of the weakly-held Co binder at the cutting edges.

As discussed in Section 2.4.1.1, the main component of cemented carbide tool is tungsten carbide (WC) that acts as the main particle, while cobalt (Co) acts as the binder. Machining

of CFRP with uncoated cemented carbide has been extensively investigated. The wear mechanism, when machining CFRP, with WC-Co cutting tools is abrasive wear. The WC particles have higher hardness, when compared to carbon fibre. The tool wear mechanism of WC cutting tool is mainly due to the hard abrasion by fractured WC grains and soft abrasion mode due to the low hardness of carbon fibre, as compared with WC grains [108, 124, 130-132]. Besides, pull-out of WC grain from the cutting edges may result in hard abrasion between the cutting tool and the workpiece, especially due to the high hardness of WC, as compared to carbon fibre. The wear of WC tool is initiated with the removal of Co binder. As the Co binder starts to be removed from the surface, crack and fracture are generated at the WC particle by brittle fracture [130-132]. Consequently, the WC particle becomes more exposed to impact loading between the cutting tool and workpiece, thus resulting in WC particle pull-out from the surface. The pits and holes found on the surface of a cutting tool show that the WC-Co has been pulled-out when the cutting tool begins to wear [67, 131]. The Co binder is weaker than the WC particle, which results in higher wear rate for Co binder, while a reasonable rate for WC particle wear. Hence, the selection of cutting tool materials is crucial when machining CFRP due to the properties of CFRP that are highly abrasive and non-homogenous.

2.4.1.4 Summary of conventional milling (CM)

Milling of CFRP is challenging due to the different properties of the matrix and carbon fibre. The primary concern in machining the polymeric matrix composite is that the cutting temperature should be below the Tg of matrix resin so as to avoid degradation in surface integrity. Several aspects could affect the machinability of the CFRP, such as fibre orientation and cutting parameters (feed, speed, and depth of cut). Due to the limitation of matrix resin processing temperature, it is proposed that machining of CFRP must be carried out at temperatures lower than the Tg. Several aspects, such as cutting parameters,

could influence the cutting temperature when milling CFRP. The cutting temperature in milling CFRP significantly affects the cutting tool wear and life, as well as the surface integrity. Due to the properties of the matrix resin, a processing temperature higher than the Tg could degrade the properties of CFRP.

The main concern in CM of CFRP is the heat generated during machining, which could degrade both workpiece and machinability. Several studies have investigated the effects of the cutting parameters, such as cutting speed [65, 69, 71], feed rate [69, 70], and depth of cut on the cutting temperature. As a result, it has been suggested that increment in cutting temperature is more apparent with increased cutting speed, especially when compared to increased feed rate [65, 71, 74]. For instance, Wang et al. [65] mentioned that the effect of increasing feed rate is more dominant with increment in cutting force, but less effect on the cutting temperature. Although increase in feed rate can significantly increase the amount of chip thickness, El-Hofy et al. [74] reported that reduction in cutting temperature was noted when increasing feed rate due to shorter machining time. At a constant cutting speed of 200 m/min, the cutting temperature reduced from 220 to 270 °C with a reduction in feed rate from 159 to 318 mm/min. Tables 2-7 and 2-8 summaries the available literature milling of CFRP employing the tungsten carbide (WC-Co) and polycrystalline diamond (PCD) end mill, respectively.

Table 2-7: Summaries of reported literature on milling of CFRP with tungsten carbide (WC-Co) end mill.

Reference	Tool Specification	Cutting Parameters	Measured output
Puw et al. [133]	*d*= 20 mm	V= 94.2, 188.4 m/min *f*= 50, 150 mm/min a_e = 1 mm FO = 0°,45°,90°,135° CE= dry	Tool wear (Vb) Cutting forces (Fx,Fy,Fx) Surface integrity Chip characteristic
Hocheng et al. [56]	*d*= 20 mm	V= 31.4, 94.2, 188.4 m/min *f*= 50, 150 mm/min a_e = 1 mm FO = 0°,45°,90°,135° CE= dry	Tool wear (Vb) Cutting forces (Fx,Fy,Fx) Surface integrity Chip characteristic
Ucar et al.[82]	*d* = 11.11 mm Helix angle, 30 °	V=18-25 m/min *f*= 76,127,178 mm/min a_e = 1 mm CE= dry	Tool wear (Vb) Cutting forces (Fx,Fy,Fx) Surface integrity Chip characteristic
Nor et. al [67]	*d*=8 mm Helix angle=30°	V= 160-200 m/min *f*=159-398 mm/min a_e= 0.71 mm CE= dry, -10°C	Tool wear (Vb) Cutting forces (Fx,Fy,Fx) Surface integrity Delamination factor
Pecat et al.[81]	*d*= 160 mm Rake angle=-12 ° Clearance angle = -7 °	V= 20, 100, 200 m/min F= 40-398 mm/min FO = 0°,+45°,90°,-45° CE= -40,20,80 & 120 °C	Cutting forces(Fx,Fy,Fz) Surface integrity
Yashiro et al. [62]	*d*=8 mm Helix angle=30 °	V= 15 – 300 m/min *f*=75-1200 mm/min CE= dry	Cutting temperature
Hosokawa et al. [134]	*d*= 4 mm Helix angle= 30 °,60 °	V= 25,75 m/min *f*= 0.025, 0.01 mm/min CE= dry	Tool wear (Vb) Cutting forces (Fx,Fy,Fx) Surface integrity
Ghafarizadeh et al. [71]	*d*= 10 mm Helix angle=30 °	V= 200- 375 m/min *f*= 400-750 mm/min a_e= 2.354 mm a_f= 0.5 mm FO = 0°,45°,90°,135° CE= dry	Cutting forces(Fx,Fy,Fz) Surface integrity Cutting temperature

d= tool diameter, V= cutting speed, f= feed rate, a_e= radial depth of cut, a_f= axial depth of cut, CE= cutting environment , FO= fibre orientation

Table 2-8: Summaries of reported literature on milling of CFRP with polycrystalline diamond (PCD) end mill.

Reference	Tool Specification	Cutting Parameters	Measured output
Hintze et al. [135]	*d*=12 mm	V= 800 m/min *f*= 6 mm/min a_e= 4 mm CE= dry	Delamination
Sorrentino et al. [136]	*d*= 40 mm	V= 100 m/min *f*= 100, 250,468 m/min a_e= 10,20,30 40 mm a_f =1.01, 1.5, 2.0 mm CE= dry	Cutting forces(Fx, Fy, Fz) Surface integrity
Wang et al.[65]	*d*= 6 mm	V= 37- 132 m/min *f*= 197 - 702 mm/min a_e= 2.32- 5.68 mm CE= dry	Cutting forces(Fx, Fy, Fz) Surface integrity Cutting temperature
El-Hofy et al. [74]	*d*= 12 mm Helix angle = -3°,0°,3°	V= 200- 300 m/min *f*= 159-318 mm/min a_e= 5 mm FO = 0°,45°,90°,135° CE= dry, chilled air	Cutting forces(Fx, Fy, Fz) Surface integrity Cutting temperature

TM= tool material, d= tool diameter, V= cutting speed, f= feed rate, a_e= radial depth of cut, a_f= axial depth of cut, CE= cutting environment , FO= fibre orientation

As for the effect of fibre orientation on cutting temperature, the results obtained in studies conducted by El-Hofy et al. [74] and Ghafarizadeh et al. [71] are inconsistent. The former observed the highest cutting temperature (293 °C) when milling at 45 ° fibre orientation, while the latter reported that the highest cutting temperature was obtained for fibre orientation at 90 ° (90 °C) and the lowest at 0 ° (50 °C). Such inconsistency could be due to the different geometries of the cutting tools employed, as well as the varying cutting parameters, which may affect the cutting temperature.

Hence, in order to reduce the effect of cutting temperature when milling CFRP, a study carried out by Nor et al. [67] revealed that the application of chilled air on the cutting tool while milling CFRP could produce a lower cutting temperature (102.8 °C) than the dry condition (133.6 °C). This could be attributed to the tool in the chilled air condition that

is less worn out, when compared to that in the dry machining condition. Chilled air removes the heat generated by the cutting tool and the workpiece. Although the cutting temperature is lower than the Tg of the epoxy (Tg= 180 °C), the thermally degraded resin was found on the machined surface, hence signifying the thermally-degraded resin. Thus, this suggests that although the cutting temperature does not reach the Tg, the combination of the cutting forces, the tool wear, and the heat generated could alter the machined surface. On top of that, Pecat et al. [81] reported that at a lower temperature (-20 and 40 °C), cracks propagating underneath the milled surface was apparent when milling CFRP at a constant speed of 100 m/min and 0.1 feed/tooth. Nonetheless, as the temperature increased (80 °C and 120 °C), the crack went invisible on the subsurface damage. This can be explained by the properties of the matrix resin that have reduced its brittleness to hold the carbon fibre. Hence, it is proposed that higher temperature increases the mobility of matrix resin (thermally damaged resin). As a result, the matrix resin could not support the carbon fibre any longer. It was also observed that cutting forces at a higher temperature are reduced, when compared to machining at a lower temperature.

In addition, surface roughness and surface integrity increased as the feed rate increased [3, 61, 82, 133, 135], but decreased with increment in cutting speed [17, 82, 137]. This can be explained as a higher feed rate generates higher chip per tooth (a_f), hence producing higher surface roughness [61, 138]. Feed rate is a critical factor in controlling delamination, as compared to cutting speed and depth of cut. Besides, increment in feed rate increases delamination on any cutting speed applied. For instance, Rahman et al. [137] observed that the surface roughness increased when 0.3 mm/rev feed rate was applied, when compared to 0.1 mm/rev feed rate. This was attributed to the increase in contact area between cutting tool and CFRP workpiece material, which further

deteriorates the surface condition and increment in chip thickness. Moreover, machining at high feed rate can increase the heat generated by both cutting tool and workpiece. Consequently, matrix smearing and thermal damage of CFRP machined surface were observed [17, 59, 126, 139].

2.4.2 Abrasive machining

Although milling of CFRP has often been performed by employing a typical milling tool, alternatively, an abrasive cutting tool could be more effective. Milling of CFRP with abrasive cutters is similar to milling of CFRP with burr milling cutter, as exhibited in Figure 2-18 (c) [3]. The cutter used in abrasive machining consists of abrasive (diamond or CBN) that typically has a negative rake angle and a small depth of cut [3]. Figure 2-20 shows the removal of materials in abrasive machining. The cutting process is carried out with several numbers of abrasive. When compared to CM, improved surface finish and less damage could be obtained with abrasive machining. The abrasive diamond cutting tool is gaining popularity for milling of CFRP due to its ability in machining at high cutting speed and feed rate, while at the same time, maintaining tool life. Although PCD could be applied in CM as the main cutting tool to promote longer tool life and to improve surface roughness, its inherently brittle feature is the main drawback. Nonetheless, the main problem when machining CFRP with abrasive cutting tool is the potential of broken fibre and thermally degraded resin to load between the diamond grit.

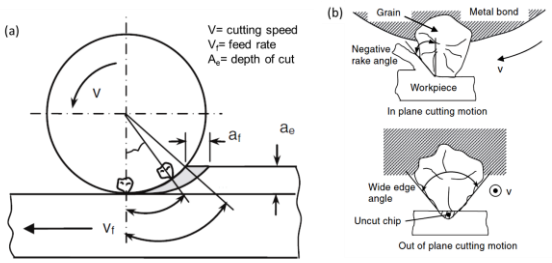

Figure 2-20: (a) Material removal with an abrasive cutter and (b) the diamond grain cutting motion (Adapted from [3]).

2.4.2.1 Cutting tool

The abrasive diamond can be deposited on the body of the cutting tool via several methods, such as resin bonding, vitrified bonding, metallic bonding, and electroplated bonding [140], based on the required application of the tools. For instance, maximum material removal rate, $Q'_{w,max}$ range from 1000 to 10000 mm^3/mms can be achieved by employing the electroplated bonding type, while vitrified bonding can offer various advantages, such as diamond strength, chip clearance, and improved surface finish [112, 141]. Typically, super-abrasive diamonds are usually deposited to the cutting tool body via electroplated Nickel (Ni) bonding to produce a single layer of diamond on the cutting tool [113, 140]. The diamond grit size is grouped into three ranges: fine, medium, and coarse, which are determined based on the application required. For example, a coarse diamond (400-600 μm) is chosen for roughing operation, while for finishing the operation, a finer (< 100 μm) grit size is applicable. Figure 2-21 shows the typical abrasive diamond tool that has often been employed for abrasive machining.

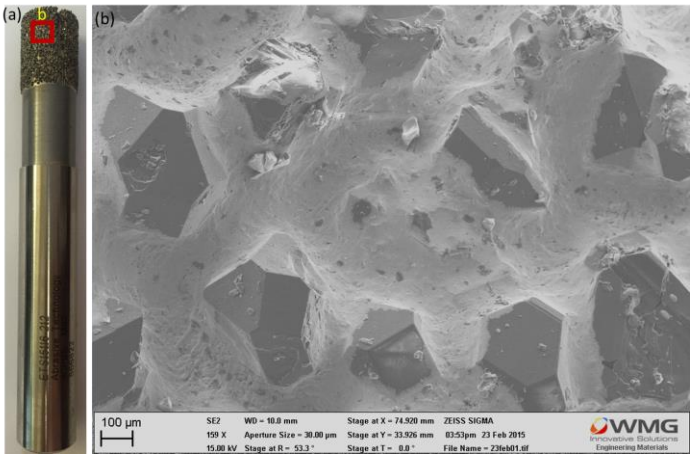

Figure 2-21: (a) Abrasive diamond tool with 420 μm diamond grain size and (b) typical geometry of abrasive diamond tool consist of randomly distributed diamond grain. This tool with 420 μm diamond abrasive grain typically employed for roughing operation.

2.4.2.2 Tool wear mechanism

Tool wear mechanism in abrasive diamond tool differs from CM tool. The types of wear observed on abrasive diamond tool are attrition wear, diamond grit fracture, and bonding fracture [142]. Attrition wear in super-abrasive diamond tool is also known as wear flat. Attrition wear occurs when the sharp peak of the abrasive diamond grit experiences wear and the active cutting edges become blunt. This can occur when machining CFRP during the material removal process; in which the diamond grain can be in contact with the workpieces, where both chemical and physical reactions take place [113, 143]. Furthermore, the flattened diamond grain is evident when the machining length was increased. Increasing wear flat of the super-abrasive diamond leads to a reduction in the active cutting edges, thus, increased cutting forces during machining. Figure 2-22 shows the attrition wear and the grain pull-out that occur on abrasive diamond tool.

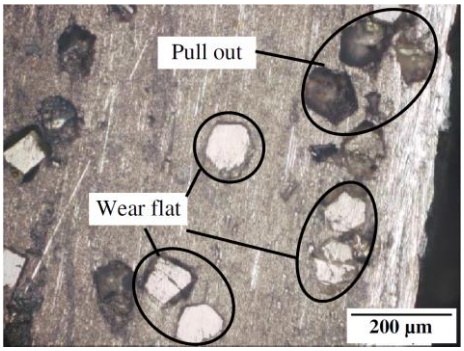

Figure 2-22: Typical wear observed on an abrasive diamond tool such as attrition wear and pull out of diamond grains. The cutting tool has an average of 91µm diamond grit size [142].

Another possible wear mechanism with abrasive diamond tool is fracturing of the diamond grain. In contrast with attrition wear, diamond grain fracture results in increased active cutting edges, where more sharp abrasive peaks are observed on the cutting tool. Moreover, another possible wear type of the abrasive diamond tool is bond fracture that leads to the diamond grain to be pulled out from the cutting tool. As a result, the number of active cutting edges on the cutting tool is reduced. Furthermore, several aspects can

lead to grain pull out, such as flattening of diamond grain, which may result in increased cutting forces during the material removal process. Hence, the high cutting force generated by fracturing of the bonding material that holds the diamond could result in pull out of the diamond grain.

2.4.2.3 Summary of abrasive machining

Abrasive machining of CFRP is mainly focused on two main aspects, which are the effects of cutting tools characteristics (abrasive types and grain size) and the cutting parameters (V, *f*, and a_e) on machinability. Machining of CFRP with abrasive diamond tool is challenging due to the high machining temperature that can lead to the dislodging of broken fibre and matrix resin between the diamond grains [113, 114]. Moreover, thermally degraded resin and broken fibre have been observed on the cutting tool with increment in machining length. Furthermore, it has been reported that the diamond grains were covered by resin and broken fibre [117]. As the machining length is increased, the heat generated by both cutting tool and workpiece can soften the material [113]. As a result, the thermally degraded resin and the broken fibre cover the active cutting edge. This problem also leads to increment in cutting force as the machining length is increased.

When comparing abrasive machining with CM in similar cutting parameters (V= 100 m/min; f= 100, 250, and 468 mm/min), Sorrentino et al. [144] reported that cutting forces, tool life, and surface roughness improved by 25 %, 60 %, and 15 %, respectively. Besides, it has been proposed that the presence of scattered individual diamond grain on the cutting tool improved the stability of the machining. Reduction in cutting force (F_{xy}) can be achieved due to the stability attained in the process and the smaller chip thickness obtained in the abrasive machining, as compared to that in CM. Reduction of cutting forces in abrasive machining due to the energy required to remove

the chip is divided into a larger number of working teeth. However, CM is limited to the number of cutting flutes. Therefore, smooth machining is achieved in abrasive machining due to small chip thickness and less vibration that result in lower cutting forces. Hence, low equivalent chip thickness in abrasive machining reduces cutting forces. Furthermore, it was reported that the abrasive grains generate a micro cutting action when machining, which leads to a reduction in cutting forces [142]. In terms of cutting parameters, the effect of feed rate is more significant, where cutting forces and surface roughness increase as the feed rate is increased [145-147]. Table 2-9 summarises the available literature on abrasive machining of CFRP performed for milling operation.

Table 2-9: Summaries of reported literature on abrasive machining of CFRP.

Reference	Tool Specification	Cutting Parameter	Measured output
Colligan and Ramulu [145]	Abrasive: Diamond *d* : 12.7, 19, 25.4 mm Grain size: 125, 180, 300, 600 μm	V= 399 m/min *f*= 0.38-1.02 m/min CE= Dry	Tool condition Cutting forces(Fx,Fy,Fz) Surface integrity
Sheikh-Ahmad et al. [148]	Abrasive: Diamond *d* :12.7 mm Grain size: 40 μm	V= 2.0, 3.3m/min f= 0.25, 0.76m/min A_e= 3.18, 12.70 mm CE= Dry	Cutting forces(Fx,Fy,Fz) Specific energy Surface integrity Cutting temperature
Soo et al. [113]	Abrasive: Diamond, CBN *d* : 10 mm Grain size:76,151, 252 μm	V= 1200 m/min *f*= 4 m/min A_e=0.5, 3 mm CE= Dry	Tool condition Cutting forces (Fx,Fy,Fz) Surface integrity
Boudelier et al. [146, 147]	Abrasive: Diamond *d* :16, 25 mm Grain size: 427,602, 852, 1182 μm	V= 400 – 1400 m/min *f*= 0.03-0.5 mm/rev A_e= 9.1 mm CE= Dry	Specific energy
Sorrentino et al. [144]	Abrasive: Diamond *d* :20 mm Grain size: 300-355 μm	V= 100 m/min *f*= 100,250,468 mm/min A_e= 10, 20 mm Environment= Dry	Tool condition Cutting forces (Fx,Fy,Fz) Surface integrity

d = tool diameter, V= Cutting speed, f= feed rate, A_e = radial depth of cut, CE=cutting environment

In terms of cutting tool characteristics, larger diamond grain is typically employed to perform roughing operations, while finer-sized diamond grain is selected for finishing operations [113, 145, 146]. For instance, Colligan and Ramulu [145] compared the varied diamond grain sizes (125, 180, 300, and 600 μm) on the surface roughness obtained on CFRP. Higher surface roughness (Ra=30-35 μm) was obtained when machining with 600 μm grits, while lower surface roughness (Ra=5-6 μm) was evident when machined with finer diamond grain size (125 μm). A similar observation was reported by Soo et al. [113], which indicated that 76 μm grain size abrasive must be employed, instead of 156 μm, to obtain a near free damage machined surface. Thus, the diamond grain size significantly affects the surface roughness in abrasive machining. Hence, as for the roughing process, the coarse diamond grit size is recommended, while for finishing operation where the surface roughness is the main criteria, finer-sized diamond grain is required.

Although smaller diamond grain size is recommended to achieve lower surface roughness, inadequate space for the chip to evacuate may be a problem. A finer grain size indicates that the density of the diamond grit is higher, when compared to coarse grain size [146, 147]. Therefore, the space between individual diamonds in the finer diamond grain is smaller compared to that with coarse diamond. For instance, coarse diamond (600 μm) has the space for chip clearance, which is larger than the finer diamond (125 μm). Although improved surface roughness can be obtained by employing finer diamond grain, the abrasive cutter with finer diamond grain is more susceptible to load with broken fibre and thermally degraded resin. The loaded materials at the cutting tool in abrasive machining reflect a similar observation with the grinding operation. When the abrasive cutter is loaded with materials, the active cutting edges are reduced. Hence, when the cutter is loaded with materials, the friction between cutting tool and workpiece materials is higher, thus leading to high cutting forces [113].

Therefore, several recommendations should be taken into consideration when machining CFRP with an abrasive tool. The selection of diamond grain depends on the surface roughness requirement. Although a finer grade of diamond is recommended to achieve lower surface roughness, the chip flow during machining must be taken into consideration.

2.5 Principle of ultrasonic assisted milling (UAM)

2.5.1 Introduction

Ultrasonic assisted machining is a hybrid technique which combines the CM mode with the vibration of cutting tool or workpiece during machining. The development of ultrasonic assisted machining, including milling, drilling, grinding, and turning is still ongoing, where some researchers have proposed different methods for ultrasonic assisted machining. However, due to the limited amount of literature reporting on ultrasonic assisted milling (UAM) of composites, especially CFRP, some of the studies discussed here include the UAM of metallic materials. The basic principles of UAM are when the high frequency (20-50 kHz) and the low amplitude vibrations (1-40 μm) are superimposed on a cutting tool or a workpiece [13, 149-151]. The ultrasonic amplitude and vibration can be applied to the workpiece or the cutting tool during the machining operation, where it can be in x, y or z-direction during UAM. It must be noted that in this research, the ultrasonic was applied on the cutting tool and vibrate in z-direction. However, UAM must not be confused with the low-frequency vibration milling (LFVM) where in LFVM, the frequency employed is usually below 200 Hz and the amplitude can reach up to 100 μm.

During UAM, the ultrasonic frequency is transferred from the spindle to the ultrasonic actuator via induction. As illustrated in Figure 2-23, during UAM**,** the transmitter segment

at the tool spindle transmits electrical signal via induction to the receiver coil of the tool holder (ultrasonic actuator) that contains piezoelectric crystals [152]. The voltage compressed the piezoelectric crystals and produced mechanical vibration. The mechanical vibration is then transferred to the cutting tool to vibrate it in an axial direction.

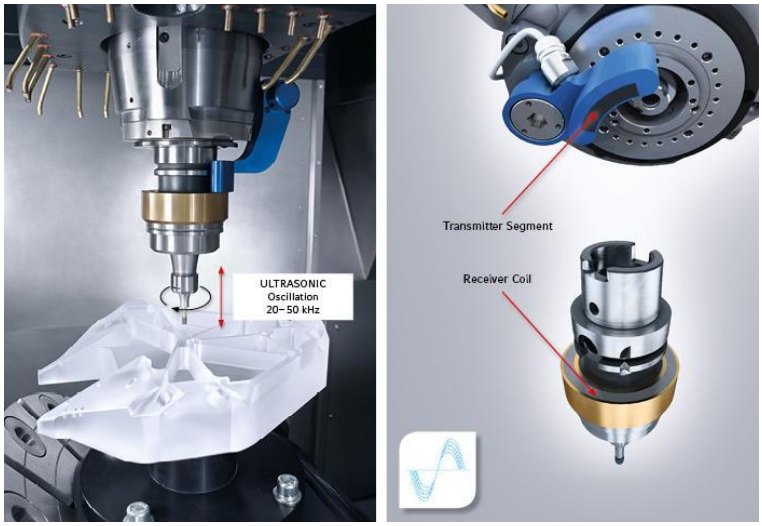

Figure 2-23: Ultrasonic assisted milling (Illustration adapted from [152])

It is claimed that the effectiveness of UAM is determined by three critical factors, which are: cutting tool or workpiece vibration frequency (*f*), vibration amplitude (*a*), and cutting speed (V). As for the ultrasonic assisted machining, the cutting speed (V) is recommended to be less than the critical speed, Vcr, to ensure the occurrence of intermittent cutting in UAM [13, 149, 150]. It has also been claimed that the effectiveness of intermittent separation between the tool and the workpiece during UAM is determined by the value of amplitude vibration and frequency, where higher value of amplitude results in a larger tool-workpiece separation during the machining process [12]. The intermittent cutting during UAM occurs when the tool-workpiece is separated at a certain time in a cutting cycle. Besides, intermittent cutting process that refers to tool-workpiece separation offers many advantages over CM in terms of machining quality and efficiency, including reduced tool force and surface roughness, improved form of accuracy, as well as enhanced tool life and material removal [13, 149, 151, 153-156]. It is also claimed that

UAM can reduce the heat accumulated between the cutting tool and the workpiece, aside from aiding in chip evacuation and removal of excess cutting fluid [149]. However, limited study has investigated the ultrasonic vibration of the cutting tool perpendicular towards feed directions, which could result in intermittent separation between the cutting tool and the workpiece.

Only limited studies have examined UAM of CFRP due to the complexity of composite structure with non-homogenous and anisotropic properties. UAM can offer several advantages for CFRP machining, especially in reducing cutting temperature that can lead to thermal degradation in composite materials.

2.5.2 Tool wear/tool life

Rapid tool wear is a major problem in machining that can lead to higher cutting forces and poor surface roughness. Thus, UAM implementation can improve and extend tool life. For example, built-up edge and adhesion of workpiece materials that are often observed in metal cutting could be reduced with UAM [154, 156]. Intermittent cutting in UAM suggests that less contact between cutting tool and workpiece could reduce wear mechanism [157]. However, Nath et al. [156] observed that the cutting tool experienced fracture and catastrophic failure when high cutting speed (15 m/s) was applied during UAM of Inconel 718. It was observed that at higher cutting speed, the cutting tool engaged with the workpiece relatively long duration and the cutting tool was attacked by tangential and radial impact during cutting. In contrast, Janghorbanian et al. [150] found that applying a low cutting speed (16-63 m/min) in UAM resulted in higher tool wear when machining stainless steel. They also asserted that at low cutting speed, the impact contact between the cutting tool and the workpieces was higher, when compared to higher cutting speed (99 m/min). The cutting tool and the workpiece have less impact

contact at higher cutting speed, where the cutting temperature is reduced and less plastic deformation occurs in UAM, as compared to CM [150]. However, Maurotto et al. [8] claimed that the tool life of carbide tool when milling stainless steel conventionally produced better tool condition, when compared with UAM. UAM with a frequency of 40 kHz produced four-times tool damages, as compared to CM, while machining with 20 kHz and 60 kHz frequencies resulted in similar tool damages as that in CM. However, varied techniques in UAM may affect the progression of tool wear and tool life [150] . For instance, Maurotto et al. [8] employed the ultrasonic vibration on cutting tool that is perpendicular towards feed direction, while Janghorbanian et al. [150] employed the ultrasonic vibration of workpiece parallel to the feed direction.

Additionally, authors claimed that the tool-workpieces ultrasonic vibration in UAM could aid in reducing cutting temperature, thus improving the life of cutting tool. The out-of-contact between cutting tool and workpiece when dry machining generates an air medium that aids in reducing the heat accumulated at the cutting tool, apart from allowing the cutting fluid to reach the maximum heat zone when machining with cutting fluid [149, 150, 158]. Nonetheless, an inconsistency emerges when Zarchi et al. [154] claimed that the vibration during UAM generated more energy that increased tool-workpiece temperature. This discrepancy is attributed to the varied techniques (UAM parameters and tool-workpiece vibration) used by researchers, which increase/decrease of cutting temperature.

2.5.3 Cutting forces

In UAM, the ultrasonic vibration affects the formation of chip, where the chips produced are smaller than the chips produced by CM [149]. The ultrasonic vibration influences the gap between the cutting tool and the workpiece material, thus leading to better chip

breaking conditions [149, 154]. Higher amplitude was found to produce smaller chips due to the larger tool-workpiece separation during material removal process in UAM, hence aiding in the chip removal at the cutting tool [9, 149, 154]. Consequently, the machining force measured in UAM is less than CM when the same machining condition was applied. In addition, improvement in the cutting forces during UAM shows promising results with different cutting tool materials and geometries, type of tool-workpiece vibration, cutting parameter, and various types of workpiece materials [149, 150, 154].

Moreover, it has been claimed that the intermittent cutting in UAM, where there is a separation between the cutting tool, indicates that no cutting occurs at a certain part in one cutting cycle, thus reducing both cutting force and shifts in cutting force pattern [154]. However, it was depends on the direction of the vibration and the method of vibration either the ultrasonic amplitude is applied on the cutting tool or the workpiece materials. It was also observed that the cutting force pattern in UAM is similar to the pulse-like profile, which indicates that the tool-workpiece was not in contact at a certain time [149]. The tool-workpiece separation aided the periodical separation between the cutting tool and the workpiece, hence, the micro-segmented cutting during the UAM reduced the cutting forces [149]. Therefore, smaller chips are produced, when compared to those generated in CM. The reduction of cutting forces was up to 19 % when 20 μm amplitude was applied, while only 6 % of reduction in cutting force when 8 μm amplitude was applied with constant parameters [154]. Thus, this result demonstrates that the tool-workpiece separation during UAM leads to reduction in cutting forces, apart from modifying the chip formation mechanism.

2.5.4 Surface roughness and integrity

Although tool life and cutting forces in UAM have displayed significant advantages over CM, improvement in roughness of the machined surface is still unclear. Razfar et al. [13] observed that surface roughness improved by 12.9% when UAM stainless steel with a cutting speed at 500 RPM and a feed rate at 0.005 mm/tooth [13]. The increase in feed rate from 0.025 to 0.1 mm/tooth resulted in increment in surface roughness for both CM and UAM. This can be attributed to the increase of uncut chip thickness, which results in higher roughness of the machined surface [9, 159]. Therefore, the effect of machining parameters in UAM, such as feed rate and speed, are similar to those in CM. Besides, it has been reported that in UAM, the friction coefficient between workpiece and cutting tool changed from semi-static to dynamic friction [13]. Hence, these changes improved the quality of the machined surface as a result of lower forces acting on the workpiece/the cutting tool. In addition, the intermittent disengagement between the tool-workpiece may create a dynamic lubrication, where cooling of cutting tool and workpiece takes place during the separation [13]. Takeyama and Iijima [7] concluded that lower cutting parameters are required in UAM to achieve lower force and enhanced surface roughness since the tool and the workpieces are separated in large part of the vibration. In contrast, Shen et al. [9] found that the ultrasonic vibration resulted in higher roughness of the aluminium surface due to increment in tool marking on the machined surface. However, enhancement of the slot width accuracy was observed.

Therefore, UAM potentially offers several advantages over CM, such as longer tool life, reduced cutting forces, and improved surface roughness. As discussed in Section 2.1.2, the processing temperature of CFRP must be below than the Tg of matrix resin. Although less work has been carried out in the light of UAM for CFRP, the intermittent separation between the cutting tool and the workpiece offered by UAM is beneficial to the

machinability of CFRP in terms of improved tool life and surface roughness, as well as reduction in lower cutting force and cutting temperature.

2.6 Measurement

2.6.1 Surface roughness

Milling of CFRP often occurs at the end of the manufacturing processes for finishing and final accuracy purposes. Thus, the quality of the machined part is essential to avoid part rejection or further remedial machining processes. Surface roughness and surface integrity constitute a significant concern for CFRP milling as the surface finish is critical in determining both machining accuracy and part performance [17]. Figure 2-24 illustrates a schematic representation of the machined surface. Surface roughness can be assessed by several roughness parameters, such as Ra (arithmetic mean value), Rp (maximum peak to mean height), Rt (maximum peak to valley height), Rv (mean to valley height), and Rz (ten-point average height). Surface roughness is often measured by using Ra value.

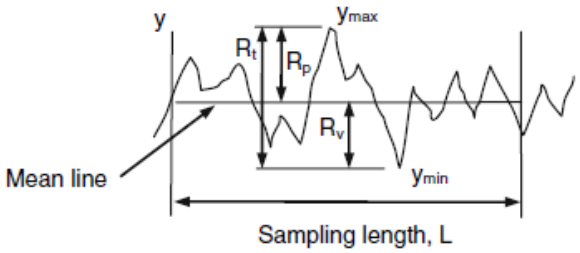

Figure 2-24: Schematic representation of the machined surface (Adapted from [3]).

Commonly, the aspect of surface roughness can be measured by using a diamond stylus. Alternatively, non-contact (optical) surface roughness measuring-devices can also be applied. A non-contact surface roughness measuring device, in fact, offers several advantages over the diamond stylus device, for example, the non-contact may not damage the soft-machined surface and it does not alter the machined surface condition. Besides,

a 3D image, such as a hole, fibre pull-out, and delamination, on the machined surface can be observed if non-contact measuring device is used.

2.6.2 Differential Scanning Calorimetry (DSC)

Differential Scanning Calorimetry (DSC) is a thermal analysis technique that provides information regarding material changes; such as the Tg, phase changes, and curing temperature. DSC is an established technique for monitoring changes in Tg of polymeric materials [160, 161]. In DSC, two pans, which are the reference's pan and sample's pan are heated or cooled at the same time. The temperature difference between both pans are maintained at zero difference as in Figure 2-25. The typical heating rate employed in DSC analysis for the polymer is 10 °C/min. A higher heating rate is not recommended as there is the potential of losing information due to the fast scanning [160, 161].

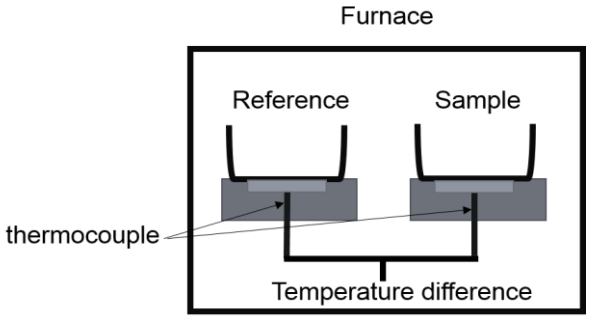

Figure 2-25: Schematic diagram of heat flux type DSC.

Nonetheless, some factors can affect the effectiveness of the measurement by using the DSC, such as heating rate, sample size, thermal contact between the pan and the sample, type of gas used (N_2, O_2, H_2), and sample purity. During measurement, the temperature difference between the sample and reference pans determines the heat flow of the materials; either exothermic or endothermic. Endothermic reactions occur when the sample absorbs heat. For instance, in order to transform a solid sample to one that is liquid, more heat flow (increment of temperature) is required to melt the sample. In

contrast to endothermic reaction, the exothermic reaction occurs when heat is released from the sample. The change of heat flow signifies that the material changes from the rigid and solid state to a glassy and rubbery state, which determines the Tg of the materials. The increase in temperature ranges consequently enhances the mobility of polymer chains [160].

Furthermore, the DSC has been extensively employed in determining material changes, especially in polymeric materials [14, 15, 43, 161]. For instance, the effect of curing on the Tg via DSC analysis has been extensively employed in many studies [14, 15, 33, 43]. DSC also has been applied to determine the effects of chemical ageing, including oxidation [35, 45], and thermal ageing [16, 44] of polymeric materials. Although DSC has been used extensively for characterisation of polymeric materials, there are limited studies involving the effect of machining on the machined surface of CFRP. Recently, some works have identified the phase changes for the machined surface of Nickel-Titanium (Ni-Ti) alloy. For instance, Kaynak et al. [162, 163] performed a DSC analysis on the machined surface of Ni-Ti alloy to investigate the phase transformation on the surface and the subsurface of the machined sample, which was induced by the cutting process. Figure 2-26 shows the DSC analysis of the machined sample from both cryogenic and dry machining conditions of Ni-Ti. The changes in Tg of machined Ni-Ti surface indicated that the machining operation did modify the chemical properties of the material. Therefore, this concludes that the DSC technique is not only limited to study polymer characterisation alone, but also to establish the effect of machining on the machined surface.

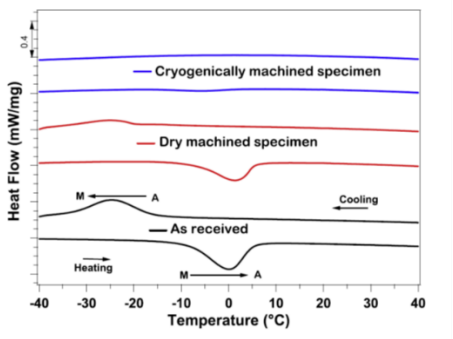

Figure 2-26: DSC analysis to investigate of effect machining process (dry and cryogenic) on NiTi structure [162].

2.6.3 Fourier Transform Infrared spectroscopy (FTIR)

Fourier Transform Infrared (FTIR) spectroscopy can be employed to study chemical property changes in a composite material since FTIR can detect small changes in the molecular structures of the polymeric composite [36, 164, 165]. FTIR is a technique where the infrared absorption peak of the molecular structure of solid, liquid or gas can be detected and it can also be used to overcome the inaccurate conclusion of thermal degradation [36]. FTIR can be utilised to study early stages of a degradation process when there are considerable changes taking place in the molecular structure material, even though the weight loss may be negligible [164, 166]. Figure 2-27 indicates the general working principle of FTIR spectroscopy. The general principles of FTIR include the infrared (IR) sources, detector, a beam splitter, and moving and fixed mirrors. During the scanning, the IR light will go through the moving and fixed mirrors. The beam splitter divides the light into two directions, which is 50 % to the fixed mirror and another 50 % to the moving mirror. Both lights from the fixed and moving mirror will reflect the beam splitter. The interference between the two light sources will give the details of the material properties wavelength.

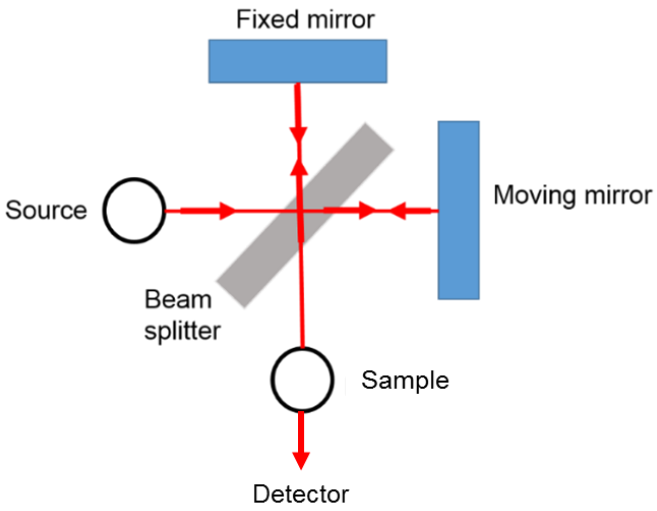

Figure 2-27: General working principle of FTIR.

Several studies have been carried out in identifying material properties changes of a polymer composite using the FTIR analysis [38, 39, 167]. The thumbprint of the polymer matrix composite can be the reference properties of the material, and the FTIR wavelength can be compared with any changes of the materials properties. For instance, the reduction of any chemical bonding detected by FTIR can give valuable information, regarding degradation, oxidation and more.

Therefore, combinations of both DSC and FTIR can compliment each other in explaining the effect of process such as in the molecular property changes of CFRP. Different thermal properties of carbon fibre and BMI resin are crucial in machining them since high processing temperature can degrade the mechanical and chemical properties of the composite. For example, the glass transition of BMI is 250 °C, while the decomposition temperature of carbon fibre is ≈3000 °C [167]. Further processing temperature on the CFRP has a detrimental effect on the composite's mechanical and chemical properties of matrix resin. CFRP experiences thermal damages or deterioration at the machined surface [22, 56, 168, 169] and there is limited research that explored the chemical properties changes and its effect on the glass transition temperature of CFRP.

Although several works have been carried out on the effect of machining on the mechanical properties [19, 20, 22, 169] of CFRP after machining, the knowledge on the effect on the chemical properties after machining is not clear yet. Thus, a combination of both DSC and FTIR can give valuable information on the effect of machining on the machined surface of CFRP in detecting the thermal and property changes of the polymeric materials [47, 166, 170, 171]. These two common techniques can be employed to identify the damage mechanism induced by the machining operation that can lead to the deterioration of the mechanical properties of CFRP.

2.7 Summary of literature review

Based on the extensive literature survey on CFRP and machining point of view, the overall literature can be summarized as depicted in the following:

- Although most parts of the aerospace application are manufactured near the net shape, machining operations, such as the finishing process to meet the final requirement, are still needed. As such, many researchers have suggested that machining of CFRP must be carried out in a dry conditions since absorption of moisture during wet machining can affect the mechanical properties of CFRP. Many researchers have reported that increasing tool wear could lead to high machining temperature while CFRP machining [5, 61, 82, 109]. They also asserted that a high temperature during machining CFRP parts leads to thermal damage and degradation of CFRP properties.
- Significant researches have been carried out to investigate the effect of machining operation on the mechanical properties of CFRP [22, 66]. However, not many have considered the chemical changes of the CFRP material properties after the machining operation. There are also limited studies on the thermal damage of CFRP machined parts after machining. Hence, there is no substantial reason or quantification proof of the claim that thermal damages and degradation of CFRP occur after machining.

- Several problems, such as rapid tool wear, due to abrasiveness of the fibre are the main concern in machining CFRP. Rapid tool wear leads to increased machining force, thus resulting in increased surface roughness. The increase in cutting temperature due to poor tool condition and high cutting force may lead to thermal damage upon the machined surface. Thus, hybrid machining, such as ultrasonic assisted milling (UAM), is an extended technique that can be applied to improve tool life, machining force, and surface quality [6, 13, 172]. The presence of cryogenic coolant in machining CFRP enhances the outcome of machining since dry environment is recommended for CFRP machining. Thus, it has been suggested that the combination of UAM with cryogenic coolant could improve the machinability of CFRP.
- DSC and FTIR are established techniques for polymer characterisation; therefore, it would be beneficial to employ both techniques to investigate the effect of matrix resin machining. The changes in chemical bond of the CFRP composite can be an indicator of the CFRP quality after the machining operations are performed.

Chapter 3 Experimental work

3.1 Workpiece material

The workpiece material employed in all experimental work was a carbon fibre reinforced polymer (CFRP) with bismaleimide 5250-4 (BMI) resin. Cytec Industries developed the Cycom 5250-4 prepreg system, and BAE Systems supplied the workpiece materials. The CFRP prepreg is the main material utilised by BAE Systems, especially in a defence aircraft. Table 3-1 shows selected mechanical and physical properties of Cycom 5250-4 prepreg system. The glass transition temperature (Tg) indicates that the maximum processing temperature for this workpiece material is 300 °C. Two different thicknesses of CFRP (5 and 10 mm) were employed in this thesis due to the availability of the supplied materials. The 5 mm CFRP was produced with the same layup sequence to ensure that the effect of the fibre orientation towards the machining outcome is negligible. Tables 3-2 and 3-3 show the prepreg sequence of the 10 mm and 5 mm thick CFRP that comprises of 75 and 32 layers of the quasi-isotropic orientation of carbon fibre, respectively. For simplicity, henceforth, CFRP with Bismaleimide 5250-4 resin will be referred as CFRP BMI 5250-4, throughout the experimental work.

Table 3-1: Selected mechanical and physical properties of CFRP BMI 5250-4 properties [173].

Properties	Value
Density	1.25 g/cc
Dry glass transition temperature, T_g	300 °C
Wet glass transition temperature, T_g	200 °C
Tensile strength	103 MPa
Flexure strength	163 MPa
Fibre volume	60 %

Table 3-2: Carbon fibre lay-up sequence for 10 mm thick CFRP BMI 5250-4.

Lay up	Fibre orientation	Lay up	Fibre orientation	Lay up	Fibre orientation
1.	45°	26.	0°	51.	90°
2.	45°	27.	90°	52.	45°
3.	45°	28.	45°	53.	45°
4.	90°	29.	45°	54.	90°
5.	0°	30.	90°	55.	45°
6.	45°	31.	45°	56.	45°
7.	45°	32.	45°	57.	0°
8.	90°	33.	0°	58.	90°
9.	45°	34.	90°	59.	45°
10.	45°	35.	45°	60.	45°
11.	90°	36.	45°	61.	90°
12.	0°	37.	90°	62.	45°
13.	45°	38.	90°	63.	45°
14.	45°	39.	45°	64.	0°
15.	90°	40.	45°	65.	90°
16.	45°	41.	90°	66.	45°
17.	45°	42.	0°	67.	45°
18.	90°	43.	90°	68.	90°
19.	0°	44.	45°	69.	45°
20.	45°	45.	45°	70.	45°
21.	45°	46.	90°	71.	0°
22.	90°	47.	45°	72.	90°
23.	45°	48.	45°	73.	45°
24.	45°	49.	90°	74.	45°
25.	90°	50.	0°	75.	45°

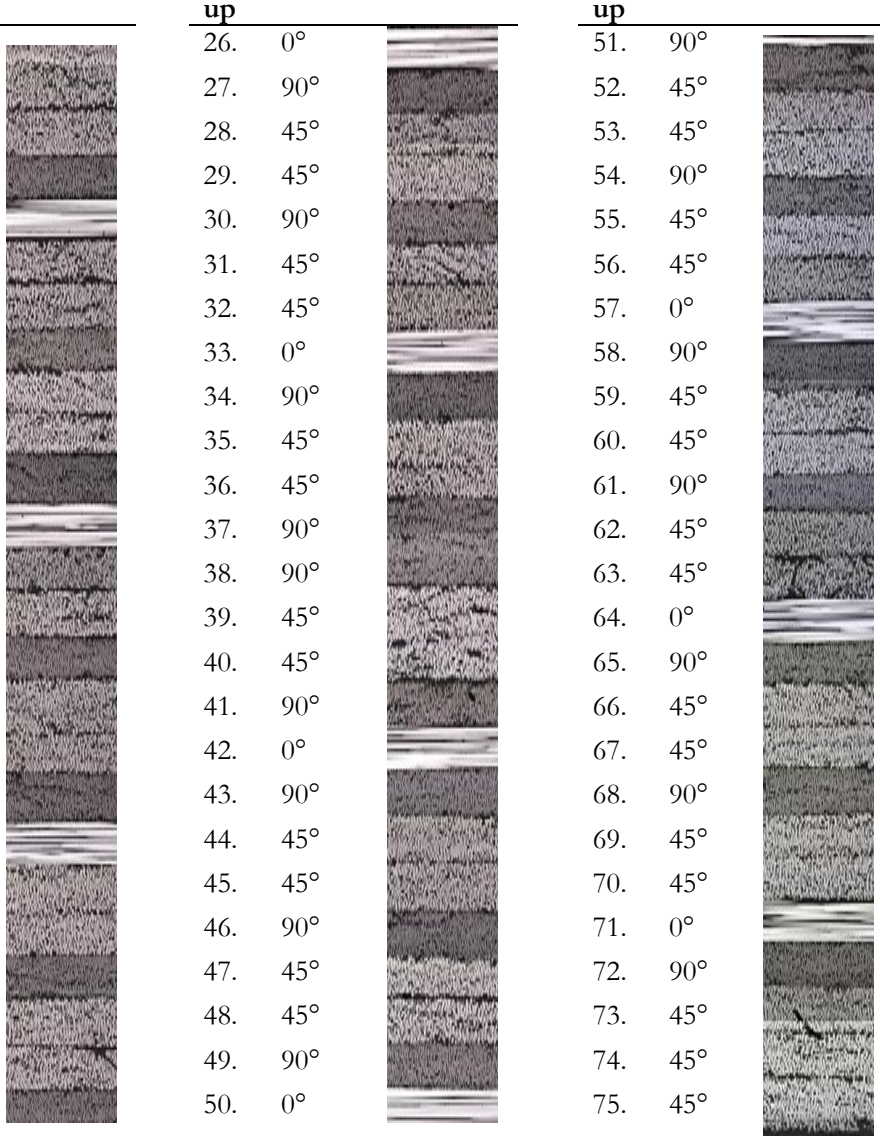

Table 3-3: Carbon fibre lay-up sequence for 5 mm thick CFRP BMI 5250-4.

Lay up	Fibre orientation	
1.	45 °	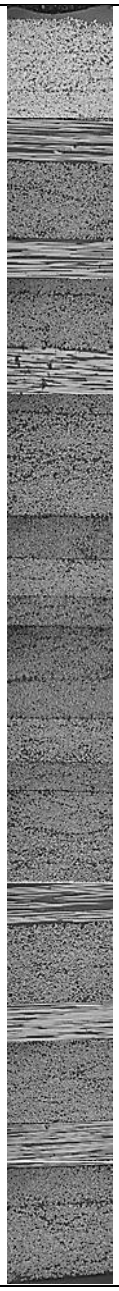
2.	45 °	
3.	45 °	
4.	0°	
5.	45°	
6.	45°	
7.	0°	
8.	45°	
9.	45°	
10.	0°	
11.	45°	
12.	45°	
13.	45°	
14.	90°	
15.	45°	
16.	90°	
17.	90°	
18.	45°	
19.	90°	
20.	45°	
21.	45°	
22.	45°	
23.	0°	
24.	45°	
25.	45°	
26.	0°	
27.	45°	
28.	45°	
29.	0°	
30.	45°	
31.	45°	
32.	45°	

3.2 Cutting Tools

Three different cutting tools, which are uncoated tungsten carbide end mill, polycrystalline diamond (PCD) end mill, and abrasive diamond tool were employed in this research. For Study 1(a), tungsten carbide end mill was employed as a main cutting tool to investigate the effect of cutting environment and machining process on the machinability (tool wear, cutting forces and surface roughness). Whereas, to investigate the effect of the cutting tool type on ultrasonic assisted milling (UAM), the straight flutes of PCD end mill tool (Study 2) and abrasive diamond tool (Study 3) were employed. Section 3.2.1 to 3.2.3 describe the specification of the cutting tools employed in this thesis.

3.2.1 Tungsten carbide end mill

Figure 3-1 shows the 10 mm diameter uncoated tungsten carbide end mill, tool code 40557 from SGS tooling was employed in Study 1(a) milling test. Figures 3-2 (a) and (b) show the top and side view of the end mill. The three flutes end mill had a cutting length of 22 mm, shank diameter of 10 mm, and helix angle of 30°. This end mill is manufactured specifically to machine the composite materials. Table 3-4 indicates the specifications of the uncoated tungsten carbide end mill.

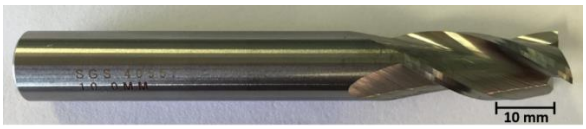

Figure 3-1: 10 mm diameter uncoated tungsten carbide end mill.

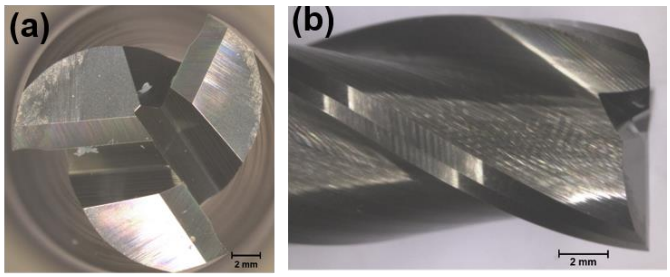

Figure 3-2: (a) Top and (b) Side view of the 10 mm uncoated tungsten carbide end mill.

Table 3-4: Specification of 40557 tungsten carbide end mill by SGS tool [128].

Parameter	Value
End Mill material	Tungsten Carbide
Carbide (WC) and Cobalt (Co) content	90 and 10 %
Tungsten carbide grain size	0.8 μm
Helix, relief and clearance angle	30°, 10° and 17°
Overall length	75 mm

3.2.2 Polycrystalline diamond (PCD) end mill

Study 2 was conducted by employing the polycrystalline diamond (PCD) end mill as a cutting tool for both conventional and ultrasonic assisted milling. Figure 3-3 shows the Exactaform 10 mm diameter of PCD end mill, tool code ETS15080-212 manufactured by Exactaform UK and was supplied by BAE Systems. This end mill has been specifically empoyed in BAE Systems for finishing operation of CFRP. The end mill has three straight flutes, a cutting length of 24 mm and an overall length of 76 mm. Figures 3-4 (a) and (b) show the top and side view of the PCD end mill employed for finishing operation of CFRP. Table 3-5 details the specification of the end mill.

Figure 3-3: 10 mm diameter of PCD end mill.

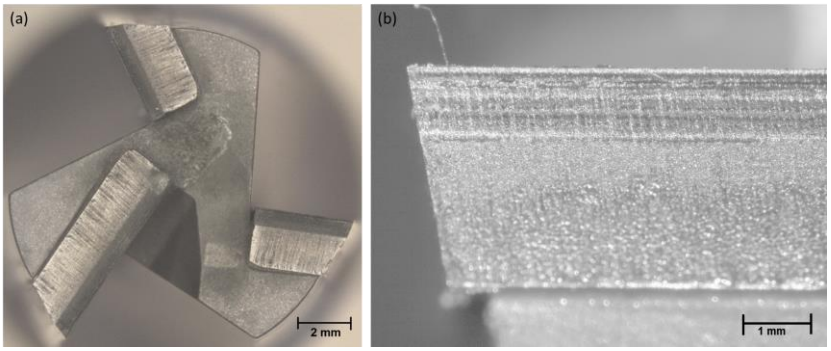

Figure 3-4: (a) Top and (b) side view of the 10 mm PCD end mill.

Table 3-5: Specifications of ETS15080-212 PCD end mill manufactured by Exactaform UK.

Parameter	Value
Insert material	Polycrystalline Diamond
End mill body material	Carbide
Diamond grade	Sub-micron
Helix , rake, primary clearance and secondary clearance angle	0°, 0°, 10°, 25°

3.2.3 Abrasive diamond milling tool

Figure 3-5 shows the Exactaform 10 mm abrasive diamond tool, tool code ETS15116-212 that was employed for both conventional (CM) and ultrasonic assisted machining (UAM) in Study 4. BAE System supplied the cutting tools. BAE System carried out the roughing of CFRP by using the abrasive diamond tool. Diamond grit with an average size of 420 μm is nickel electroplated on the body of the cutting tool. Figure 3-6 shows the top and side view of the cutting tool. The cutting tool specification was summarised in Table 3-6.

Figure 3-5: 10 mm diameter of the super abrasive diamond tool with 420 μm grit size of the diamond.

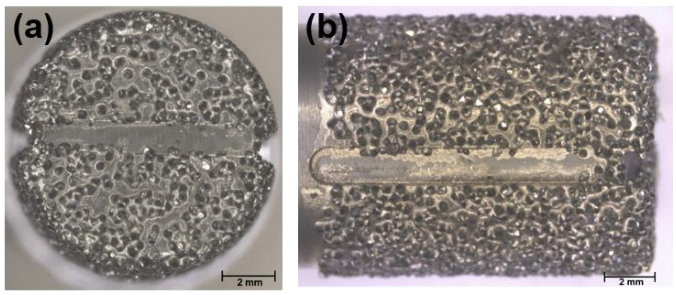

Figure 3-6: Top and side view of the 10 mm diameter of the abrasive diamond tool.

Table 3-6: Specifications of the ETS15116-212 abrasive diamond tool.

Parameter	Value
End Mill material	Carbide
Coating	Diamond
Diameter, D	10 mm
Diamond grit size	420 μm

3.3 Experimental equipment and methodology

3.3.1 Machine tool

The experimental work was carried out using an ultrasonic 65 DMU manufactured by DMG as shown in Figure 3-7 (a). The 5-axis machine tool has a maximum spindle speed of 18000 rpm and feed rate of 40000 mm/min. The maximum work area that the machine tool can accommodate is 650 x 650 x 560 mm in x, y, and z-direction, respectively. The ultrasonic assisted working mechanism is explained in detail in Section 2.5. Figure 3-7 (b) shows the ultrasonic actuator that was employed in this study. The value of the frequency is displayed on the machine controller whilst the value of the actual peak-to-peak amplitude have to be measured. Therefore, Section 3.3.4.1 explained the method to measure the ultrasonic amplitude prior machining. The direction of the ultrasonic amplitude was in the z-direction, which is perpendicular to the feed direction during milling.

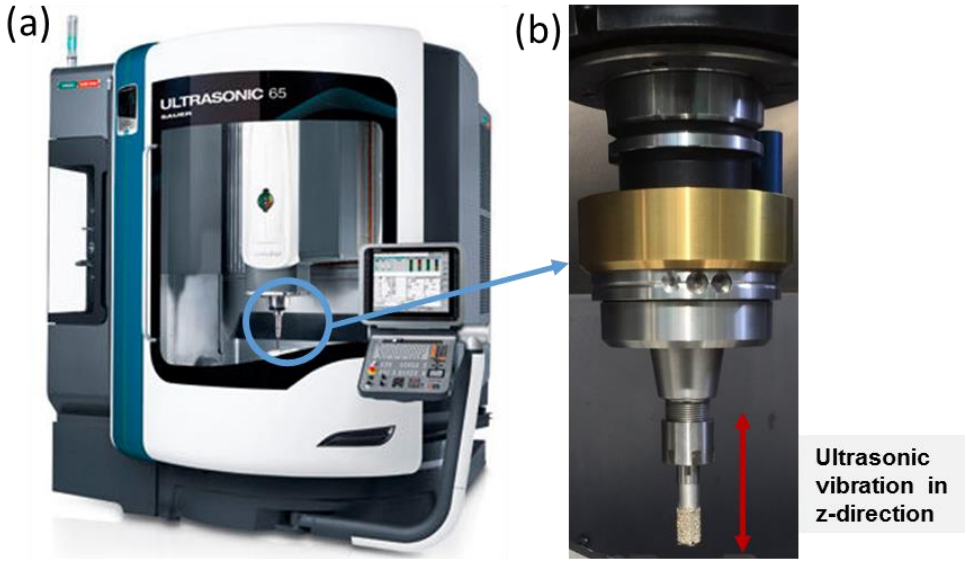

Figure 3-7: (a) Ultrasonic 65 DMU (image not in scale) and (b) 10 mm cutting tool attached to the ultrasonic actuator.

3.3.2 CO_2 cryogenic application

Some of the works in Study 1(a) were carried out employing CO_2 cryogenic cutting medium. The CO_2 was supplied from outside the machine tool using a Cool Clean Technologies ChilAire™ Lite CO_2 cooling system. The main components of the CO_2 ChilAire™ Lite system are; CO_2 liquid supply, compressed clean air supply, coaxial coolant spray hose, and the applicator nozzle. Figure 3-8 shows the schematic of the CO_2 cryogenic cooling system. During machining, the applicator nozzle sprayed the CO_2 ice crystals to cool the cutting tool. CO_2 liquid and compressed air are fed into the ChilAire™ Lite main system. The CO_2 liquid was supplied via a standard CO_2 liquid cylinder, and the clean air dry was supplied via available compressed air system in machine shop WMG. The CO_2 liquid and compressed air that were combined in the main ChilAire™ Lite system and transferred to the applicator nozzle. The pressure of the CO_2 ice crystal can be controlled by increasing the pressure of the CO_2 liquid and the compressed clean air.

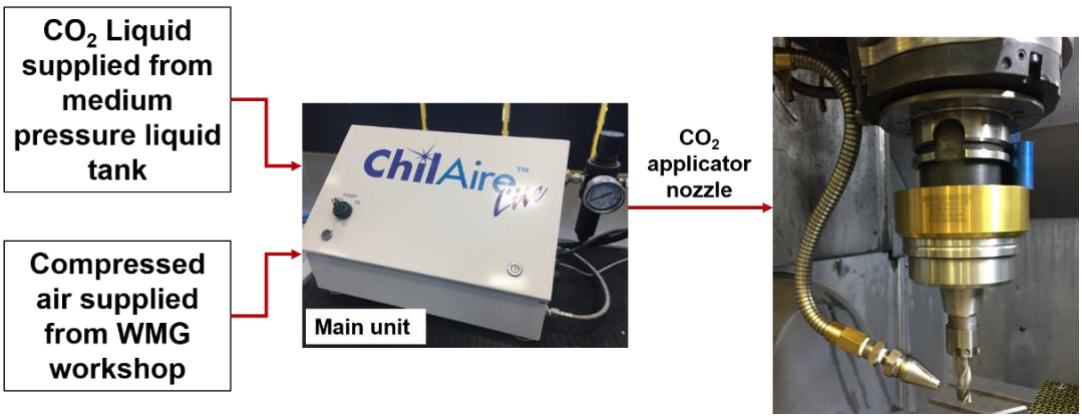

Figure 3-8: Schematic of working mechanism of CO_2 cryogenic cooling.

3.3.3 Cutting fluid application

For conventional cutting fluid media, the cutting fluid was supplied through the nozzles inside the machine tool. The cutting fluid employed throughout this study was Blasocut BC 25 MD cutting fluid and was manufactured by Blaser Swisslube. The cutting fluid contains 62 % of mineral oil and 3 % of water before diluting with water prior to machining. Mini jet mix emulsion mixer was used to mix the cutting fluid with the water and refractometer was employed to measure the concentration of the mixture that is in between 6 to 9 % (i.e.: 6 % of cutting fluid and 94 % of water).

3.3.4 Analysis equipment and procedure

3.3.4.1 Ultrasonic amplitude

Equipment

The Ultrasonic 65 machine tool provides the value of frequency and the percentage of the ultrasonic amplitude before the machining was performed. Therefore, to determine the actual peak-to-peak of ultrasonic amplitude a Keyence LK-H008 laser measurement sensor was employed. This device can produce 0.005 μm repeatability and 0.05 % accuracy of measurement. The laser device was connected to a LK-G5001 controller,

power supply, and a personal computer that was installed with a LK-Navigator 2 software as shown in Figure 3-9.

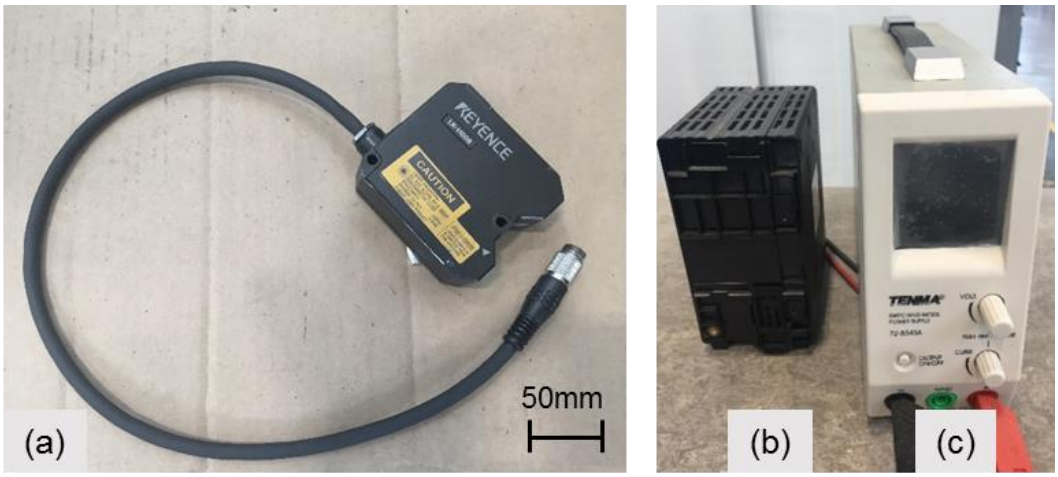

Figure 3-9: (a) Keyence LK-H008 and (b) Keyence LK G5001 controller and (c) power supply for the ultrasonic amplitude measurement.

Method

The ultrasonic amplitude was measured prior to UAM testing. The Keyence laser was mounted on the machine bed using a fixture, and the cutting tool was located in the middle of the laser sensor. The LK-Navigator 2 software received the signal detected by the laser, and the amplitude was measured three times to ensure the repeatability. To measure the ultrasonic amplitude using this device, it is necessary to find a flat surface on the cutting tool to make sure that the laser reflected the device during measurement.

Therefore, to ease the amplitude measurement, a 10 mm x 10 mm of an aluminium strip was glued on the top side of the tungsten carbide end mill (Study 1(a)), Figure 3-10. Work carried out by David Ray (WMG intern) indicates that the effectiveness of this method reduce over time. This can be explained by the glue starting to melt because the heat produced by the ultrasonic vibration on the cutting tool (Appendix A). Therefore, for PCD (Study 2) and abrasive diamond tool (Study 3), the amplitude measurement was

carried out by pointing the laser into a flat surface on the cutting tool. Figure 3-11 (a) shows the ultrasonic amplitude measurement before and after the ultrasonic amplitude is turned on. The 'ultrasonic off' in Figure 3-11 (a) indicates the natural frequency of the machine tool. Figure 3-11 (b) shows the peak-to-peak amplitude of the cutting tool vibration with the average value of 5 μm when the ultrasonic amplitude is 60 %, and 38000 Hz frequency was applied.

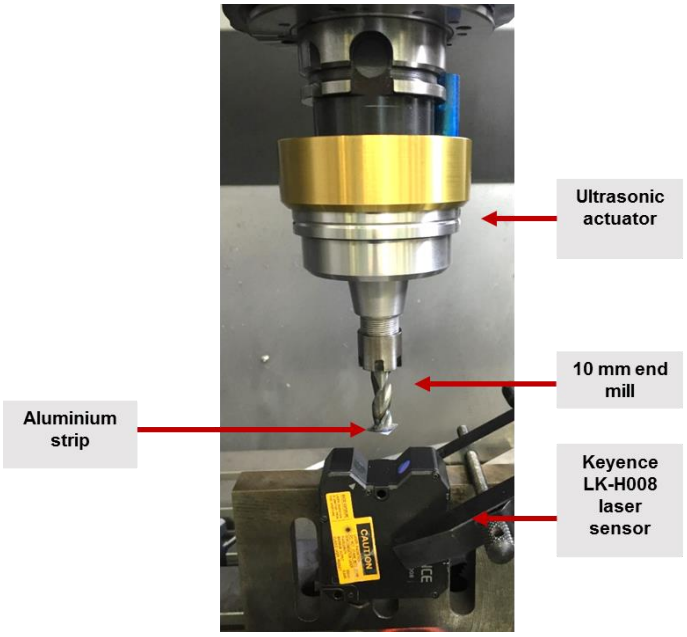

Figure 3-10: Method for ultrasonic amplitude measurement using the Keyence model LK-H008.

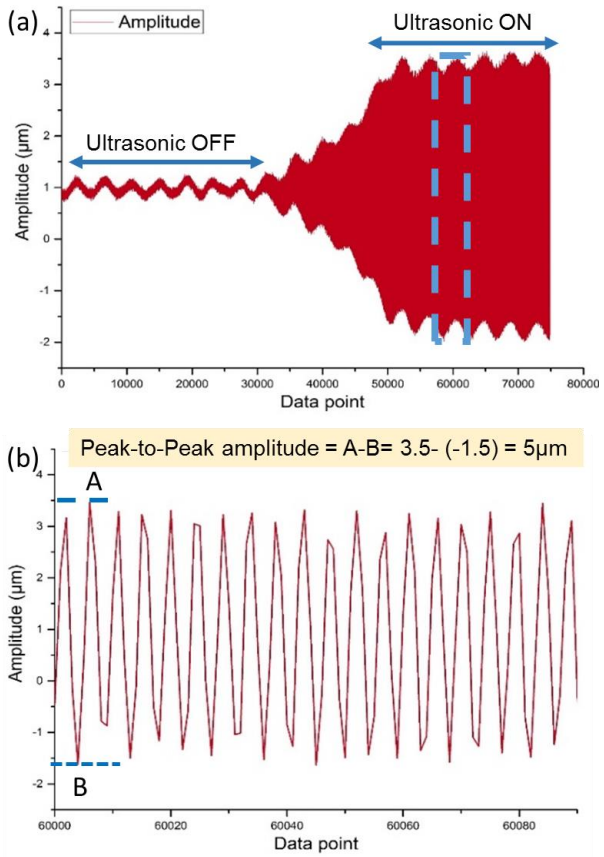

Figure 3-11: Graph showing (a) ultrasonic amplitude measured by Keyence LK-H008 before and after amplitude is turn on and (b) zoom in the image of ultrasonic amplitude indicates that the peak-to-peak amplitude was approximately 5 µm.

3.3.4.2 Cutting forces

Equipment

Measuring the cutting force during machining is important to monitor the progression of tool wear, the quality of the machined part, and the machinability of the material. The cutting force during milling was measured using a Kistler 9257B multi-component piezoelectric dynamometer as in Figure 3-12. The dynamometer was firmly mounted on the machine bed, and a fixture was attached to the dynamometer to secure the workpieces. During machining, the cutting forces measured by the dynamometer with a sampling rate of 40000 Hz were transformed from the electrical charges to a voltage by the Kistler multi-channel charge amplifier (Type 5070). Then, the amplified voltage was processed by the Kistler data acquisition (Type 5697 A) connected to a personal computer

running the Dynoware software. The sensitivity of the multi-channel charge amplifier (Type 5070) was set according to the Kistler's recommendation. The dynamometer was calibrated using known a load (1, 2 and 3 kg) prior to machining to ensure the accuracy of the measurement. Figure 3-13 shows the typical cutting forces recorded during milling. Cutting forces were recorded in the x-direction (Fx = feed force), y-direction (Fy = normal force) and z-direction (Fz= thrust force). The thrust force (Fz) is not considered in this study as the value recorded for the thrust force was significantly low, in the range between 0 to 5 N. The natural frequency of the dynamometer was 3 kHz. The Kistler dynamometer calibration certificate was attached in Appendix B.

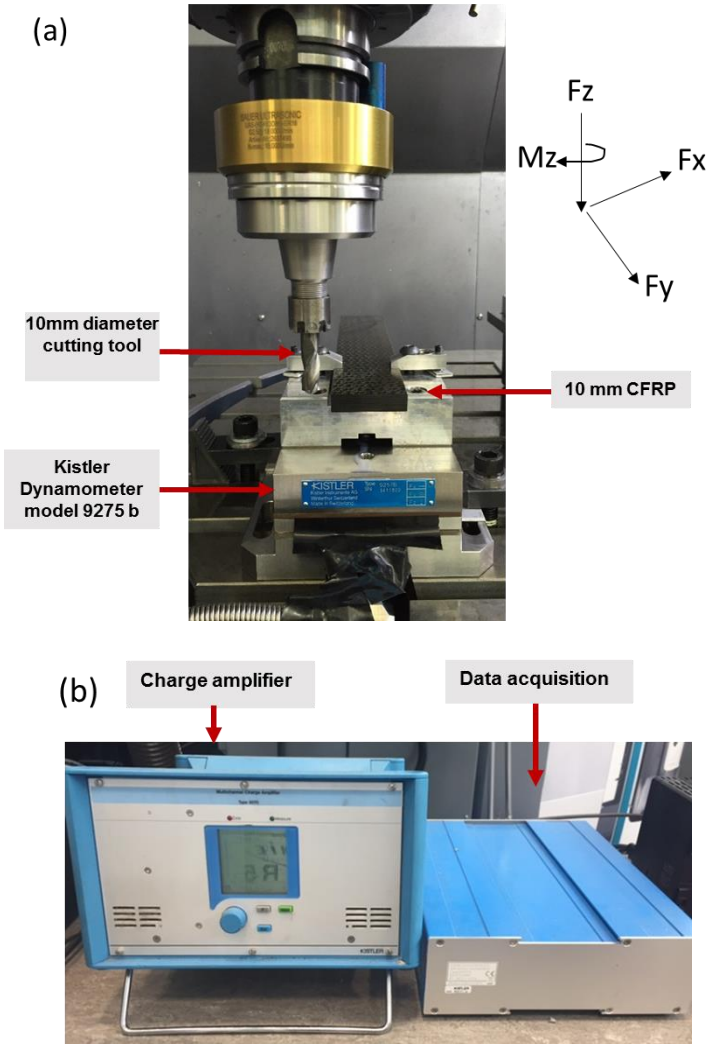

Figure 3-12: (a) Set up of Kistler Dynamometer and (b) charge amplifier and data acquisition for cutting force measurement.

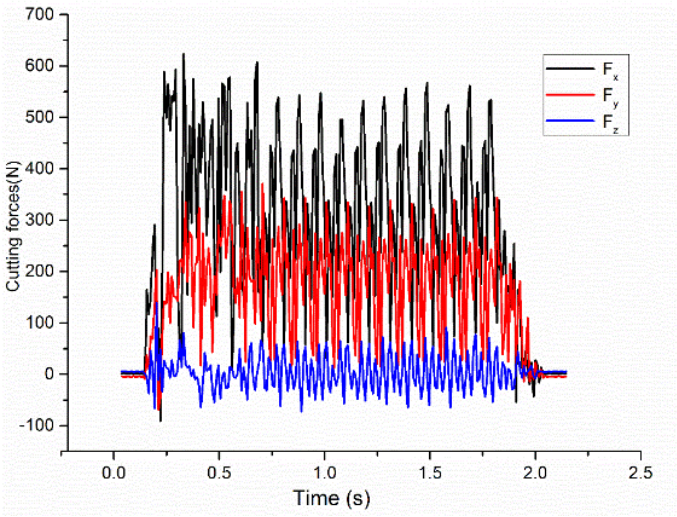

Figure 3-13: Typical cutting force data measured for milling operation indicated that the cutting force in z-direction has an average of 0 to 5 N.

3.3.4.3 Tool wear

Equipment

The progression of tool wear was observed using a Nikon microscope model SMZ 74 ST, Figure 3-14. The microscope is equipped with the ZEISS Axiocam ERc 5s camera. The camera was connected to the personal computer running the ZEN image capture and analysis software. The system was calibrated using a standard microscope eyepiece graticule before tool wear measurement were conducted.

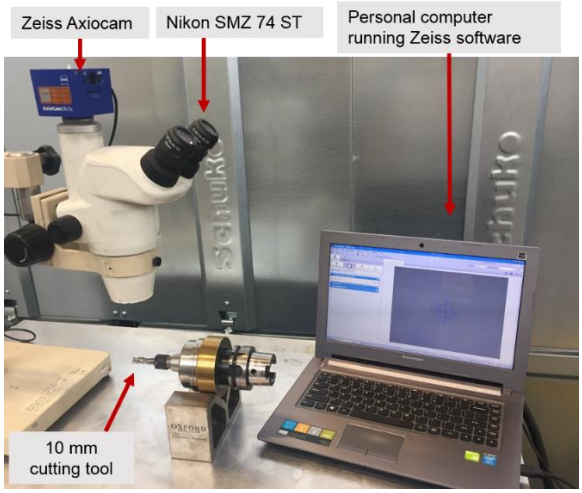

Figure 3-14: Nikon SMZ 74 ST microscope equipped with Zeiss Axiocam camera set up for tool wear analysis.

Method

The progression of tool wear for PCD and tungsten carbide end mill was measured by monitoring the flank wear at the clearance face of the cutting tool. The measurement of the flank wear (Vb) was based on ISO 8688 [174]. Figures 3-15 and 3-16 show the method of measuring the flank wear of the tungsten carbide and PCD end mill, respectively. Maximum flank wear recommended by the SGS tool for the tungsten carbide end mill was maximum Vb= 300 μm and maximum flank wear recommended by BAE system for the PCD end mill tool was maximum Vb =110 μm [175].

The average of the maximum flank wear for both end mill was considered as in equation (3.1) for evaluation:

$$\text{Flank wear} = \text{Maximum of } [(A_0 - A_{3000}), [(B_0 - B_{3000}), [(C_0 - C_{3000})] \quad \ldots\ldots\ldots\ldots \quad (3.1)$$

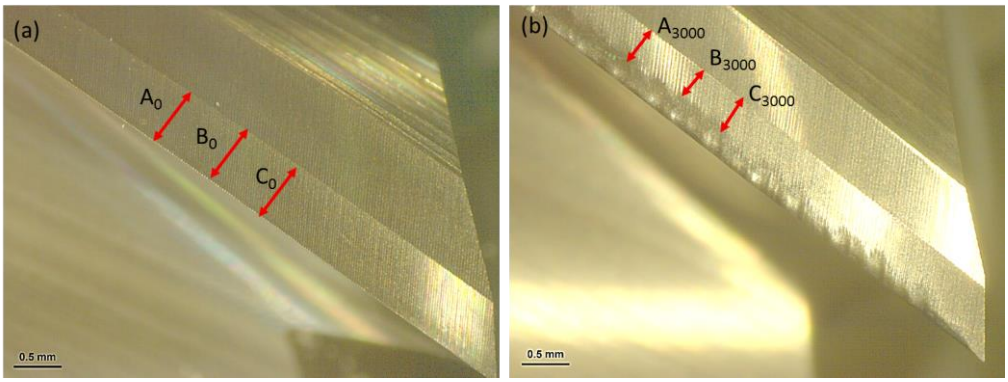

Figure 3-15: Measurement of flank wear for tungsten carbide end mill; (a) new cutting edge and (b) worn out cutting edge after milling CFRP; A_{3000}, B_{3000} and C_{3000} indicates 3000 mm machining length.

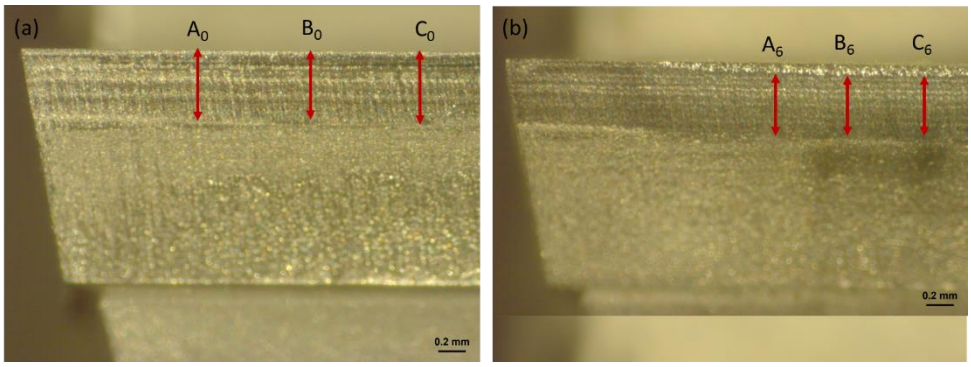

Figure 3-16: Measurement of flank wear for PCD end mill; (a) new cutting edge and (b) worn out cutting edge after milling CFRP; A_6, B_6 and C_6 indicates 6 m machining length.

Due to the complexity of the abrasive diamond tool geometry, that has a scattered diamond grit on the tool body, the progression of the tool diameter for the abrasive diamond tool was monitored by slotting the graphite plate as shown in Figure 3-17. Progression of tool wear for the abrasive diamond tool (Section 3.2.3) was measured by monitoring the diameter of the tool after every 1 m machining length. It has been suggested that increasing or decreasing of the cutting tool diameter can be observed by measuring the width of the slotted graphite plate [113, 114, 143]. The slotting of graphite

plate was carried out at every 1 m machining length with cutting speed of 50 m/min and feed rate of 1 mm/min. Minimum cutting parameters and 2 mm thickness of graphite plate was chosen to avoid the slotting method giving any effect to the cutting tool. The reduction of the tool diameter was measured based on the slotting width on the graphite plate. The width of the slotted area on the graphite plate was measured at 2, 4, and 6 mm height from the bottom surface of the slot area.

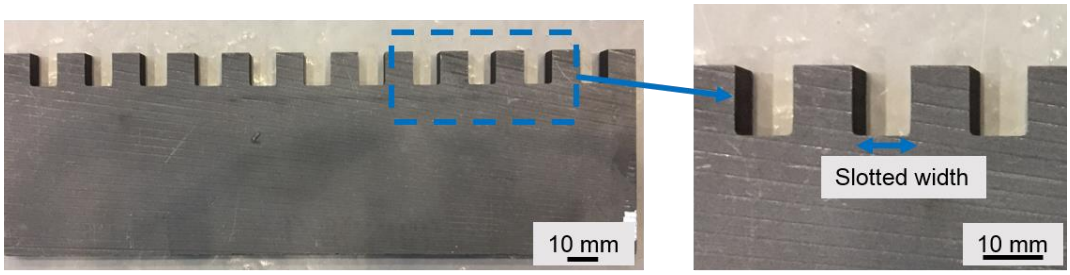

Figure 3-17: Slotting of graphite plate for tool diameter measurement for abrasive diamond tool.

3.3.4.4 Cutting temperature

Equipment

As discussed in Section 2.1, machining of CFRP must be carried out below the glass transition temperature (Tg) of the matrix resin. Therefore, monitoring the cutting temperature while machining is critical to avoid thermal damages that can affect the quality of the machined part. The cutting temperature was measured using the FLIR T250 thermal camera during machining as shown in Figure 3-18. The feature of the thermal camera is that it can create a visual and infrared non-radiometric of MPEG-4 videos file. A 3.1 Mpixel digital camera can produce a clear view of the thermal distribution when machining is performed. Thermal sensitivity of the thermal camera was 0.08 °C at 30 °C and a spectral range of 7.5 to 13 μm [176]. The accuracy of the measurement is 2 % from the reading. To obtain an accurate measurement from the thermal camera, the boiling

water temperature (100 °C) was measured by the thermal camera to ensure that the value was right.

Figure 3-18: FLIR thermal camera model T250 [176].

3.3.4.5 Tool-CO_2 nozzle distance

Equipment

When applying CO_2, it was necessary to measure the optimum distance between the nozzle and cutting tool. This measurement is required to provide the effectiveness of cooling during machining. K-type thermocouple from Picotech was utilised to measure the CO_2 temperature. The K-type thermocouple can measure the temperature in a range of -75 to 250 °C and has an accuracy of 2 % as shown in Figure 3-19. The K-type thermocouple was connected to the Picotech thermocouple data logger model TC-08. The thermocouple data logger was connected to the PC with Picolog software for analysis. The thermocouple data logger has a temperature accuracy reading of 0.2 % and ±0.5 °C. The distance between the CO_2 nozzle applicator and the cutting tool was measured using the Mitutoyo Vernier calliper.

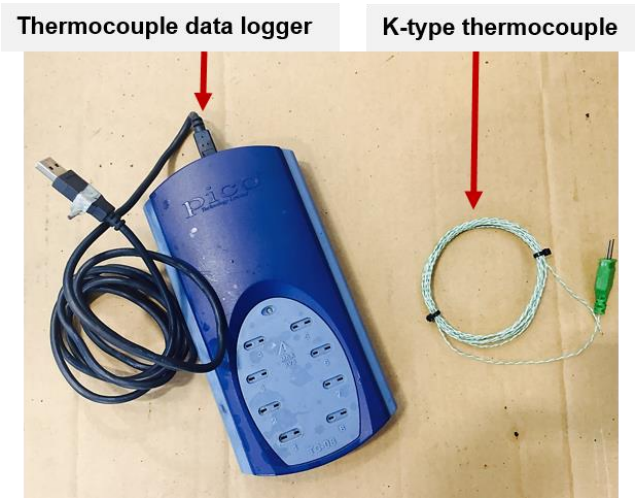

Figure 3-19: Picotech thermocouple data logger model TC-08 and K-type thermocouple.

Method

Figure 3-20 shows the set up for measuring the temperature of CO_2 that comes out from the nozzle. The temperature of CO_2 was measured in between 0 to 25 mm distance from the cutting tool and a temperature over distance. The CO_2 manufacturer also suggested that the nozzle should be pointed between 15 ° to 60 ° towards the cutting tool to produce an optimum cooling outcome at the cutting tool [177].

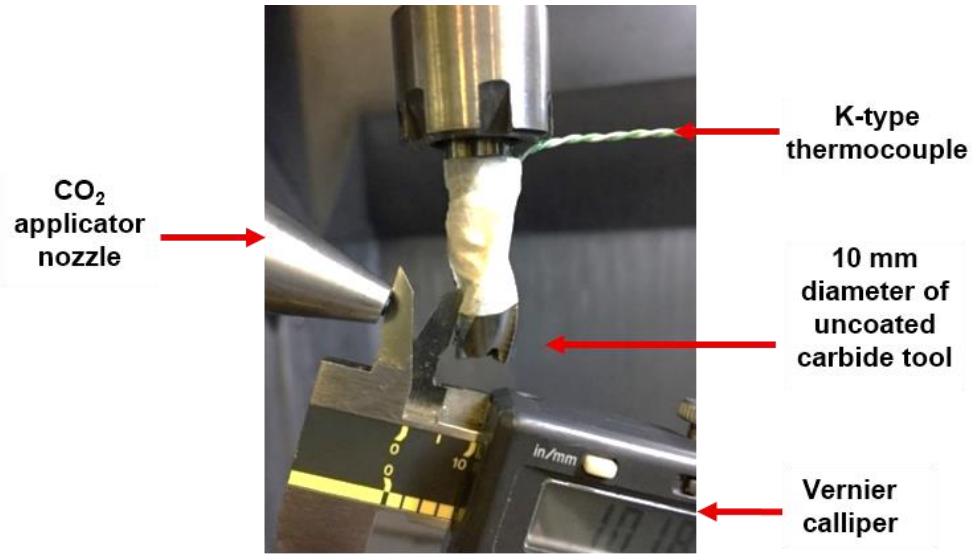

Figure 3-20: Temperature measurement for determining the relationship between the nozzle distance and the temperature of the CO_2 cryogenic from the applicator nozzle.

3.3.5 Post machining analysis equipment and procedure

3.3.5.1 Surface roughness and cutting tool condition

Equipment

Figure 3-21 shows the Alicona InfiniteFocus that can measure the surface roughness and 3D micro coordinate measurement. The Alicona InfiniteFocus offers a non-contact measurement that could give several benefits to the measurement of the machined surface where the non-contact/optical measurement does not alter the surface, and it has the fastest measurement than the Talysurf. Alicona InfiniteFocus is capable of measuring with 2.5 X to 100 X magnification with the vertical resolution of 10 nm. The accuracy capable by this equipment is 0.05 % [178].

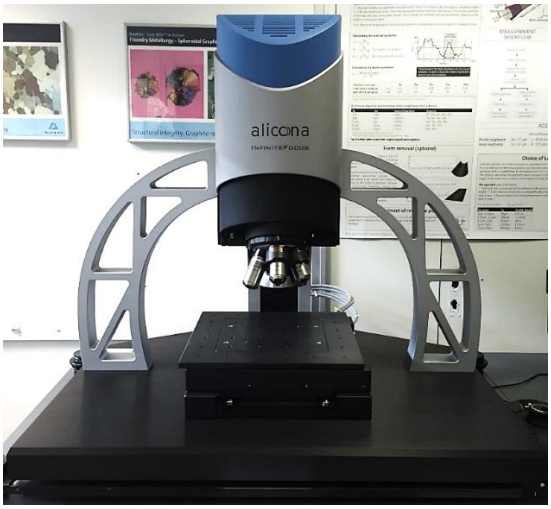

Figure 3-21: Alicona InfiniteFocus.

Methods

All surface roughness of the machined surface was measured at 10 X magnification with a vertical resolution of 100 nm. As recommended in the literature, the surface roughness, Ra was employed to measure the roughness of the milled surface under different machining parameters. The measurement was set at 4 mm transverse length and 0.8 mm

cut-off value. The sample was cut into 10 x 10 x 45 mm dimension and was cleaned using the ultrasonic bath with acetone to remove debris on the machined surface before the measurement was performed. The analysis was repeated three times at each point to ensure repeatability, and an average was calculated afterwards.

In addition to surface roughness, the tool condition for the abrasive diamond tool was measured using the Alicona InfiniteFocus. The topography of the cutting tool was scanned with the 5 X magnification with a vertical resolution of 100 nm as shown in Figure 3-22 (a). Figure 3-22 (b) shows the 2D image analysis where the area of the cutting tool covered by the matrix resin and carbon fibre was measured. The area of the cutting tool covered by the matrix resin was measured after the milling test was carried out.

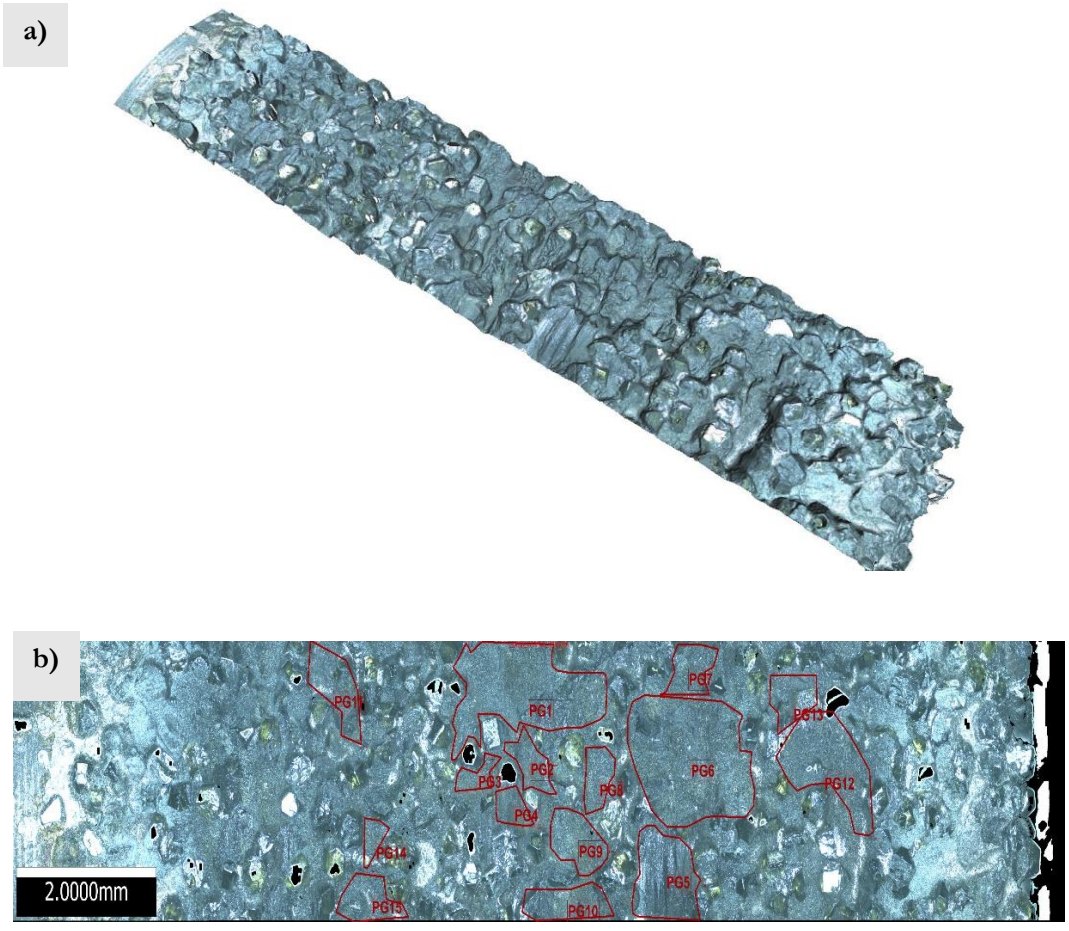

Figure 3-22: (a) Scanned image of the abrasive diamond tool and (b) image processing to measure the area of the cutting tool that covered by the matrix resin and broken fibre.

3.3.5.2 Scanning electron microscopy (SEM) micrograph

Equipment

Additional information on surface integrity and cutting tool condition were obtained using the ZEISS Sigma scanning electron microscope (SEM) as shown in Figure 3-23. SEM can attain higher magnification images which could not be achieved by the optical microscope and it could could magnify the image from 10 X to 100000 X magnification. This equipment is also equipped with the Energy Dispersive Spectroscopy (EDS) to identify the sample elements and their compositions.

Figure 3-23: Zeiss Sigma scanning electron microscope.

Method

The machined surface was cut into a section of 10 x 10 x 10 mm and was cleaned using the acetone bath. The samples were dried before being coated with gold on the surface. The machined CFRP surface sample needs to be coated with gold since CFRP does not have an excellent conductivity for voltage to charge the sample. For the cutting tool examination, the cutting tool was cleaned prior to the SEM analysis where it was secured on the tool holder that can be fixed in the SEM working table inside the chamber.

3.3.5.3 Sample preparation for thermal analysis

To investigate the effect of machining environment on the machined CFRP surface, the machined surface needs to be transformed into powder. The sample tested by thermogravimetric (TGA), differential scanning (DSC) and Fourier transform Infrared (FTIR) was prepared by transforming the machined CFRP surface to a powder form. Therefore, the sharp scalpel was used to ensure that the shaving method does not affect the material. The thickness of the sample was measured before and after the shaving processes using vernier callipers. An average of 400 to 500 μm thickness and 150 mm length machined surface of CFRP was shaved from the machined surface, Figure 3-24.

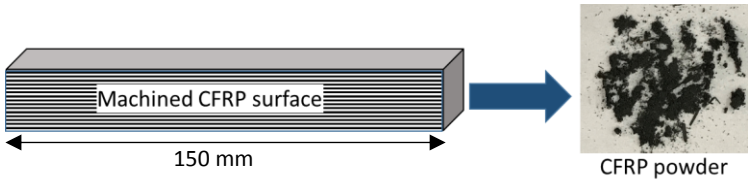

Figure 3-24: Transformation of the machined CFRP surface into CFRP powder for thermal analysis test.

3.3.5.4 Thermogravimetric analysis (TGA)

Equipment

Thermogravimetric analysis (TGA) is usually utilised for the thermal analysis of polymeric materials, such as thermoplastic and thermoset. Materials characterisation from TGA can provide chemical and physical properties information of the test sample. Information such as decomposition, vaporization, oxidation, dehydration and reaction process of test sample can be obtained from TGA [179]. The basic principle of TGA is monitoring the weight loss or gain of test sample over temperature (heated, cooled, or isothermal) with a constant heating rate and the stepwise changes in mass indicate that the chemical/physical changes of the materials over temperature. Therefore, TGA of the pure (unmachined) CFRP was conducted before performing the thermal analysis of the

CFRP using the differential scanning (DSC) analysis to indicate the starting decomposition temperature of the resin. In this study, Mettler Toledo supplied the TGA equipment as shown in Figure 3-25. The equipment is capable of measuring the sample at a temperature ranging from room temperature up to 1100 °C with an accuracy of ±1 °C [180] and a heating rate of 0.02 to 250 °C/min.

Figure 3-25: TGA by Mettler Toledo [179].

Method

Before the material characterisation was performed in TGA, the sample needs to be prepared and measured. The sample preparation was discussed in Section 3.3.5.3. An alumina crucible was chosen in this test because it can withstand a temperature up to 1000 °C, Figure 3-26. The sample was measured approximately 6 mg before the test was carried out and the crucible with a sample is then located inside the test furnace. The sample decomposition property was evaluated from 25 to 600 °C with a constant heating rate of 10 °C/min and the nitrogen gas was supplied to the furnace at a constant rate of 150 mL/min. The result from the TGA was analysed using the STAR-e software provided by Mettler Toledo and plotted using the Origin software. The derivative of the weight loss curve indicates the temperature that the sample starts to decompose, and the decomposition temperature is the maximum testing temperature that can be used in the DSC analysis.

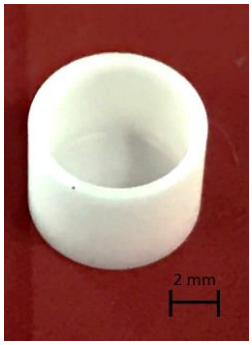

Figure 3-26: Alumina crucible that capable to withstand temperature up to 1000 °C that was used in TGA analysis.

3.3.5.5 Differential Scanning Calorimetry (DSC)

Equipment

To investigate the effect of the machining environment on the machined surface, it is important to monitor the glass transition temperature (Tg) of the matrix resin. Therefore, Differential Scanning Calorimetry (DSC) as shown in Figure 3-27 was employed to measure the glass transition temperature in this research. Much information can be obtained from the DSC analysis such as specific heat capacity, enthalpy change, solid-solid transition, melting point, crystallinity, and glass transition temperature (Tg). The fundamental principle of DSC is heat flow changes between the reference and the sample when heated or cooled with a constant heating rate. The details on the DSC working mechanism have been explained in Section 2.6.2. The DSC is capable of testing the material at a temperature from -150 to 700 °C with a constant heating rate in the range of 0.02 to 300 °C/min depending on the test material [181]. The temperature accuracy and precision offered by this equipment was ±0.2 °C and ±0.02 °C, respectively [181].

Figure 3-27: DSC1 by Mettler Toledo.

Method

The weight of the test sample and reference sample (empty crucible) were measured before the DSC analysis was performed. The weight of the test sample was approximately 6 mg. Aluminium crucible was chosen in this test due to the test temperature does not exceed 600 °C, Figure 3-28. After the weighted sample have been placed inside the crucible, the crucible needs to seal with the cap using a crimper. To avoid the sample bursting out from the sealed crucible during heating, it is important to make a hole on the crucible cap after sealing the crucible, Figure 3-28 (b). The sample was heated from 25 to 350 °C with a constant heating rate of 10 °C/min, and the nitrogen gas was supplied to the furnace at a constant rate of 150 mL/min. The results obtained from DSC was analysed using the STAR-e software provided by Mettler-Toledo and plotted using the Origin software.

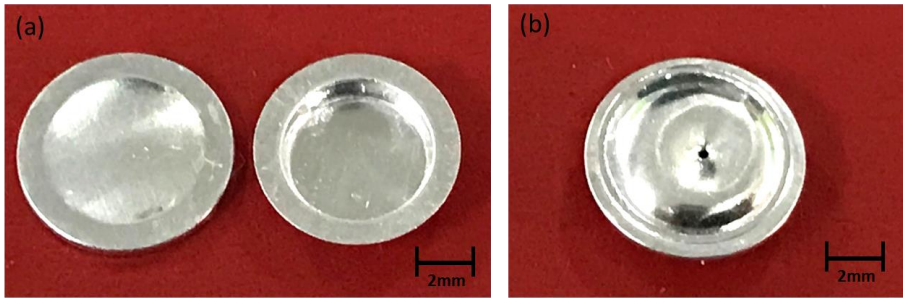

Figure 3-28: (a) Crucible cap and pan and (b) sealed crucible with a hole made on the cap.

3.3.5.6 Fourier Transform Infrared spectroscopy (FTIR)

Equipment

The changes in the glass transition temperature (Tg) are related to the changes of the chemical property of the matrix resin. Therefore, Fourier Transforms Infrared spectroscopy (FTIR) was employed to detect the changes on the chemical property of the matrix resin after machining. FTIR is an analytical technique to determine the chemical composition of the organic and polymeric materials. FTIR is capable of determining the functional groups, bonding type and materials compound. Therefore, the effect of machining environment on the chemical property changes of the matrix resin was determined by FTIR. The working mechanism is discussed in Section 2.6.3. The FTIR equipment employed in this study was Tensor 27 (Figure 3-29) that was supplied by Bruker, and it can scan the sample from 400 to 7000 cm^{-1} with a standard KBr beam splitter.

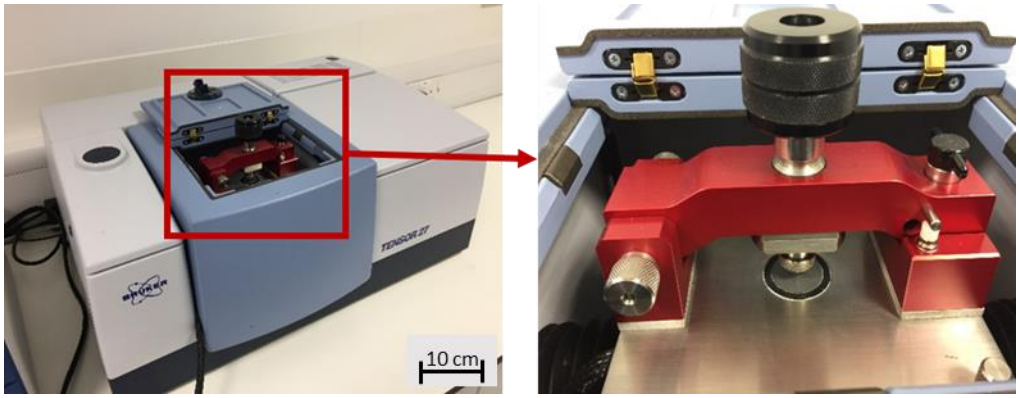

Figure 3-29: Fourier transforms infrared (FTIR) spectroscopy model Tensor 27 by Bruker.

Method

The machined surface sample used in this test was prepared as explained in Section 3.3.5.3 and only a small amount of test sample range 2 mg needed to perform this test. The FTIR scans collected the wavenumber ranging from 700 to 4000 cm^{-1}. The resolution employed was 4 cm^{-1} and a scan time was 32 seconds. Before scanning of the test sample, the

background scanning was carried out to detect any molecule such as water that was present in the test chamber and the background scanning spectrum was then subtracted from the sample spectrum to ensure the accuracy of the scanning. To ensure the repeatability of the data produce by FTIR, it is important to run the test several times. Five samples were taken randomly from the machined surface (for each machining length), and for each sample, the scanning was repeated three times. The data were normalised by dividing the data with the maximum peak value obtained from scanning to ensure that the peak was comparable. The data was analysed using OPUS software, provided by Bruker, and plotted using the Magicplot™ software.

3.4 Experimental studies

3.4.1 Study 1(a): Machinability of CFRP in dry, conventional cutting fluid and CO_2 cryogenic machining environment.

Study 1(a) was aimed to investigate the effect of the machining environment in terms of tool wear, cutting forces, and surface roughness. In this study, three different machining conditions, which are dry, conventional cutting fluid (CCF), CO_2 cryogenic (CO_2) were investigated, and the uncoated tungsten carbide end mill was employed (Section 3.2.1). All machining environments were tested with conventional (CM) and ultrasonic assisted milling (UAM). The CFRP strip (45 mm x 10 mm) was mounted on the dynamometer for the force measurement and the CFRP panel (300 mm x 10 mm) was fixed on the fixture for the tool wear progression. Tool wear was monitored and the machined surface for roughness analysis was cut at every 600 mm machining length. Figure 3-30 shows the experimental set up of the test. The FLIR thermal camera was located at 30 cm distance from the CFRP panel for the temperature measurement. For CO_2 cutting media, the CO_2 was supplied from outside the machine tool. The constant CO_2 pressure of 6.2 MPa and

compressed air pressure of 0.5 MPa were applied to obtain a consistent supply of CO_2 ice crystal with a rate of 6 kg/hour. The detail of the set up was explained in Section 3.3.2. For CCF condition, the cutting fluid was supplied through the nozzles inside the machine tool. The ultrasonic amplitude was measured before the milling test was performed and the procedure for the amplitude measurement has been discussed in Section 3.3.4.1. Table 3-7 shows the cutting parameters employed in this test.

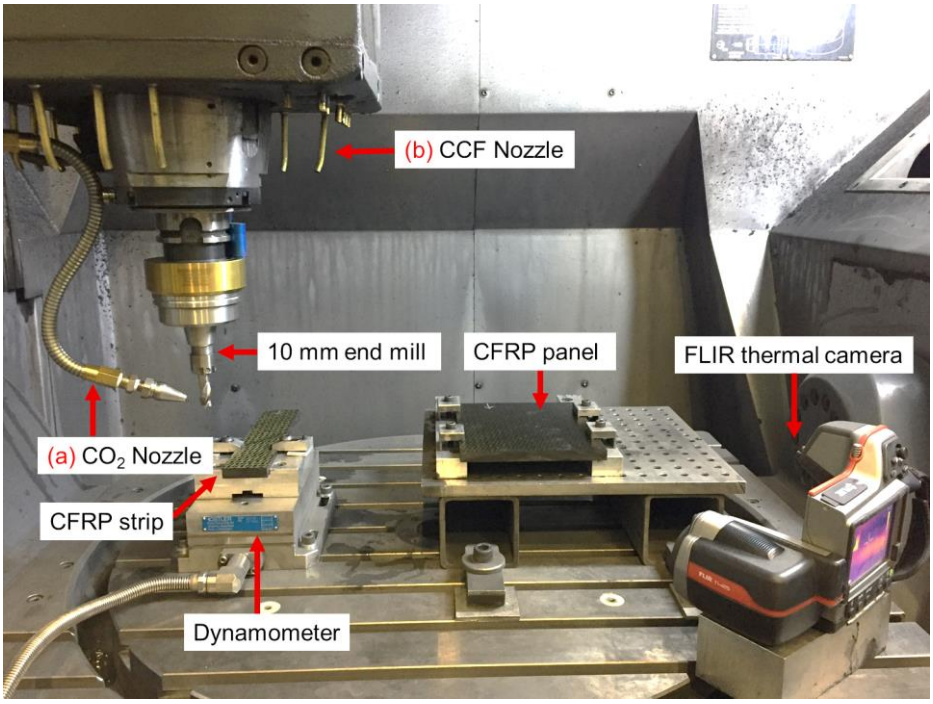

Figure 3-30: Experimental set-up when milling CFRP labelled (a) indicates the CO_2 cryogenic nozzle and (b) indicates the CCF nozzle.

Table 3-7: Machining parameter for Study 1(a).

Parameter		**Value**
Cutting tool		10 mm diameter uncoated tungsten carbide
CFRP thickness		10 mm
Cutting speed, V		500 m/min
Feed rate, f		800 mm/min
Radial depth of cut, a		1 mm
Ultrasonic-assisted	Frequency, *f* Amplitude, A	38000 Hz ≈ 5 μm peak-to-peak
Machining environments		Dry CCF CO_2

3.4.2 Study 1(b): Post machining analysis to understand the effect of machining environment on the machined CFRP surface

The objective of this study was to investigate the effect of machining environment (Study 1(a)) on the chemical properties of the machined CFRP surface. As mentioned earlier, the cutting temperature in machining polymeric materials was limited to the glass transition temperature (Tg). Therefore, it is necessary to study the effect of the machining environment on the machined surface that can affect the degradation of the property of the CFRP. The effect of the machining environment on the Tg was studied using the DSC. The sample was taken from 1, 2, and 3 m machining length machined surface from Study 1(a), and the sample preparation was explained in Section 3.3.5.3. Five different samples were randomly taken from each machining length for the analysis. The detail of DSC analysis procedure was explained in Section 3.3.5.5.

In addition to the DSC analysis, to investigate the effect of machining environment on the chemical properties of the machined CFRP surface was carried out using FTIR. The machined surface sample was taken from 1, 2, and 3 m machining length of the machined CFRP surface. Five different samples were randomly taken from each machining length for the analysis. The scanning procedure was repeated five times for each sample, and the procedure of the measurement was explained in Section 3.3.5.6.

3.4.3 Study 2: Machinability of CFRP using the PCD end mill

In this study, the aim was to investigate the effect of UAM over CM with respect to tool wear, cutting forces, and surface quality. This test also aimed to investigate the effect of the tool type on the effectiveness of UAM over CM. The equipment set up and CFRP workpiece dimension for this study is similar to Study 1(a) as shown in Section 3.4.1. The cutting tool employed in this study was PCD end mill (Section 3.2.2). The CFRP employed in this milling test was 5 mm thick due to the limited supply of the 10 mm thick CFRP. The cutting parameters used in this test were recommended by BAE Systems and both CM and UAM employed the same cutting parameters, and all machining test was carried out in dry condition. Table 3-8 shows the cutting parameters employed in this test. The ultrasonic amplitude was measured before the milling test was performed and the procedure for the amplitude measurement has been discussed in Section 3.3.4.1

Table 3-8: Machining parameter for Study 2.

Parameter		**Value**
Cutting tool		PCD end mill
Cutting tool diameter		10 mm
CFRP thickness		5 mm
Cutting speed		500 m/min
Feed rate		800 mm/min
Depth of cut		1 mm
Ultrasonic-assisted	Frequency	38000 Hz
	Amplitude	≈ 5μm peak-to-peak

3.4.4 Study 3: Machinability of CFRP using the abrasive diamond milling tool

Figure 3-31 shows the set-up for the milling test employing the abrasive diamond tool. This study aims to investigate the effectiveness of the ultrasonic assisted machining in

terms of tool wear, cutting forces, and surface roughness. It has been previously observed that the main problem when machining with the abrasive diamond tool after a certain machining length, the resin started to build-up on the cutting tool [175]. The workpieces configuration for tool wear and cutting force was similar to Study 1(a) (Section 3.4.1). In this test, the reduction of the abrasive diamond tool was measured using the graphite plaque. The width of the slotted graphite was assumed to have a similar diameter with the cutting tool. The cutting tool diameter was measured at every one-metre machining length. This method has been explained in Section 3.3.4.3. The cutting parameters employed were recommended by BAE Systems, and both CM and UAM employed the same cutting parameters. The ultrasonic amplitude was measured before the milling test was performed and the procedure for the amplitude measurement has been discussed in Section 3.3.4.1. All tests were carried out in a dry condition. The parameters that were employed in this study was tabulated in Table 3.9.

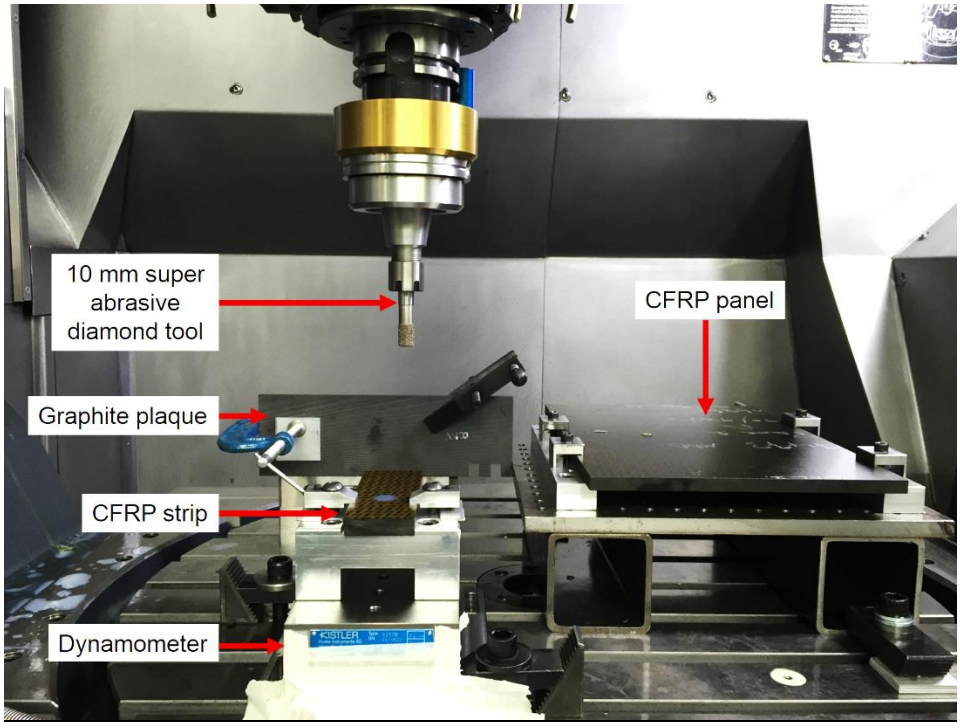

Figure 3-31: Experimental set-ups for milling of CFRP employing the abrasive diamond tool.

Table 3-9: Machining parameter for Study 3.

Parameter		**Value**
Cutting tool		10 mm abrasive diamond tool
Workpiece thickness		10 mm
Cutting speed		565 m/min
Feed rate		1500 mm/min
Depth of cut		1 mm
Ultrasonic-assisted	Frequency	38000 Hz
	Amplitude	≈ 5 μm peak-to-peak

Chapter 4 Results and Analysis

4.1 Study 1(a): Machinability of CFRP in dry, conventional cutting fluid and CO_2 cryogenic machining environments

This study examined the effects of cutting environments, which were dry, conventional cutting fluid (CCF), and CO_2 on the machinability of CFRP BMI 5250-4 for the aspects of tool wear, cutting forces, and surface roughness. The experimental methodology is described in Section 3.4.1. Meanwhile, as for CO_2 cutting environment, as mentioned in Section 3.3.4.5, it is important to ascertain the occurrence of continuous cooling of cutting tool during machining. Besides, the distance between the nozzle and the cutting tool was maintained at a maximum of 17 mm distance to obtain a temperature below - 60 °C at the cutting tool, as presented in Figure 4-1.

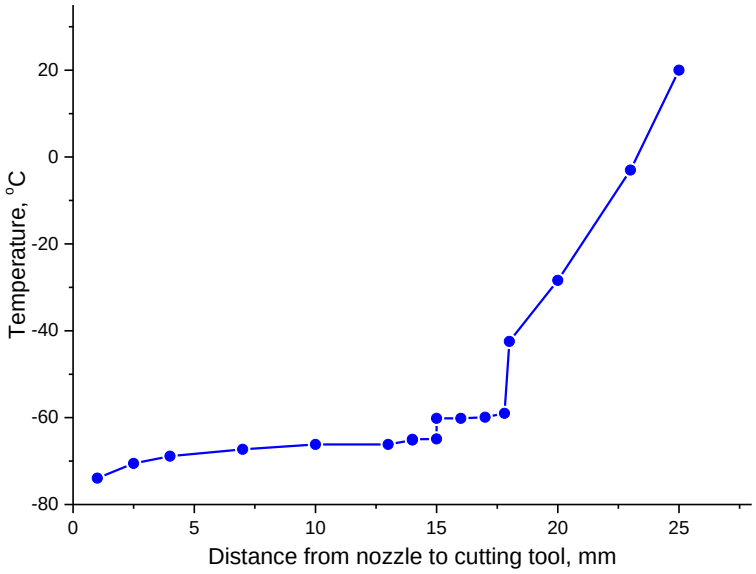

Figure 4-1: Relationship between the distance of cutting tool and CO_2 cryogenic applicator nozzle with CO_2 temperature.

4.1.1 Tool wear and cutting temperature

The progression of flank wear when milling CFRP with uncoated tungsten carbide end mill in various machining environments for CM and UAM is shown in Figures 4-2 (a) and (b), respectively. An increase in the machining length showed increment in tool wear for all machining environments.

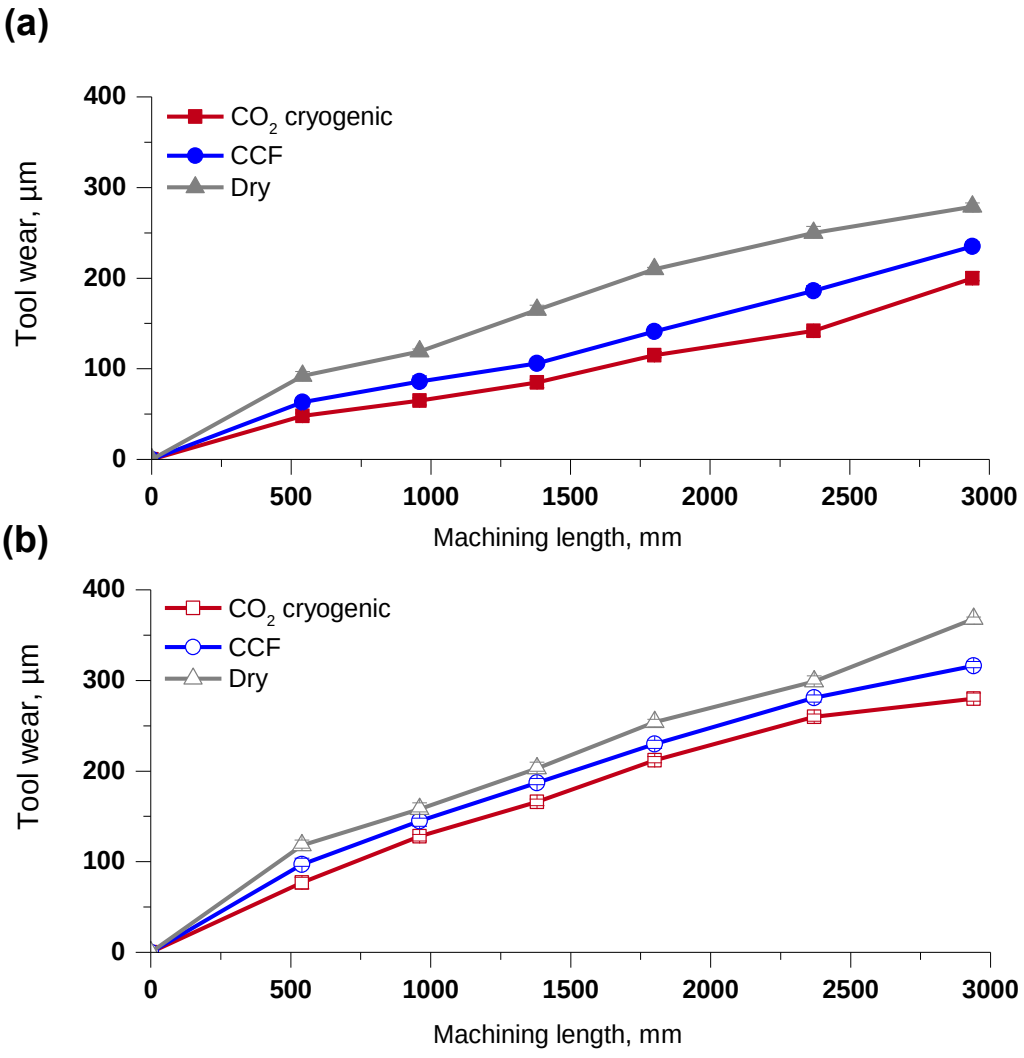

Figure 4-2: Progression of tool wear of (a) CM and (b) UAM in dry, CCF and CO_2 cryogenic environments.

The results plotted in Figures 4-2 (a) and (b) exhibit that the tool wear pattern in all machining environments is similar for both CM and UAM. Nevertheless, the tool wear measured for UAM was 30 to 40 % higher, as compared to CM, for all machining

environments, as tabulated in Table 4-1. This can be attributed to the mechanism of UAM, which vibrates, rotates, and moves when machining, while in CM, the tool does not vibrate during the machining. Hence, the motions of cutting tools generate more interaction between the cutting tool and the CFRP workpiece, which deteriorates the cutting tool [8]. Further elaboration on the effect of ultrasonic vibration that is perpendicular to the feed direction is given in Study 2 (Section 4.3).

Table 4-1: Comparison of maximum flank wear between CM and UAM at the end of the milling test (after 3000 mm machining length) a) CO_2 b)CCF and c) dry machining environment.

Machining environments	Maximum flank wear for CM (μm)	Maximum flank wear for UAM (μm)	Percentage different when comparing between UAM-CM
a) CO_2	200	280	40 %
b) CCF	235	316	35 %
c) Dry	279	368	32 %

Figure 4-3 shows the tool wear at 3000 mm for both CM and UAM in CO_2, CCF, and dry machining environments. It is suggested that the tool wear for UAM is higher than CM for all machining environments. As a result, the highest tool wear was observed when CFRP was milled in a dry environment for CM and UAM after 3000 mm machining length, when compared to both CCF and CO_2 environments. Milling of CFRP with the presence of CO_2 resulted in the lowest tool wear of over 3000 mm machining length, when compared to dry and CCF environments for both CM and UAM. CM and UAM in a dry environment resulted in 279 and 368 μm flank wear after 3000 mm machining length, respectively. Meanwhile, as for CCF, the tool wear measured for CM was 235 μm and 316 μm for UAM. Lower tool wear was recorded in CO_2 environment, where the flank wear for CM was 200 μm, and 280 μm for UAM at the end of the test.

Table 4-2 summarises the progression of tool wear for both CM and UAM in CO_2, CCF, and dry environments at 500 mm and 3000 mm machining length.

Table 4-2: Tool wear for CM and UAM at 500 and 3000 mm machining length.

Process	Condition / Length, mm	Flank wear (Vb), µm		
		CO_2	CCF	Dry
CM	500	48	63	92
	3000	200	235	279
UAM	500	77	97	118
	3000	280	316	368

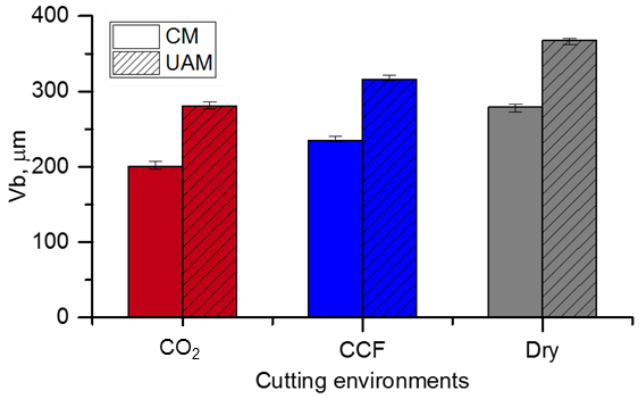

Figure 4-3: Comparison of flank wear,Vb at 3000 mm for CM and UAM in different cutting conditions.

In order to gain better understanding pertaining to the effects of cutting environment with the progression of tool wear, the cutting temperature during milling was recorded by the FLIR thermal camera. Figure 4-4 shows the cutting temperatures for CM and UAM in dry and CO_2 environments. Figure 4-5 shows the infrared (IR) measurement of cutting temperature recorded by the FLIR thermal camera for UAM in a dry environment at 3000 mm machining length. The cutting temperatures recorded for both CM and UAM in dry and CO_2 environments indicate similar trend regardless of the process. The cutting temperature obtained by CO_2 machining was 30 to 50 % lower than the dry machining in both CM and UAM. At 3000 mm machining length, the cutting temperature measured for CO_2 was 115 °C for CM and 140 °C for UAM. On the other hand, as for the dry

machining, the cutting temperatures measured for CM and UAM had been in the range of 170 to 200 °C. The increment in cutting temperature upon increased machining length can be explained by the progression of tool wear, as shown in Figures 4-2 (a) and (b). Nevertheless, only 10 to 15 % of variance between the cutting temperatures had been recorded for CM and UAM. This finding contradicts several researches, in which they claimed that the implementation of UAM reduces cutting temperature due to the periodical separation between the cutting tool and the workpieces [157, 182-184].

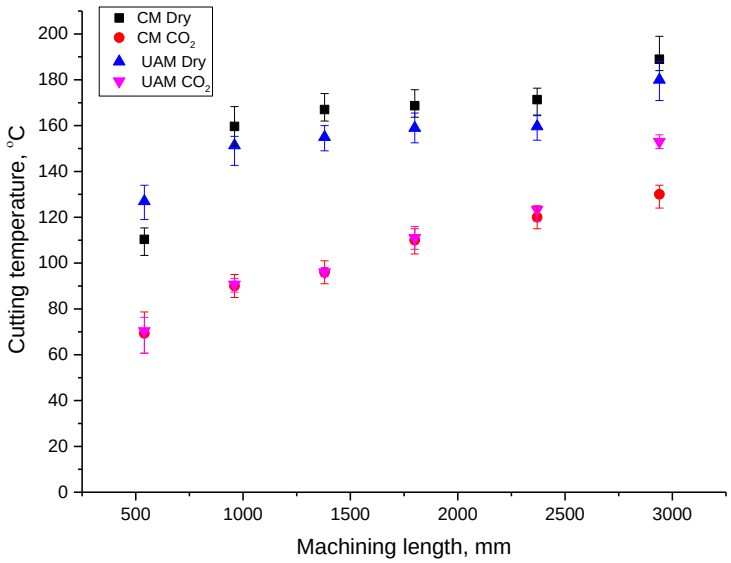

Figure 4-4: Cutting temperature for CM and UAM in dry and CO_2 environment recorded by FLIR thermal camera.

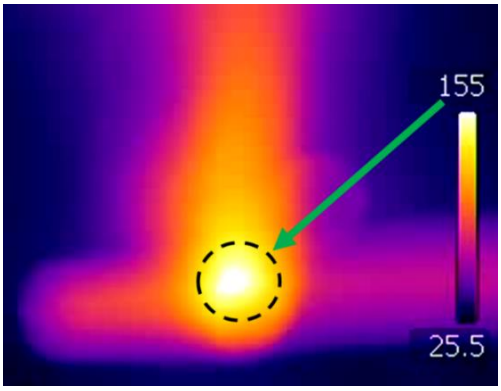

Figure 4-5: Infrared measurement of cutting temperature indicates that the maximum and minimum temperature for UAM in dry environment at 3000 mm.

As for machining in dry environments, the condition of the cutting tool deteriorated due to the heat generated during the cutting process. When milling with CCF, the cutting temperature recorded by the FLIR thermal camera was within the range of 27 to 32 °C. This finding is similar to that retrieved by Dahnel et al. [120] when measuring the cutting temperature during milling of CFRP. During CCF, continuous cooling of the cutting tool and the CFRP workpiece retained the strength of the CFRP. Thus, higher tool wear was observed for both CM and UAM in CCF, when compared to CO_2. Machining of CFRP with the presence of CO_2 improved the progression of tool wear by 28 % and 23 % for CM and UAM, respectively, in comparison to dry and CCF machining environments. The presence of CO_2 improved the tool wear due to the continuous cooling effect on the cutting tool, which assisted in removing the heat generated by the cutting tool and in reducing the temperature of the cutting tool [18, 78, 86].

However, in contrast with Budwannachai et al. [97] and Barnes et al. [90], the tool wear for cryogenic drilling was higher, in comparison to the dry drilling of CFRP. This could be attributed to the method employed by the cryogenic cooling during the drilling, where the cutting tool is not continuously cooled, which resulted in higher tool wear. Nonetheless, in this present study, the cutting tool was continuously cooled by CO_2, where the temperature of the CO_2 emitted from the applicator nozzle was maintained at -60 °C. As mentioned earlier, the distance between the cutting tool and the CO_2 applicator nozzle was kept at a distance less than 17 mm (Figure 4-1) to ascertain that the temperature at the cutting tool was always below -60 °C. As a result, by maintaining the temperature of CO_2 emitted from the nozzle, the continuous cooling of the cutting tool during milling improved the tool wear when milling with the presence of CO_2.

Although CO_2 was supplied directly to the cutting tool when machining was performed, it is proposed that the heat generated by the cutting tool and the workpiece softened the

workpiece materials. The heat generated by the cutting tool was removed, but concurrently, the strength of the workpieces reduced. As a result, the reduction in material strength and the removal of heat by CO_2 aided in improving the tool wear in the CO_2 environment. Another possible explanation for the enhanced tool wear in CO_2 environment when machining CFRP is due to the high pressure of the CO_2 coolant emitted from the nozzle. The high pressure of the CO_2 removed broken fibre, and at the same time, reduced the abrasion between the cutting tool and the workpiece. Therefore, this present study shows that the implementation of CO_2 cryogenic coolant directly to the cutting tool can improve the tool wear when machining CFRP, in comparison to both dry and CCF conditions.

Figures 4-6 to 4-8 show the SEM micrographs of tool wear for the dry, CCF and CO_2 environments in CM and UAM after 3000 mm machining length, respectively. The images taken in SEM indicate that the cutting tool experienced the same wear mechanism regardless of the process and machining environments.

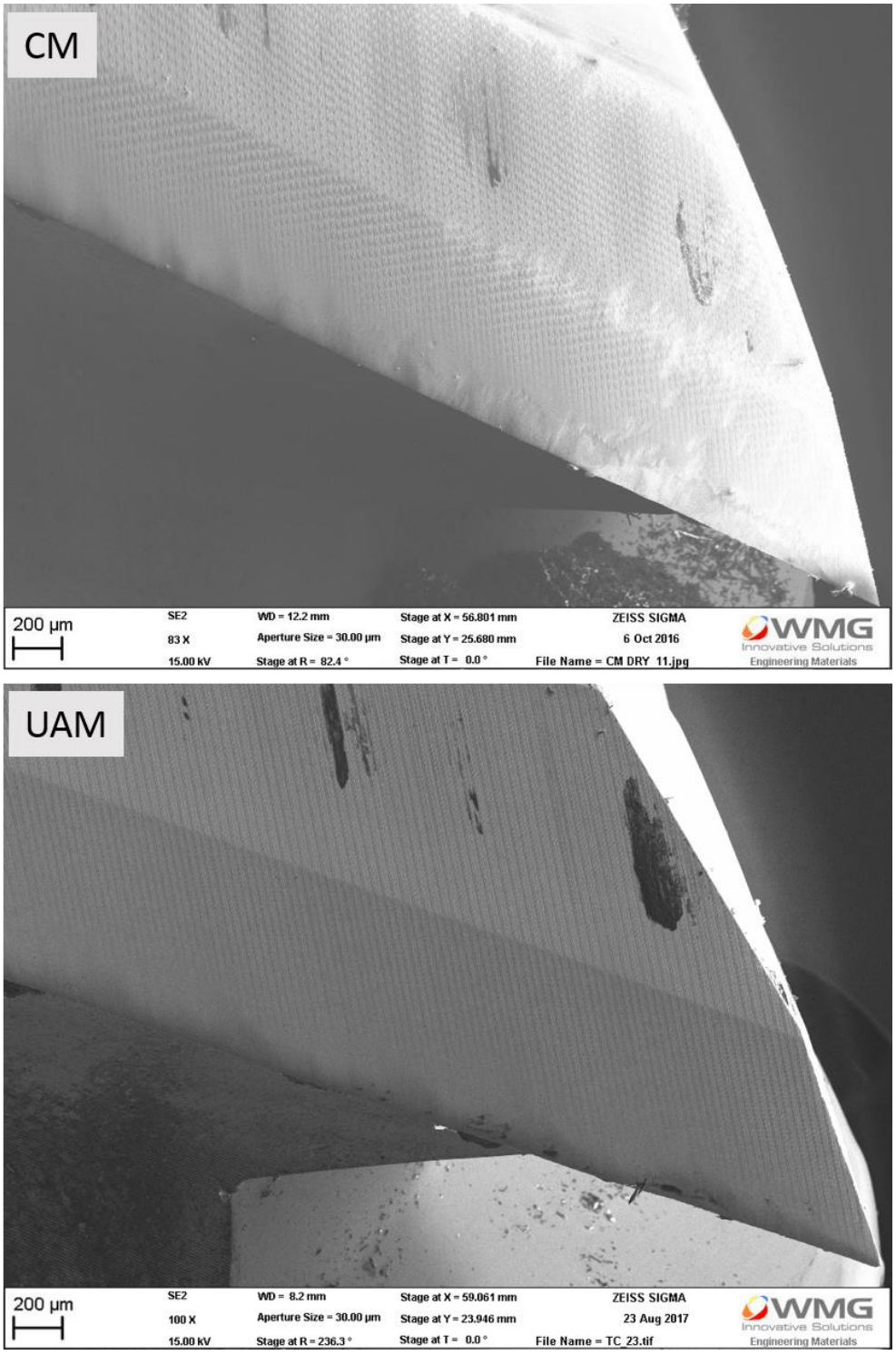

Figure 4-6: SEM micrographs of tungsten carbide end mill for (a) CM and (b) UAM in dry environment after 3000 mm machining length.

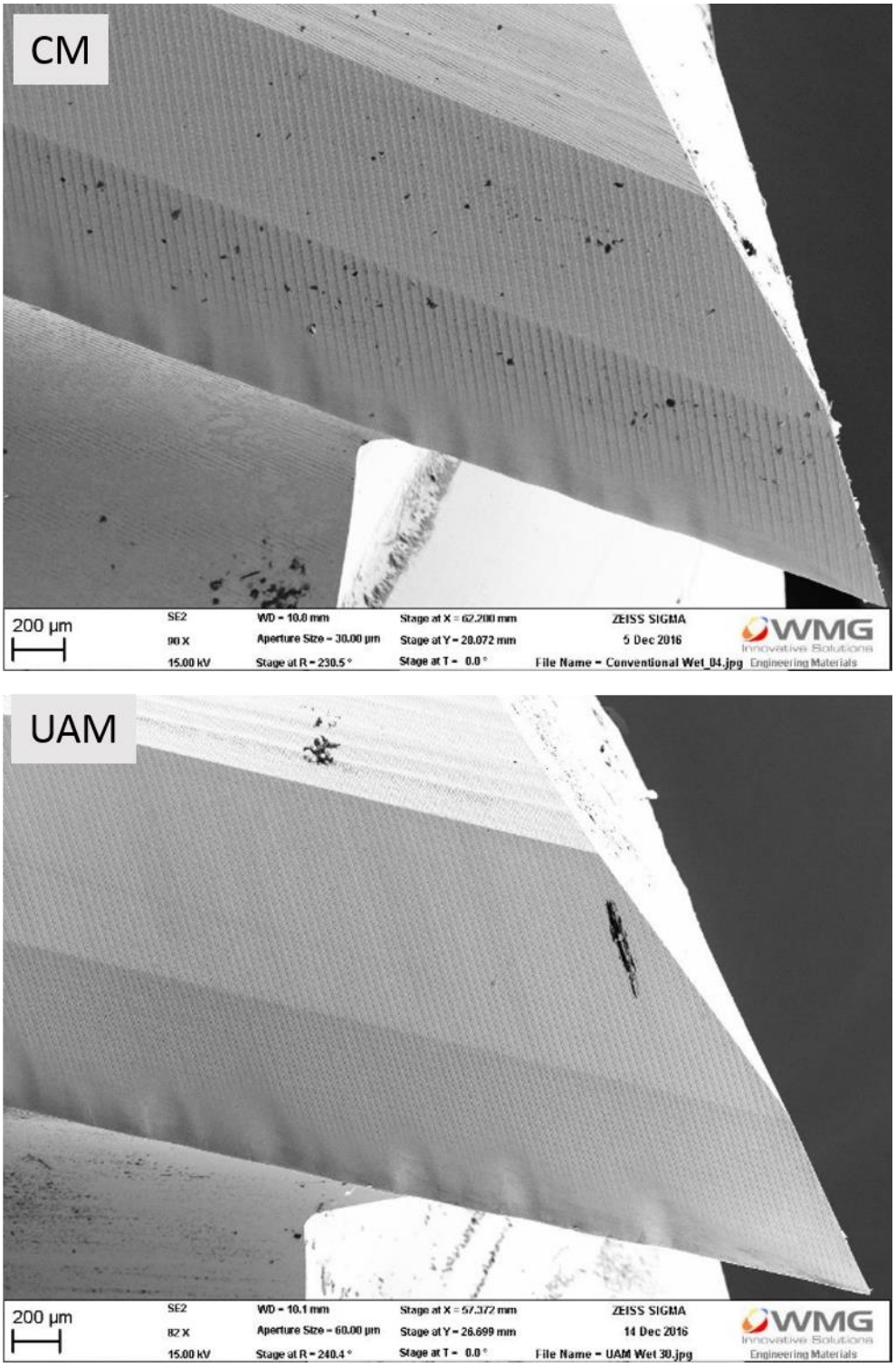

Figure 4-7: SEM micrographs of tungsten carbide end mill for (a) CM and (b) UAM in CCF environment after 3000 mm machining length.

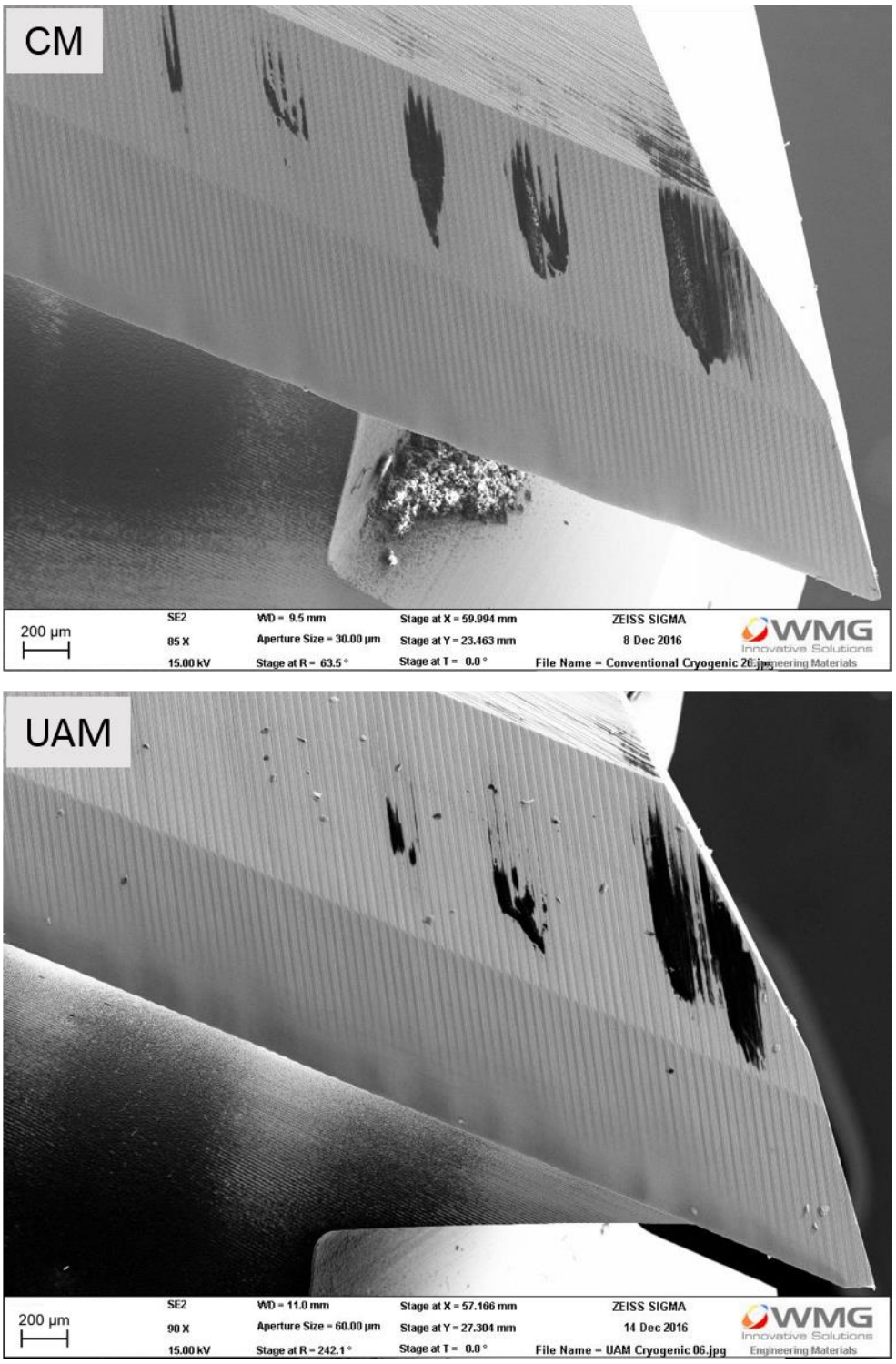

Figure 4-8: SEM micrographs of tungsten carbide end mill for (a) CM and (b) UAM in CO_2 environment after 3000 mm machining length.

When milling CFRP, the dominant tool wear mechanism in both CM and UAM with different machining environments (dry, CCF, and CO_2) was abrasive wear at the cutting edge. It was also observed the serrated surface of the cutting edges and the formation of scar on the flank surface. Figure 4-9 (a) shows the cutting edge of the carbide end mill that was used for UAM in dry environment after 3000 mm machining length. It was observed that the tungsten carbide (WC) and the cobalt (Co) binder were removed from the tool surface, as shown in Figure 4-9 (b). The wear observed in the carbide cutting tool was mainly due to the rubbing mechanism that occurred between the clearance face of the cutting tool and the CFRP workpiece [67, 108, 109, 185]. The edges rounding at the cutting edge is the dominant effect when machining CFRP with the carbide cutting tool. Additionally, the rubbing action between the clearance face and the surfaces of the CFRP workpieces resulted in wear on the clearance face of the tool. This argument is supported by Figure 4-9 (a) that shows the edge rounding effect of the cutting edges after machining the CFRP over 3000 mm length.

Wear mechanism of the WC-Co end mill is summarised as follows:

a) The wear is initiated by the removal of Co binder, where the evidence of void with a size of less (< 0.8 μm) than the WC particle was found on the tool surface. The hardness of Co (H_{Co} = 400-1200 HV) that is lower than the WC (H_{WC}= 2100 HV) and the carbon fibre (H_{CF} = 800-1000 HV) eases removal during machining [52, 80, 108].
b) As the cutting progressed, the Co binder with the broken carbon fibre abraded the surface of the tool, which resulted in dislodged WC particles. Due to the naturally brittle characteristic of the WC particles, cracks and fractures of the WC particles were also observed, as shown in Figure 4-9 (b).

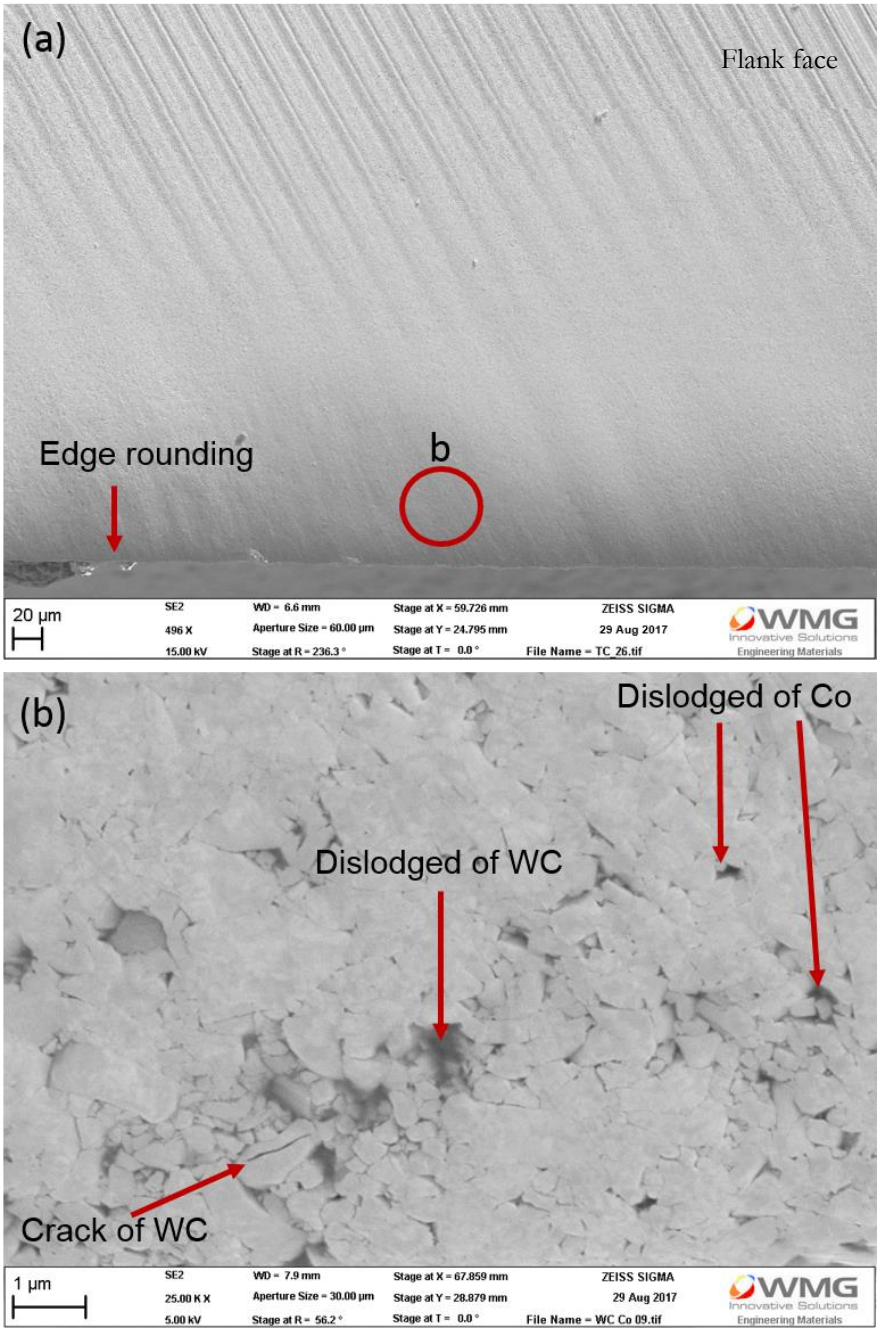

Figure 4-9: (a)SEM micrographs of worn end mill used for UAM dry after cutting 3000 mm of CFRP at cutting speed of 500 m/min and feed rate of 800 mm/min and (b) high magnification of SEM of 'b'.

From Figure 4-10, it was observed that the smooth surface of the cutting edges turn into serrated condition when it started to wear out. It was also observed that the wear scar (notch) formation on the flank surface of the cutting tool that was used form CM and UAM for all cutting environments. It is suggested that the serrated condition of the cutting edges and the wear scar on the cutting tool are due to the quasi-isotropic orientation of the carbon fibre. The distance for each scar on the cutting tool had been within the range of 450 to 630 μm. However, when comparing the distance between the scars on the cutting tool with the fibre orientation, there is no direct correlation between them. Although there was a claimed that the wear scar is apparent when machining 0 ° fibre orientation (parallel to the cutting direction) because of the compressive strength that was generated between the cutting tool and the workpiece materials [7, 137, 186]. The fibre tends to fail due to buckling mechanism, while the cutting tool was under a higher pressure against the hard fibres due to the feed motion [59, 133], therefore producing a wear scar on the cutting tool surface. However, there is no strong evidence which fibre orientation that caused the wear scar in this study.

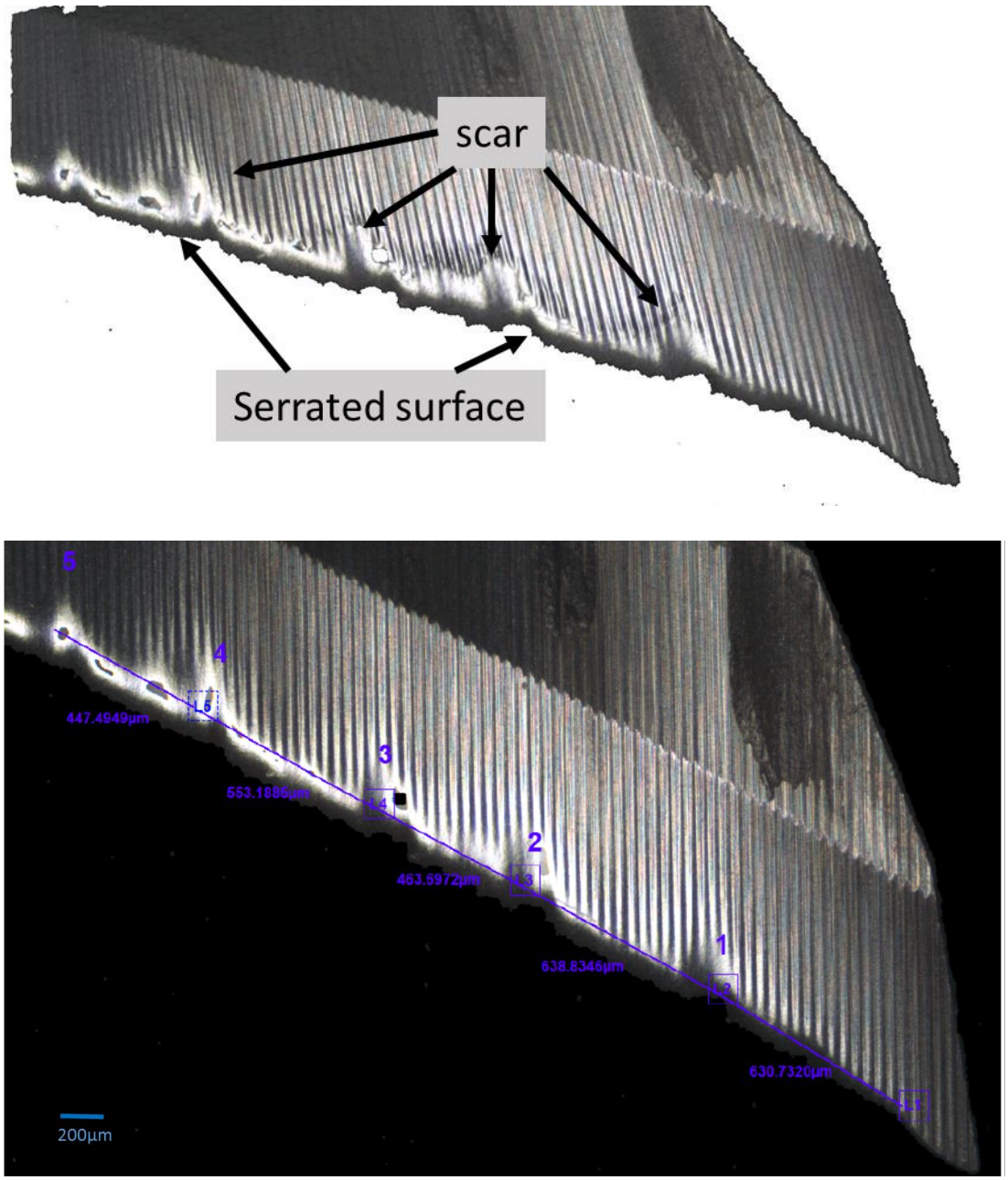

Figure 4-10: Cutting tool condition examined using Alicona surface profiler. The scanned image of the cutting tool indicated that the cutting edge of the cutting tool experienced 'segregated' and formation of scar on the cutting tool surface.

Interestingly, the wear scar (notch) appeared more apparent on the cutting tool in the CCF condition as the cutting fluid retained the strength of the CFRP. Meanwhile, as for dry and CO_2 environments, matrix softening induced by the generated heat aided in the reduction of the wear scar. In order to reduce the effect of fibre orientation on the scar formation, it is recommended to employ a lower cutting speed and the fibre orientation

should be less than 90 °. However, in the present study, constant cutting parameters were employed, and CFRP was fabricated based on industrial applications.

4.1.2 Cutting forces

The effects of different machining environments on the cutting forces for CM and UAM are presented in Figures 4-11 and 4-12. The error bars represent both maximum and minimum values of the recorded cutting forces. The feed force (Fx) and the normal force (Fy) increased as the machining length increased, as a result of the increasing tool wear. The cutting forces obtained from CM were higher by 16 to 35 % than the UAM for all machining environments.

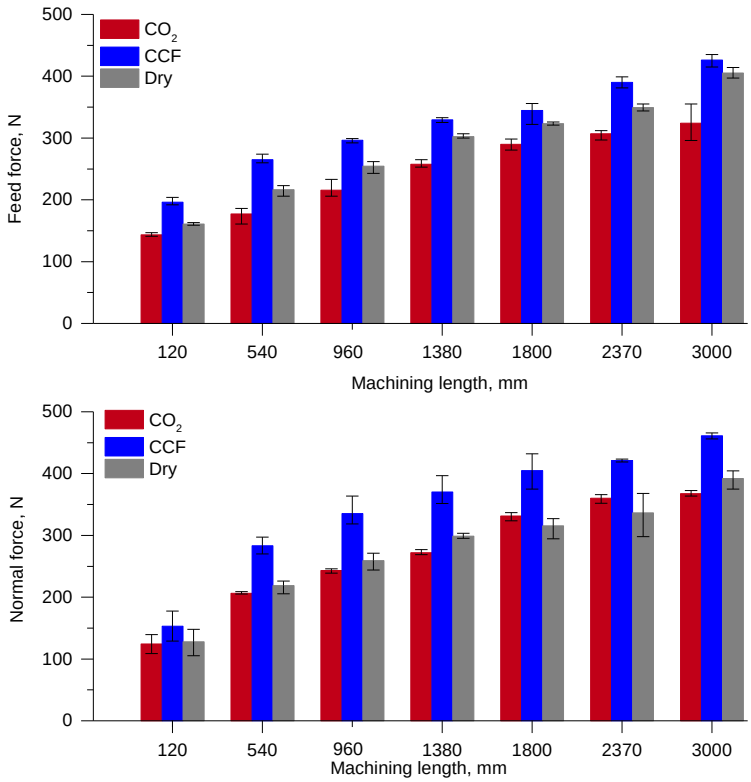

Figure 4-11: Feed force (Fx) and normal force (Fy) for CM over 3000 mm length.

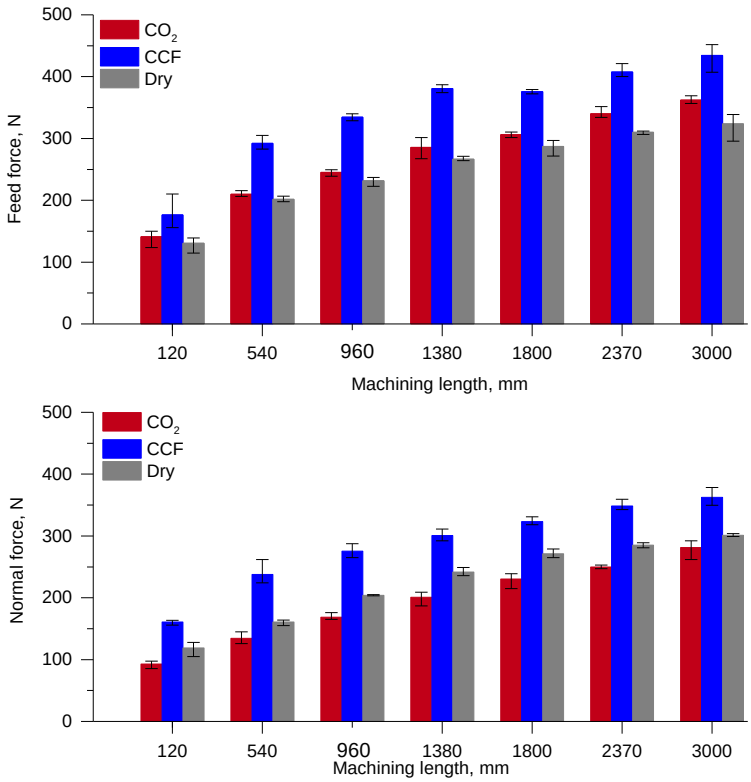

Figure 4-12: Feed force (Fx) and normal force (Fy) for UAM over 3000 mm length.

Table 4-3: Cutting forces for UAM and CM at 3000 mm machining length.

	Cutting forces	Dry	CCF	CO_2
CM	Fx, N	405	426	324
	Fy, N	391	461	367
UAM	Fx, N	301	362	281
	Fy, N	323	434	362

Table 4-3 tabulates both feed and normal forces for UAM and CM when milling at different machining conditions at 3000 mm machining length. The feed forces (Fx) for CM and UAM measured for CCF (426 and 362 N) were the highest, followed by dry (405 and 301 N), and CO_2 (324 and 281 N) machining, respectively. Meanwhile, cutting forces for UAM were the lowest when compared to CM for all machining environments. Although the tool wear recorded in CM were lower when compared with UAM (in Section 4.1.1), the cutting forces recorded for UAM were the lowest at all environments, in comparison to CM. This reduction of cutting forces in UAM is attributed to the cutting

mechanism of UAM. The vibration of the cutting tool in the z-direction that is perpendicular to the feed direction generated a hammering effect between the cutting tool and the workpiece. The ultrasonic vibration further aided in fracturing of the inherently brittle carbon fibre.

In addition, Figures 4-11 and 4-12 show that the cutting forces measured for dry and CO_2 have minimal variance, but both cutting forces are lower than that of CCF by 10-15 %. Although the cutting temperature slightly increased in CO_2, this cutting temperature aided in softening the matrix resin, hence resulting in lower cutting forces, when compared to CCF and dry conditions. As for dry machining, the cutting temperature was higher when compared to CO_2. Although high tool wear was generated in dry machining, the high cutting temperature softened the matrix resin, thus resulted in lower cutting force.

As for CCF, the continuous cooling of the cutting tool and the workpiece retained the strength of CFRP. This resulted in high cutting forces in CCF, when compared to CO_2 and dry machining environments. The effect of temperature on CFRP materials has been well discussed in the literature [83, 98, 100]. The tensile strength and the modulus of CFRP were found to decrease as the temperature increased. Previous study also reported that the residual and the mechanical stress of CFRP reduced as the temperature increased [98]. Thus, this explains the cutting forces for CO_2, CCF, and dry machining environments for both CM and UAM. Regarding machining environments, lower cutting forces were recorded with CO_2 (324 and 281 N, respectively) because the tool wear for CO_2 was lower, when compared to both dry and CCF machining.

Although tool wear condition for the cutting tool used in CCF machining was lower when compared with dry machining, the continuous cooling of the CFRP during the machining retained the strength of the materials [97, 120], which resulted in high cutting forces for

CCF machining. As discussed earlier in Section 4.1.1, the cutting temperature (60-120 °C) in CO_2 environment was lower, when compared to machining in the dry condition (100-200 °C). Nevertheless, the tool wear in dry machining condition was higher, in comparison to the CCF machining environment; the heat generation during the dry machining softened the matrix material, thus reducing the cutting forces in the dry machining. Therefore, high machining temperatures obtained in the dry machining softened the material properties and reduced the cutting forces, when compared to CCF machining. The strength of CFRP bond was reduced as the temperature increased. As mentioned by Katz et al. [30], as the temperature increased from 25 to 250 °C, the strength of CFRP reduced by 90 % of its initial strength. This is in agreement with the findings reported by Pecat et al. [81], where the workpiece temperature (120 °C) was found higher than the Tg (60 °C) of the epoxy, which softened CFRP, thermally degraded matrix resin, and caused visible damages on the subsurface up to 500 μm underneath.

4.1.3 Surface roughness

The average of the surface roughness, Ra, for CM and UAM in different machining conditions (dry, CCF, and CO_2 cryogenic) are plotted in Figures 4-13 (a) and (b), respectively. The error bars represent both maximum and minimum value of the Ra measured. The surface roughness for CM was lower than that for UAM in all machining environments. Both CM and UAM demonstrated a similar pattern of surface roughness, where the surface roughness increased as the machining length increased. Table 4-4 presents the Ra for CM and UAM in different cutting environments at 500 and 3000 mm machining length.

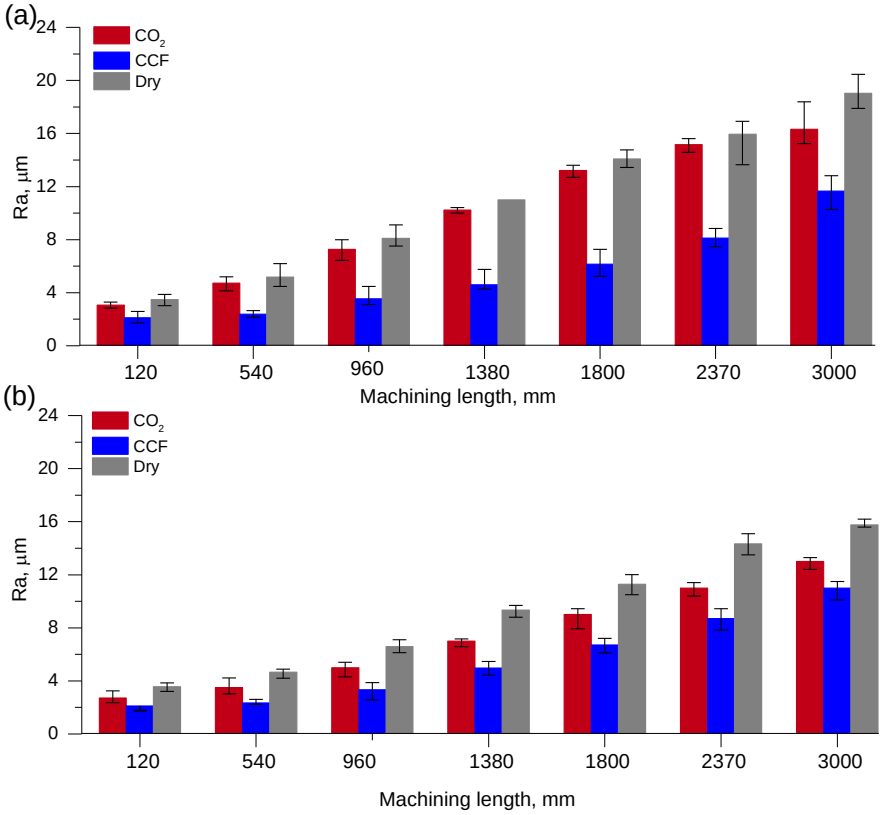

Figure 4-13: Average surface roughness, Ra for (a) CM and (b) UAM over 3000 mm length

Table 4-4: Ra for CM and UAM at 500 and 3000 mm machining length in the different cutting environment

		Ra, µm		
	Environments / **Cutting length, mm**	**Dry**	**CCF**	**CO_2**
CM	540	4.6	2.3	3.5
	3000	15.7	11	13
UAM	540	5.2	2.4	4.7
	3000	19	12	17

When compared in terms of process, Figure 4-14 shows that UAM exhibits higher surface roughness, as compared to CM for all machining environments. The average surface roughness obtained by UAM was 10 to 30 % higher than CM for all machining environments. The increase of surface roughness is associated to the progression of tool wear and cutting force during machining. This finding is a reasonable evidence to support

the correlation between tool wear, cutting temperature, and cutting forces when milling CFRP in different machining environments.

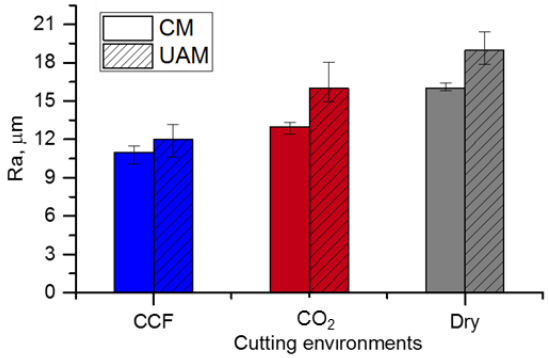

Figure 4-14: Surface roughness of machined CFRP surface at 3000 mm for CM and UAM in different cutting environments.

The surface roughness measured for both CM and UAM in dry environments were 17-30 % and 11-36 % higher, when compared to CO_2 and CCF environments, respectively. The CCF machining environment enhanced the surface roughness, when compared to both dry and CO_2 machining environments. This finding is attributed to the progression of tool wear and cutting forces. As discussed in Sections 4.1.1 and 4.1.2, the progression of tool wear and cutting forces when milling CFRP depends on the cutting environment. The increase in tool wear in dry machining resulted in the increasing cutting temperature. As mentioned earlier, the strength of CFRP is reduced as the cutting temperature increases. As a result, the dry machined surface is prone to fibre pull out, matrix cracking, and matrix smearing.

As for CCF, the continuous cooling of the cutting tool and workpiece during machining resulted in enhanced surface roughness. Taking into consideration the cutting temperature in CCF, which is within the range of 25 to 35 °C, the matrix resin strongly holds the carbon fibre since the effect of matrix softening is insignificant. Moreover, the presence of cutting fluid aided chip removal in CCF. This trend is similar to that reported by Dahnel et al. [120], whereby surface roughness improved with CCF, when compared

to CO_2 and dry machining environments at CFRP milling. They also mentioned that the effect of CO_2 on surface roughness is insignificant, as compared to CCF, mainly because the CO_2 only cooled the cutting tool, while in CCF, the cutting fluid cooled both cutting tool and workpiece simultaneously.

However, the effect of tool wear and the cutting temperature on the dry machined surface is more apparent. At 3000 mm machining length, the Ra measured for dry UAM was 20 μm, while for CM was 16 μm. In machining the polymeric matrix composite, the high machining temperature would eventually reduce the cutting force due to the softened matrix materials. Nonetheless, at this stage, the softened matrix resin could not hold the fibre strongly, thus deteriorating the quality of machined surface. The softening of the matrix resin can also lead to fibre pull-out and fibre matrix de-bonding. Moreover, the strength of CFRP reduced as the machining temperature increased [30]. This explains the effect of machining environment (dry, CCF, and CO_2) on surface roughness for machined surfaces. This study also demonstrates that the surface roughness measured for UAM is higher than that of the CM for all machining environments. It should be noted that the cutting tool oscillation that is perpendicular to the feed direction in UAM, consequently, affected the surface roughness. Figures 4-15 and 4-16 illustrate the machined surfaces for dry, CCF, and CO_2 environments in CM and UAM, respectively. One can observe that the machined surface for all machining environments experienced fibre pull-out, matrix smearing, and fibre-matrix de-bonding on the machined surfaces.

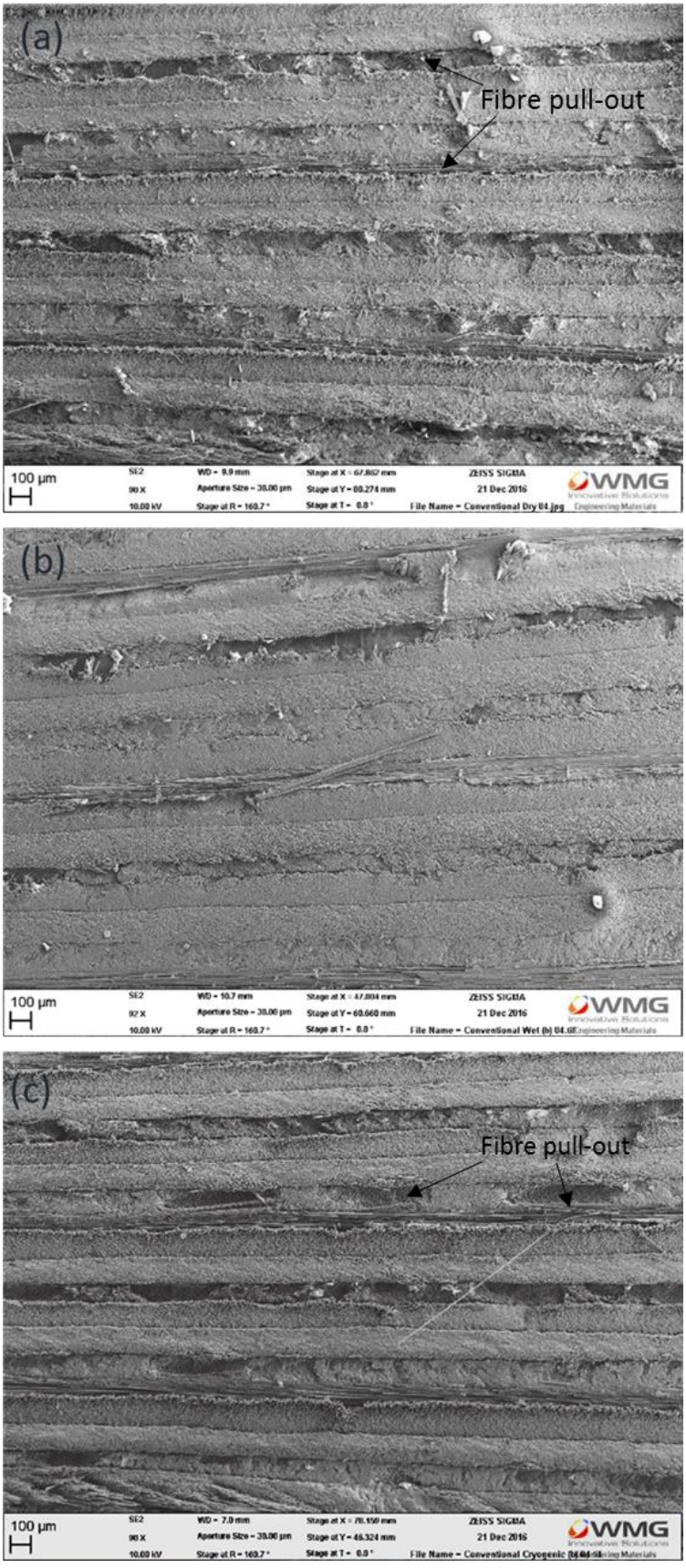

Figure 4-15: SEM micrographs of machined CFRP surface of CM in (a) dry, (b) CCF and (c) CO_2 environments at 3000 mm machining length.

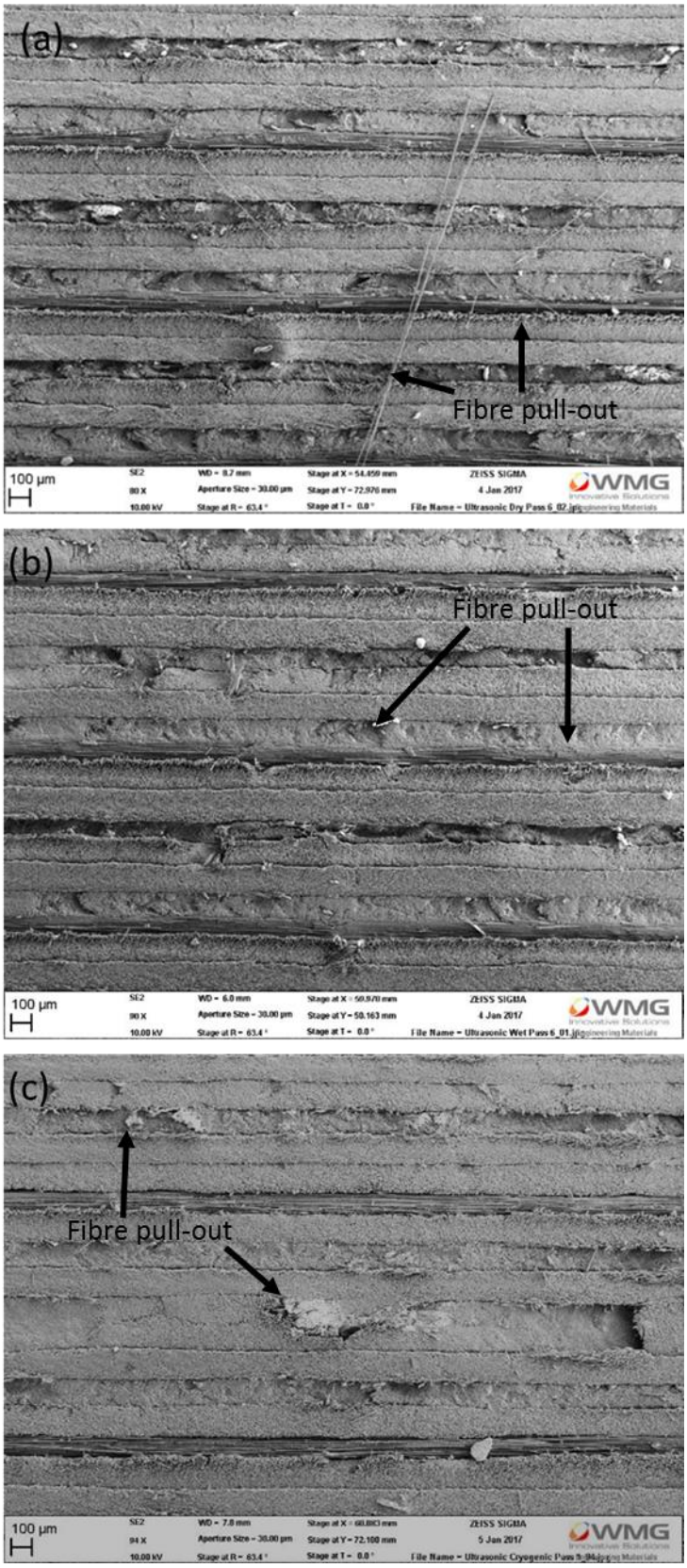

Figure 4-16: SEM micrographs of machined CFRP surface of UAM in (a) dry, (b) CCF and (c) CO_2 environments at 3000 mm machining length.

Next, Figures 4-17 and 4-18 exhibit the surface topography and the roughness profile for CM and UAM in dry environment, respectively. Whilst for CM and UAM in CCF and CO_2 machining environments, the surface topography and roughness profile are presented in Appendix C. The surface roughness profile for CM machined surface indicated that the profile height for the dry, CCF, and CO_2 cryogenic were between -70 and 50 µm, while the profile height for the UAM machined surface was higher, which was between -100 and 100 µm. As discussed before, ultrasonic vibration on cutting tools deteriorates the machined surface condition, thus, resulting in higher surface roughness in UAM, as compared to CM.

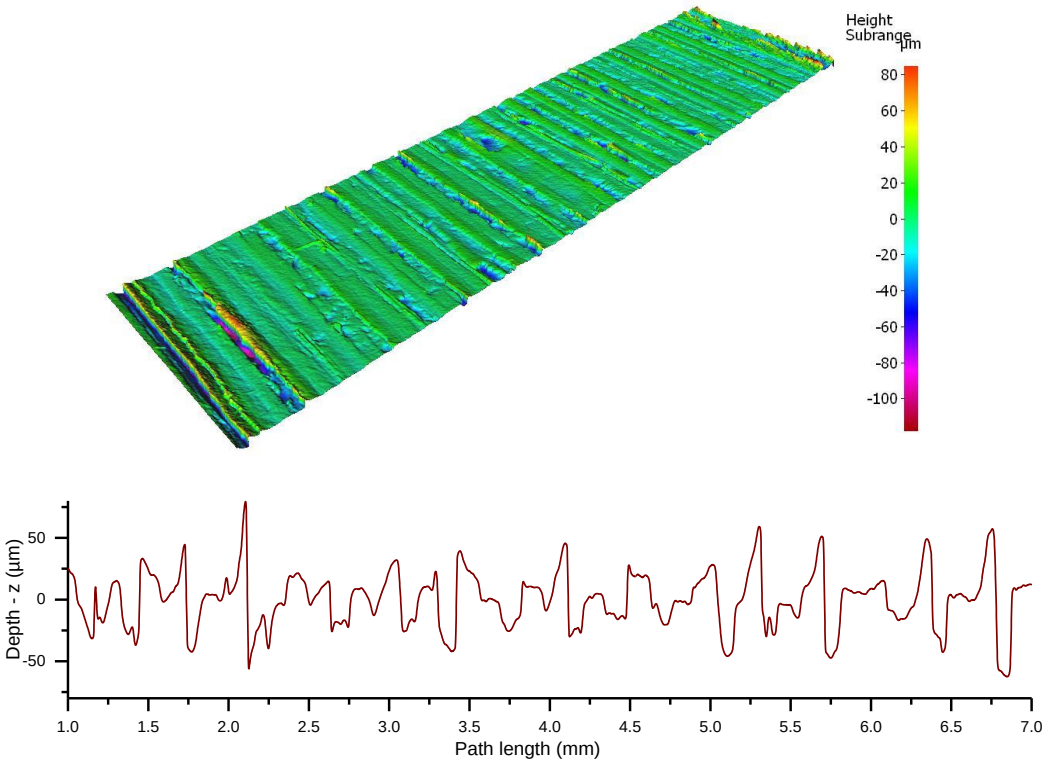

Figure 4-17: Machined surface topography and roughness profile for CM in dry environment machined surface taken in the Alicona with 5X magnification with Ra of 19.4 µm.

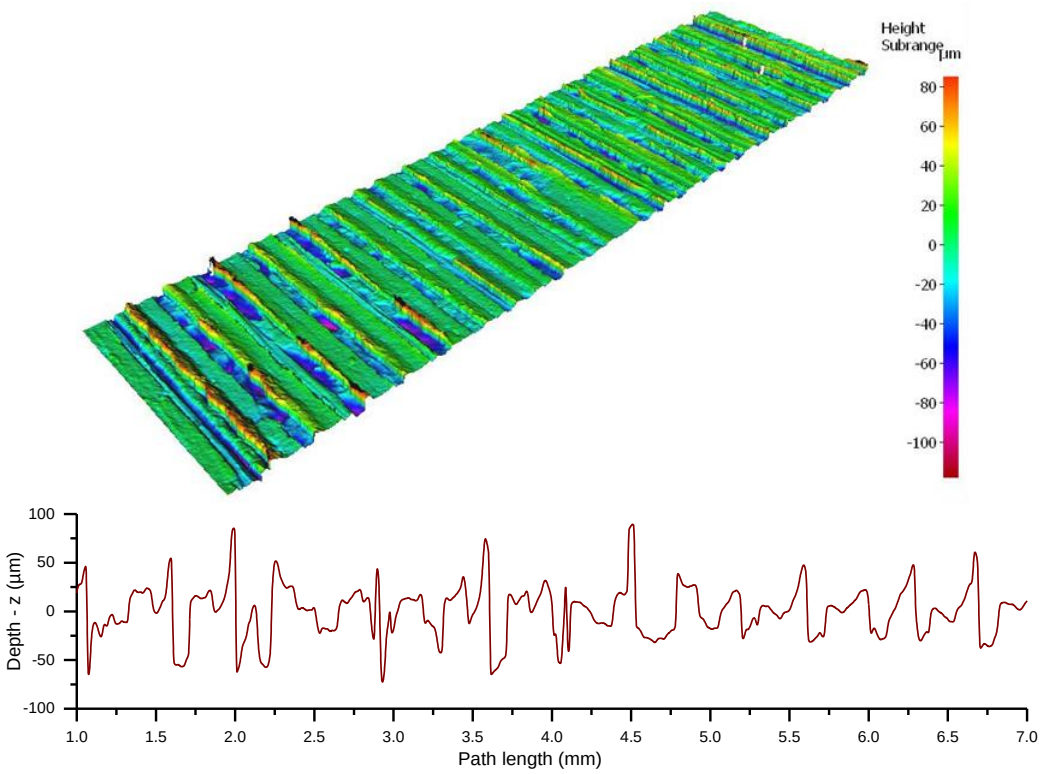

Figure 4-18: Machined surface topography and roughness profile for UAM in dry environment machined surface taken in the Alicona with 5X magnification with Ra of 19.3 µm.

4.1.4 Summary from Study 1(a)

Study 1(a) focused on investigating the effects of different cutting environments (dry, CCF, and CO_2) and processes (CM and UAM) on tool wear, cutting forces, and surface roughness. As such, several important findings can be drawn and are depicted in the following:

- The progression of tool wear for both CM and UAM displayed a similar trend when machining in dry, CCF, and CO_2 machining environments. The highest tool wear was obtained by the dry machining, followed by CCF and CO_2. High tool wear in the dry condition was observed due to the heat generated by the cutting tool, while the workpiece deteriorated the cutting tool. The cutting temperature recorded for the dry environment in UAM and CM are in between 120 and

200 °C, while CO_2 was between 60 and 120 °C and CCF was between 28 to 32 °C. The differences in cutting temperature may contribute to the progression of tool wear. As for CCF and CO_2, the presence of cutting fluid aided in heat removal, which enhanced tool wear.

- In terms of cutting force, the vibration of the cutting tool aided in fracturing the carbon fibre in UAM, which resulted in lower cutting force for UAM, in comparison to that for CM, in all machining environments. Although the tool wear in dry environment was higher than CCF and CO_2, heat generated between the cutting tool and the workpiece softened the matrix resin. Therefore, the cutting force in dry machining is lower due to reduction in material strength. In CCF, the flood cooling of the cutting tool and the workpiece materials retained the material strength. Therefore, the cutting forces in CCF had been observed to be higher.
- The surface roughness measured for UAM was higher than the CM for all machining environments could be attributed to the ultrasonic vibration that was perpendicular direction to the feed direction of the machining. Therefore, rougher surface was obtained in UAM, when compared to CM. However, the implementation of UAM, in this case, did not display any beneficial output to the machining outcome, as indicated in the milling process of CFRP. Conventional machining considerably helps to reduce the tool wear that occurs at the cutting edges. Therefore, in order to investigate the effect of the cutting environments on the machined surface, Study 1(b) was designed to explore the effect of cutting environments upon the machined surface. The machined surfaces from Study 1(a) were analysed by employing the DSC and FTIR analysis.

4.2 Study 1(b): Post machining analysis to understand the effect of machining environments on the machined CFRP surface

This study was designed to investigate the effects of machining environments (dry, CCF, and CO_2) on the shifts in chemical properties of the machined CFRP surfaces. The samples used in this study were taken from Study 1(a), and the sample preparation is as discussed in Section 3.3.5.3.

The DSC was employed to detect the changes that took place in Tg, while FTIR spectroscopy was applied to identify the changes that occurred in chemical properties of the CFRP, which consisted of Bismaleimide 5250-4 (BMI 5250-4) as the matrix resin. In addition, Thermogravimetric (TGA) and DSC analyses were performed on the pure sample of CFRP (un-machined) confirm that the method does not affect the properties of the CFRP. The methodology of the study is as discussed in Section 3.4.4.

Figure 4-19 presents the TGA curve for the pure sample, which indicates that the weight loss of the sample began at 350 °C. Therefore, the result from TGA indicates that the temperature range for DSC analysis of machined sample was from 25 to 350 °C. Next, Figure 4-20 displays the DSC curve of the powder sample for pure CFRP (un-machined) that remained at 272 °C, which indicates that the shaving method proposed in Section 3.3.5.3 did not have any affect upon the properties of the materials.

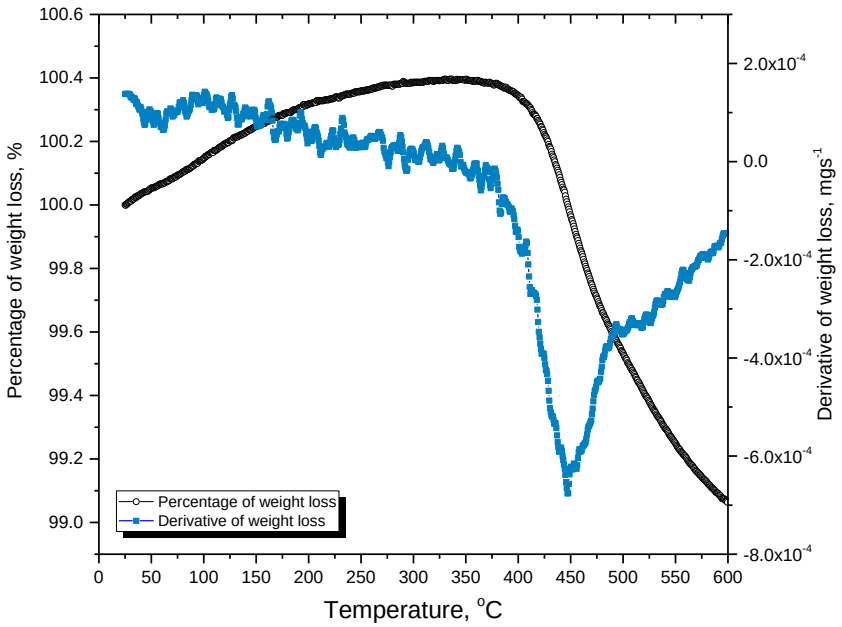

Figure 4-19: TGA analysis of a pure sample of CFRP consist of BMI 5250-4 as a matrix resin indicates that the weight loss starts at 350 °C.

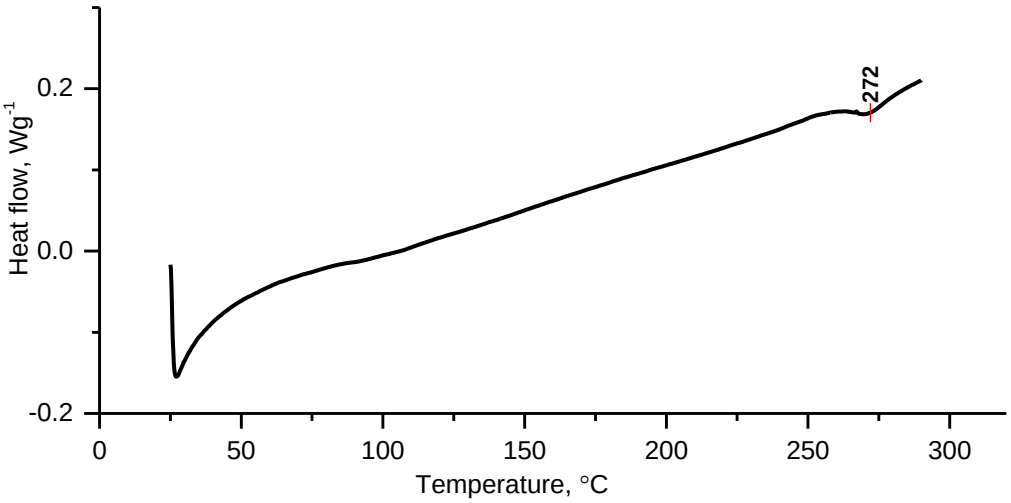

Figure 4-20: DSC analysis of pure sample of CFRP indicates the Tg for the BMI 5250-4 was at 272 °C.

4.2.1 DSC analysis of machined CFRP surface

The DSC analysis of the machined CFRP surfaces (all samples were taken at 3000 mm machining length) of CM and UAM for dry, CCF, and CO_2 machining environments is shown in Figures 4-21 and 4-22. The DSC analysis indicates that the Tg for the dry machining environment (at 3000 mm) of both CM and UAM had been shifted due to the high cutting temperature during machining. Nevertheless, the Tg of the machined surfaces of CM and UAM in CCF and CO_2 machining environments remained at 272 °C. This indicates that the cutting temperatures in CCF and CO_2 machining environments did not exceed the Tg of matrix resin, which could lead to the shift or elimination of the Tg.

Modification of the Tg at 272 °C for the machined surfaces of CM and UAM in dry condition (Figures 4-21(a) and 4-22(a)) from the DSC scan analysis indicates significant depolymerisation and chemical degradation of the material properties. The elimination of the Tg peak at 272 °C also suggests that the cutting temperature when machining via CM and UAM in dry condition exceeded 272 °C. However, the measured cutting temperature (180 - 200 °C) for the dry machining environment at 3000 mm length indicates that the temperature was below the Tg. This suggests that the cutting temperature recorded by the IR thermal camera is not the actual cutting temperature when machining CFRP as it is higher than the Tg. The shift in Tg further indicates the changes that took place in both chemical and mechanical properties of the thermoset over temperature [171].

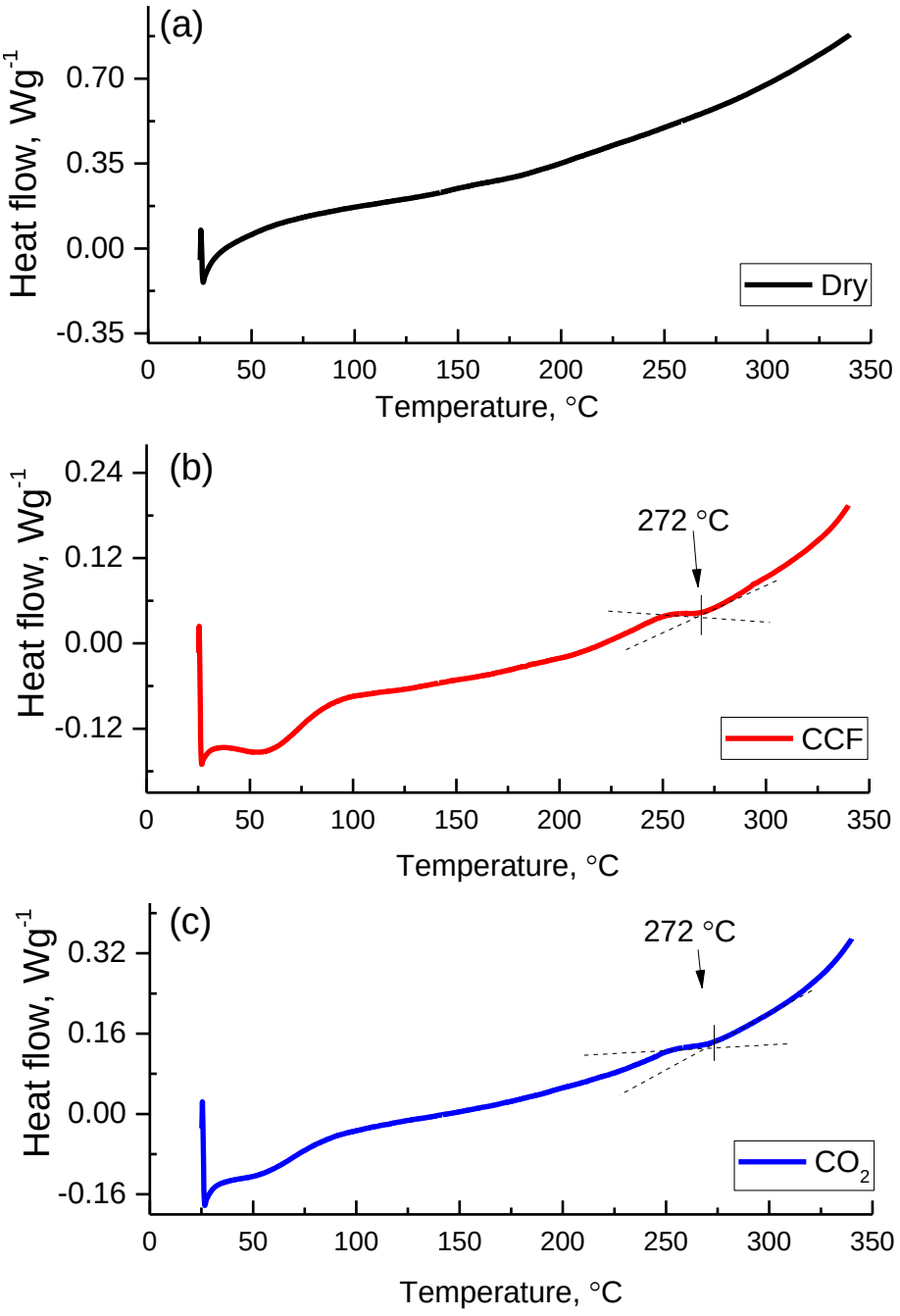

Figure 4-21: Differential scanning analysis (DSC) of CM machined surface at 3000 mm machining length with a heating rate of 10°C/min from 25 to 340 °C. Samples were taken from dry, CCF and CO_2 environments.

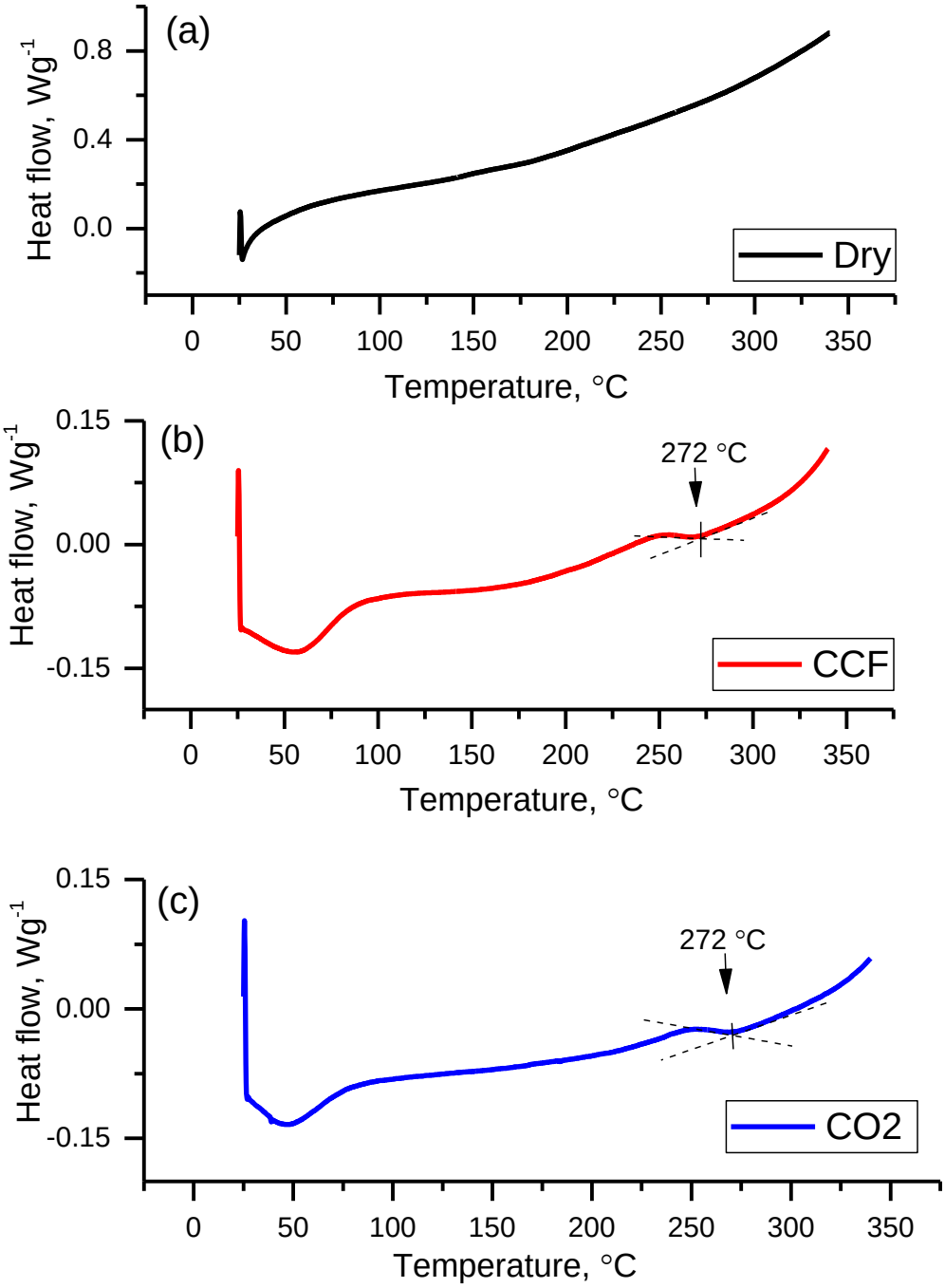

Figure 4-22: Differential scanning analysis (DSC) of UAM machined surface at 3000 mm machining length with a heating rate of 10°C/min from 25 to 340 °C. Samples were taken from dry, CCF and CO_2 environments.

This finding is also supported by the SEM micrograph for the dry machined surfaces, where apparent evidence of fibre pull-out and matrix smearing on the machined surfaces suggest that the material properties in CFRP did alter due to the high cutting temperature, as depicted in Figure 4-23. Similar works investigating the ageing of polymeric materials also observed the elimination of the Tg peak after ageing of the material occurred under certain conditions [35, 44, 45]. Therefore, the findings obtained in this present work demonstrate that the cutting temperature effects could yield a similar effect on the changes in material properties after machining. The variation in the Tg indicates that molecular changes do affect both mechanical and physical properties of the materials in various ways [45].

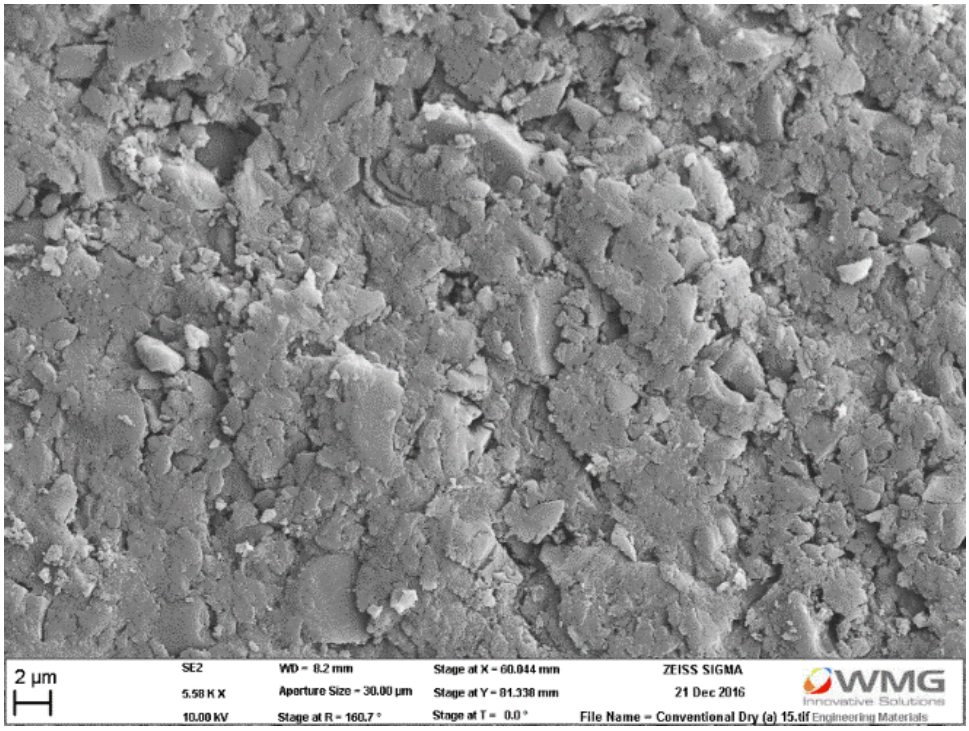

Figure 4-23: SEM micrograph of the CM machined surface in a dry environment indicate that the matrix was smeared and thermally degraded matrix resin was found on the machined surface.

4.2.2 FTIR analysis of machined CFRP surface

In an attempt to confirm that the cutting temperature and the machining environments do have a substantial effect on the BMI 5250-4 chemical bonding that also led to the elimination of Tg, FTIR analysis of machined CFRP surfaces was carried out. Table 4-5 presents the major absorption peak of the IR spectra for CFRP, and the assignment of each peak based on the available literature.

Table 4-5: Assignment of wavelength number of the CFRP with BMI 5250-4 resin by the FTIR analysis [14, 36, 38, 39, 41, 47, 171].

Wavelength (cm^{-1})	Definition / possible bonding for wavenumber
3700-3000	-OH hydroxyl functional group
2250	Aromatic nitrile C≡N
1583	Stretching vibration of C=C in benzene ring
1502	Stretching vibration of C=C in benzene ring
1470	Various aliphatic and imide, CH, CH_2, CH_3
1226	C-H
1143	Stretching vibration of C-O in benzene ring
1103	Symmetrical stretching vibration of C-O ring
825	maleimide C=C
686	C-H

The DSC analysis of the machined surfaces for CM and UAM in dry environment at 3000 mm machining length indicates that the changes in chemical properties occurred prior to the shift of the Tg. These changes could be attributed to the high cutting temperature induced by dry machining over CCF and CO_2 environments, which leads to alteration of chemical properties. The recorded cutting temperatures for CM and UAM of CFRP point out that the cutting temperatures were below the Tg, as portrayed in Figure 4-4. Nevertheless, the shifting of the Tg suggests that the actual cutting temperatures were higher than the values recorded, therefore, it is necessary to detect the

chemical bond changes that took place prior to that. Figures 4-29 to 4-34 illustrate the major peak absorption of the machined CFRP surfaces for CM and UAM in dry, CCF, and CO_2 environments, respectively. The IR absorption peaks for all machining environments showed similarity in shapes and positions of the bonds. However, in certain cases, the intensity of the peak differed, hence suggesting that the cutting temperature induced the chemical property changes of the BMI 5250-4 matrix resin. Based on Figures 4-24 to 4-29, the FTIR absorption peaks for dry, CCF, and CO_2 environments for CM and UAM display the comparable patterns of absorption.

Interestingly, in CM dry environment (sample was taken at 3000 mm machining length), an unusual peak was observed at the region of 2405 to 2233 cm^{-1}, thus suggesting the appearance of aromatic nitrile bond [36, 41, 187, 188] in the machined CFRP surface. However, this aromatic nitrile bond was not observed in CM (CCF and CO_2) and UAM (dry, CCF, and CO_2). Similar observation has been reported by [36, 41], indicating that the presence of aromatic nitrile bond is typically observed after pyrolysis of polymeric materials. Additionally, Regnier et al. [41] reported that thermal degradation of the BMI began from 400 °C to 600 °C to produce isocyanate-derived product, such as nitrile bonding. Therefore, this finding suggests that for machined CFRP surface in dry environment at 3000 mm machining length, the cutting temperature at the primary shear zone could exceed 400 °C to generate isocyanate-derived product. As such, the vibration of the cutting tool aided in removing the heat generated at the primary shear zone. This also suggests that the cutting mechanism in UAM aided heat removal between the cutting tool and the workpiece materials [6, 13, 154], thus reducing the degradation process of the machined surface. When compared to the machining conditions, i.e. CM and UAM, it was observed that machined CFRP surface does not give any substantial difference to the shift in chemical properties. However, as for the machining environments (dry, CCF,

and CO_2), a significant difference was noted in the chemical properties changes, where the intensity changes had been rather apparent.

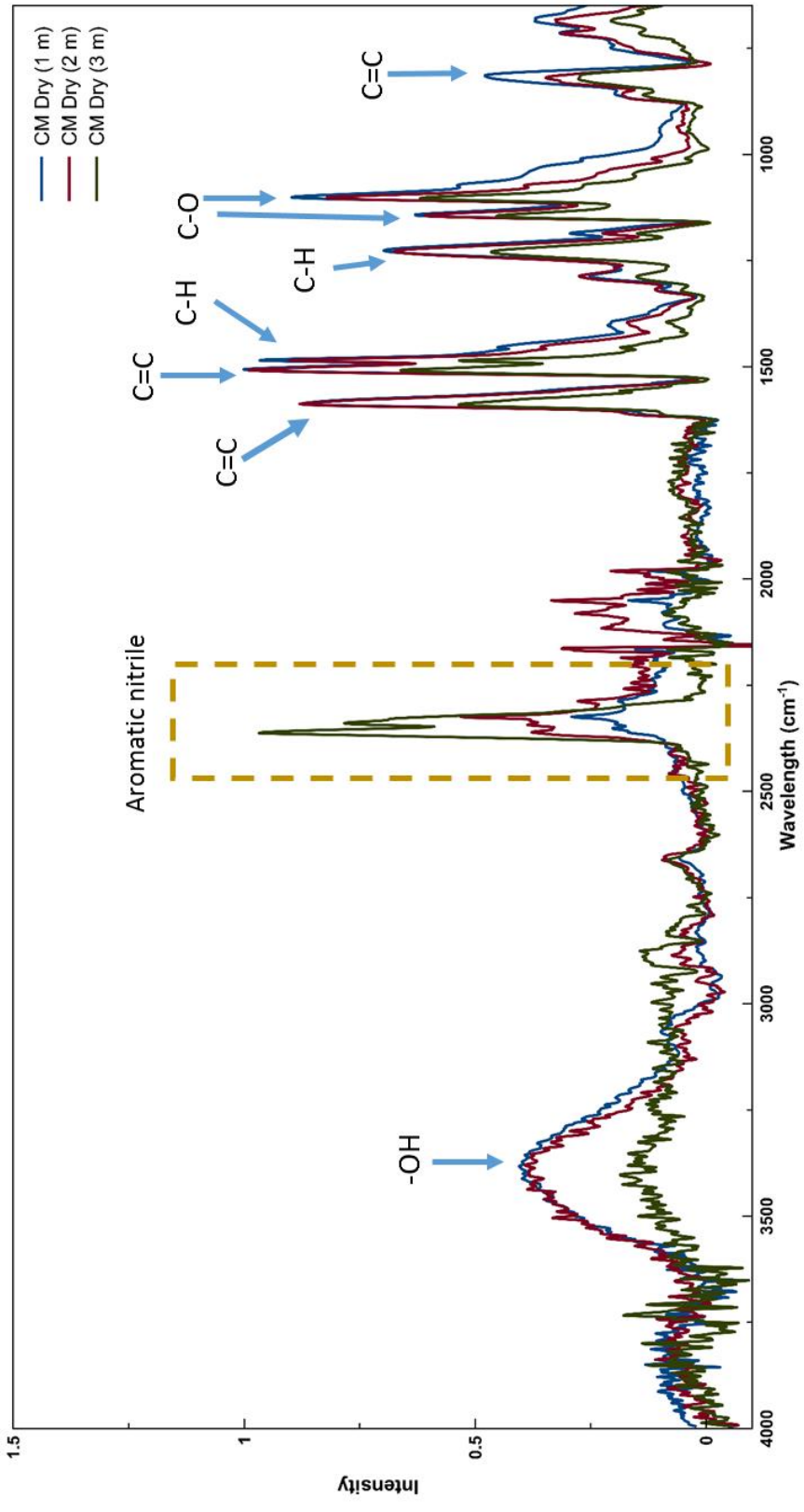

Figure 4-24: FTIR Spectra for machined CFRP surface for CM in dry environment from 4000 to 600 cm^{-1} for 3 m machining length.

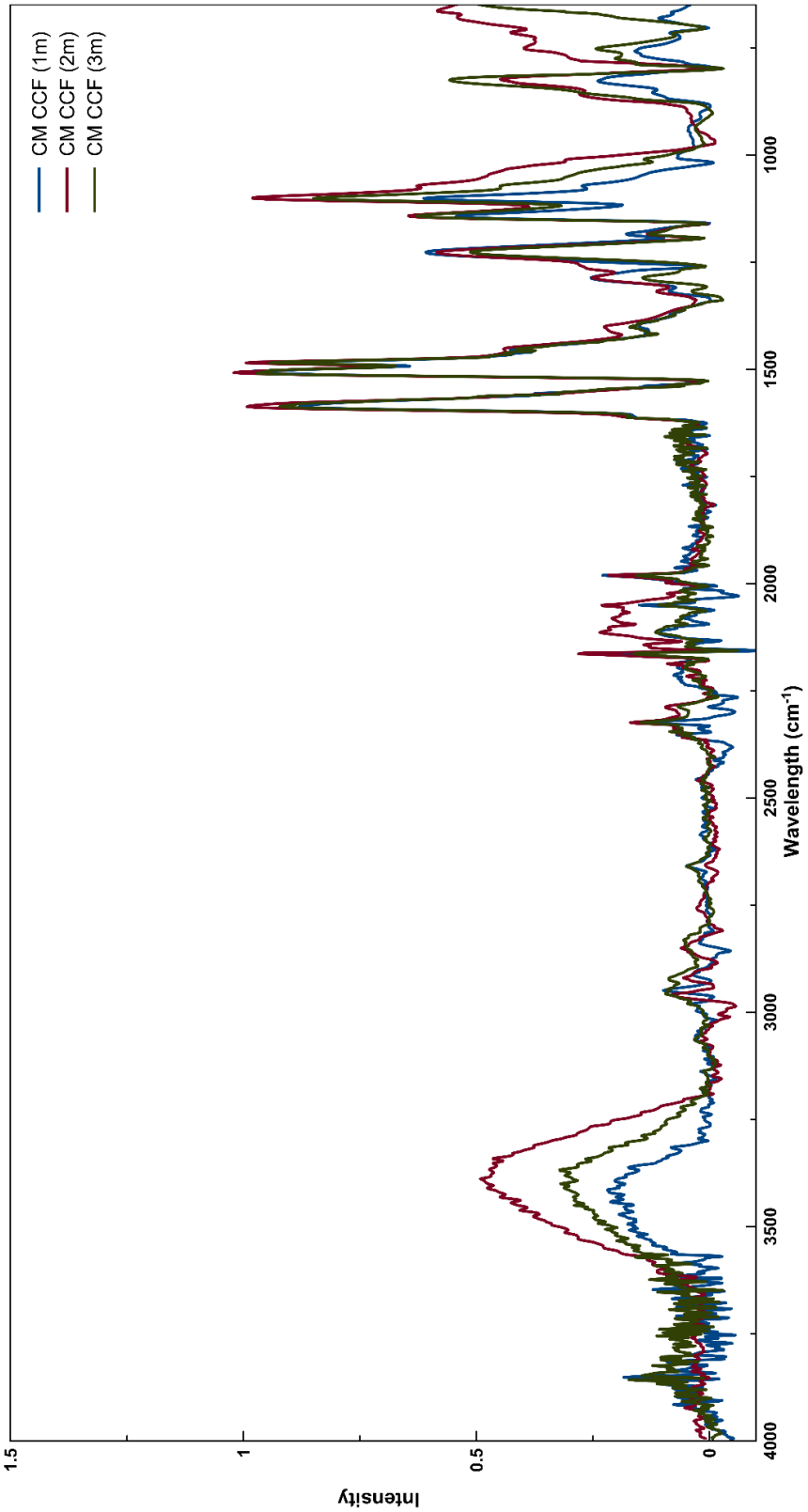

Figure 4-25: FTIR Spectra for machined CFRP surface for CM in CCF environment from 4000 to 600 cm^{-1} for 3 m machining length.

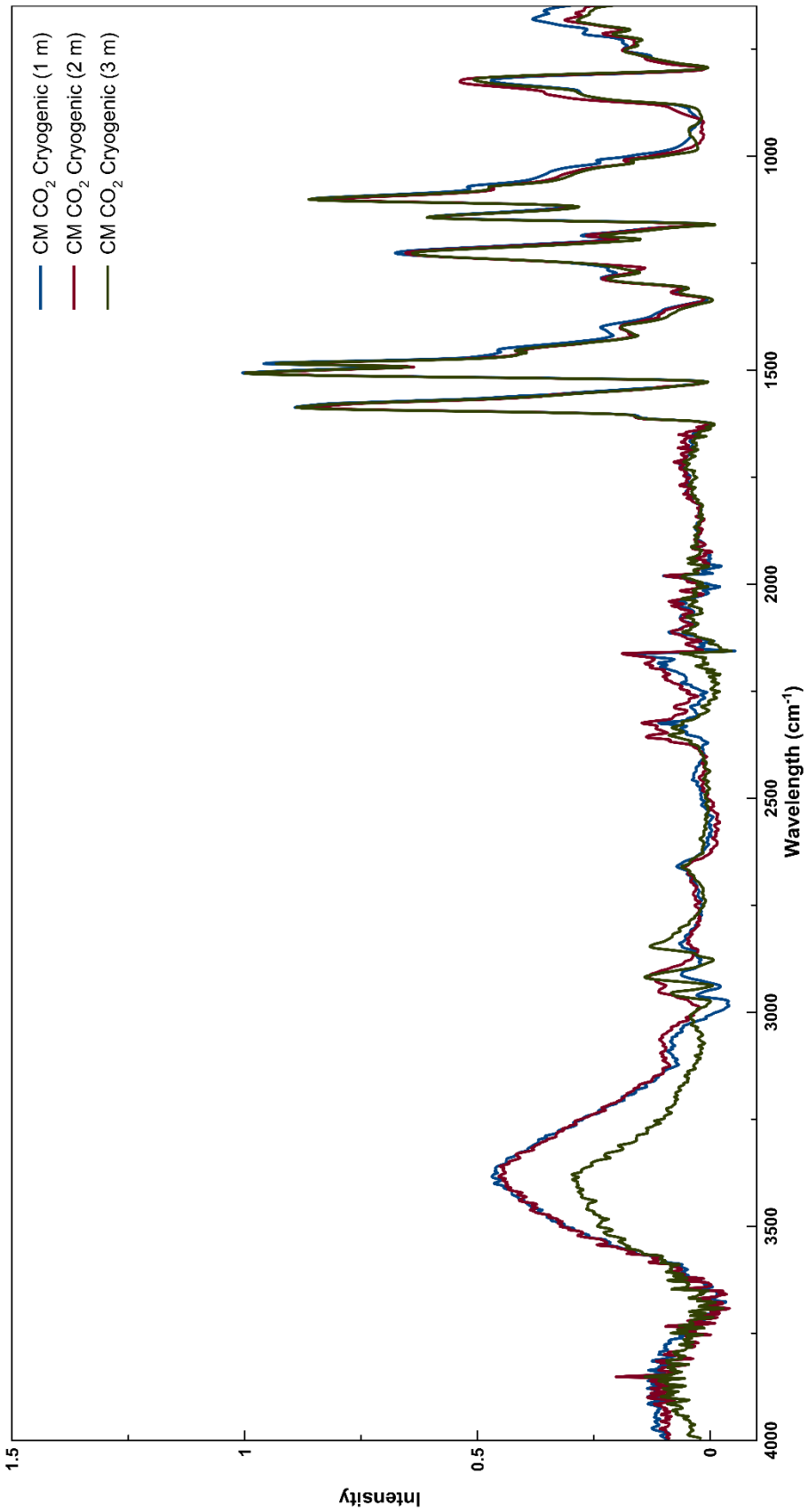

Figure 4-26: FTIR Spectra for machined CFRP surface for CM in CO_2 environment from 4000 to 600 cm^{-1} for 3 m machining length.

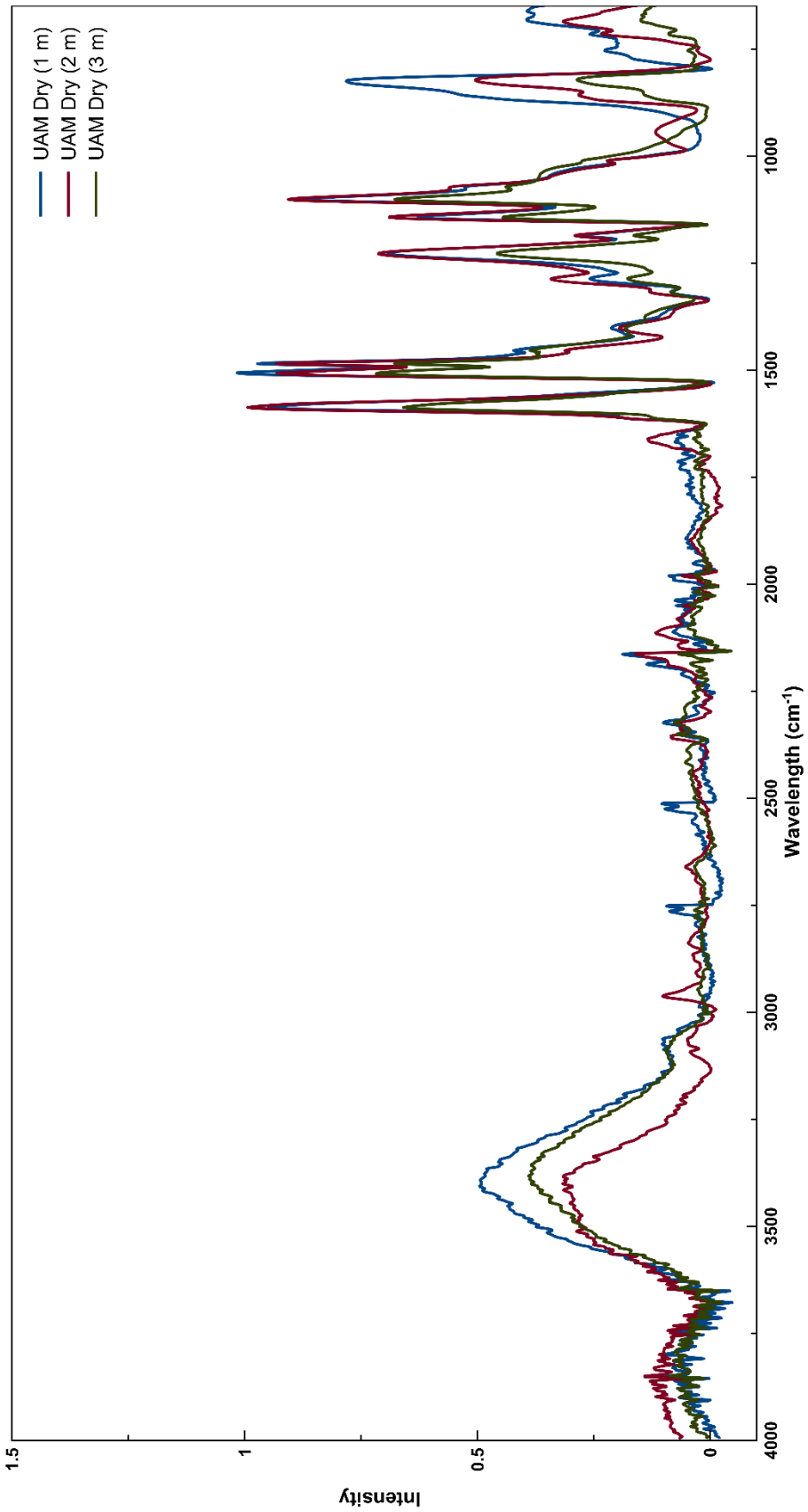

Figure 4-27: FTIR Spectra for machined CFRP surface for UAM in dry environment from 4000 to 600 cm^{-1} for 3 m machining length.

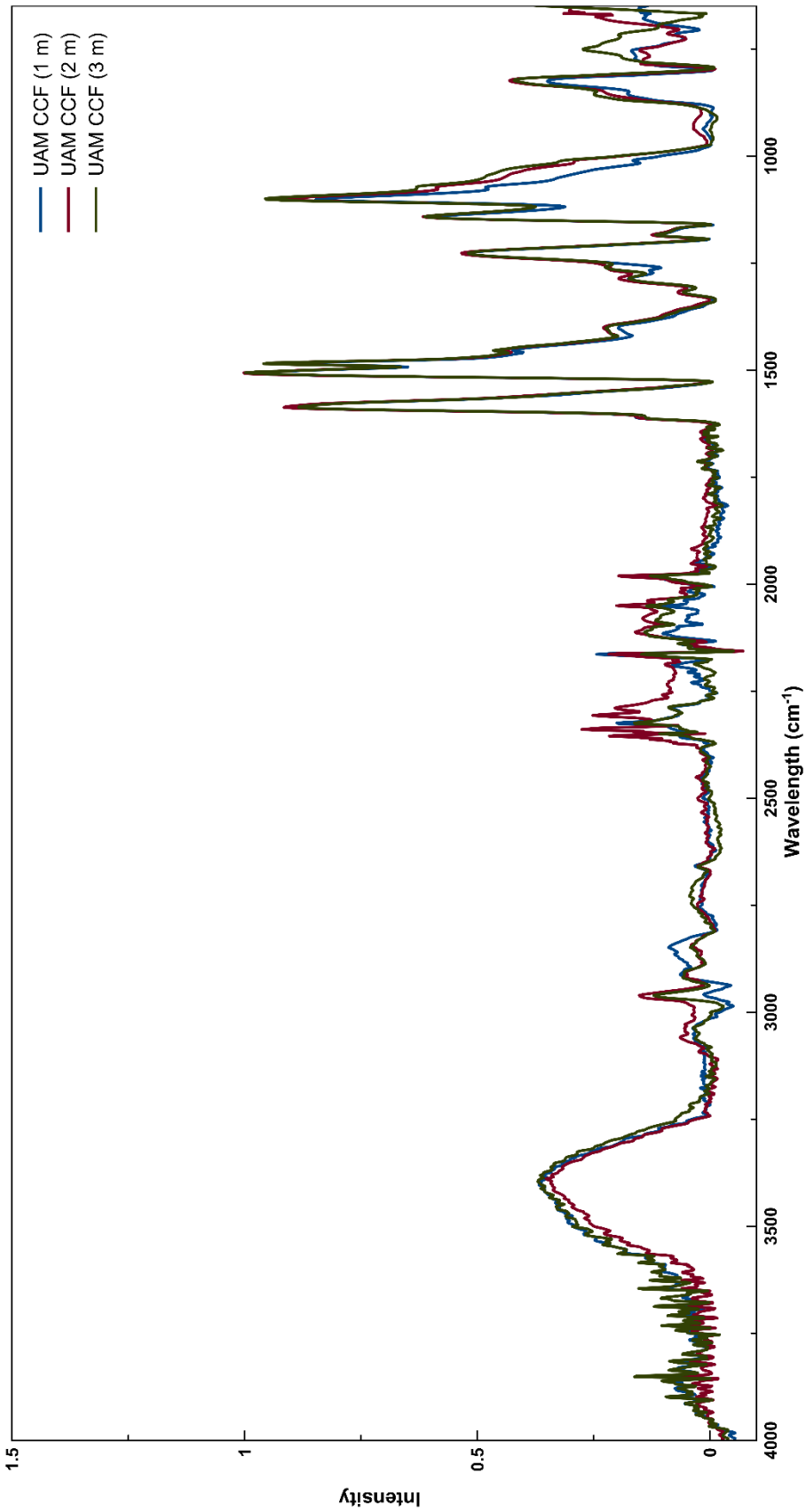

Figure 4-28: FTIR spectra for machined CFRP surface for UAM in CCF environment from 4000 to 600 cm^{-1} for 3 m machining length.

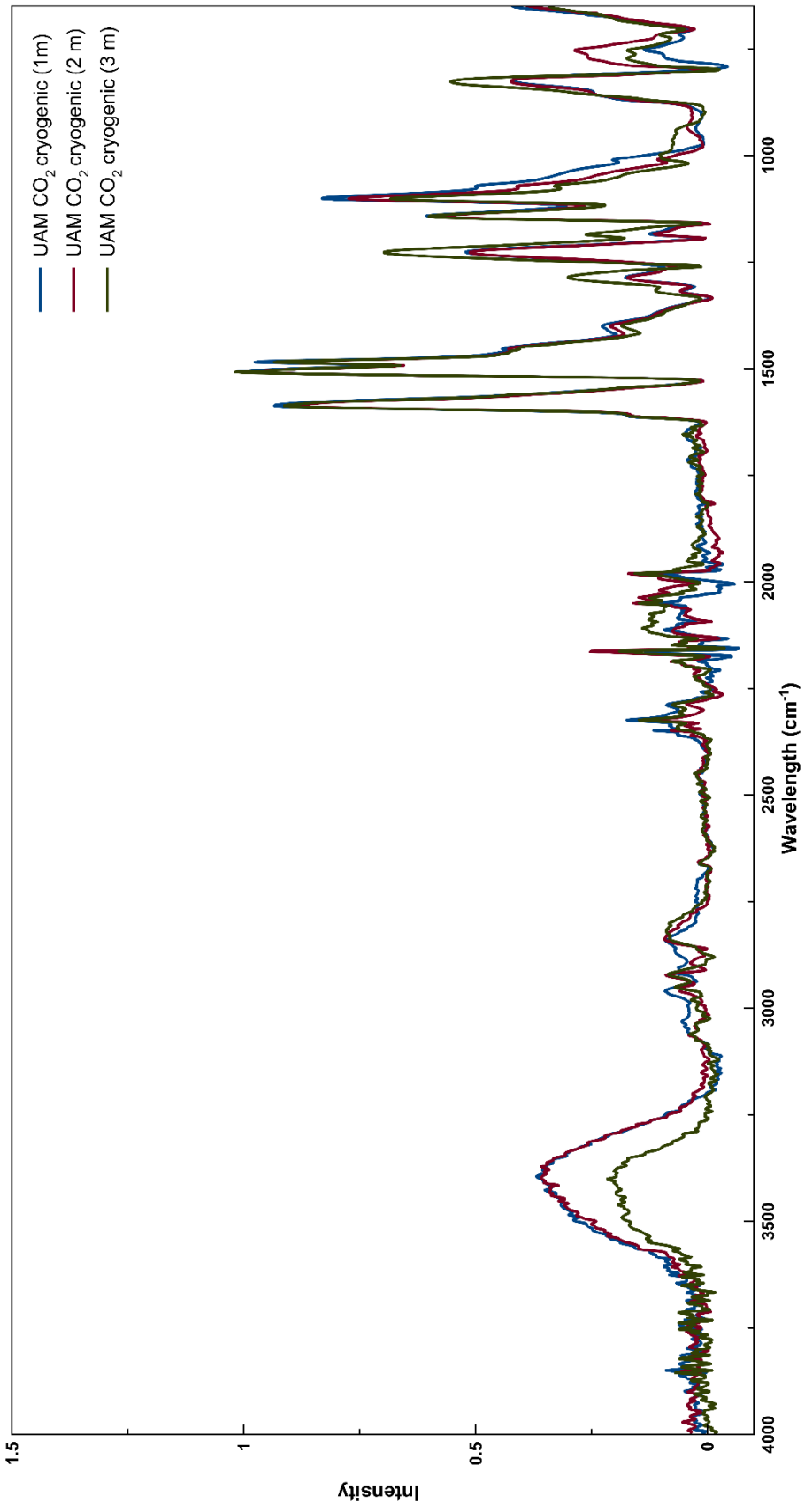

Figure 4-29: FTIR spectra for machined CFRP surface for UAM in CO_2 environment from 4000 to 600 cm^{-1} for 3 m machining length.

4.2.2.1 Region of 3700 cm^{-1} to 3000 cm^{-1}

In the region between 3700 and 3000 cm^{-1}, the formation of hydroxyl (–OH) functional groups had been noticed. The broad wavelength spectra centred at 3400 cm^{-1} of –OH were observed. Figure 4-30 illustrates the -OH region from 3700 to 3000 cm^{-1} for CM (a-c) and UAM (d-f) in dry, CCF, and CO_2 environments, respectively. Significant reduction of the -OH intensity was clearly observed in the conventional dry machining, as compared to CCF and CO_2 machining environments. The formation of -OH is expected due to the post-curing mechanism of the BMI resin system. Nonetheless, the changes in the intensity of -OH, when comparing the different machining environments, were not obvious. This can be attributed to the cutting temperature effect, which is not continuous on the CFRP that could generate the thermal oxidative effect upon the machined CFRP surfaces. Moreover, a prior study on the curing mechanism of CFRP that consisted of BMI resin mentioned that the formation of –OH (at the wavelength of 3473 cm^{-1}) can be linked to ether crosslinks via hydration over a 10-hour period [14].

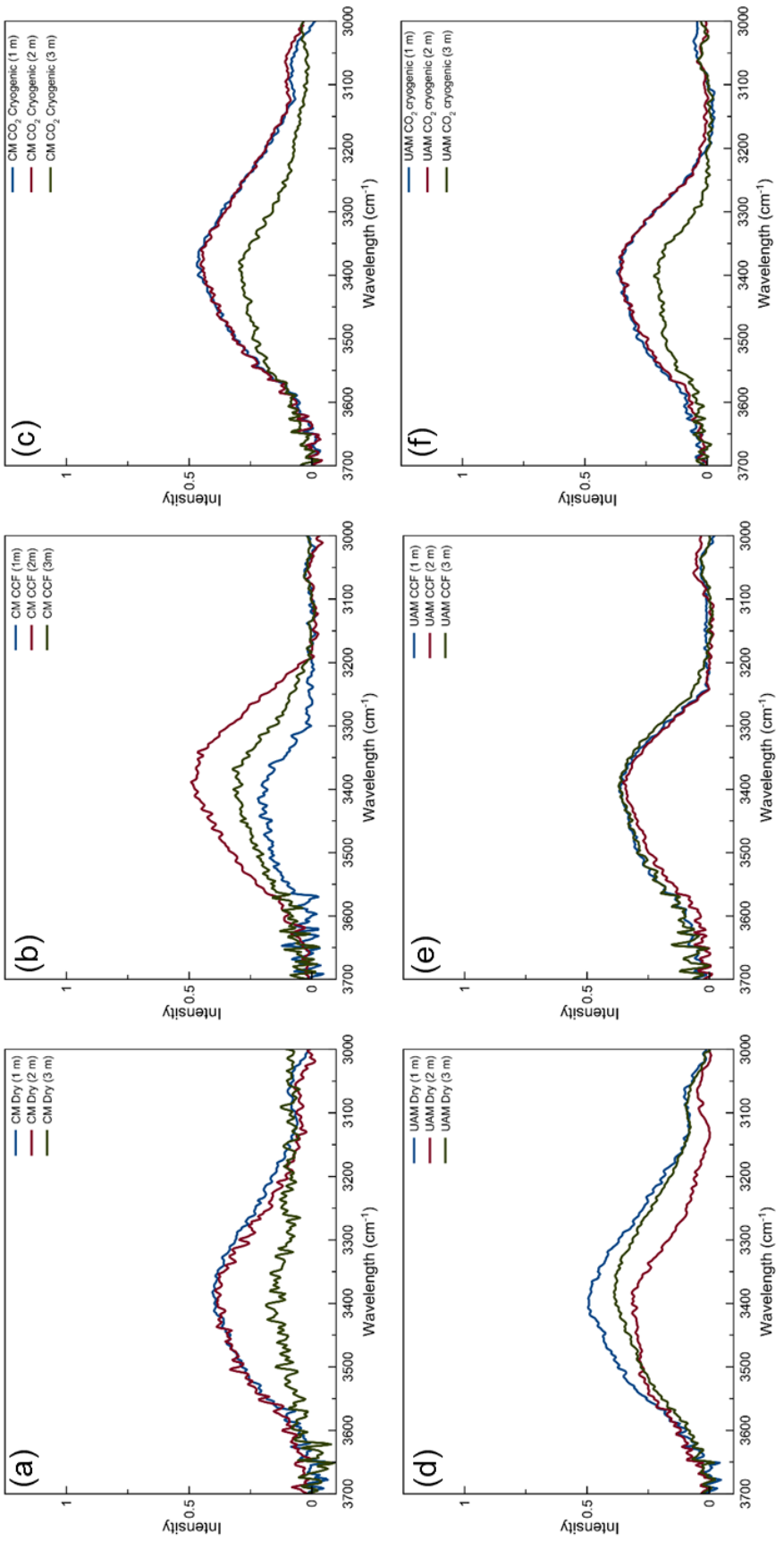

Figure 4-30: Changes in intensity for a region of 3700 to 3000 cm^{-1} for conventional (a-c) and ultrasonic assisted milling (d-e).

4.2.2.2 Region of 1700 cm^{-1} to 1300 cm^{-1}

Figures 4-31 (a) to (f) display the region of three peaks between wavenumber 1583 cm^{-1} and 1502 cm^{-1} (stretching of C=C in benzene ring), as well as 1470 cm^{-1} (various aliphatic and imide). CM and UAM machined CFRP surfaces for dry machining environment, as portrayed in Figures 4-36 (a) and (d), exemplify the reduction of the intensity of peaks from 1 to 3 m machining length. In contrast, the peaks for CM and UAM in CCF and CO_2 machining (Figures 4-31 b, c, e, and f) are consistent. Hence, no substantial variance could be found in the intensities of CCF and CO_2 machining environments, as illustrated in those figures. The increased cutting temperature over the machining length reduced the intensity of carbon-carbon double bond (C=C) in the dry machining environment for both machined CFRP surfaces of CM and UAM. The reduction of the intensity of C=C can be explained by further post-curing effect to the materials in dry environment. On the other hand, the intensities in CCF and CO_2 cryogenic environments remained unchanged.

This finding is in agreement with the results reported by Morgan [14] and Khatjeh [16], where they pointed out that the curing mechanism occurs at three C=C. However, the curing is not apparent in phenyl and ally, where C=C can be noted. The consistency of the peak intensities for CCF and CO_2 cryogenic conditions for both CM and UAM can be explained by the cutting temperatures measured, which are lower than the Tg during the machining operation. Thus, the post-curing effect at the peaks of 1583, 1502, and 1470 cm^{-1} for CCF and CO_2 cryogenic machined CFRP surfaces does not occur. In addition, Dao et al. [171] asserted that the reduction of intensity at ≈1502-1511 cm^{-1} signifies that the BMI has experienced ageing.

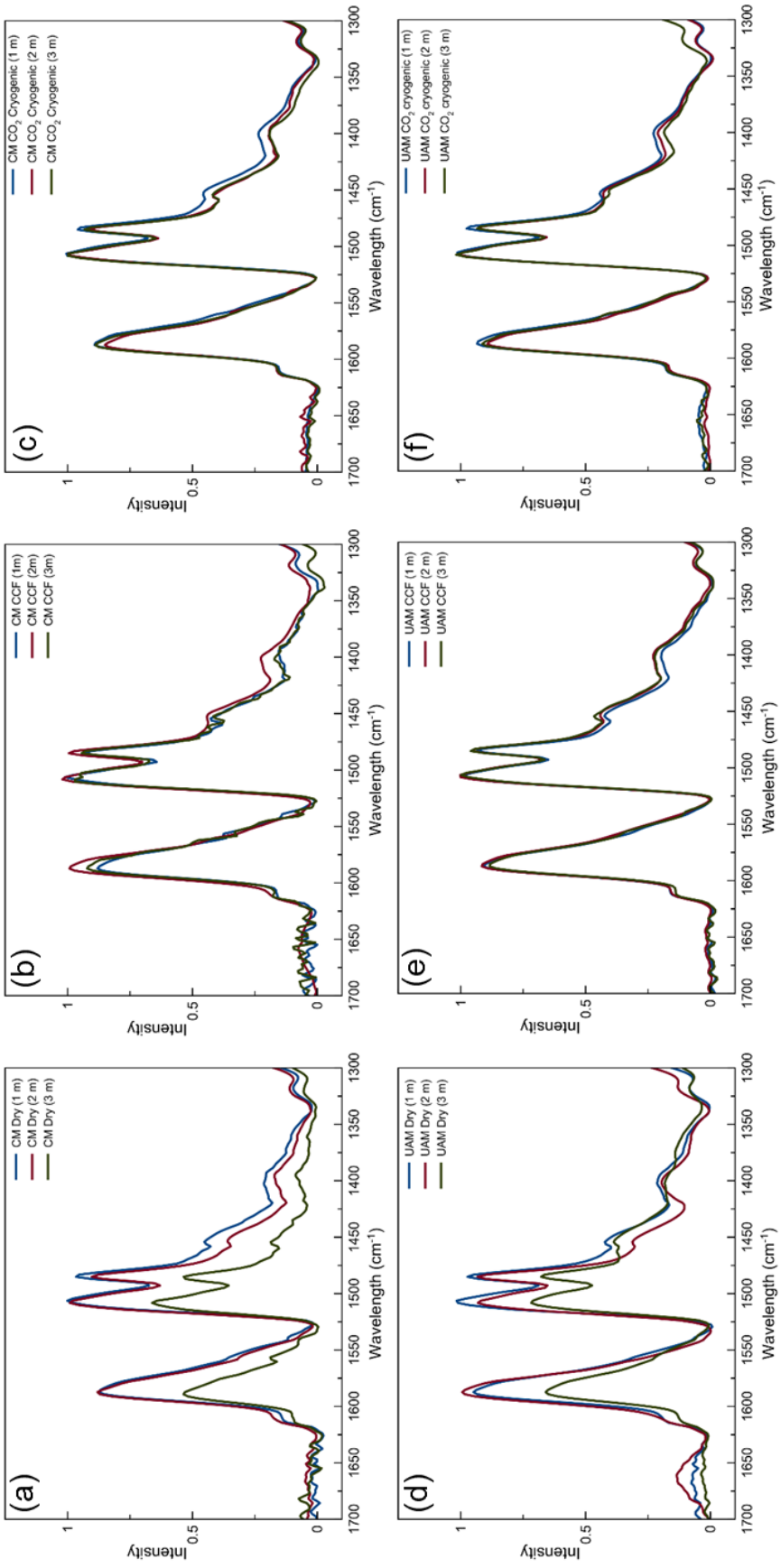

Figure 4-31: Changes in intensity for a region of 1700 to 1300 cm-1 for conventional (a-c) and ultrasonic assisted milling (d-e).

4.2.2.3 Region of 1300 cm^{-1} to 1000 cm^{-1}

Figures 4-32 (a) to (f) indicate the peak in the region between 1300 cm^{-1} and 1000 cm^{-1} for CM and UAM in different machining conditions, which are dry, CCF, and CO_2 cryogenic. The peak at 1226 cm^{-1} indicates the carbon-hydrogen (C-H) bonding, while peaks at 1143 cm^{-1} and 1103 cm^{-1} are attributed to the symmetrical stretching vibration of the carbon-oxygen (C-O) in the benzene ring. Moreover, the pattern of the intensity of the peak shows that the CM and UAM project a similar pattern in the decrease of peak for dry and CO_2 cryogenic conditions. However, the peak intensity for CCF machining condition shows increased intensity at 1103 cm^{-1}. Significant changes of the peak intensity from 1 to 3 m machining length of the machined surfaces for CM and UAM CFRP samples are presented in Figures 4-32 (a) and (d). The intensities of the C-O peaks for CM and UAM dry decreased as the machining length increased. This can be attributed to the increase in the cutting temperature from 100 to 220 °C as the machining length increases. The intensity of the peaks at 1226 cm^{-1} for CCF and CO_2 cryogenic machining conditions for both CM and UAM shows the consistency of the peaks throughout the machining length. However, for the dry machining condition for both CM and UAM, a reduction in C-O intensity can be observed.

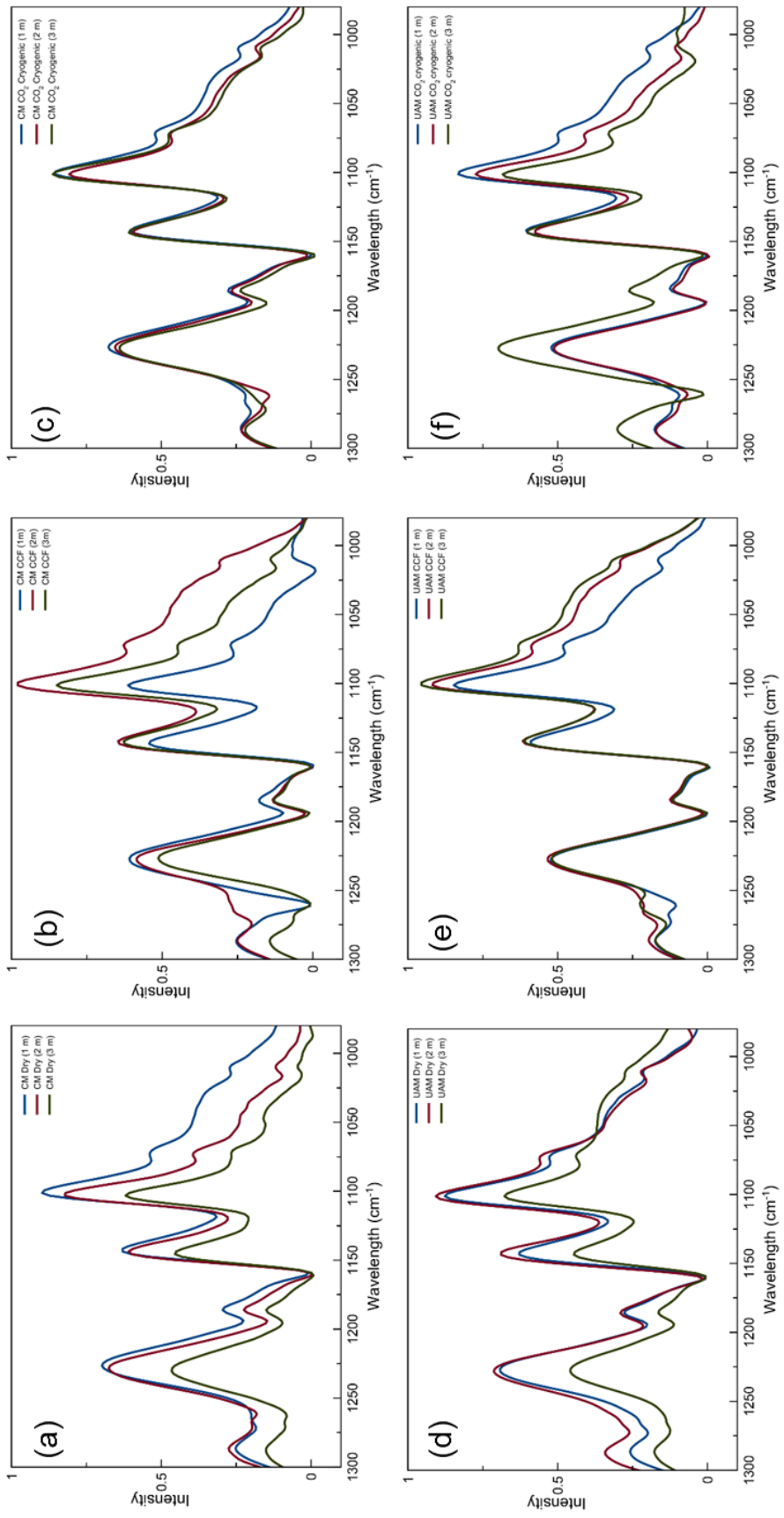

Figure 4-32: Changes in intensity for a region of 1300 to 1000 cm^{-1} for conventional (a-c) and ultrasonic assisted milling (d-e).

4.2.2.4 Region of 950 cm^{-1} to 700 cm^{-1}

Figures 4-33 (a) to (f) display the wavelength spectra for the region between 950 and 700 cm^{-1} of the machined CFRP surfaces for CM and UAM. Figures 4-33 (a) and (d) represent CM and UAM in dry condition that reflect significant reduction of the intensity of maleimide (C=C) at 825 cm^{-1}. Next, Figures 4-33 (b) and (e) display the CM and UAM in CCF condition, showing that the intensity of the C=C is inconsistent. Meanwhile, Figures 4-33 (c) and (f) that represent CM and UAM in CO_2 cryogenic condition demonstrate that the intensity of maleimide (C=C) is nearly unchanged after 3 m of machining length. It is assumed that the presence of –OH group in the conventional cutting fluid affected the chemical properties of CFRP. Nonetheless, no significant variance had been noted for the machined CFRP surfaces in CO_2 cryogenic condition, thus suggesting that the low cutting temperature (70-110 °C) was obtained due to CO_2 cryogenic cutting condition that aided in maintaining the CFRP chemical structure. Certainly, the significant reduction in maleimide (C=C) for dry condition machined surface of CFRP can be explained due to the higher cutting temperature (180-200 °C), when compared with CCF and CO_2 cryogenic conditions. Besides, it is assumed that further post-curing occurred in dry machining condition. Moreover, thermally degraded resin and broken fibres were found on the cutting tool, as shown in Figure 4-34, indicating that the CFRP with BMI 5250-4 was not completely cured.

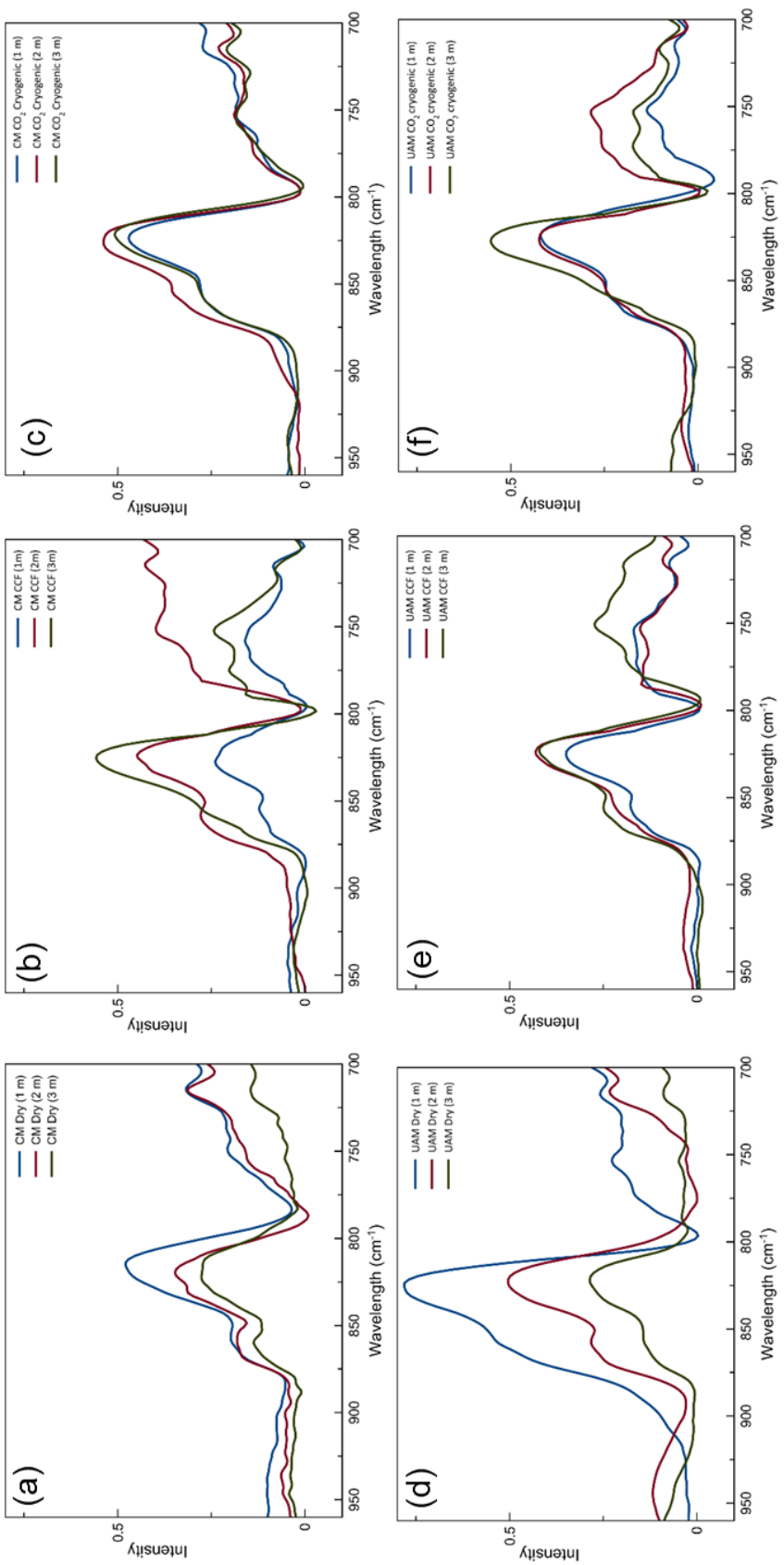

Figure 4-33: Changes in intensity for a region of 950 to 700 cm^{-1} for conventional (a-c) and ultrasonic assisted milling(d-e).

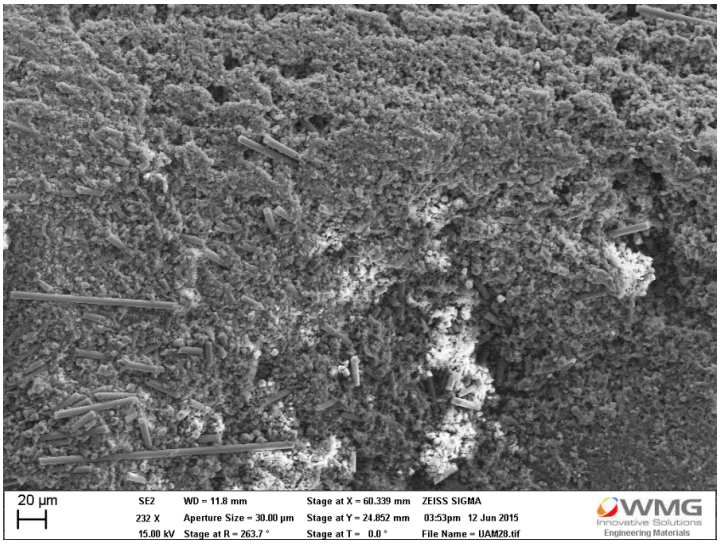

Figure 4-34: SEM micrograph of thermally degraded resin and broken fibres were found in between the diamond grit indicates that the BMI 5250-4 resin is not fully cured.

Furthermore, the reduction in maleimide bond (C=C) suggests that the high machining temperature induces further post-curing effect on the machined surface, thus deteriorating the mechanical properties of CFRP. This indicates that the BMI 5250-4 resin experiences more curing reaction due to the increase in cutting temperature as the machining length increases.

This present work confirms that the curing reaction of CFRP is incomplete after the standard composite fabrication and post-cure. The elimination of the Tg curve in Figures 4-21 and 4-22 suggests that the chemical properties of the machined CFRP surfaces have been changed/modified due to high cutting temperature in dry machining condition. Therefore, further curing effect on CFRP could occur by the service environment condition, thus resulting in changes of the Tg and the degradation of mechanical properties [14]. For instance, Morgan et al. [14] found the same reduction in the maleimide bond (at 825 cm^{-1}) when investigating the effect of curing temperature upon BMI. They further explained that the increase in curing temperature hiked the Tg and hence, degrades the mechanical properties of the BMI composite. Nonetheless, the increase/decrease of the maleimide (C=C) group in CM (CCF and CO_2) does not project

any substantial changes. Even though the sample taken for the FTIR refers to the machined CFRP surface, one can observe that even without ageing the materials, high cutting temperature induced by machining process can initiate degradation of materials. Although the application of cutting fluid could decrease the cutting temperature, it is well-agreed by several researchers that the application of coolant base is not recommended in machining composite, specifically thermoset, where absorption of moisture is high and can lead to hydrolysis of materials.

Therefore, the results obtained from DSC analysis and FTIR spectroscopy reveal that milling of CFRP in dry environment could lead to alteration in chemical properties of BMI 5250-4 matrix resin. The formation of isocyanate-derived product, as observed for CM dry at 3000 mm machining length, suggests that the actual cutting temperature could possibly reach 400 °C. Although the result obtained from Study 1(a) suggests that the application of UAM could lead to increased tool wear and surface roughness due to the vibration of the cutting tool. Results from FTIR indicate that the vibration of the cutting tool aided in removal of heat generated. Furthermore, milling of CFRP with CCF indicates that the presence of water molecule (-OH) in CCF could deliberately alter the chemical properties in BMI 5250-4 matrix resin. Hence, based on the DSC and FTIR results on the machined CFRP surfaces, it is proposed that milling of CFRP with CO_2 is recommended due to the fact that the machining environment does not affect the chemical properties of BMI 5250-4 matrix resin, while at the same time, improves the aspect of machinability. This result also suggests that the combination of DSC and FTIR analysis could be beneficial in determining thermal degradation of machined CFRP surfaces.

4.2.3 Summary from Study 1(b)

This study addressed the effect of machining environments on BMI 5250-4 chemical properties. Therefore, summaries of results obtained by DSC and FTIR analysis are outlined as follows:

- The results from DSC and FTIR analyses demonstrated that the combination of both techniques revealed the initial thermal degradation of CFRP. The DSC results revealed that higher cutting temperature (exceeding 180 °C) could lead to changes in material properties by examining the shift of Tg for BMI resin. It was observed that the initial Tg at 272 °C was eliminated in dry machining environment for both CM and UAM at 3000 mm machining length, thus suggesting that the actual cutting temperature exceeded the Tg.
- Further analysis of the machined surface by FTIR indicates that chemical changes occur prior to the cutting temperature. It was observed that in CM dry, the presence of a peak at 2250 cm^{-1} signifies the aromatic nitrile bond (C=N). The presence of the aromatic nitrile bond that is typically observed during thermal degradation of BMI above 400 °C points out that the high cutting temperature in the dry environment of CM degraded the property of BMI. However, the presence of aromatic nitrile in UAM machined CFRP surface was not observed because the ultrasonic vibration cutting mechanism in UAM aided in removal of heat generated by cutting tool and workpiece.
- Furthermore, reduction of maleimide bond (C=C) at 825 cm^{-1} in CM and UAM dry environments indicate that further post-curing occurred in both processes.
- Although the samples examined for FTIR were the machined surface of CFRP, it is now clearly understood that even without ageing the materials; the machining process can initiate degradation of materials. Besides, it is well-agreed by several

researchers that the application of cutting fluid is not recommended in machining composite, specifically for thermoset, where the absorption of moisture is high that can lead to hydrolysis of materials.

- The high cutting temperature generated during the machining of CFRP can initiate more crosslinking effect to CFRP and further deteriorates chemical and mechanical properties. Thus, the machining temperature can alter the properties of the materials even without ageing the materials for a certain amount of time.
- The changes of Tg in CFRP materials indicate the occurrence of chemical property degradation and depolymerisation of polymeric materials. Hence, further post-curing of BMI 5250-4 and its composite could reduce the mechanical properties of the material and further initiate more damages, such as crack propagation.

4.3 Study 2: Machinability of CFRP using PCD end mill

The purpose of Study 2 was to investigate the effect of cutting tool type (tool materials and geometry) on UAM. The direction of cutting tool vibration that is perpendicular to the feed direction was proposed in contributing to the degradation of cutting tool condition and machined surface in UAM, regardless of the type of the cutting tool employed. Hence, this study employed the straight flute geometry (helix angle, $\lambda = 0$ °) of 10 mm diameter PCD end mill in order to investigate the effect of tool type on the machinability of UAM. Thus, the cutting parameters employed in the present study are similar to those in Study 1(a) (Section 4.1) in order to observe the effect of cutting tool type on the machinability of UAM. The study also investigated the effect of UAM, in comparison to CM, in terms of tool wear, cutting forces, and surface roughness.

4.3.1 Tool wear

Wear progression of polycrystalline diamond (PCD) end mill that was used for CM and UAM were shown in Figure 4-35. The tool wear was measured at each of three flutes of the PCD end mill. The error bars represent both maximum and minimum values of the flank wear measurement from the three flutes. When milling of CFRP with PCD end mill for both CM and UAM, it was observed that the tool wear increased gradually as the machining length increased. Nevertheless, some minimal differences by 5 to 10 % had been noted between the tool wear measured for CM and UAM up to 8 m, in which both machining processes showed a similar trend of tool wear. When approaching 10 m machining length, the end mill used for UAM reached the maximum wear band, and the test was stopped. The end mill used for CM, on the other hand, could machine further

up to 15 m in length before the end mill reached the maximum wear band, as recommended by the industry, which was 110 µm.

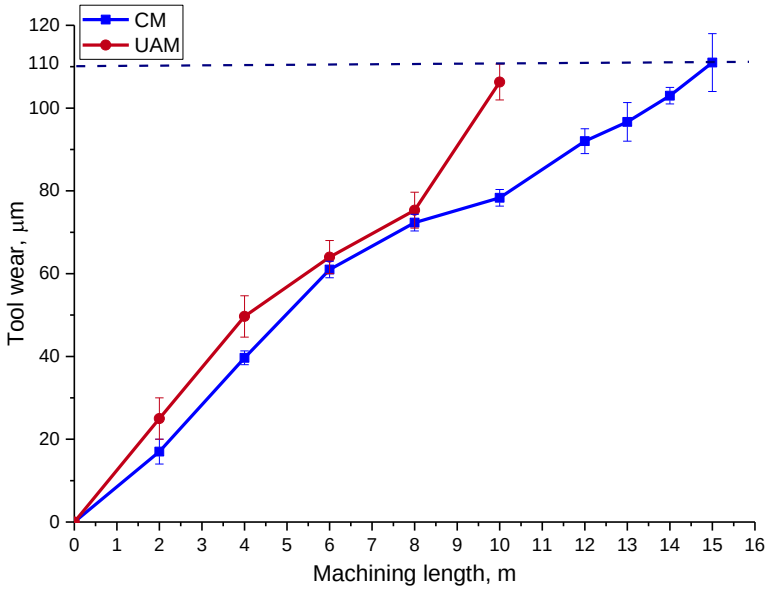

Figure 4-35: Progression of tool wear for CM and UAM over 10 metre machining length.

At 10 m machining length, the end mill used for UAM exhibited the maximum recommended wear band (110 µm), whereas the wear measured for CM was 80 µm. The end mill used for CM enhanced the tool wear by 29 %, when compared to the end mill used for UAM. This result, nonetheless, contradicts with another finding [150] that claimed the presence of ultrasonic vibration during milling could longer the tool life, as compared to the CM. Nevertheless, the direction of the ultrasonic vibration was in parallel with the feed direction and the intermittent separation of tool-workpiece aided in improving the tool life. However, the direction of the ultrasonic vibration in the present study was in a perpendicular direction with the feed direction, thus could be attributed to the high tool wear in UAM and the intermitted separation between the cutting tool and workpiece did not take place. Figure 4-36 displays the tool motion during CM and UAM. Moreover, it is noted that from Figure 4-36(b) that the cutting tool used in UAM travelled more than the CM in one cutting cycle.

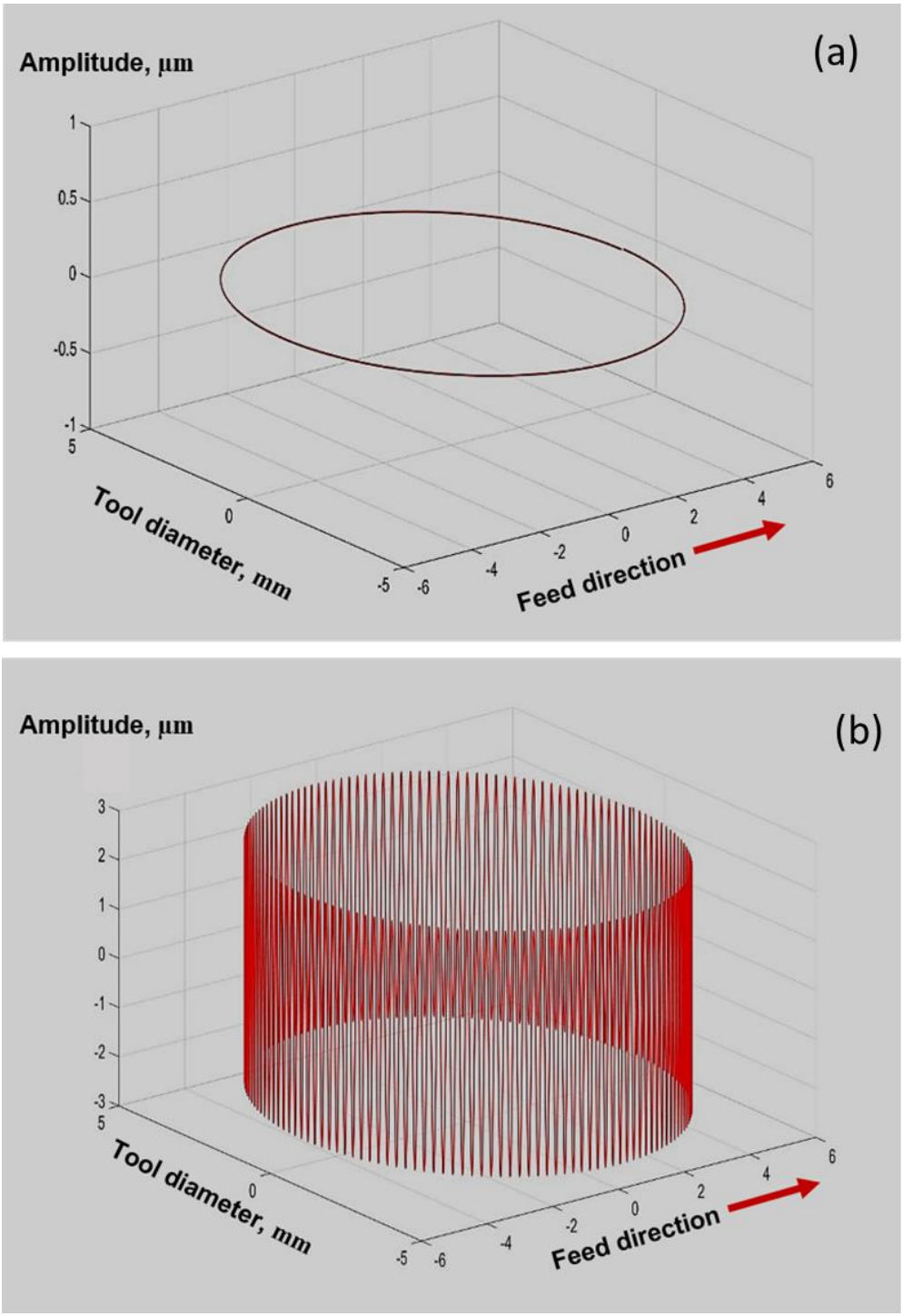

Figure 4-36: Tools motion for (a) CM and (b) UAM over one cutting cycle of cutting speed (500 m/min), feed rate (0.8 m/min) and peak-to-peak amplitude (5 µm) indicates that the cutting tool used for UAM create more tool-workpiece contact compared with CM. MATLab simulation was carried out by Aniruddha Gupta.

Therefore, the increase in tool wear for UAM can be attributed to the motion of the cutting tool, mainly due to the ultrasonic vibration. Furthermore, several aspects, such as

rotation, vibration, and movement of the end mill, during the UAM increased the contact length of tool-workpiece, hence creating more abrasion and interaction. As a result, after 8 m of machining length, the PCD end mill could not sustain the impact between the tool and the workpieces, thus reaching the maximum wear band when the machining is no further than 10 m. In contrast with UAM, the end mill used for CM only rotated and moved along the machine path, thus reducing the contact length between end mill and CFRP workpiece.

Furthermore, increase in the contact between cutting tool and workpieces when milling with the assistance of the ultrasonic amplitude in the present study is in agreement with prior researches [8, 149, 150]. Notably, the increased contact length between the cutting tool- and the workpiece creates a continuous interaction between the both. Besides, other work suggests that the complexity of tool movement, which vibrates in the perpendicular direction (z-direction) to the feed direction, deteriorates the tool condition in UAM, when compared with CM [8, 9, 149]. Although both findings employed different types of workpieces, it is important to note that the direction of the ultrasonic vibration contributes to a significant effect on the progression of tool wear in UAM. Therefore, higher tool wear for the cutting tool used in UAM can be concluded due to the continuous interaction between the cutting tool and the workpieces. Such continuous interaction degrades the condition of the cutting tool in UAM, when compared to that of CM. Thus, based on tool wear results, it can be concluded that the ultrasonic vibration that is perpendicular to the feed direction failed in offering any beneficial outcome in tool wear, especially for milling operation in this case.

Figure 4-37 shows the new PCD end mill, while Figures 4-38 and 4-39 exhibit the worn end mill for CM and UAM, respectively. Irregular and groove surfaces could be observed on the tool surface for the worn tool for CM (Figure 4-38 (b)) and UAM (Figure 4-39 (b)).

However, no material adhesion was noted on the cutting edge for both tools. The wear of the PCD was initiated with abrasion between the PCD and the workpiece.

In addition, the void that was observed on the tool surface is evidence of the removal of Cobalt (Co) binder, as projected in Figures 4-38 (b) and 4-39 (b). The hardness of Co (H_{Co} = 400-1200 HV), which is lower than the diamond particle ($H_{Diamond}$ = 10000 HV) and the carbon fibre (H_{CF} = 800-1000 HV), eases their removal during machining [52, 80, 108]. Moreover, the presence of the free Co binder and the broken fibre abraded the tool surface and the workpieces as the machining length was increased. The continuous abrasion between Co and broken fibre with the tool surface and the workpiece could lead to diamond particle breakage and more removal of Co binder due to the impact during machining [125]. This can also be supported by the characteristic of the diamond that has lower toughness, when compared to Co binder and carbon fibre [110, 124].

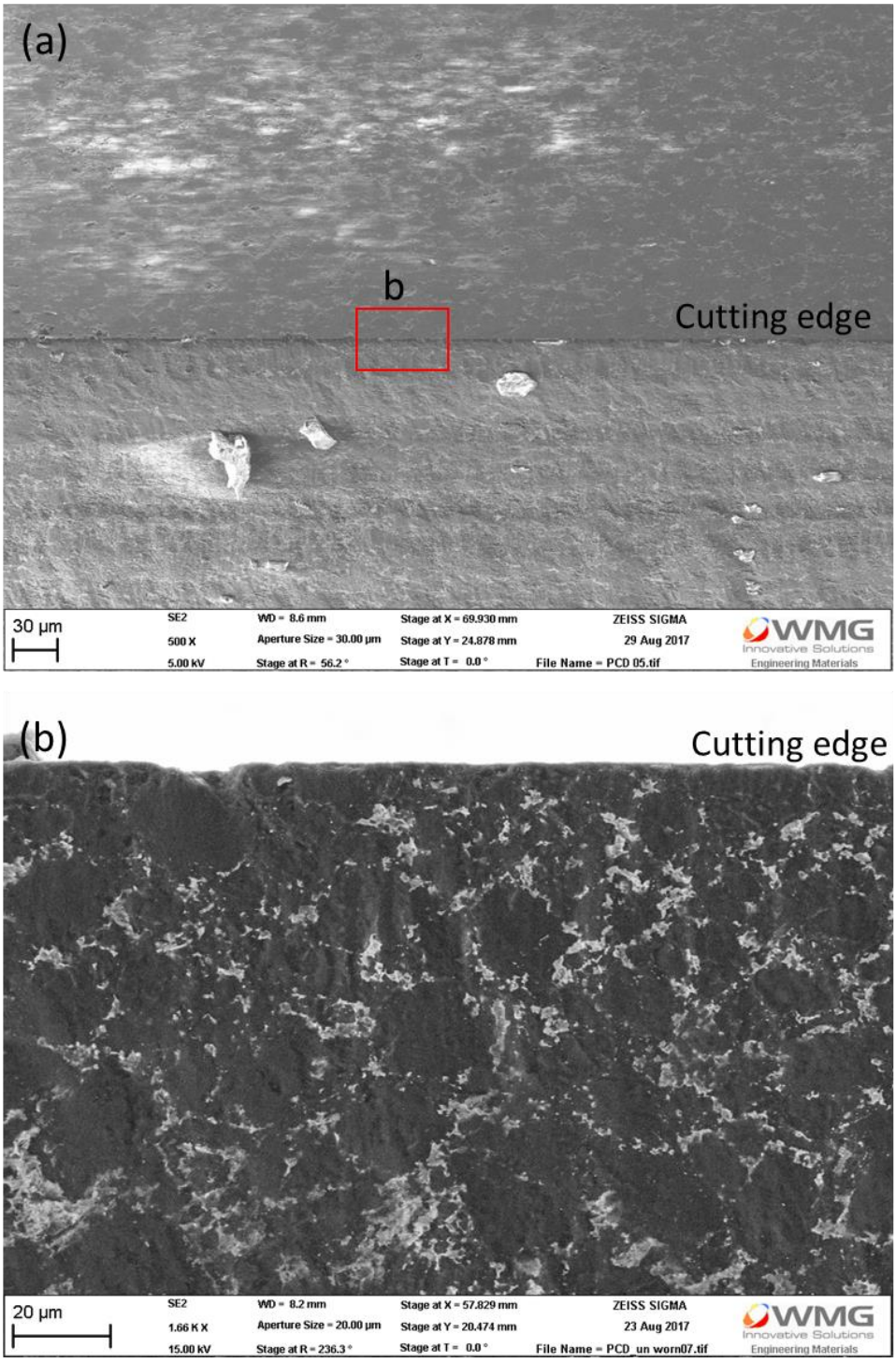

Figure 4-37: (a) SEM micrographs of cutting edge of new PCD end mill and (b) high magnification SEM micrograph of 'b' indicates that the white spots are the cobalt binder (Co) and dark spots are the diamond particles.

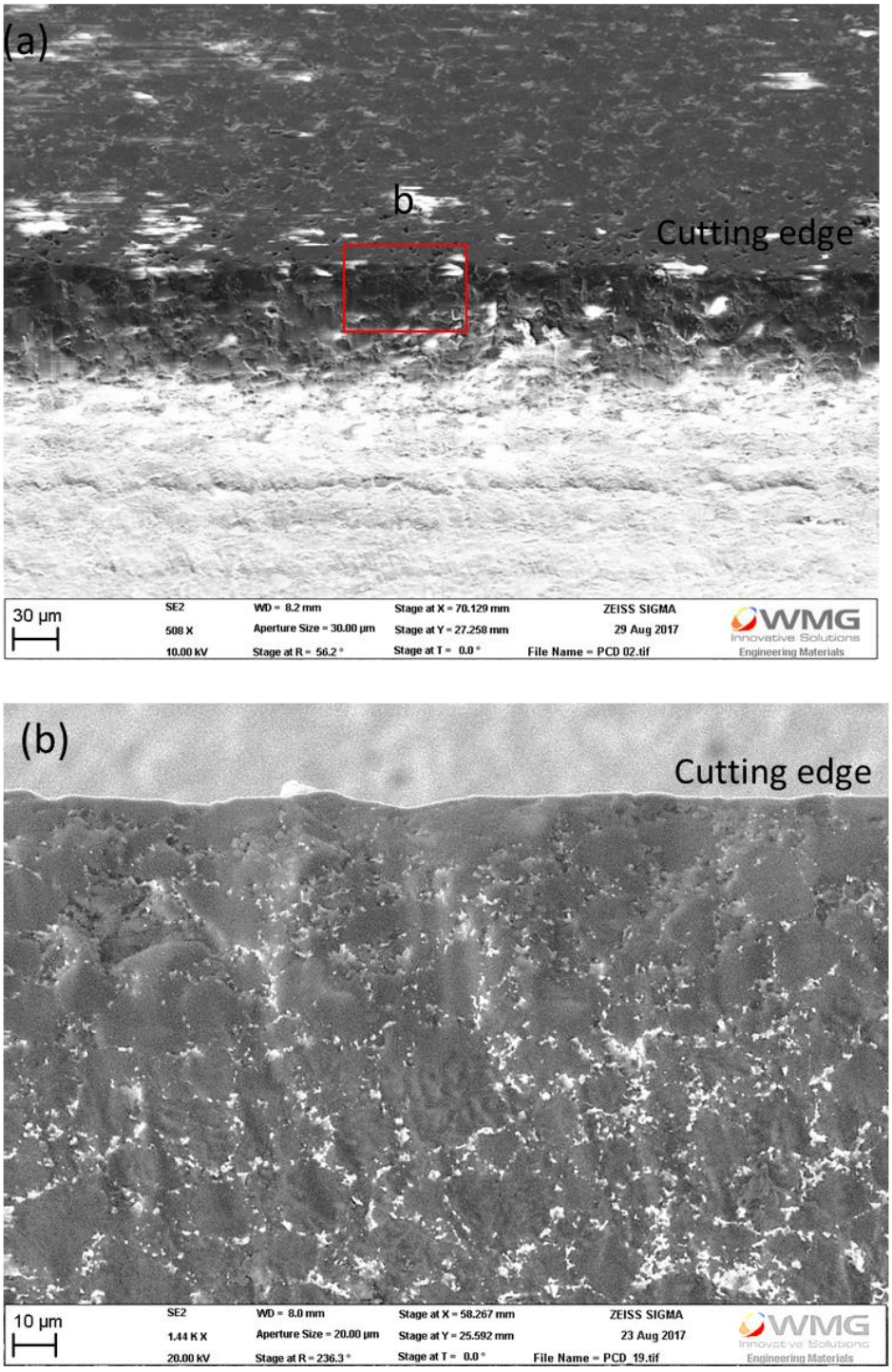

Figure 4-38: (a) SEM micrographs of a PCD end mill cutting edge used for CM after 10 metres machining length and (b) high magnification SEM micrograph of 'b' indicates the worn out surface and the removal of Co binder.

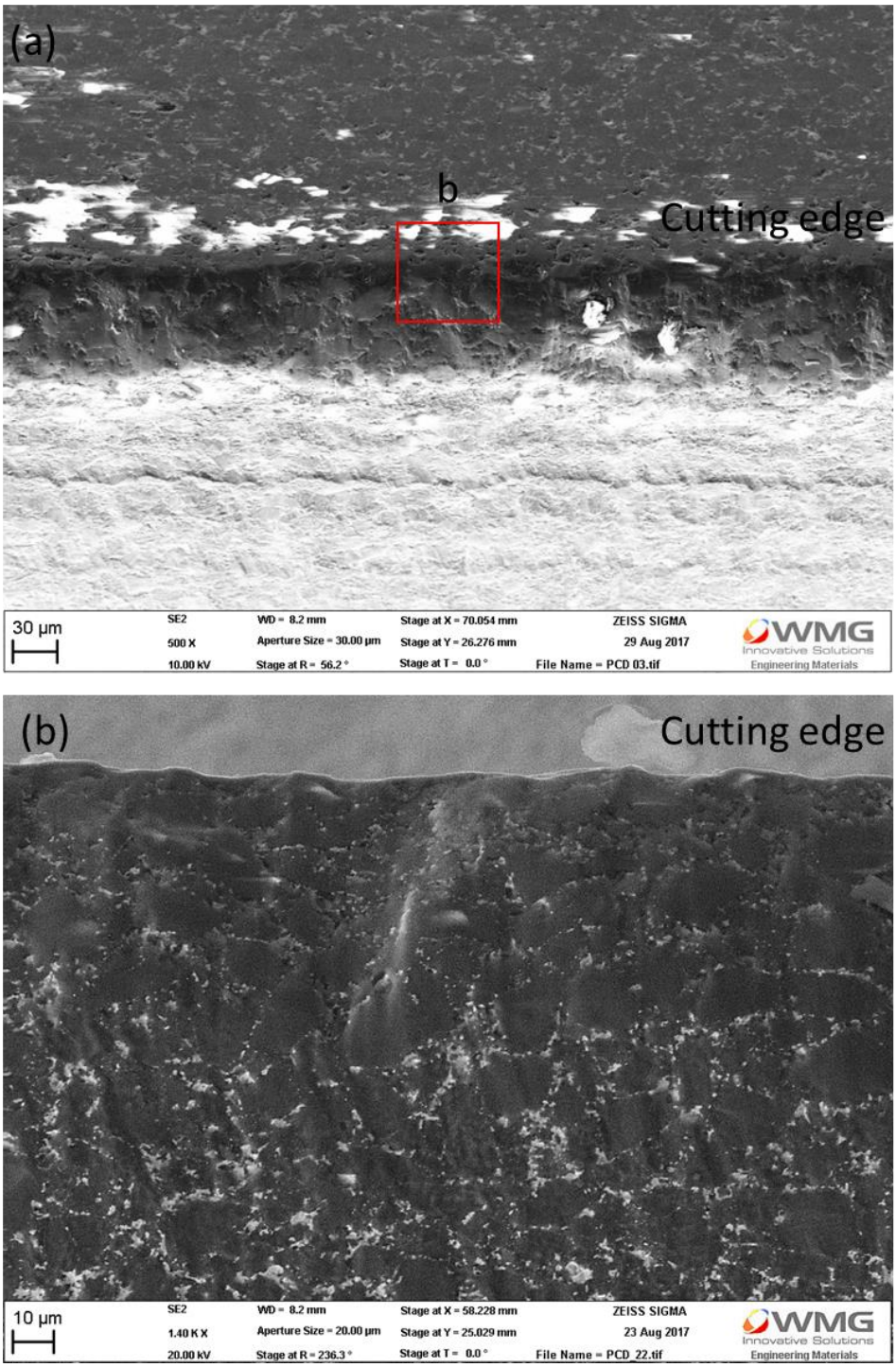

Figure 4-39: (a) SEM micrographs of a PCD end mill cutting edge used for UAM after 10 metres machining length and (b) high magnification SEM micrograph of 'b' indicates the worn out surface and the removal of Co binder.

Additionally, higher tool wear rate in the cutting tool used for UAM can be supported by the mechanism of Co binder loss, which leads to the fracture of diamond particle. During UAM, the frequency employed was 38000 Hz with peak-to-peak amplitude of 5 μm. The combination of high frequency with ultrasonic amplitude leads to the continuous vibration of the cutting tool while cutting. As a result, the PCD tool used in UAM condition was continuously abraded with the CFRP workpiece, thus reducing tool life. It is noted that the cutting tool condition for both CM and UAM had been similar when examined under SEM. Thus, one can conclude that the ultrasonic vibration of the cutting tool accelerates the wear on the cutting edges of PCD at 8 m of machining length, where the Co binder is severely dislodged in the cutting tool. The different hardness between the carbon fibre and the matrix resin also causes stress alteration and consequent fatigue on the cutting tool [118]. Hence, it is reasonable that the wear rate for the first 8 m of machining length is similar for both CM and UAM.

This rather contradicting result may be due to the vibration of the cutting tool that is perpendicular to the feed directions. A prior study mentioned that enhanced tool wear could be achieved via UAM operation. However, the result presented by [150] employed the ultrasonic vibration in the feed direction during milling. Similar observation was reported by [119] when machining CFRP, where the main mechanism was mainly attributed to the different hardness of carbon and matrix. Hence, it is suggested that the vibration of the cutting tool increases the abrasion between the cutting tool and the workpiece, thus leading to more removal of Co binder.

Therefore, the results of tool wear obtained from Study 2 conclude that the cutting tool geometry between PCD and WC-Co end mill does not have a significant effect upon tool wear, where higher tool wear was reflected in UAM, when compared with CM, in Studies 1(a) and 2. Hence, the direction of ultrasonic vibration, which is in the

perpendicular direction to the feed direction, could be a reason for the deterioration of tool wear.

4.3.2 Cutting forces

Figure 4-40 compares the feed force (Fx) and the normal force (Fy) for both CM and UAM. The effects of cutting speed, feed rate, and depth of cut are negligible because both CM and UAM employed constant parameters. The cutting forces in both x- and y-directions were increased as the machining length was increased. Besides, both feed and normal forces for UAM were 10 % lower than the CM with over 10 m machining length. At 10 m machining length, the feed force (Fx) measured for UAM was 429 N and 468 N for CM, while the normal forces were 244 N and 278 N for UAM and CM, respectively. The feed force is higher than the normal force for both UAM and CM due to the frictional force in the feed direction [148].

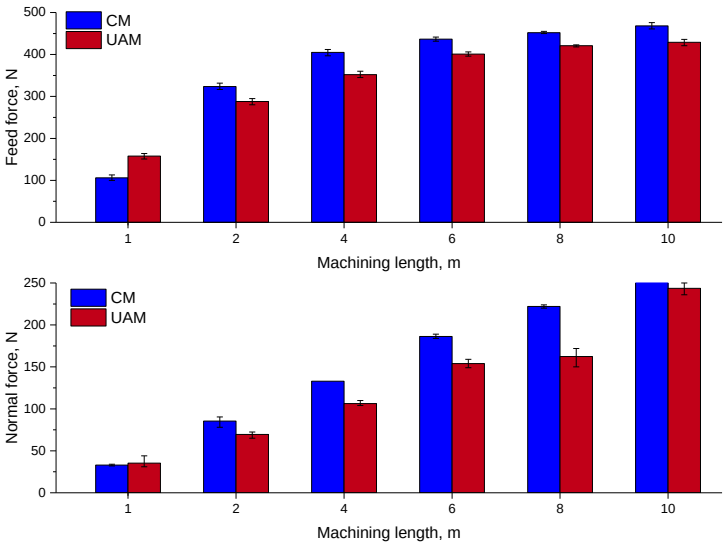

Figure 4-40: Feed force (F_x) and normal force (Fy) for CM and UAM over 10 metre machining length.

As mentioned in the literature, the cutting force during milling of CFRP exerts a strong correlation with the progression of tool wear [65, 136, 189]. The progression of tool wear usually affects the cutting forces during machining. However, in this present study, lower cutting force (10 to 15 %) was obtained by UAM, when compared with CM. Nevertheless, Section 4.3.1 shows that the tool wear of CM is lower than that of UAM. This could be attributed to the minimal variance of progression of tool wear between CM and UAM for the first 8 m. At 10 m machining length, the tool wear measured for UAM was 110 μm and 78 μm for CM. Furthermore, as mentioned by many researchers [6, 7, 156], a significant reduction in cutting forces and improved tool wear can be achieved by UAM due to its intermittent cutting, where the cutting tool engaged from the workpiece can be observed. Nevertheless, the intermittent separation between the cutting tool and the workpiece in the present study did not occur. The intermittent cutting produced zero cutting forces, thus reducing the average cutting forces. However, Figure 4-41 shows that the cutting forces for CM and UAM are comparable for this study. The sampling rate employed during the force measurement was 40000 Hz, and the ultrasonic frequency was set at 38000 Hz. Thus, it has been expected that the dynamometer is capable of collecting all the force data during machining since the sampling rate is higher than the ultrasonic frequency. The increase and the decrease of the cutting force in the zoom image (Figure 4-41) are due to the interrupted cutting in milling, where the cutting flute enters and exits the workpiece in a cutting cycle.

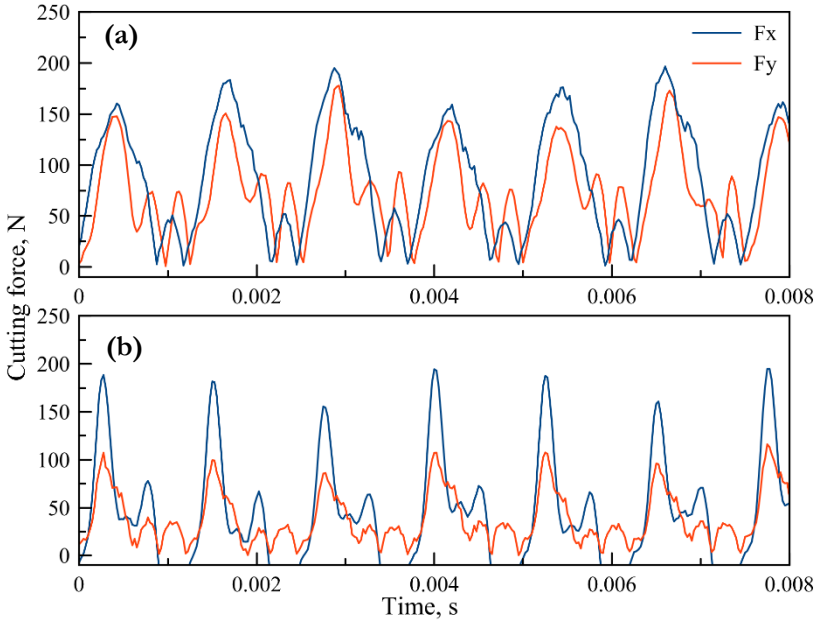

Figure 4-41: Typical cutting force data for a) CM and b) UAM at 2 metre machining length indicate that the cutting forces pattern for UAM and CM are comparable.

Although the intermittent cutting did not take place in this study, a minimal reduction (5-10 %) of the cutting forces that was recorded for UAM could be attributed to the ultrasonic vibration of the cutting tool during milling. Hence, it is suggested that the continuous interaction between the cutting tool and the workpieces has altered the mechanism of chip formation, where the ultrasonic vibrations aided in chip breakage, aside from generating thinner and smaller chips [157, 190]. This is opposed to metal cutting, where the mechanism of chip formation is mainly due to plastic deformation of the workpiece materials. However, the chip formation mechanism of CFRP [54, 57, 191] is mainly due to carbon fibre fracture and brittle fracture of matrix resin. Besides, no evidence displays that the carbon chip produced by UAM is smaller than that produced by CM.

4.3.3 Surface roughness

Figure 4-42 compares the average surface roughness, Ra, of the machined surfaces for CM and UAM with over 10 m machining length. The value of the average surface roughness for both CM and UAM increased as the machining length was increased, while the error bars represent both maximum and minimum values of the surface roughness. The average surface roughness showed that the value measured for UAM was higher by 5 to 10 %, when compared to CM, although low cutting forces were recorded for UAM.

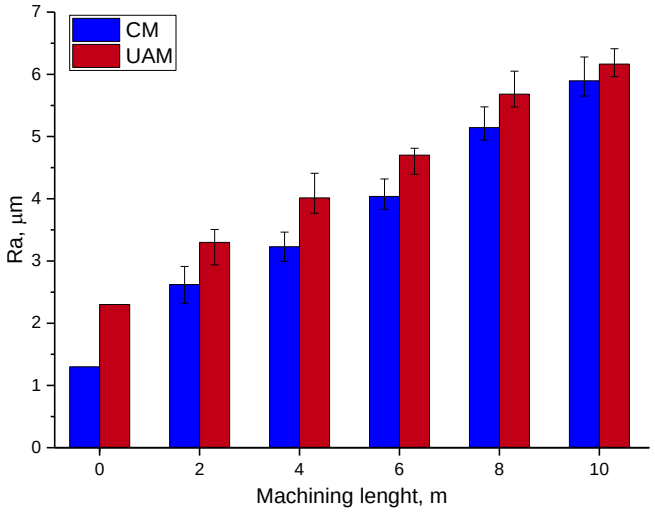

Figure 4-42: Surface roughness, Ra of CM and UAM over 10 metre machining length.

Increment in surface roughness of UAM machined surface is attributed to the higher tool wear in UAM than CM. In addition, poor surface roughness obtained by UAM is attributed to the ultrasonic vibration that was superimposed onto the cutting tool during the machining process. This extra movement of the cutting tool in UAM degrades the surface roughness, when compared with the CM machined surface. Moreover, Study 1(a) also found that rougher surface was obtained when milling CFRP with UAM, as compared with CM. Although varied cutting tool geometries were employed in Studies 1(a) and 2, the ultrasonic vibration of the cutting tool during UAM that is perpendicular to the feed direction contributed to the rougher surface in UAM.

When the cutting tool was still sharp at 0.5 m machining length (Vb=18 μm), the surface roughness measured for CM was 1.3 μm, while the UAM machined surface was 2.3 μm. Further milling of CFRP up to 10 m showed that the surface roughness for CM was 5.8 μm, and UAM was 6.2 μm, which refers to 7 % higher than CM. These results are in line with those reported by Maurotto et al. [8], whereby surface roughness of stainless steel obtained by UAM was higher, when compared with that of CM. Moreover, obvious tool marking was noticed on the machined surface when employed in high frequency (20 to 60 kHz), when compared with CM. Nonetheless, insignificant difference was found when the sub-surface metallography for both processes had been examined. The complexity of the motion in the UAM can be attributed to the degradation of the machined surface quality [9]. In contrast with Razfar et al. [13], the enhanced surface roughness can be obtained when machining carbon steel with implementation of ultrasonic vibration on the workpiece. They further claimed that the improvement was attributed to the direction of the vibration, which is in the same direction with the feed direction. However, in the present work, ultrasonic vibration was applied perpendicular to the feed direction.

Although the characteristics and the properties of workpiece materials employed in other studies [8, 9, 13, 192] differed from CFRP materials, it is agreed that the direction of the cutting tool and workpiece vibrations during UAM displays a significant effect on the surface roughness of the workpiece. Moreover, the characteristic of CFRP composite materials, which is non-homogenous, is more complicated, when compared to metal. The quasi-isotropic layer of carbon fibre in the workpiece employed in this study also complicated the progression of surface roughness. Furthermore, the difference properties of carbon fibre and matrix resin further complicated the CFRP machining process, in comparison to metal machining.

Figures 4-43 and 4-44 illustrate the surface topography and the roughness profile of the machined surfaces of CM and UAM at 10 m machining length. The profile height for CM was in the range of -15 to 10 μm with an average surface roughness of 5.4 μm, while the average surface roughness of UAM, Ra was 6.2 μm with a profile height between -20 and 10 μm. As discussed earlier, rougher surface was noted for UAM. The UAM surface topography and profile obtained from Alicona InfiniteFocus, as given in Figure 4-44, exhibit the irregular surface for UAM machined surface. The lower peak on the surface roughness profile indicates the voids, while the higher peaks signify fibre pull-out observed on the UAM machined surface. Hence, it is proposed that the tool vibration that is perpendicular to the feed direction deteriorates the machined surface. The complexity of tool movement in ultrasonic assisted machining, which vibrates, rotates, and moves, at the same time, affects the surface roughness [6, 9, 149].

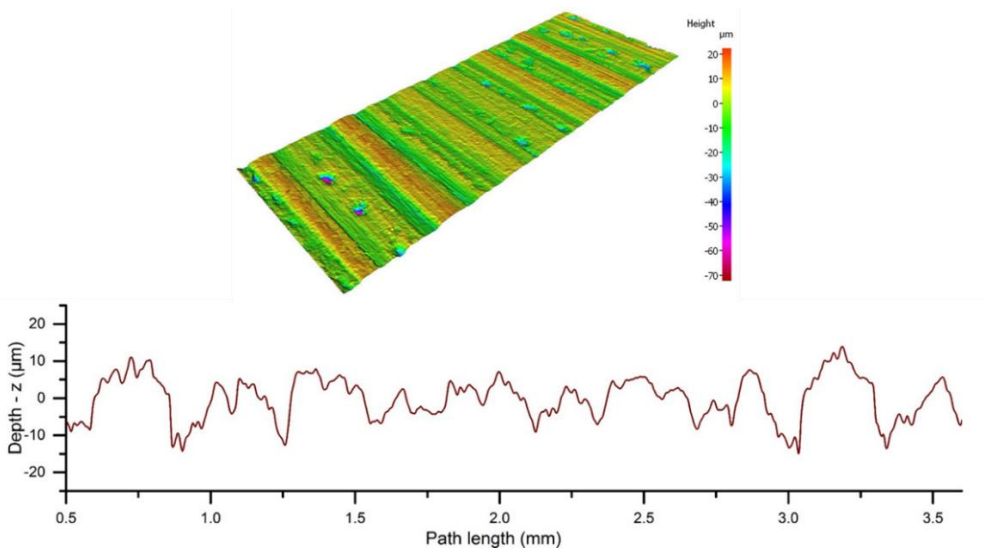

Figure 4-43: Surface topography and roughness profile of the CM surface produced by the Alicona with 5 X magnification with an average surface roughness, Ra of 5.4 μm at 10 m machining length.

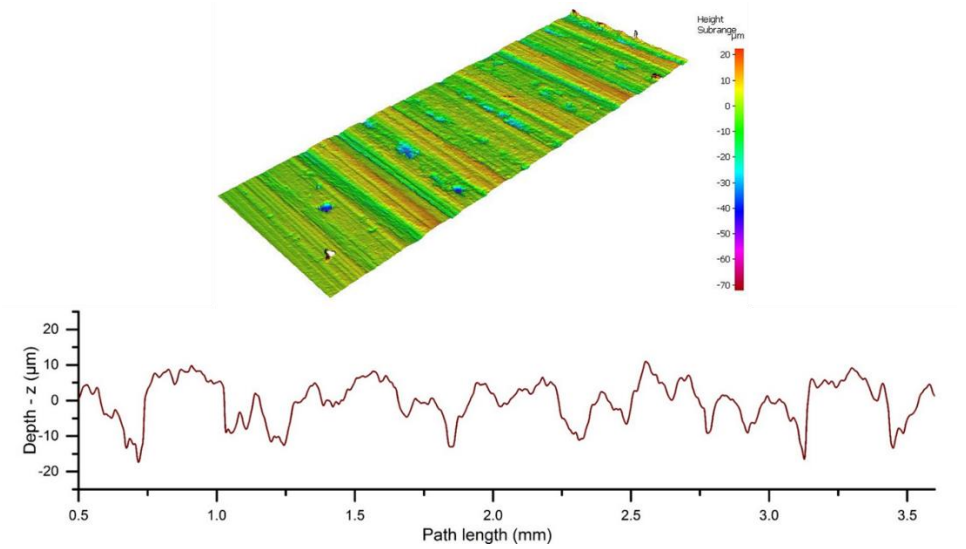

Figure 4-44: Surface topography and roughness profile of the UAM surface produced by the Alicona with 5 X magnification with an average surface roughness, Ra of 6.2 µm at 10 m machining length.

Although some studies have reported that the implementation of ultrasonic could improve surface roughness, most of the claims were observed when machining homogeneous materials, such as aluminium and titanium alloys. However, in the present study, the properties of CFRP employed are non-homogenous with quasi-isotropic orientation.

Additionally, based on the surface topography for both CM and UAM, matrix smearing and holes were noted on the machined surface. The holes that appeared on the machined surface indicated that the fibres were pulled out from the surface. At 10 m machining length, where tool wear and cutting forces for both CM and UAM were higher, it is plausible that the heat generated by cutting tool and workpiece is higher. Consequently, the high cutting temperature could reduce the strength between carbon fibre and matrix resin, thus enabling fibre to be pulled out and causing holes on the machined surface. Figures 4-45 and 4-46 illustrate the machined CFRP surfaces for CM and UAM taken in SEM, respectively. It was observed that the machined surface for CM was smooth, as

compared to that of UAM. As reported by Ramulu et al. [139], the presence of matrix smearing on the machined surface can affect the value of the surface roughness. A lower surface roughness can be obtained when the matrix is smeared over the machined surface. However, when the matrix is smeared at a certain area on the machined surface, fibre can be pulled out from the machined surface, thus generating higher roughness. Thus, Figures 4-45 (b) and 4-46 (b) display higher magnification images of the machined surface taken in SEM for both CM and UAM at 10 m machining length, respectively.

Damage such as fibre pull-out, fibre-matrix de-bonding, and matrix smearing, were observed on the machined surfaces of CM and UAM. However, it is evident that the UAM machined surface has fibres being pulled-out from the surface and voids can be observed, as shown in Figure 4-46 (b). In addition, the SEM images also reveal that the resin was thermally degraded during the machining processes due to high tool wear that led to high cutting temperature. On the other hand, the matrix smearing on CM surface is evident of lower surface roughness obtained in CM, when compared to UAM. This explains the variance between the surface roughness values obtained by the machined surfaces of CM and UAM.

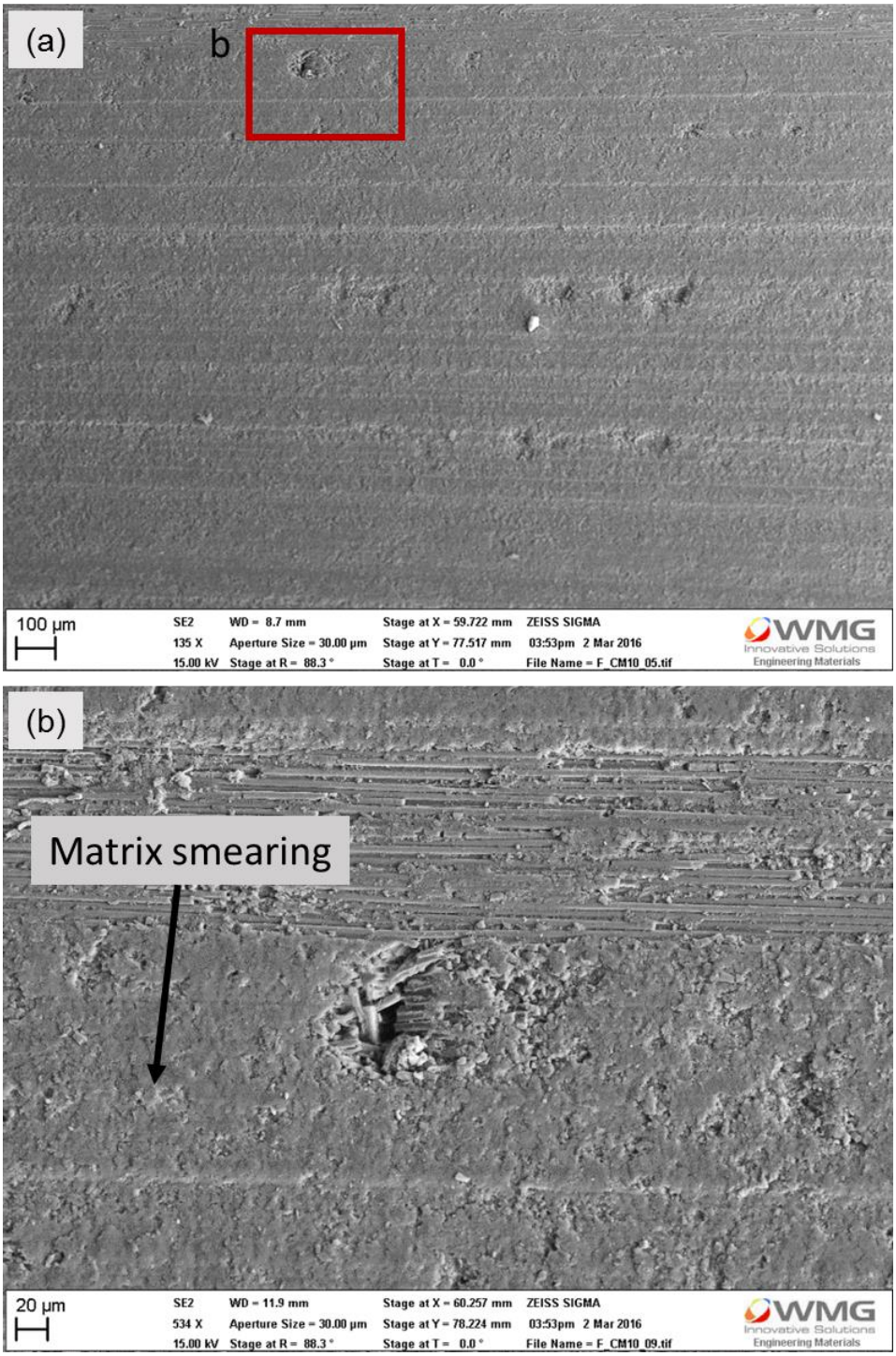

Figure 4-45: (a) SEM micrographs of CM of CFRP machined surface at 10 m machining length and (b) high magnification SEM micrograph of 'b' indicates that the matrix was smearing on the machined surface.

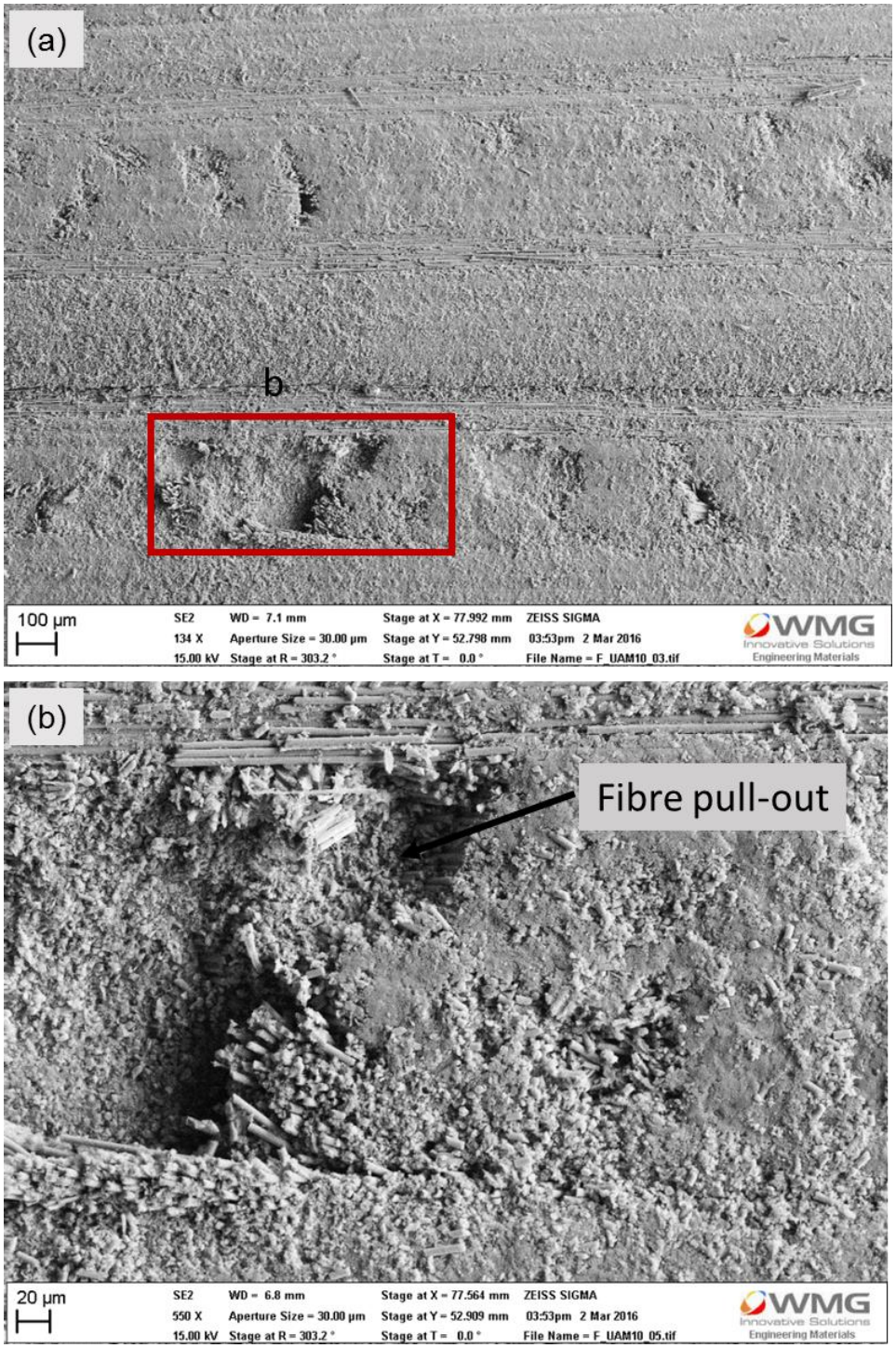

Figure 4-46: (a) SEM micrographs of UAM of CFRP machined surface at 10 m machining length and (b) high magnification SEM micrograph of 'b' indicates that the surface experienced fibre pull-out and created the void on the machined surface.

4.3.4 Post machining analysis of machined CFRP surface

4.3.4.1 DSC and FTIR analysis of machined CFRP surface

As discussed in Study 1(b) (Section 4.2), the elimination of the Tg for BMI 5250-4 indicates that the high cutting temperature has deliberately changed the chemical properties of the matrix resin during machining. Therefore, in this subsection, only the machined CFRP surface sample at 10 m machining length (high temperature and high tool wear) had been incorporated for analyses to ensure that the repeatability of the results obtained in Study 1(b). Figure 4-47 compares the DSC analysis of un-machined and machined CFRP surfaces for both CM and UAM at 10 m machining length. The un-machined sample of CFRP indicates that the Tg of the BMI 5250-4 matrix resin was at 272 °C. However, for CM and UAM machined CFRP surfaces; the Tg curves were not observed. This suggests that at this machining length, the cutting temperatures of CM (145 °C) and UAM (130 °C) have affected the chemical properties of the machined surfaces, as portrayed in Appendix D.

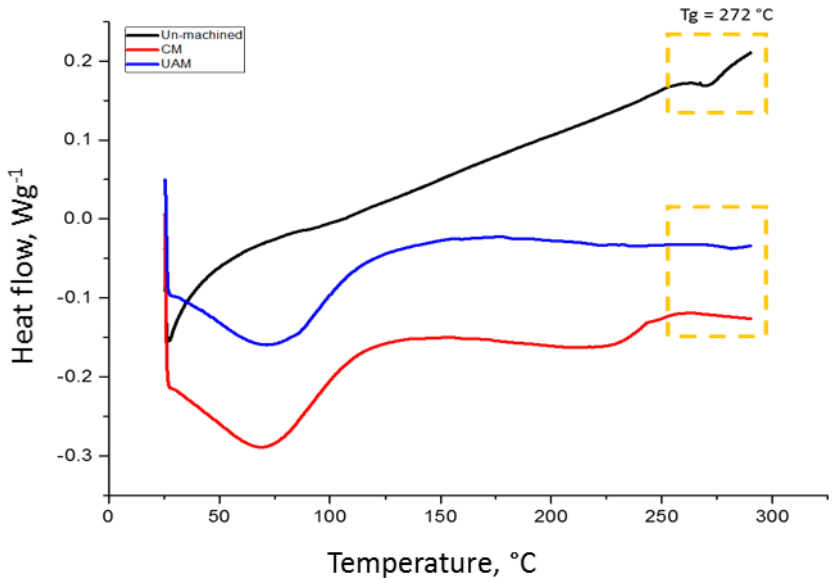

Figure 4-47: DSC analysis of machined CFRP surface at 10 m machining length indicates the Tg for CM and UAM were eliminated suggesting that the chemical property of the machined surface have been changed because of high cutting temperature at the end of machining test.

Apart from the DSC analysis of the machined CFRP surface, FTIR analysis was performed to determine the changes that took place in the chemical properties of the machined surface. Similar to Study 1(b), the formation of aromatic nitrile bond was observed in CM machined CFRP surface sample, but not for UAM machined CFRP surface sample, as illustrated in Figure 4-48. Therefore, these results confirm that the formation of aromatic nitrile at the region of 2405 to 2233 cm^{-1} suggest the occurrence of thermal degradation for the machined CFRP surfaces. This finding also confirms that DSC and FTIR could be used to determine the degradation of machined surfaces.

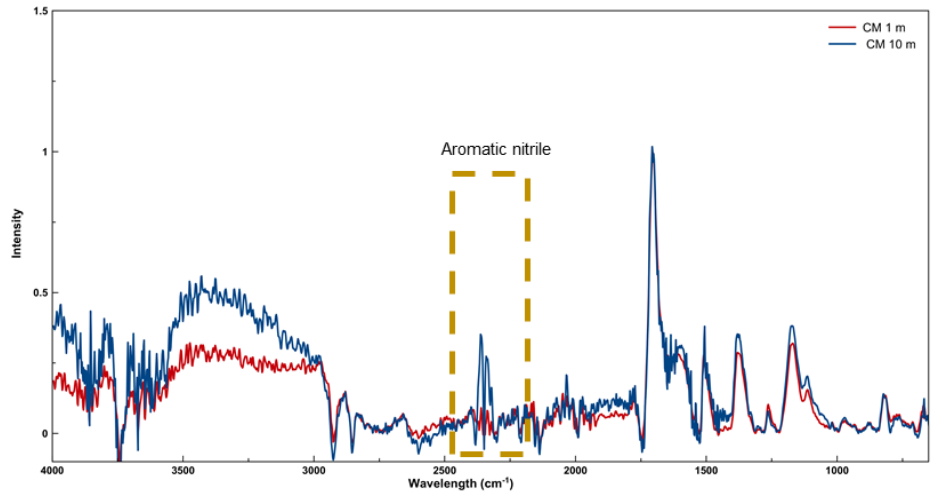

Figure 4-48: FTIR Spectra for machined CFRP surface for CM in dry environment from 4000 to 600 cm^{-1} for 1 and 10 m machining length.

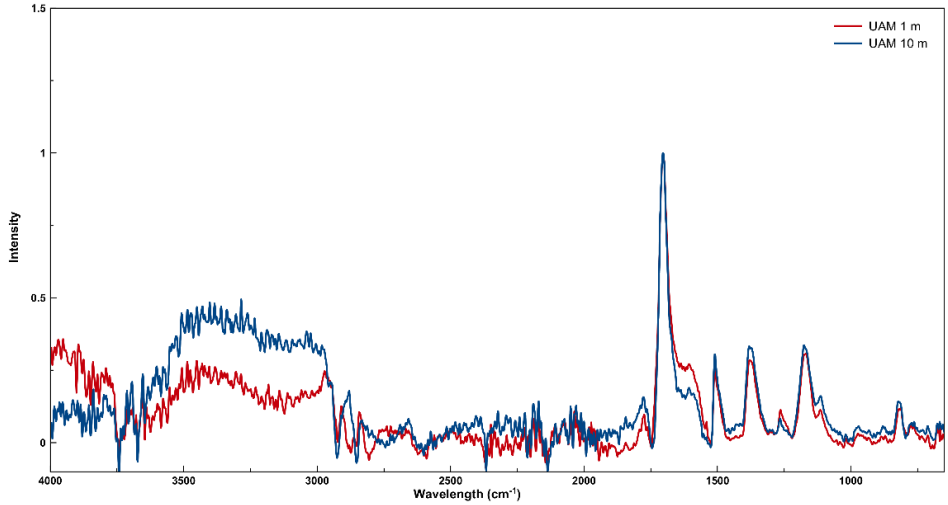

Figure 4-49: FTIR Spectra for machined CFRP surface for UAM in dry environment from 4000 to 600 cm^{-1} for 1 and 10 m machining length.

4.3.5 Summary from Study 2

Study 2 has shown that the application of ultrasonic vibration on cutting tool during milling of CFRP did not exert any beneficial effect to tool wear and cutting forces. The results obtained from DSC and FTIR also revealed that the formation of isocyanate-derived product was observed on CM machined surface, which is similar to the result obtained in Study 1(d). Therefore, the findings from this study can be summarized as follows:

- The results obtained in Study 2 indicate that the cutting tool geometry did not significantly influence the tool wear. Therefore, the vibration of the cutting tool that is perpendicular to the feed direction did not display a beneficial effect upon tool wear in UAM.
- From Study 2, it can be concluded that the PCD end mill used for CM could machine further up to 15 m before reaching the maximum flank wear, as recommended by the industry. However, the PCD end mill used for UAM only machined up to 10 m before it attained the maximum flank wear. There is a marginal difference (5-8 %) in the progression of tool wear for the end mill used in CM and UAM for the first 8 m of machining length. However, the PCD end mill for UAM is only capable to machine up to 10 m before it reached 110 μm. Hence, for the first 10 m, the effect of tool wear in the analysis is negligible.
- The cutting force for UAM is 10 % lower when compared with CM. This may be due to the cutting tool vibration in UAM that increases the fracturing mechanism of carbon fibre, thus reducing the cutting forces in UAM. However, the cutting tool vibration that is perpendicular to the feed direction leads to a rougher machined surface due to discovery of fibre pull-out on the UAM machined surface, while matrix smearing on the CM-machined surface.

- It is suggested that the ultrasonic vibration that is perpendicular to the feed direction deteriorates the machined surface in UAM and increases tool wear of the cutting tool used for UAM.
- Post-machining analysis on the machined surface by DSC indicates that the Tg has been eliminated due to the high cutting temperature. Inspection by FTIR suggests that the formation of aromatic nitrile bond in CM-machined CFRP surface indicates that the machined surface has been thermally degraded.

4.4 Study 3: Machinability of CFRP using an abrasive diamond milling tool

Studies 1(a) and 2 employed the typical end mill tool to perform CFRP milling. As mentioned earlier in the literature review, application of abrasive diamond tool as a cutting tool to perform CFRP milling has been increasing due to the advantages offered by the abrasive, especially when high cutting speed and feed rate is necessary. Therefore, this study investigated the effect of UAM, in comparison to CM in terms of tool wear, cutting forces, and surface roughness. Constant cutting parameters of speed (565 m/min), feed rate (1500 mm/min), and depth of cut (1 mm) were applied, as shown in Section 3.4.4. Both CM and UAM employed the 10 mm diameter of the abrasive diamond tool with an average of 420 μm diamond grit, which is commonly used for roughing of CFRP at the BAE Systems.

4.4.1 Tool wear

Figure 4-50 demonstrates the progression of the cutting tool diameter based on the slot width for CM and UAM over the 10 m machining length. The error bars represent the difference for maximum and minimum averages of the slot width measured. The diameter of abrasive diamond tool was examined by monitoring the width of a slot cut on a

graphite plate, as elaborated in Section 3.3.4.3. In fact, reduction of the cutting tool diameter for both milling processes demonstrated a similar pattern for the first three metres. The decrease in the cutting tool diameter is attributed to the initial condition of the sharp abrasive peaks, indicating rapid tool wear [113]. Nonetheless, CM beyond 3 m increases the diameter of the cutting tool. It was also observed that after three metres of machining length, the broken fibre and the degraded resin began to adhere to the cutting tool used for CM. In contrast, the tool diameter of UAM constantly decreased, and it was observed that the less degraded resin and broken fibre adhered to the tool surface. At the end of the test, the tool diameter for CM had increased from 9.94 to 9.975 mm, while for the UAM, the cutting tool diameter reduced from 9.955 to 9.935 mm.

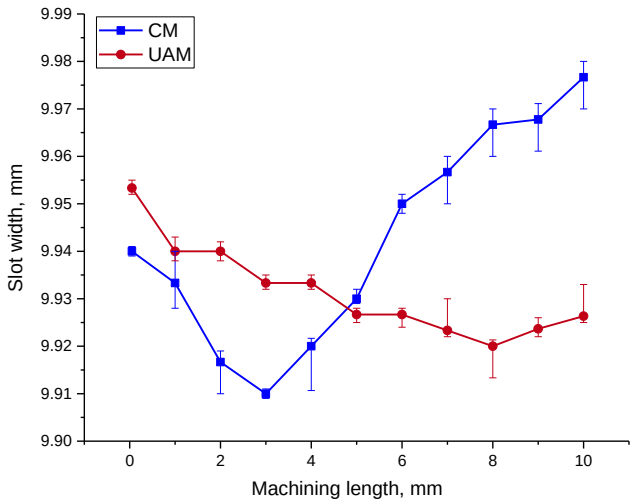

Figure 4-50: Progression of tool diameter of an abrasive diamond tool for CM and UAM over 10 m machining length.

Figures 4-51 (a, b, c, d, e, and f) show the optical microscopy images of the cutting tools used for CM and UAM at 0.5, 5.0, and 10.0 m machining length. It was observed that the cutting tools used for CM adhered to the broken fibre and the degraded resin between the diamond grit at 5 and 10 m machining length, as shown in Figures 4-51 (b) and (c), respectively. Thus, the degraded resin and the broken fibre that adhered to the tool surface contribute to the increasing tool diameter for CM, as shown in Figure 4-50. The

adhered material observed on the cutting tool surface is typically observed on the grinding tool. The increment in the cutting tool diameter for CM after 3 m of machining length is associated with the increasing heat generated as the machining length is increased. The heat generated during machining deformed and degraded the matrix resin. This occurrence is similar to the observations described in [113, 141, 193], where thermally degraded matrix resin was loaded between the diamond grits in CM.

In contrast with CM, adhesion of thermally degraded matrix resin and broken fibre onto the cutting tool used for UAM are not so apparent. This finding is consistent with the results obtained by other researchers [142, 194], where the motions of the cutting tool in UAM reduce the chances for the materials to adhere between the diamond grits. The cutting tool motion of the UAM, which vibrates, rotates, and moves during cutting, improved chip circulation. However, as for CM, the broken fibre and the thermally degraded resin did not have a sufficient medium to evacuate from the cutting tool and the machined CFRP surface. As a result, the broken fibre and the thermally degraded resin were found on the cutting tool.

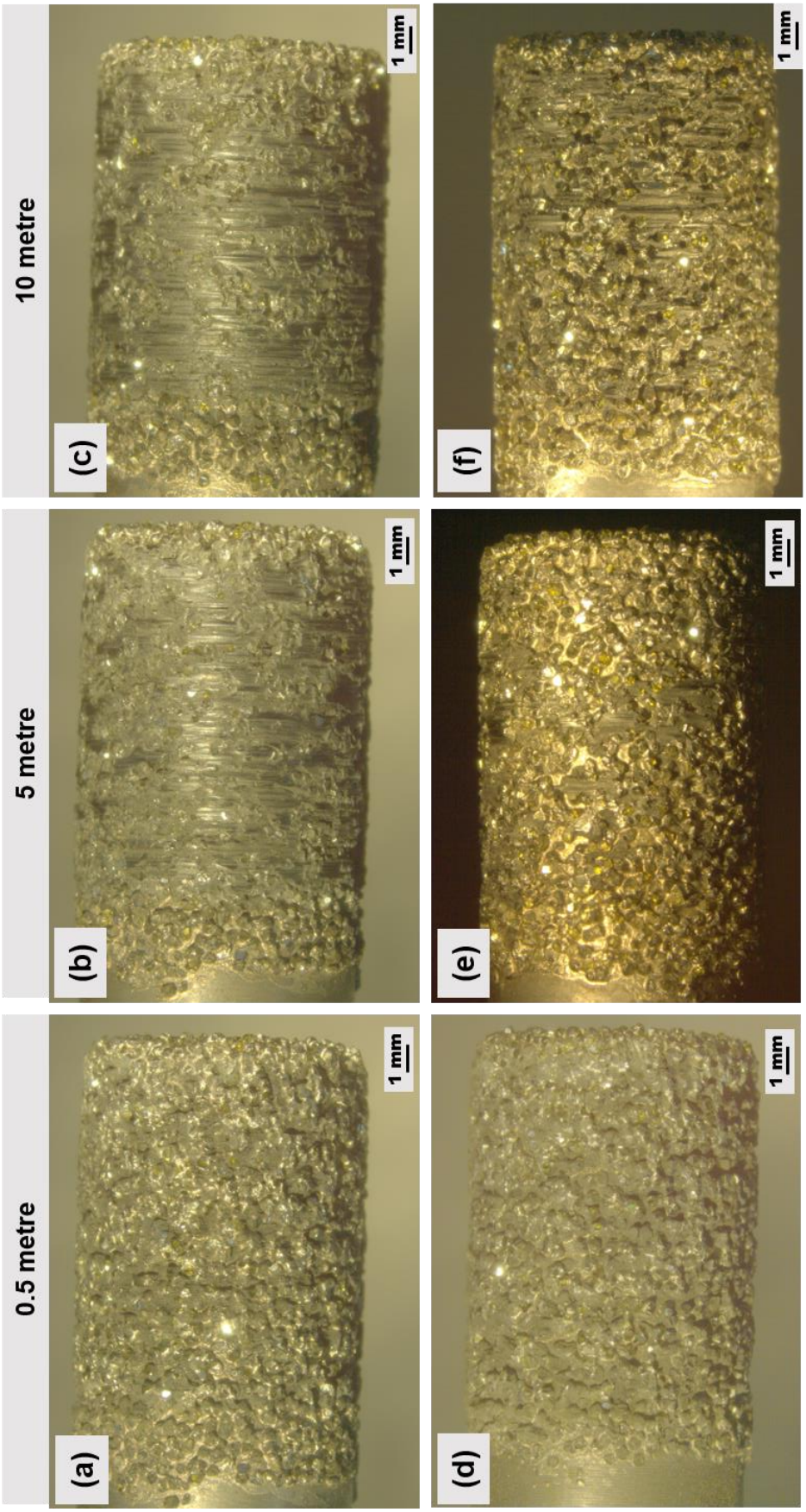

Figure 4-51: Optical microscopy images of an abrasive diamond tool for (a-c) CM and (d-f) UAM over 0.5, 5 and 10 metre machining length

At the end of the 10 m machining length, in order to remove the adhered material on the cutting tool, both cutting tools were cleaned using an ultrasonic bath and acetone. However, the materials that were still intact to the cutting tool used for CM signify that the matrix resin had been degraded during machining. This could be attributed to the high cutting temperature as the machining length increases, and the tools were loaded with the adhered materials. In order to quantify the area of the cutting tool covered by the degraded resin and broken fibre, a 2D image processing method was performed. Figures 4-52 (a) and (b) display the images of the scanning area of the cutting tool used for the CM taken in Alicona InfiniteFocus, whereas Figure 4-52 (b) presents the areas of the cutting tool that was adhered by the degraded resin and broken fibres. The total area covered by the thermally degraded resin and broken fibre on the cutting tool used for CM was 30.35 mm^2, while 17.11 mm^2 for UAM, which is 44 % less than the tool used for CM. Appendix F shows the total area covered by the degraded resin and the broken fibre on the abrasive tool used for CM and UAM.

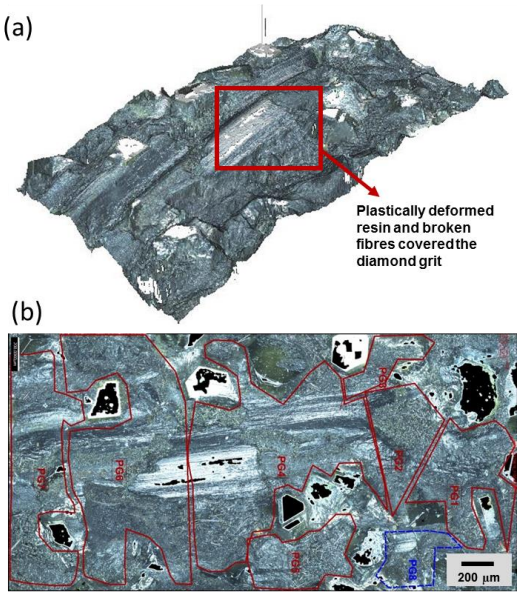

Figure 4-52: (a) Image of a cutting tool used for CM scanned by Alicona using 5x magnification and (b) areas of cutting tool that covered by the degraded resin.

The wear of the abrasive tool for both UAM and CM is presented in Figures 4-53 and 4-54. Two wear mechanisms were observed on both cutting tools, which are a fracture of the diamond grain and the bond fracture. Figures 4-53 illustrates the cutting tool used for UAM, which also indicates that the cutting tool experienced a bond fracture between the diamond grit and the nickel bond, along with the sharp abrasive peaks of the diamond grits. The ultrasonic vibration generated the micro-cracks on the diamond grit, which created sharper cutting edges on the cutting tool. As a result, more active cutting edges had been observed on the cutting tool used for UAM, when compared to CM. Higher magnification SEM images, as shown in Figures 4-54 (a) and (b), indicate that the cutting tool used for CM experienced grain pull-out, bond fracture between diamond grit and nickel bond, as well as micro-fracture of diamond grit. As for the cutting tool used for CM, the diamond grit was completely covered by the degraded resin and broken fibre. Hence, the effective cutting edges on the cutting tool used for CM had been reduced. Nonetheless, the attritions wear, which indicates the wear flat of the abrasive that is commonly observed on the grinding tool, was not apparent in this study.

Figure 4-53: SEM micrographs of a cutting tool used for UAM indicates that the cutting tool experienced microcrack and the sharp abrasive peak of the diamond grit after 10 metre machining length.

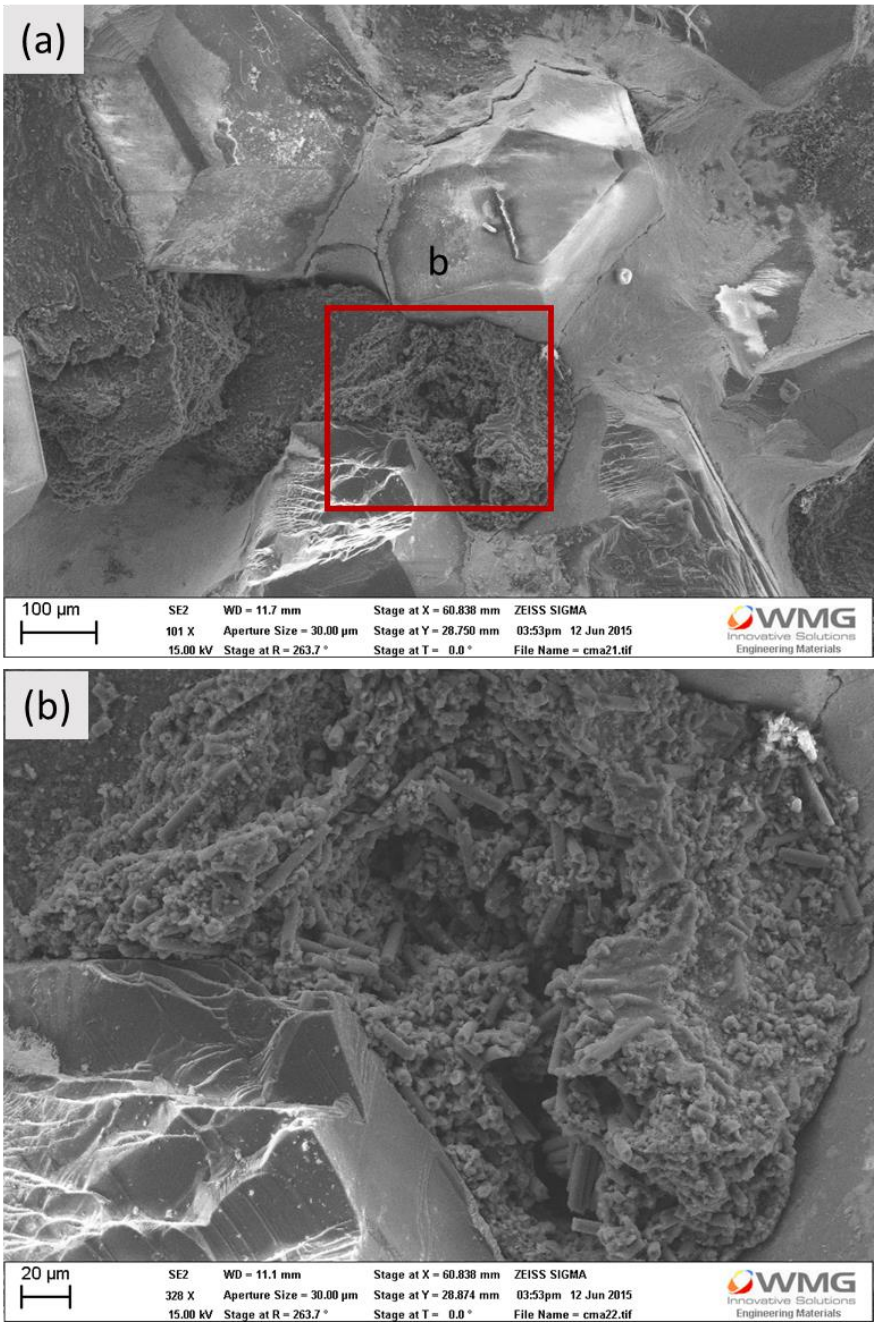

Figure 4-54: (a) SEM micrographs of a cutting tool used for CM and (b) higher magnification of SEM micrograph of 'b' indicates that the cutting tool was loaded with broken fibres and degraded resin after 10 meter machining length.

Figure 4-55 shows the energy disperse spectroscopy (EDS) analysis of the materials adhered to the cutting tool that was used for CM. It was confirmed that from the EDS analysis, the materials adhered in between the diamond grit was carbon elements.

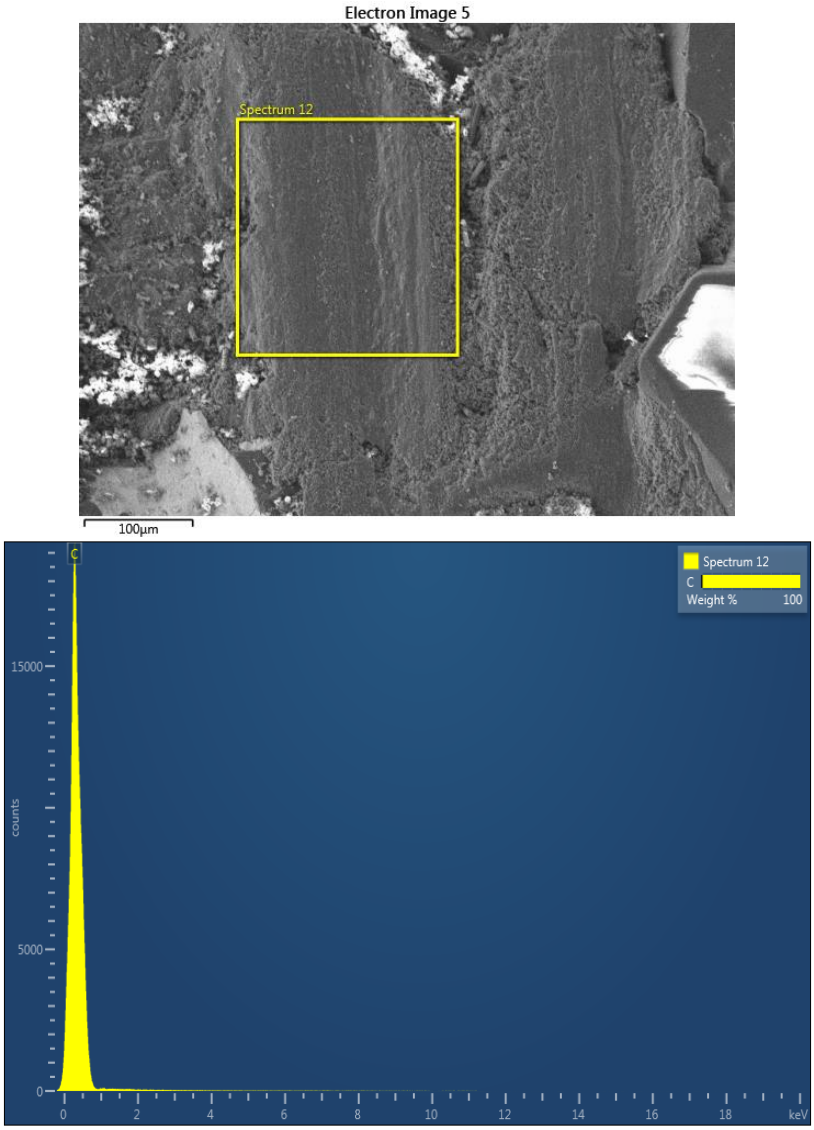

Figure 4-55: EDS for the materials adhered to the abrasive diamond tool used for CM indicates that the materials sticking were a carbon element.

4.4.2 Cutting forces

Figure 4-56 presents the feed force (Fx) and the normal force (Fy) for both CM and UAM. The error bars indicate both maximum and minimum cutting forces recorded during the measurement. The feed and normal forces show similar pattern, where both forces were found to increase as the machining length increased.

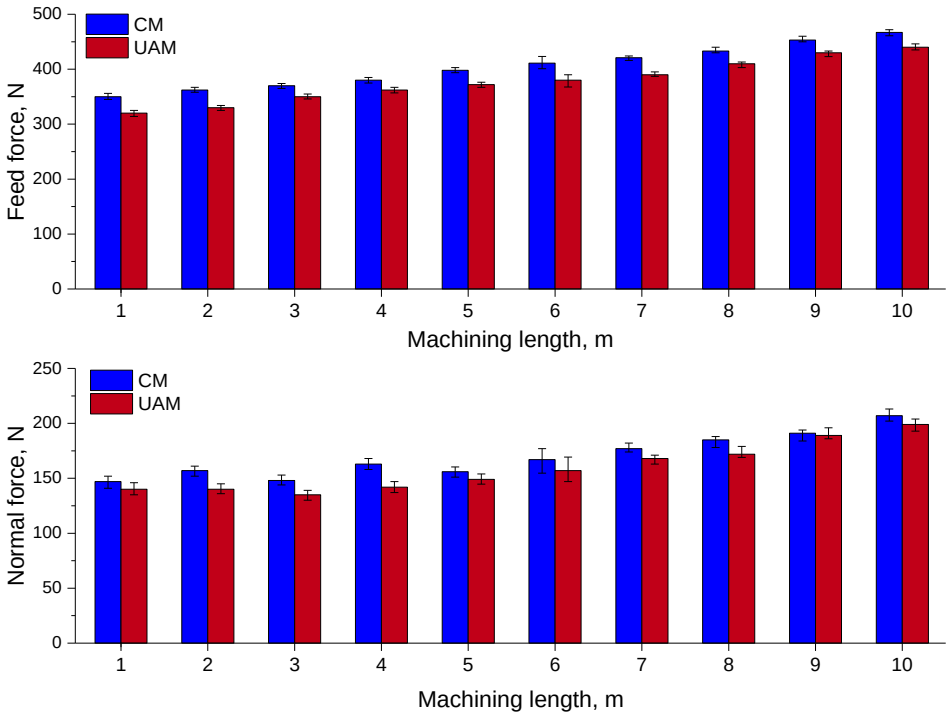

Figure 4-56: Feed force (Fx) and normal force (Fy) for CM and UAM over 10 metre machining length.

Both feed and normal forces of UAM were found to increase up to 10 % of the force reductions, in comparison to CM. Higher cutting forces were observed for CM, as compared to UAM, throughout the milling operation. At the end of the test, the feed force measured where the cutting tool of the CM loaded with degraded resin and broken fibre was 470 N, while 440 N was measured for UAM. As discussed in Section 4.4.1, the cutting tool diameter for CM started to increase after 3 m of machining length, which led to the increase in cutting force. This is due to the degraded matrix resin and the broken

fibre that were transferred to the tool in CM, than that in UAM, hence causing higher obstruction in CM, as presented in Figure 4-51 (c). The deformed resin and the broken fibres that covered the diamond grit in CM reduced the active cutting edges. Due to the increasing number of diamond cracks and inactive cutting edges in CM, a greater frictional interaction was initiated between the cutting tool and the workpiece. Material loaded on the cutting tool generated a rubbing effect between the loaded materials and the workpiece, thus increasing the cutting force. However, as for UAM, the sharp abrasive peaks aided the cutting mechanism of the carbon fibre. The degraded resin, however, did not cover the diamond grit, thus maintaining the active cutting edges. Ding et al. [142] also reported that the presence of active cutting edge from the sharp abrasive peak of the diamond aided in the cutting process, which then reduces the cutting forces in UAM.

4.4.3 Surface roughness

The average surface roughness, Ra, for CM and UAM over 10 m machining length is shown in Figure 4-57. The error bars represent both maximum and minimum values of the measured surface roughness. The surface roughness measured for CM was 20 % higher, when compared to the machined surface of UAM. As the machined length increased, the surface roughness increased in both UAM and CM. The progression of surface roughness can be related to the cutting tool condition and the cutting forces of both processes, as explained in Sections 4.4.1 and 4.4.2. The cutting tool used for CM was loaded with degraded resin and broken fibre as the cutting length increased. Besides, the diamond grits were covered with degraded resin and broken fibre, as illustrated in Figures 4-51 (a), (b), and (c), thus resulting in the decrease of active cutting edges on the cutting tool used for CM. As a result, the cutting action reflected a form of friction, instead of fracturing the workpiece materials. In contrast with CM, the tool vibration,

which is due to the ultrasonic motion in UAM, aided in fracturing the fibre, which resulted in better surface condition, when compared to CM. As depicted in Section 4.4.1, the diamond grain fracture that was observed on the cutting tool used for UAM creates more active cutting edges on the cutting tool.

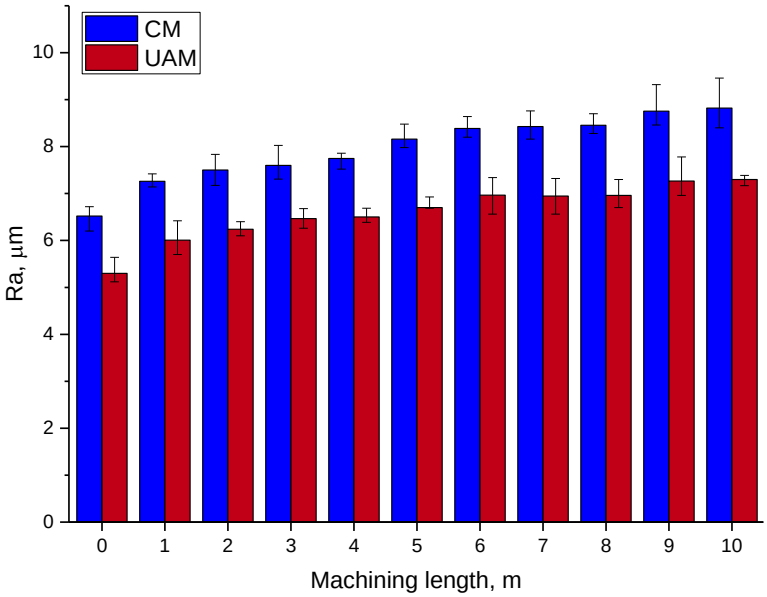

Figure 4-57: Surface roughness for CM and UAM.

Further inspection of the surface condition in SEM after 10 m length showed that the CM-machined surface experienced matrix smearing, fibre pull-out, and fibre-matrix cracking, as illustrated in Figure 4-58. Furthermore, it was observed that the matrix had smeared on the machined surface and the fibre-matrix de-bonding occurred. This occurrence can be attributed to the high cutting forces required for the material removal processes due to poor tool conditions for CM at this machining length. These are also attributed to the cutting tool condition that is loaded with degraded resin and broken fibres, which covered the diamond grit on the cutting tool used for CM [113, 114, 141]. On the contrary, Figure 4-59 displays that the UAM-machined surface experienced fibre pull-out that generated voids and holes on the machined surface.

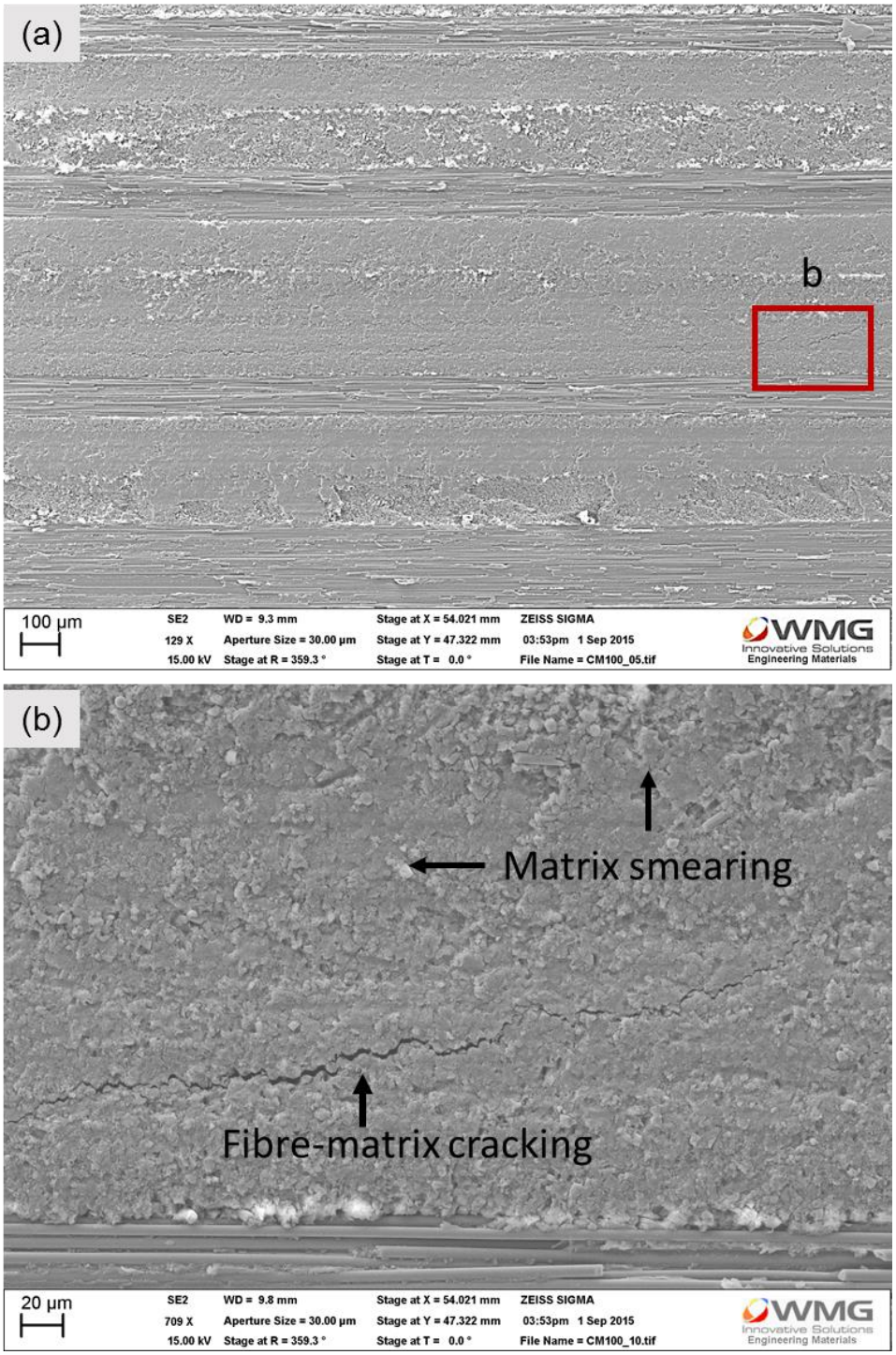

Figure 4-58: (a) SEM micrograph of CM machined CFRP surface at 10 m machining length and (b) high magnification of 'b' showing that the surfaces were covered with the degraded resin and experienced fibre-matrix cracking.

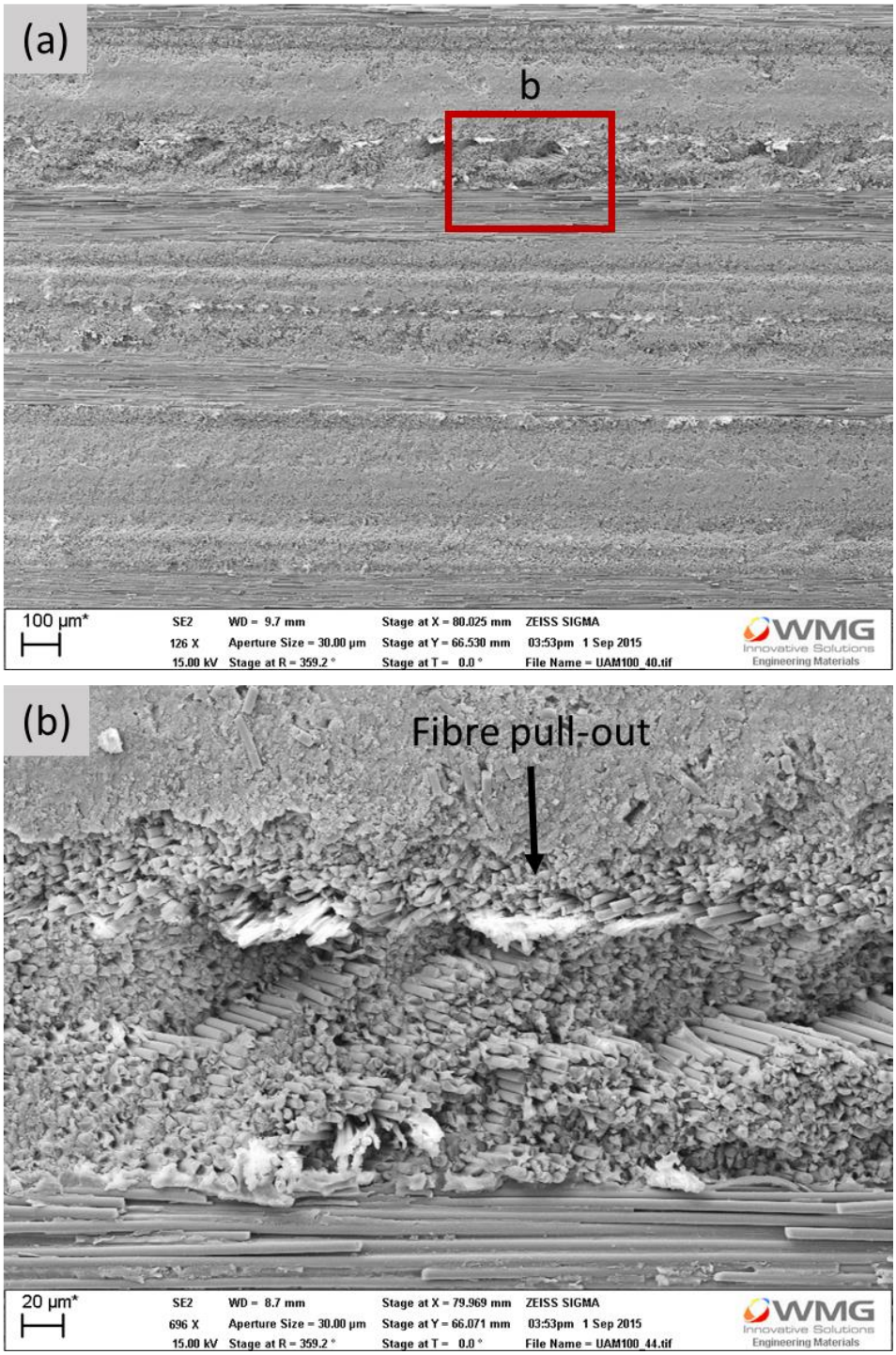

Figure 4-59: (a) SEM micrograph of UAM machined CFRP surface at 10 m machining length and (b) high magnification of 'b' showing that the fibre being pulled out from the surface and generates voids and holes on the machined surface.

Next, Figures 4-60 and 4-61 exhibit the surface topography and the roughness profile for both CM- and UAM-machined surface at 10 m machining length. The surface roughness profile for CM and UAM indicated that the wavelength of the profile did not share a similar trend. The surface profile of the CM indicated that the peaks and the troughs were between -10 and 20 μm, while the average surface roughness was 8.5 μm at 10 m machining length. These signify that the smeared matrix resin was found on the CM machined surface. On the other hand, the height distribution of the UAM was between -25 and 20 μm, whereas the average surface roughness at 10 m machining length was 7.2 μm. The UAM-machined surface profile showed that the height of the profile was distributed irregularly. This can be explained due to the occurrences of fibre pull-out and void that were observed on the machined surface of the UAM, as shown in Figure 4-65. Although the average surface roughness for CM was higher when compared to that of UAM, the surface profile for UAM indicated that the tool vibrations during machining could be attributed to the variations of the profile height. Ramulu et al. [139] reported that the smeared matrix on the machined surface could result in lower surface roughness. However, as for the CM-machined surface, the distribution of the fibre pull-out and the matrix smearing on the machined surface had not been apparent.

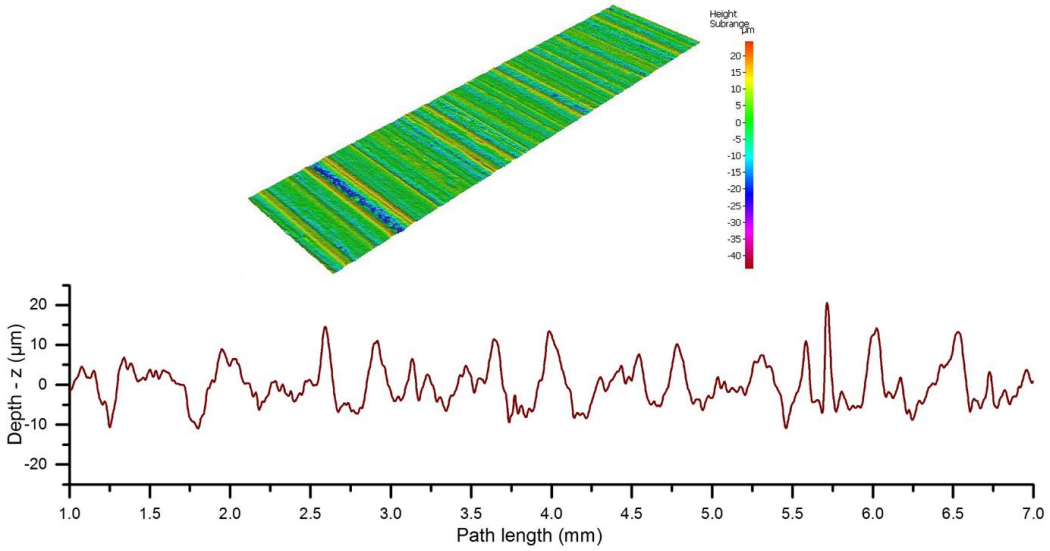

Figure 4-60: Surface topography and roughness profile of the CM surface produced by the Alicona with 5X magnification with the average surface roughness, Ra of 8.5 µm

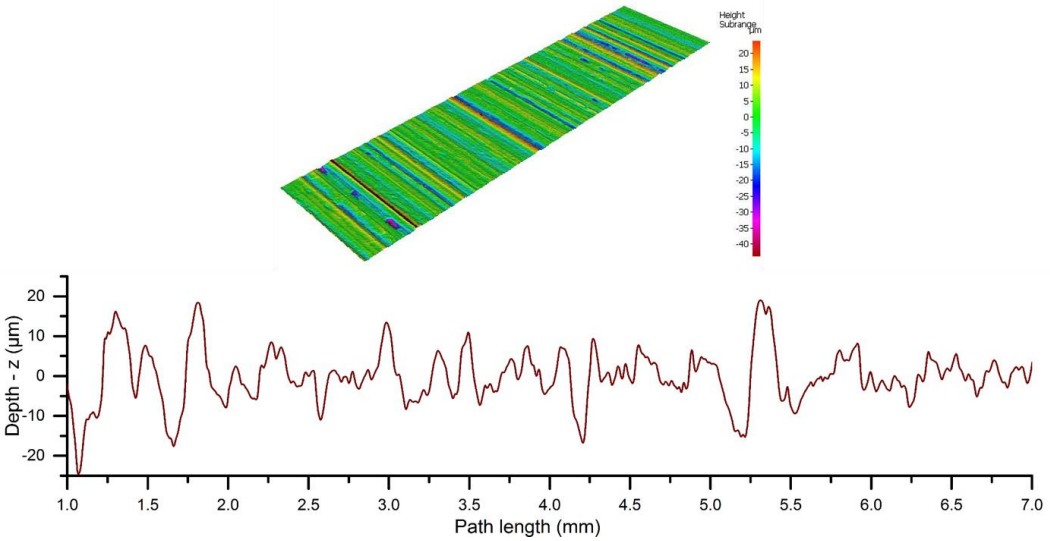

Figure 4-61: Surface topography and roughness profile of the UAM surface produced by the Alicona with 5X magnification with Ra of 7.2 µm.

4.4.4 Summary from Study 3

When milling CFRP with the presence of ultrasonic vibration on the cutting tool employing the abrasive diamond tool, the improvement of the cutting tool condition on the abrasive diamond tool used for UAM could be beneficial for CFRP machinability. Hence, the findings from Study 3 are summarized as follows:

- Milling of CFRP with the presence of ultrasonic vibration on the cutting tool improved the condition of the tool, as compared to the CM. The amount of degraded resin and broken fibre that adhered to the cutting tool used for UAM had been 44% less than the cutting tool used for CM. The ultrasonic vibration that is perpendicular to the feed direction reduced the chances of the CFRP chip to get stuck between the diamond grits. The cutting tool used for CM was loaded with broken fibre and degraded resin as the machining length was increased.
- The main wear mechanisms for the cutting tool used for UAM were grain fracture of the diamond grain and micro-crack of the nickel bond. Whereas, the cutting tool used for CM experienced bond fracture between nickel bond and diamond grain, which led to diamond grain pull-out and micro-fracture of the diamond grit. The cutting tool condition for both CM and UAM significantly affected the cutting forces and the machined surface condition.
- The cutting forces in CM was 5 to 10 % higher compared to the UAM because the cutting tool used for CM was loaded with degraded resin and broken fibre. Meanwhile, the cutting tool used for UAM had fracture of the diamond grain, which is beneficial in generating more cutting edges due to the formation of sharp diamond abrasive peaks. Consequently, the cutting forces measured in UAM significantly reduced, when compared to that in CM. As for the machined surfaces, the cutting

tool condition significantly affected the surface roughness and the integrity of the machined surface. Matrix smearing, fibre-matrix cracking, and fibre pull-out were observed on CM-machined CFRP surface, whereas fibre pull-out was apparent on the UAM-machined surface.

- Thus, the application of ultrasonic vibration on the abrasive diamond tool significantly improved the cutting tool condition, which reduced cutting forces and enhanced the condition of machined surface, when compared to that in CM.

4.5 Overall discussion

4.5.1 Effects of cutting processes and environments on the tool wear, cutting forces and surface roughness

Previous studies [12, 13, 150, 154] have reported that the application of ultrasonic assisted machining when milling metal enhanced the aspect of machinability in terms of longer tool life, lower cutting forces, and improved surface roughness. However, the different directions of the ultrasonic vibration, cutting parameters, and workpiece materials have made understanding UAM of CFRP a difficult task. This study proves that the application of the typical end mill tool, which is uncoated WC-Co end mill (Study 1(a)), and PCD end mill (Study 2), when milling CFRP with the presence of ultrasonic vibration at the cutting tool that is perpendicular towards feed direction had been non-beneficial to tool wear and surface roughness.

The tool wear measured for UAM is higher than CM for both cases. For Study 1(a), the tool wear for UAM was higher 30 to 40 %, when compared to CM, while for Study 2, the PCD tool used for CM could travel an extra 5 m before reaching its maximum wear. This is attributed to the ultrasonic vibration of the cutting tool that is perpendicular towards the feed direction during milling. Moreover, the intermittent separation between the

cutting tool and the workpiece in UAM claimed by other studies is not observed in this research.

In terms of surface roughness, the higher surface roughness obtained by UAM-machined surface can be attributed to the back and forth motion of the cutting tool, as well as the quasi-isotropic carbon fibre orientation that may lead to the degradation of machined surface quality. Although the ultrasonic vibration of cutting tool in UAM did not improve tool wear and surface roughness in Studies 1(a) and 2, both studies showed that the cutting forces obtained by UAM are lower, as compared to CM. This can be attributed to the ultrasonic vibration of the cutting tool that aided in brittle fracture of carbon fibre.

In contrast with Studies 1(a) and 2, Study 3 displayed that milling of CFRP with abrasive diamond tool could offer some beneficial outcomes to tool condition, cutting forces, and surface roughness. Besides, it has been reported that the main problem when milling CFRP with abrasive diamond tool is the resin built-up between the diamond grits, which may increase cutting forces and reduce the quality of machined surface [113]. In this present research, the ultrasonic vibration of cutting tool created a sufficient medium for the carbon chip to be removed during machining. The results from Study 3 also show that less degraded resin and broken fibre adhered to the cutting tool used for UAM, while the cutting tool used for CM was loaded with degraded resin and broken fibre. As a result, when the test was terminated at 10 m of machining length, the area of the cutting tool used for CM was loaded with degraded resin and broken fibre, which was 44 % higher than those found on the UAM cutting tool. Hence, for UAM, the cutting forces had been reduced by 10 %, while the surface roughness improved by 20 %, when compared to CM.

In terms of machining environment, the dry environment is recommended when machining CFRP due to the nature of the resin that is susceptible to moisture absorption.

However, machining of CFRP higher than the Tg of matrix resin may lead to degradation of CFRP. Study 1(a) compared the effects of machining environments, which were dry, CCF, and CO_2 cryogenic cutting media when milling CFRP conventionally and with ultrasonic assistance. It was found that milling with CO_2 cutting media improved the tool wear of the uncoated WC-Co end mill up to 28 % when compared to dry and CCF machining environments. Besides, the high pressure of CO_2 directed towards the cutting tool aided in removing the heat generated and the chip produced. Milling of CFRP in dry environment resulted in high cutting temperature that ranged from 100 to 220 °C. Meanwhile, machining of CFRP with CCF resulted in higher tool wear and cutting forces due to the flood cooling of both cutting tool and workpieces. However, it was observed that milling with CCF resulted in improved surface roughness, when compared to dry and CO_2.

Overall, it can be concluded that the vibration of the cutting tool that is perpendicular towards the feed direction when milling of CFRP with typical end mill tool is not beneficial for tool wear and surface roughness. However, the ultrasonic vibration that aided in brittle fracture of the carbon fibre could reduce the cutting forces. Although UAM displayed lower cutting forces for all environments, milling of CFRP conventionally is recommended to obtain improved tool wear and improved surface roughness.

4.5.2 Effect of machining environment on machined CFRP surfaces

As mentioned in the literature, the machining of CFRP is limited below the Tg of matrix resin. Machining of CFRP higher than the Tg may lead to the degradation of matrix resin and in the quality of machined surface. Therefore, monitoring the cutting temperature is crucial when milling CFRP. In study 1(a), three different cutting environments were employed to investigate the effects of machining environment on the aspect of machinability (tool wear, cutting forces, and surface roughness), while Study 1(b) was designed to investigate the effects of the machining environments on the chemical properties of BMI 5250-4 matrix resin.

Although the cutting temperature measured by the thermal camera failed to reach Tg (less than 272 °C), elimination of Tg at 272 °C in DSC analysis for machined samples of CM and UAM dry at 3000 mm signified that the actual cutting temperature is higher than the Tg. Besides, the results from FTIR revealed that CM and UAM dry experienced further post-curing for matrix resin. This is explained by the reduction of maleimide (C=C) bond at 825 cm^{-1}, which was often observed while curing BMI resin.

Furthermore, formation of isocyanate-derived product at a wavelength of 2250 cm^{-1} revealed that the actual cutting temperature for CM dry at 3000 mm might reach 400 °C. Moreover, formation of isocyanate-derived product often occurs when the BMI resin is thermally degraded at temperatures between 400 and 600 °C. Interestingly, the formation of isocyanate-derived product was only observed at the CM dry, but none was recorded at UAM dry, although elimination of Tg and reduction of maleimide (C=C) had been noted. This finding is similar to Study 2, where the formation of isocyanate-derived product was only observed at the CM dry machined surface. Therefore, from Study 1(a) and Study 2, it can be concluded that the ultrasonic vibration of the cutting tool during

UAM could attribute to reduction in cutting temperature. The result obtained from FTIR also revealed that the application of conventional cutting fluid could affect the chemical properties of the BMI 5250-4 matrix resin. This was observed especially when machining CFRP with CCF, where inconsistency of C=C had been recorded due to the presence of –OH. Therefore, machining of CFRP in a dry environment is not recommended mainly because high cutting temperature may degrade the product.

No study has looked into the effect of machining upon machined CFRP surface for chemical properties in matrix resin especially in the changes of the Tg and the effect on the resin chemical bonding. Thus, this finding contributes to the body of knowledge regarding the effect of machining environment upon CFRP machined surface. As no study has identified the effect of machining environment upon matrix resin, the method and data of this study can serve as a benchmark for future work focusing on the effect of machining environment/temperature upon matrix resin.

Chapter 5 Conclusions

5.1 Conclusions for literature review

Based on the extensive literature survey pertaining to CFRP machining and BMI 5250-4 thermal history, several conclusions on prior studies are drawn, as follows:

- Machining of CFRP is limited to the glass transition temperature (Tg) of the matrix resin. Although machining with the presence of cutting fluid could result in a reduction of cutting temperature, it is not recommended to machine CFRP with the presence of cutting fluid. Further post-processing of the machined part has to remove the moistures absorbed during the machining. Therefore, it is proposed that machining of cryogenic coolant could be beneficial for machining CFRP.
- The ultrasonic assisted milling (UAM) has displayed some beneficial outcomes for machinability of metallic materials. The ultrasonic vibration of cutting tool/workpiece during machining is proposed to reduce the heat generated by the cutting tool and the workpiece. Therefore, the implementation of UAM in CFRP is suggested to improve the machinability in terms of tool wear, cutting force, and surface roughness, as well as to reduce cutting temperature.
- Thermal analysis study of polymeric material has been well established. Analysis methods, such as differential scanning calorimetry (DSC), thermogravimetric analysis (TGA), and Fourier transform infrared spectroscopy (FTIR), are some of the methods employed to investigate the properties of the polymeric materials. Therefore, these methods are proposed to investigate the effect of machining condition and environments on the machined CFRP surface.

5.2 Conclusions for experimental work

5.2.1 Study 1(a): Machinability of CFRP in dry, conventional cutting fluid and CO_2 cryogenic machining environment

Based on the observations made, as well as the analysis of UAM and conventional milling (CM) of CFRP with constant speed (500 m/min), feed (800 mm/min), and radial depth of cut (1 mm), the following conclusions are drawn:

- From Study 1(a), it is proposed that the effect of ultrasonic vibration that is perpendicular to the feed direction is not beneficial for machinability. It was observed that the tool wear of UAM was higher than CM in all machining environments.
- The highest tool wear was obtained by dry, followed by CCF, and CO_2. High tool wear in dry condition is proposed due to the heat generated by the cutting tool and the workpiece that deteriorates the cutting tool. Meanwhile, in CCF and CO_2, the presence of cutting fluid aided in heat removal that improved tool wear.
- As for cutting force, the vibration of the cutting tool aided in fracturing the carbon fibre in UAM, therefore, the cutting force in UAM was lower than the CM for all machining environments.
- The implementation of CO_2 during milling reduced the cutting temperature by 30 - 50 %, as compared to dry machining.
- UAM recorded higher surface roughness than in CM for all machining environments .The complexity of cutting tool movement in UAM resulted in rougher surface for all machining conditions.

- The machined surface obtained by CCF environments resulted in lower surface roughness. It is proposed that the flood cooling during CCF retained the strength of the CFRP.
- Therefore, from Study 1(a), it can be concluded that, in terms of processes, UAM did not show any beneficial output on tool wear and surface roughness. The cutting tool vibration that is in perpendicular to the feed direction added to the complexity of the tool movement. However, the ultrasonic vibration of the cutting tool aided in the fracturing mechanism of carbon fibre, thus resulting in lower cutting force. Machining with presence of CO_2 could be beneficial in reducing the cutting temperature, improving tool wear and reducing the cutting force as well as maintained the properties of the CFRP.

5.2.2 Study 1(b): Post machining analysis to understand the effect of machining environment on the machined CFRP surface

Based on DSC and FTIR analysis on machined surfaces obtained from Study 1(a), several conclusions can be made, as follows:

- The results obtained from DSC analysis of the machined surfaces demonstrated that the machining environment did influence the Tg of the Bismaleimide 5250-4 (BMI 5250-4) matrix resin. The Tg values for both UAM and CM in dry environment at 3000 mm machining length were eliminated, thus suggesting that the cutting temperature has altered the chemical properties of BMI 5250-4. This also suggests that the cutting temperature, during machining, could exceed 272 °C.

- Further analysis on the machined surface by FTIR revealed that the machined surface of CM in dry environment formed isocyanate-derived product (aromatic nitrile) from 2405 to 2233 cm^{-1} that had been observed in thermal degradation of BMI 5250-4, which suggests that the machined surface has been thermally degraded. The formation of isocyanate-derived product was observed when the BMI was thermally degraded at 400 °C. Therefore, this suggests that the cutting temperature for CM dry at 3000 mm could reach as high as 400 °C.
- The reduction of intensity in maleimide bond at 825 cm^{-1} that was observed in curing of BMI 5250-4 suggests that further curing had occurred in both CM and UAM dry environment. It is proposed that the heat generated during machining may cause further crosslinking effect on the BMI 5250-4 resin.
- The FTIR results on CCF-machined surface revealed that some of the chemical bonds had been modified by the presence of hydrogen bonding (-OH) in the water molecule. Meanwhile, as for the machined CFRP surface in the CO_2 environment, the intensity of the chemical bond was more stable, hence suggesting that the CO_2 environment did not have a substantial effect on CFRP.
- Based on Study 1(b), it is proposed that the CO_2 environment is a suitable environment in CFRP machining due to the reduction of cutting temperature that is offered by CO_2 and the minimal effect on the chemical properties of BMI 5250-4.
- The thermal analyses methods (TGA, DSC, and FTIR) that are often used for polymeric material have been proven to be beneficial in investigating the effect of machining on the machined CFRP surface.

5.2.3 Study 2: Machinability of CFRP using the PCD end mill

Based on the observations made, as well as the analyses of UAM and CM of CFRP with constant speed (500 m/min), feed (800 mm/min), and radial depth of cut (1 mm), the following conclusions are drawn:

- In Study 2, the tool wore out faster during UAM, when compared with CM. The PCD end mill used for CM can machine further 15 m before it reached its maximum wear band. However, the PCD end mill used for UAM can machine only 10 m before it reached its maximum wear band. Thus, it is proposed that the ultrasonic vibration in UAM that is perpendicular to the feed direction generates more friction between the cutting tool and the machined surface. Therefore, it can be concluded that the ultrasonic vibration of cutting in milling is not beneficial for tool wear, regardless the tool geometry.
- In terms of cutting forces, the maximum cutting forces recorded for UAM had been lower (10 %) when compared to CM. Tool vibration aided the material removal process in UAM.
- However, the average surface roughness, Ra, for UAM was higher between 5 and 25 %, when compared to CM. Worse surface quality in UAM can be attributed to the motion of the tool, which was perpendicular to the machining direction, hence generating rougher machined surface.
- The reduction in cutting force for UAM had been due to ultrasonic vibration that aided in fracturing the carbon fibre and the brittle fracture of the CFRP.
- Therefore, the application of ultrasonic vibration in UAM produced higher tool wear and rougher surface, when compared with CM. The ultrasonic vibration

aided in fracturing mechanism and resulted in reducing the cutting forces in UAM.

- Post-machining analysis on samples derived from Study 1(b) revealed that the presence of isocyanate-derived product (aromatic nitrile bond) in the sample indicates that the machined CFRP surface for CM has been thermally degraded. However, the presence of nitrile bond was not observed in UAM-machined CFRP surface. This finding confirms that the cutting mechanism in UAM aided in the heat removal that is generated by cutting tool and workpieces. As a result, UAM could be beneficial in reducing the effect of temperature upon machined surface.

5.2.4 Study 3: Machinability of CFRP using abrasive diamond tool

Based on the observations made and the analyses of UAM and CM of CFRP with constant speed (565 m/min), feed (1500 mm/min), and radial depth of cut (1 mm), the following conclusions are drawn:

- The presence of ultrasonic vibration on the diamond abrasive tool during UAM resulted in better tool condition, when compared to CM. Diamond abrasive tool used for UAM resulted in 44 % less adhesion of broken fibre and thermally degraded resin, when compared to the tool used for CM. The ultrasonic vibration of the cutting tool aided in the evacuation of broken fibre and degraded resin; therefore less material adhered between the abrasive diamond grits.
- Fracture of diamond grit on cutting tool used for UAM generated more active cutting edges on the abrasive diamond tool. However, from an abrasive diamond tool used for CM, the fracturing of nickel bond was observed, and micro-cracks

in the diamond grits were noted after 10-metre machining length, which could lead to pull-out of diamond grit from the cutting tool, thus suggesting that UAM can prolong tool life.

- The conditions of the abrasive diamond tool significantly affected the cutting forces and the surface roughness obtained in CM and UAM. As the abrasive diamond tool was covered with broken fibre and degraded resin in CM, it was observed that the cutting forces (Fx and Fy) in CM had been 10 - 15 % higher, when compared to UAM. However, in UAM, the presence of more active cutting edges was noted and the ultrasonic vibration aided in removal of materials.
- Surface roughness measured for CM was in the range of 6.8 to 9 μm, whereas surface roughness measured for UAM was in the range of 5.5 to 6 μm. It was observed that on CM-machined surface, the matrix was smearing and fibre-matrix de-bonding. The condition of the cutting tool used for CM that was covered with broken fibres and degraded resin generated higher cutting forces that led to more damages. Meanwhile, in UAM, the ultrasonic vibration of the cutting tool generated void and holes on the machined surface.
- Therefore, the application of ultrasonic vibration on the cutting tool could increase tool life, improve surface roughness, and lower cutting forces when CFRP is machined with diamond abrasive tool.

5.3 Overall conclusions

This research has developed both knowledge and understanding pertaining to the effect of machining environment/process upon thermal behaviour of BMI 5250-4 matrix and machinability of CFRP. Therefore, the overall conclusions of this research are listed in the following:

- The Differential Scanning Calorimetry (DSC) and the Fourier transform infrared (FTIR) analysis were employed in this study to investigate the effect of machining environment on the machined surface. It is observed that in dry machining for CM and UAM at 3000 mm machining length, the Tg of the BMI 5250-4 matrix resin has been eliminated due to the high cutting temperature. Therefore, the elimination of the Tg suggests that the chemical properties of the BMI 5250-4 resin have experienced changes.
- The FTIR results suggest that the machined surface of CM dry at 3000 mm machining length is thermally degraded due to the formation of isocyanate-derived product (aromatic nitrile bond) at 2405 to 2233 cm^{-1} and the reduction of maleimide bond at 825 cm^{-1} that is often observed in curing mechanism of BMI 5250-4. The formation of isocyanate-derived product is often observed when BMI is thermally degraded from 400 to 600 °C, hence suggesting the actual cutting temperature at 3000 mm machining length that may hit as high as 400 °C. However, the formation of isocyanate-derived product is not observed for UAM machined surface, thus suggesting that the ultrasonic vibration of the cutting tool may reduce the cutting temperature at the primary shear zone.
- Application of CCF can be beneficial for machinability. However, the results retrieved from FTIR indicate that the presence of moisture (-OH) could affect the properties of BMI 5250-4.

- Results obtained from DSC and FTIR analyses display that it is not recommended to machine CFRP in a dry and CCF environment. Therefore, it is proposed that the application of CO_2 when machining CFRP could be beneficial to the machinability of CFRP and it does not affect the chemical properties of the BMI 5250-4 resin.
- It is proposed that in a milling operation when employing typical end mill (Studies 1(a) and 2), the ultrasonic vibration that is perpendicular direction with the feed direction generates more interaction between the tool and the workpieces, hence resulting in higher tool wear and surface roughness, regardless of the cutting tool geometry employed. Although higher tool wear and surface roughness are associated to UAM, it can be observed that the cutting forces in UAM are lower compared to that of CM. Besides, it is proposed that the ultrasonic vibration aids in brittle fracture of the carbon fibre that leads to a reduction in cutting forces.
- When employing abrasive diamond tool to perform milling of CFRP, it is observed that UAM has some beneficial outcomes (tool condition, cutting forces, and surface roughness) with fewer material adhesion on the abrasive diamond tool. As a result, the cutting forces and the surface roughness in UAM are lower, when compared to those of CM. However, in Studies 1(a) and 2 (WC and PCD end mill), higher tool wear is observed in UAM, when compared with CM.
- The application of CO_2 machining environment in Study 1(a) results in improved tool wear, reduced cutting forces, and improved surface roughness. It is observed that the application of CO_2 in machining CFRP could remove the heat generated and reduce the cutting temperature. However, the application of CO_2 in UAM does not show improvement in machinability. In all cases (dry, CCF, and CO_2), the results obtained for CM have always improved than UAM.

- The application of UAM for CFRP is not beneficial for the aspect of machinability due to the complexity of the tool vibration and the heterogeneous property of CFRP. Evidence derived from the FTIR analysis shows that the isocyanate-derived product is not observed for the UAM-machined surface in Study 1(b), while Study 2 indicates that the application of UAM could be beneficial in reducing the effect of cutting temperature on CFRP.

Chapter 6 Future work

Results obtained from Studies 1 to 3 has established the knowledge of the effect of machining of CFRP machined surface and machinability of UAM. Therefore, future work listed below are still needed to extend the knowledge.

- The effect of chemical properties changes can be extended by investigating the effect of the machining environment to the internal damages of the CFRP. The knowledge on how much the distance beneath the machined surface that affected by the machining environment could be beneficial.
- The effect of chemical properties changes can be extended to be in a relationship with the mechanical property changes. It is expected that the reduction in the chemical property changes of the CFRP can lead to the reduction in the mechanical properties changes. Further analysis such as investigation on the strength of the materials can be employed to explain the effect of the materials properties changes.
- Development of measuring tool tip temperature while machining CFRP composite must be explored because least research focused on the actual machining temperature. High machining temperature while machining of CFRP composite is critical, hence, the simulation of the machining temperature of the composite is crucial.
- Variation of ultrasonic and machining parameters such as cutting speed, feed rate, ultrasonic amplitude and ultrasonic frequency and low feed rate could give an overall overview on the effectiveness of the UAM.
- Least research was done on simulation of the effect of the ultrasonic assisted machining on the composite materials. Finite element analysis (FMEA) which is well established in metal cutting can be employed to get a better understanding on the ultrasonic assisted machining of the composite materials.

References

[1] J. Hale. (2006). *Boeing 787 from the Ground Up*. Available: http://www.boeing.com/commercial/aeromagazine/articles/qtr_4_06/index.html (Assessed 15 September 2016).

[2] (2017). *Composites: Airbus continues to shape the future*. Available: http://www.airbus.com/newsroom/news/en/2017/08/composites--airbus-continues-to-shape-the-future.html (Assessed 20 March 2017).

[3] J. Y. Sheikh-Ahmad, *Machining of polymer composites*: Springer, 2009.

[4] F. C. Campbell, *Structural composite materials*: ASM international, 2010.

[5] R. Teti, "Machining of Composite Materials," *CIRP Annals - Manufacturing Technology,* vol. 51, pp. 611-634, 2002.

[6] M. M. A. Zarchi, M. R. Razfar, and A. Abdullah, "Influence of ultrasonic vibrations on side milling of AISI 420 stainless steel," *The International Journal of Advanced Manufacturing Technology,* vol. 66, pp. 83-89, 2013.

[7] H. Takeyama and N. Iijima, "Machinability of Glassfiber Reinforced Plastics and Application of Ultrasonic Machining," *CIRP Annals - Manufacturing Technology,* vol. 37, pp. 93-96, 1988.

[8] A. Maurotto and C. T. Wickramarachchi, "Experimental investigations on effects of frequency in ultrasonically-assisted end-milling of AISI 316L: A feasibility study," *Ultrasonics,* vol. 65, pp. 113-120, 2016.

[9] X.-H. Shen, J. Zhang, D. Xing, and Y. Zhao, "A study of surface roughness variation in ultrasonic vibration-assisted milling," *The International Journal of Advanced Manufacturing Technology,* vol. 58, pp. 553-561, 2012.

[10] V. A. Phadnis, F. Makhdum, A. Roy, and V. V. Silberschmidt, "Experimental and Numerical Investigations in Conventional and Ultrasonically Assisted Drilling of CFRP Laminate," *Procedia CIRP,* vol. 1, pp. 455-459, 2012.

[11] V. A. Phadnis, F. Makhdum, A. Roy, and V. V. Silberschmidt, "Ultrasonically-assisted drilling in CFRP composites," in *ECCM15—15th European conference on composite materials*, 2012, pp. 24-28.

[12] M. M. A. Zarchi, M. R. Razfar, and A. Abdullah, "Research on the importance of tool–workpiece separation in ultrasonic vibration–assisted milling," *Proceedings of the Institution of Mechanical Engineers, Part B: Journal of Engineering Manufacture,* vol. 231, pp. 600-607, 2015.

[13] M. Razfar, P. Sarvi, and M. A. Zarchi, "Experimental investigation of the surface roughness in ultrasonic-assisted milling," *Proceedings of the Institution of Mechanical Engineers, Part B: Journal of Engineering Manufacture,* vol. 225, pp. 1615-1620, 2011.

[14] R. J. Morgan, E. Eugene Shin, B. Rosenberg, and A. Jurek, "Characterization of the cure reactions of bismaleimide composite matrices," *Polymer,* vol. 38, pp. 639-646, 1997.

[15] R. J. Morgan, R. J. Jurek, A. Yen, and T. Donnellan, "Toughening procedures, processing and performance of bismaleimide-carbon fibre composites," *Polymer,* vol. 34, pp. 835-842, 1993.

[16] A. Khajeh, F. Mustapha, M. T. H. Sultan, G. Bánhegyi, Z. Karácsony, and V. Baranyai, "The effect of thermooxidative aging on the durability of glass fiber-reinforced epoxy," *Advances in Materials Science and Engineering,* vol. 2015, 2015.

[17] M. Ramulu, "Machining and surface integrity of fibre-reinforced plastic composites," *Sadhana,* vol. 22, pp. 449-472, 1997.

[18] A. A. Khan and M. I. Ahmed, "Improving tool life using cryogenic cooling," *Journal of Materials Processing Technology,* vol. 196, pp. 149-154, 2008.

[19] V. Tagliaferri, G. Caprino, and A. Diterlizzi, "Effect of drilling parameters on the finish and mechanical properties of GFRP composites," *International Journal of Machine Tools and Manufacture,* vol. 30, pp. 77-84, 1990.

[20] M. Saleem, L. Toubal, R. Zitoune, and H. Bougherara, "Investigating the effect of machining processes on the mechanical behavior of composite plates with circular holes," *Composites Part A: Applied Science and Manufacturing,* vol. 55, pp. 169-177, 2013.

[21] J. Liu, D. Zhang, L. Qin, and L. Yan, "Feasibility study of the rotary ultrasonic elliptical machining of carbon fiber reinforced plastics (CFRP)," *International Journal of Machine Tools and Manufacture,* vol. 53, pp. 141-150, 2012.

[22] M. Haddad, R. Zitoune, H. Bougherara, F. Eyma, and B. Castanié, "Study of trimming damages of CFRP structures in function of the machining processes and their impact on the mechanical behavior," *Composites Part B: Engineering,* vol. 57, pp. 136-143, 2014.

[23] J. Sheikh-Ahmad and A. H. Shahid, "Effect of edge trimming on failure stress of carbon fibre polymer composites," *International Journal of Machining and Machinability of Materials,* vol. 13, pp. 331-347, 2013.

[24] M. M. Schwartz, "Composite Materials-Properties, Nondestructive Testing, and Repair, vol. 1," ed: Prentice Hall Inc, New Jersey, USA, 1997.

[25] P. K. Mallick, *Fiber-reinforced composites: materials, manufacturing, and design*: CRC press, 1993.

[26] M. Balasubramanian, *Composite materials and processing*: CRC press, 2013.

[27] K. K. Chawla, *Composite materials: science and engineering*: Springer, 2012.

[28] D. Gay, *Composite materials: design and applications*: CRC press, 2014.

[29] M. A. Meyers and K. K. Chawla, *Mechanical behavior of materials* vol. 547: Cambridge University Press Cambridge, 2009.

[30] A. Katz, N. Berman, and L. C. Bank, "Effect of high temperature on bond strength of FRP rebars," *Journal of Composites for Construction,* vol. 3, pp. 73-81, 1999.

[31] A. Katz and N. Berman, "Modeling the effect of high temperature on the bond of FRP reinforcing bars to concrete," *Cement and Concrete Composites,* vol. 22, pp. 433-443, 2000.

[32] J. Boyd, "Bismaleimide Resins," in *ASM Handbook*, ed, 2001, pp. 97-104.

[33] J. E. Lincoln, R. J. Morgan, and E. E. Shin, "Fundamental investigation of cure-induced microcracking in carbon fiber/bismaleimide cross-ply laminates," *Polymer composites,* vol. 22, pp. 397-419, 2001.

[34] Y. Li, J. Miranda, and H.-J. Sue, "Hygrothermal diffusion behavior in bismaleimide resin," *Polymer,* vol. 42, 2001.

[35] L.-R. Bao and A. F. Yee, "Effect of temperature on moisture absorption in a bismaleimide resin and its carbon fiber composites," *Polymer,* vol. 43, pp. 3987-3997, 2002.

[36] R. Torrecillas, N. Regnier, and B. Mortaigne, "Thermal degradation of bismaleimide and bisnadimide networks—products of thermal degradation and type of crosslinking points," *Polymer Degradation and Stability,* vol. 51, pp. 307-318, 1996.

[37] W. Shaoquan, D. Shangli, G. Yu, and S. Yungang, "Thermal ageing effects on mechanical properties and barely visible impact damage behavior of a carbon fiber reinforced bismaleimide composite," *Materials & Design,* vol. 115, pp. 213-223, 2017.

[38] X. Lv, R. Wang, W. Liu, and L. Jiang, "Effect of thermal-oxidative aging on carbon fibre-bismaleimide composites," *Pigment & Resin Technology,* vol. 41, pp. 34-41, 2012.

[39] X. Liu, Y. Yu, and S. Li, "Study on cure reaction of the blends of bismaleimide and dicyanate ester," *Polymer,* vol. 47, pp. 3767-3773, 2006.

[40] Y. Li, J. Miranda, and H.-J. Sue, "Hygrothermal diffusion behavior in bismaleimide resin," *Polymer,* vol. 42, pp. 7791-7799 2001.

[41] N. Regnier and B. Mortaigne, "Thermal behavior of bismaleimide resin," *Polymers for Advanced Technologies,* vol. 5, pp. 513-520, 1994.

[42] J.-S. Chen, C. K. Ober, M. D. Poliks, Y. Zhang, U. Wiesner, and C. Cohen, "Controlled degradation of epoxy networks: analysis of crosslink density and glass transition temperature changes in thermally reworkable thermosets," *Polymer,* vol. 45, pp. 1939-1950, 2004.

[43] A. Khattab, "Cure Cycle Effect on High-Temperature Polymer Composite Structures Molded by VARTM," *Journal of Composites,* vol. 2013, p. 6, 2013.

[44] T. K. Tsotsis, S. Keller, K. Lee, J. Bardis, and J. Bish, "Aging of polymeric composite specimens for 5000 hours at elevated pressure and temperature," *Composites science and technology,* vol. 61, pp. 75-86, 2001.

[45] T. K. Tsotsis and S. M. Lee, "Long-term thermo-oxidative aging in composite materials: failure mechanisms," *Composites science and technology,* vol. 58, pp. 355-368, 1998.

[46] Y. Wang, J. Meng, Q. Zhao, and S. Qi, "Accelerated ageing tests for evaluations of a durability performance of glass-fiber reinforcement polyester composites," *Journal of Materials Science & Technology,* vol. 26, pp. 572-576, 2010.

[47] S. Chandran M, M. Krishna, and K. S. Rai, "Preparation and characterization of chain-extended bismaleimide/carbon fibre composites," *International Journal of Polymer Science,* 2010.

[48] E. Martuscelli, P. Musto, G. Ragosta, and G. Scarinizi, "A polymer network of unsaturated polyester and bismaleimide resins: 1. Kinetics, mechanism and molecular structure," *Polymer,* vol. 37, pp. 4025-4032, 1996.

[49] J. K. Pandey, K. R. Reddy, A. P. Kumar, and R. Singh, "An overview on the degradability of polymer nanocomposites," *Polymer degradation and stability,* vol. 88, pp. 234-250, 2005.

[50] P. Musto, G. Ragosta, P. Russo, and L. Mascia, "Thermal-oxidative degradation of epoxy and epoxy-bismaleimide networks: kinetics and mechanism," *Macromolecular chemistry and physics,* vol. 202, pp. 3445-3458, 2001.

[51] X. Lv, R. Wang, W. Liu, and L. Jiang, "Surface and interface properties of carbon fiber composites under cyclical aging," *Applied Surface Science,* vol. 257, pp. 10459-10464, 2011.

[52] E. M. Trent and P. K. Wright, *Metal cutting*: Butterworth-Heinemann, 2000.

[53] S. Kalpakjian, *Manufacturing engineering and technology*: Pearson Education India, 2001.

[54] A. Koplev, A. Lystrup, and T. Vorm, "The cutting process, chips, and cutting forces in machining CFRP," *Composites,* vol. 14, pp. 371-376, 1983.

[55] D. Arola, M. Ramulu, and D. H. Wang, "Chip formation in orthogonal trimming of graphite/epoxy composite," *Composites Part A: Applied Science and Manufacturing,* vol. 27, pp. 121-133, 1996.

[56] H. Hocheng, H. Y. Puw, and Y. Huang, "Preliminary study on milling of unidirectional carbon fibre-reinforced plastics," *Composites Manufacturing,* vol. 4, pp. 103-108, 1993.

[57] D. H. Wang, M. Ramulu, and D. Arola, "Orthogonal cutting mechanisms of graphite/epoxy composite. Part I: unidirectional laminate," *International Journal of Machine Tools and Manufacture,* vol. 35, pp. 1623-1638, 1995.

[58] D. H. Wang, M. Ramulu, and D. Arola, "Orthogonal cutting mechanisms of graphite/epoxy composite. Part II: multi-directional laminate," *International Journal of Machine Tools and Manufacture,* vol. 35, pp. 1639-1648, 1995.

[59] H. Puw and H. Hocheng, "Milling of polymer composites," *Manufacturing Engineering and Materials Processing,* vol. 53, pp. 267-294, 1999.

[60] K. Palanikumar and J. P. Davim, "Assessment of some factors influencing tool wear on the machining of glass fibre-reinforced plastics by coated cemented carbide tools," *Journal of Materials Processing Technology,* vol. 209, pp. 511-519, 2009.

[61] J. P. Davim and P. Reis, "Damage and dimensional precision on milling carbon fiber-reinforced plastics using design experiments," *Journal of Materials Processing Technology,* vol. 160, pp. 160-167, 2005.

[62] T. Yashiro, T. Ogawa, and H. Sasahara, "Temperature measurement of cutting tool and machined surface layer in milling of CFRP," *International Journal of Machine Tools and Manufacture,* vol. 70, pp. 63-69, 2013.

[63] L. Sorrentino, S. Turchetta, L. Colella, and C. Bellini, "Analysis of Thermal Damage in FRP Drilling," *Procedia Engineering,* vol. 167, pp. 206-215, 2016.

[64] J. L. Merino-Pérez, R. Royer, S. Ayvar-Soberanis, E. Merson, and A. Hodzic, "On the temperatures developed in CFRP drilling using uncoated WC-Co tools Part I: Workpiece constituents, cutting speed and heat dissipation," *Composite Structures,* vol. 123, pp. 161-168, 2015.

[65] H. Wang, J. Sun, J. Li, L. Lu, and N. Li, "Evaluation of cutting force and cutting temperature in milling carbon fiber-reinforced polymer composites," *The International Journal of Advanced Manufacturing Technology,* vol. 82, pp. 1517-1525, 2016.

[66] M. Haddad, R. Zitoune, F. Eyma, and B. Castanié, "Machinability and surface quality during high speed trimming of multi directional CFRP," *International Journal of Machining and Machinability of Materials,* vol. 13, pp. 289-310, 2013.

[67] M. K. Nor Khairusshima, C. H. Che Hassan, A. G. Jaharah, A. K. M. Amin, and A. N. Md Idriss, "Effect of chilled air on tool wear and workpiece quality during milling of carbon fibre-reinforced plastic," *Wear,* vol. 302, pp. 1113-1123, 2013.

[68] Z. Jia, R. Fu, F. Wang, B. Qian, and C. He, "Temperature effects in end milling carbon fiber reinforced polymer composites," *Polymer Composites,* 2016.

[69] K. Kerrigan, J. Thil, R. Hewison, and G. E. O'Donnell, "An Integrated Telemetric Thermocouple Sensor for Process Monitoring of CFRP Milling Operations," *Procedia CIRP,* vol. 1, pp. 449-454, 2012.

[70] K. Kerrigan and G. E. O'Donnell, "On the Relationship between Cutting Temperature and Workpiece Polymer Degradation During CFRP Edge Trimming," *Procedia CIRP,* vol. 55, pp. 170-175, 2016.

[71] S. Ghafarizadeh, G. Lebrun, and J.-F. Chatelain, "Experimental investigation of the cutting temperature and surface quality during milling of unidirectional carbon fiber reinforced plastic," *Journal of Composite Materials,* vol. 50, pp. 1059-1071, 2016.

[72] W. Hintze, C. Schütte, and S. Steinbach, "Influence of the Fiber Cutting Angle on Work Piece Temperature in Drilling of Unidirectional CFRP," in *New Production Technologies in Aerospace Industry*, B. Denkena, Ed., ed: Springer International Publishing, 2014, pp. 137-143.

[73] N. F. H. A. Halim, H. Ascroft, and S. Barnes, "Analysis of Tool Wear, Cutting Force, Surface Roughness and Machining Temperature During Finishing Operation of Ultrasonic Assisted Milling (UAM) of Carbon Fibre Reinforced Plastic (CFRP)," *Procedia Engineering,* vol. 184, pp. 185-191, 2017.

[74] M. H. El-Hofy, S. L. Soo, D. K. Aspinwall, W. M. Sim, D. Pearson, R. M'Saoubi*, et al.*, "Tool Temperature in Slotting of CFRP Composites," *Procedia Manufacturing,* vol. 10, pp. 371-381, 2017.

[75] V. S. Sharma, M. Dogra, and N. Suri, "Cooling techniques for improved productivity in turning," *International Journal of Machine Tools and Manufacture,* vol. 49, pp. 435-453, 2009.

[76] N. S. Kalsi, R. Sehgal, and V. S. Sharma, "Cryogenic Treatment of Tool Materials: A Review," *Materials & Manufacturing Processes,* vol. 25, pp. 1077-1100, 2010.

[77] R. Ghosh, Z. Zurecki, and J. H. Frey, "Cryogenic machining with brittle tools and effects on tool life," in *ASME 2003 International Mechanical Engineering Congress and Exposition*, 2003, pp. 201-209.

[78] V. Singh, S. Ghosh, and P. V. Rao, "Grindability Improvement of Composite Ceramic with Cryogenic Coolant," in *Proceedings of the World Congress on Engineering*, 2010.

[79] Y. Yildiz and M. Nalbant, "A review of cryogenic cooling in machining processes," *International Journal of Machine Tools and Manufacture,* vol. 48, pp. 947-964, 2008.

[80] G. T. Smith, *Cutting tool technology: industrial handbook*: Springer Science & Business Media, 2008.

[81] O. Pecat, R. Rentsch, and E. Brinksmeier, "Influence of milling process parameters on the surface integrity of CFRP," *Procedia CIRP,* vol. 1, pp. 466-470, 2012.

[82] M. Ucar and Y. Wang, "End-milling machinability of a carbon fiber reinforced laminated composite," *Journal of advanced materials,* vol. 37, pp. 46-52, 2005.

[83] R. P. Reed and M. Golda, "Cryogenic properties of unidirectional composites," *Cryogenics,* vol. 34, pp. 909-928, 1994.

[84] Y. Yildiz and M. M. Sundaram, "Cryogenic machining of composites A2 - Hocheng, H," in *Machining Technology for Composite Materials*, ed: Woodhead Publishing, 2012, pp. 365-393.

[85] P. Blau, K. Busch, M. Dix, C. Hochmuth, A. Stoll, and R. Wertheim, "Flushing Strategies for High Performance, Efficient and Environmentally Friendly Cutting," *Procedia CIRP,* vol. 26, pp. 361-366, 2015.

[86] M. I. Ahmed, A. F. Ismail, Y. A. Abakr, and A. K. M. N. Amin, "Effectiveness of cryogenic machining with modified tool holder," *Journal of Materials Processing Technology,* vol. 185, pp. 91-96, 2007.

[87] C. Machai, H. Abrahams, and D. Biermann, "Machining of β-Titanium Under Cryogenic Conditions: Process Cooling by CO2-Snow," in *Future Trends in Production Engineering: Proceedings of the First Conference of the German Academic Society for Production Engineering (WGP), Berlin, Germany, 8th-9th June 2011*, G. Schuh, R. Neugebauer, and E. Uhlmann, Eds., ed Berlin, Heidelberg: Springer Berlin Heidelberg, 2013, pp. 109-120.

[88] S. Y. Hong and Y. Ding, "Cooling approaches and cutting temperatures in cryogenic machining of Ti-6Al-4V," *International Journal of Machine Tools and Manufacture,* vol. 41, pp. 1417-1437, 2001.

[89] J. C. Aurich, P. Mayer, B. Kirsch, D. Eifler, M. Smaga, and R. Skorupski, "Characterization of deformation induced surface hardening during cryogenic turning of AISI 347," *CIRP Annals - Manufacturing Technology,* vol. 63, pp. 65-68, 2014.

[90] S. Barnes, P. Bhudwannachai, and A. N. Dahnel, "Drilling performance of carbon fiber reinforced epoxy composite when machined dry, with conventional cutting fluid and with a cryogenically cooled tool," in *ASME 2013 International Mechanical Engineering Congress & Exposition, IMECE*, 2013.

[91] T. Xia, Y. Kaynak, C. Arvin, and I. S. Jawahir, "Cryogenic cooling-induced process performance and surface integrity in drilling CFRP composite material," *The International Journal of Advanced Manufacturing Technology,* vol. 82, pp. 605-616, 2016.

[92] M. Dix, R. Wertheim, G. Schmidt, and C. Hochmuth, "Modeling of drilling assisted by cryogenic cooling for higher efficiency," *CIRP Annals - Manufacturing Technology,* vol. 63, pp. 73-76, 2014.

[93] K. V. B. S. Kalyan Kumar and S. K. Choudhury, "Investigation of tool wear and cutting force in cryogenic machining using design of experiments," *Journal of Materials Processing Technology,* vol. 203, pp. 95-101, 2008.

[94] Z. Y. Wang and K. P. Rajurkar, "Cryogenic machining of hard-to-cut materials," *Wear,* vol. 239, pp. 168-175, 2000.

[95] D. Bhattacharyya, M. N. Allen, and S. J. Mander, "Cryogenic machining of Kevlar composites," *Material and manufacturing process,* vol. 8, pp. 631-651, 1993.

[96] D. Bhattacharyya and D. P. W. Horrigan, "A study of hole drilling in Kevlar composites," *Composites Science and Technology,* vol. 58, pp. 267-283, 1998.

[97] P. Bhudwannachai, "Performance evaluation and analysis of the use of CO2 cooling for conventional drilling of carbon fibre reinforced plastics," PhD, Warwick Manufacturing Group, University of Warwick, United Kingdom, 2014.

[98] R. Y. Kim and S. L. Donaldson, "Experimental and analytical studies on the damage initiation in composite laminates at cryogenic temperatures," *Composite Structures,* vol. 76, pp. 62-66, 2006.

[99] T. Inoue, M. Hagino, M. Matsui, and L. W. Gu, "Cutting characteristics of CFRP materials with end milling," 2009, pp. 710-713.

[100] J. B. Schutz, "Properties of composite materials for cryogenic applications," *Cryogenics,* vol. 38, pp. 3-12, 1998.

[101] A. Rivera-Moreno, L. E. Hernández-Castillo, H. R. Siller, A. Elías-Zúñiga, and C. A. Rodríguez-González, "Influence of CO2 Cooling on the Orthogonal Cutting of Elastomers," *Ingeniería mecánica, tecnología y desarrollo,* vol. 4, pp. 177-183, 2013.

[102] S. Thirumalai Kumaran, T. J. Ko, C. Li, Z. Yu, and M. Uthayakumar, "Rotary ultrasonic machining of woven CFRP composite in a cryogenic environment," *Journal of Alloys and Compounds,* vol. 698, pp. 984-993, 2017.

[103] S. Arul, L. Vijayaraghavan, S. K. Malhotra, and R. Krishnamurthy, "The effect of vibratory drilling on hole quality in polymeric composites," *International Journal of Machine Tools and Manufacture,* vol. 46, pp. 252-259, 2006.

[104] M. Hojo, S. Matsuda, B. Fiedler, T. Kawada, K. Moriya, S. Ochiai*, et al.*, "Mode I and II delamination fatigue crack growth behavior of alumina fiber/epoxy laminates in liquid nitrogen," *International Journal of Fatigue,* vol. 24, pp. 109-118, 2002.

[105] R. F. Pinto, G. Catalanotti, and P. P. Camanho, "Measuring the intralaminar crack resistance curve of fibre reinforced composites at extreme temperatures," *Composites Part A: Applied Science and Manufacturing,* vol. 91, Part 1, pp. 145-155, 2016.

[106] K.-H. Im, C.-S. Cha, S.-K. Kim, and I.-Y. Yang, "Effects of temperature on impact damages in CFRP composite laminates," *Composites Part B: Engineering,* vol. 32, pp. 669-682, 2001.

[107] X. Wang, P. Y. Kwon, C. Sturtevant, D. Kim, and J. Lantrip, "Tool wear of coated drills in drilling CFRP," *Journal of Manufacturing Processes,* vol. 15, pp. 127-135, 2013.

[108] S. Rawat and H. Attia, "Wear mechanisms and tool life management of WC–Co drills during dry high speed drilling of woven carbon fibre composites," *Wear,* vol. 267, pp. 1022-1030, 2009.

[109] A. I. Azmi, R. J. T. Lin, and D. Bhattacharyya, "Tool wear prediction models during end milling of glass fibre-reinforced polymer composites," *The International Journal of Advanced Manufacturing Technology,* vol. 67, pp. 701-718, 2013.

[110] V. P. Astakhov and J. P. Davim, "Tools (geometry and material) and tool wear," in *Machining*, ed: Springer, 2008, pp. 29-57.

[111] W. König, C. Wulf, P. Graß, and H. Willerscheid, "Machining of Fibre Reinforced Plastics," *CIRP Annals - Manufacturing Technology,* vol. 34, pp. 537-548, 1985.

[112] A. Gilpin, "Tool solutions for machining composites," *Reinforced Plastics,* vol. 53, pp. 30-33, 2009.

[113] S. L. Soo, I. S. Shyha, T. Barnett, D. K. Aspinwall, and W.-M. Sim, "Grinding performance and workpiece integrity when superabrasive edge routing carbon fibre reinforced plastic (CFRP) composites," *CIRP Annals - Manufacturing Technology,* vol. 61, pp. 295-298, 2012.

[114] M. H. El-Hofy, S. L. Soo, D. K. Aspinwall, W. M. Sim, D. Pearson, and P. Harden, "Factors Affecting Workpiece Surface Integrity in Slotting of CFRP," *Procedia Engineering,* vol. 19, pp. 94-99, 2011.

[115] K. Colligan and M. Ramulu, "The effect of edge trimming on composite surface plies," *Manufacturing Review(USA),* vol. 5, pp. 274-283, 1992.

[116] A. H. N. F. Huda, H. Ascroft, and S. Barnes, "Machinability Study of Ultrasonic Assisted Machining (UAM) of Carbon Fibre Reinforced Plastic (CFRP) with Multifaceted Tool," *Procedia CIRP,* vol. 46, pp. 488-491, 2016.

[117] J. Sheikh-Ahmad, N. Urban, and H. Cheraghi, "Machining damage in edge trimming of CFRP," *Materials and Manufacturing Processes,* vol. 27, pp. 802-808, 2012.

[118] P. S. Sreejith, R. Krishnamurthy, S. K. Malhotra, and K. Narayanasamy, "Evaluation of PCD tool performance during machining of carbon/phenolic ablative composites," *Journal of Materials Processing Technology,* vol. 104, pp. 53-58, 2000.

[119] C. Dold, M. Henerichs, L. Bochmann, and K. Wegener, "Comparison of Ground and Laser Machined Polycrystalline Diamond (PCD) Tools in Cutting Carbon Fiber Reinforced Plastics (CFRP) for Aircraft Structures," *Procedia CIRP,* vol. 1, pp. 178-183, 2012.

[120] A. Dahnel, C. Kibbler, S. Barnes, and H. Ascroft, "Study of cutting forces and surface roughness in milling of Carbon Fibre Composite (CFC) with conventional and

pressurized CO2 cutting fluids," in *ASME 2015 International Mechanical Engineering Congress and Exposition*, 2015.

[121] A. Azmi, "Chip formation studies in machining fibre reinforced polymer composites," *International Journal of Materials and Product Technology,* vol. 46, pp. 32-46, 2013.

[122] Anonymous. (11 September). *Cutting Tool Materials*. Available: http://www.mitsubishicarbide.com/en/technical_information/tec_other_data/tec_other_data_top/tec_other_data_technical/tec_cutting_tool_materials (Assessed 2 April 2016)

[123] J. R. Ferreira, N. L. Coppini, and G. W. A. Miranda, "Machining optimisation in carbon fibre reinforced composite materials," *Journal of Materials Processing Technology,* vol. 92–93, pp. 135-140, 1999.

[124] J. A. Arsecularatne, L. C. Zhang, and C. Montross, "Wear and tool life of tungsten carbide, PCBN and PCD cutting tools," *International Journal of Machine Tools and Manufacture,* vol. 46, pp. 482-491, 2006.

[125] Q. S. Bai, Y. X. Yao, P. Bex, and G. Zhang, "Study on wear mechanisms and grain effects of PCD tool in machining laminated flooring," *International Journal of Refractory Metals and Hard Materials,* vol. 22, pp. 111-115, 2004.

[126] J. Sheikh-Ahmad and J. P. Davim, "5 - Tool wear in machining processes for composites A2 - Hocheng, H," in *Machining Technology for Composite Materials*, ed: Woodhead Publishing, 2012, pp. 116-153.

[127] P. J. Heath, "Developments in applications of PCD tooling," *Journal of Materials Processing Technology,* vol. 116, pp. 31-38, 2001.

[128] K. S. Tool, "General Purpose End Mill," ed.

[129] F. Girot, L. N. L. D. Lacalle, A. Lamikiz, D. Iliescu, and M. E. Gutierrez, "Machinability aspects of polymer matrix composite," in *Machining Composite Materials*, J. P. Davim, Ed., ed: John Wiley & Sons, 2010, pp. 39-112.

[130] M. Masuda, Y. Kuroshima, and Y. Chujo, "Failure of tungsten carbide-cobalt alloy tools in machining of carbon materials," *Wear,* vol. 169, pp. 135-140, 1993.

[131] R. I. Blombery, C. M. Perrot, and P. M. Robinson, "Abrasive wear of tungsten carbide-cobalt composites. I. Wear mechanisms," *Materials Science and Engineering,* vol. 13, pp. 93-100, 1974.

[132] J. Larsen-Basse, C. M. Perrott, and P. M. Robinson, "Abrasive wear of tungsten carbide—cobalt composites. I. Rotary drilling tests," *Materials Science and Engineering,* vol. 13, pp. 83-91, 1974.

[133] H. Y. Puw and H. Hocheng, "Machinability test of carbon fiber-reinforced plastics in milling," *Materials and Manufacturing Processes,* vol. 8, pp. 717-729, 1993.

[134] A. Hosokawa, N. Hirose, T. Ueda, and T. Furumoto, "High-quality machining of CFRP with high helix end mill," *CIRP Annals - Manufacturing Technology,* 2014.

[135] W. Hintze, D. Hartmann, and C. Schütte, "Occurrence and propagation of delamination during the machining of carbon fibre reinforced plastics (CFRPs) – An experimental study," *Composites Science and Technology,* vol. 71, pp. 1719-1726, 2011.

[136] L. Sorrentino and S. Turchetta, "Milling of carbon fiber-reinforced plastics: analysis of cutting forces and surface roughness," 2011.

[137] M. Rahman, S. Ramakrishna, J. R. S. Prakash, and D. C. G. Tan, "Machinability study of carbon fiber reinforced composite," *Journal of Materials Processing Technology,* vol. 89–90, pp. 292-297, 1999.

[138] J. P. Davim, P. Reis, and C. C. António, "A study on milling of glass fiber reinforced plastics manufactured by hand-lay up using statistical analysis (ANOVA)," *Composite Structures,* vol. 64, pp. 493-500, 2004.

[139] M. Ramulu, C. Wern, and J. Garbini, "Effect of fibre direction on surface roughness measurements of machined graphite/epoxy composite," *Composites Manufacturing,* vol. 4, pp. 39-51, 1993.

[140] J. Kopac and P. Krajnik, "High-performance grinding—a review," *Journal of Materials Processing Technology,* vol. 175, pp. 278-284, 2006.

[141] D. Biermann and M. Feldhoff, "Abrasive points for drill grinding of carbon fibre reinforced thermoset," *CIRP Annals - Manufacturing Technology,* vol. 61, pp. 299-302, 2012.

[142] K. Ding, Y. Fu, H. Su, X. Gong, and K. Wu, "Wear of diamond grinding wheel in ultrasonic vibration-assisted grinding of silicon carbide," *The International Journal of Advanced Manufacturing Technology,* vol. 71, pp. 1929-1938, 2014.

[143] D. K. Aspinwall, S. L. Soo, D. T. Curtis, and A. L. Mantle, "Profiled superabrasive grinding wheels for the machining of a nickel based superalloy," *CIRP Annals-Manufacturing Technology,* vol. 56, pp. 335-338, 2007.

[144] L. Sorrentino, S. Turchetta, and C. Bellini, "Analysis of carbon fibre reinforced polymers milling by diamond electroplated tool," *Diamond and Related Materials,* vol. 76, pp. 184-190, 2017.

[145] K. Colligan and M. Ramulu, "Edge trimming of graphite/epoxy with diamond abrasive cutters," *Journal of Manufacturing Science and Engineering,* vol. 121, pp. 647-655, 1999.

[146] A. Boudelier, M. Ritou, S. Garnier, and B. Furet, "Optimization of process parameters in CFRP machining with diamond abrasive cutters," in *Advanced Materials Research*, 2011, pp. 774-783.

[147] A. Boudelier, M. Ritou, S. Garnier, and B. Furet, "Investigation of CFRP machining with diamond abrasive cutters, Journal of Composite and Advanced Materials," *Revue des composites et des matériaux avancés,* vol. 23, pp. 425-436, 2013.

[148] J. Sheikh-Ahmad and J. Mohammed, "Optimization of Process Parameters in Diamond Abrasive Machining of Carbon Fiber-Reinforced Epoxy," *Materials and Manufacturing Processes,* vol. 29, pp. 1361-1366, 2014.

[149] X.-H. Shen, J.-H. Zhang, H. Li, J.-J. Wang, and X.-C. Wang, "Ultrasonic vibration-assisted milling of aluminum alloy," *The International Journal of Advanced Manufacturing Technology,* vol. 63, pp. 41-49, 2012.

[150] J. Janghorbanian, M. R. Razfar, and M. M. A. Zarchi, "Effect of cutting speed on tool life in ultrasonic-assisted milling process," *Proceedings of the Institution of Mechanical Engineers, Part B: Journal of Engineering Manufacture,* vol. 227, pp. 1157-1164, 2013.

[151] E. Uhlmann, F. Protz, B. Stawiszynski, and S. Heidler, "Ultrasonic Assisted Milling of Reinforced Plastics," *Procedia CIRP,* vol. 66, pp. 164-168, 2017.

[152] D. Mori. (2015, 02 January). *Advanced Technologies by DMG MORI*. Available: http://us.dmgmori.com/technical-press/advanced-technologies/sauer-represents-the-advanced-technologies-of-dmg-mori/386006 (Assessed 13 January 2016).

[153] R. Zemann, L. Kain, and F. Bleicher, "Vibration Assisted Machining of Carbon Fibre Reinforced Polymers," *Procedia Engineering,* vol. 69, pp. 536-543, 2014.

[154] M. M. A. Zarchi, M. R. Razfar, and A. Abdullah, "Investigation of the effect of cutting speed and vibration amplitude on cutting forces in ultrasonic-assisted milling," *Proceedings of the Institution of Mechanical Engineers, Part B: Journal of Engineering Manufacture,* vol. 226, pp. 1185-1191, 2012.

[155] V. Ostasevicius, R. Gaidys, R. Dauksevicius, and S. Mikuckyte, "Study of Vibration Milling for Improving Surface Finish of Difficult-to-Cut Materials," *Strojniški vestnik-Journal of Mechanical Engineering,* vol. 59, pp. 351-357, 2013.

[156] C. Nath and M. Rahman, "Effect of machining parameters in ultrasonic vibration cutting," *International Journal of Machine Tools and Manufacture,* vol. 48, pp. 965-974, 2008.

[157] M. N. Kumar, S. K. Subbu, P. V. Krishna, and A. Venugopal, "Vibration Assisted Conventional and Advanced Machining: A Review," *Procedia Engineering,* vol. 97, pp. 1577-1586, 2014.

[158] D. E. Brehl and T. A. Dow, "Review of vibration-assisted machining," *Precision Engineering,* vol. 32, pp. 153-172, 2008.

[159] J.-D. Kim and E.-S. Lee, "A study of the ultrasonic-vibration cutting of carbon-fiber reinforced plastics," *Journal of materials processing technology,* vol. 43, pp. 259-277, 1994.

[160] G. W. H. Höhne, W. Hemminger, and H.-J. Flammersheim, "Theoretical Fundamentals of Differential Scanning Calorimeters," in *Differential Scanning Calorimetry*, ed: Springer, 1996, pp. 21-40.

[161] S. Mutlur, "Thermal analysis of composites using DSC," in *Advanced topics in characterization of composites*, M. R.Kessler, Ed., ed: Trafford, 2004.

[162] Y. Kaynak, H. Tobe, R. D. Noebe, H. E. Karaca, and I. S. Jawahir, "The effects of machining on the microstructure and transformation behavior of NiTi Alloy," *Scripta Materialia,* vol. 74, pp. 60-63, 2014.

[163] Y. Kaynak, S. Manchiraju, and I. S. Jawahir, "Modeling and Simulation of Machining-induced Surface Integrity Characteristicsof NiTi Alloy," *Procedia CIRP,* vol. 31, pp. 557-562, 2015.

[164] M. Celina, D. K. Ottesen, K. T. Gillen, and R. L. Clough, "FTIR emission spectroscopy applied to polymer degradation," *Polymer Degradation and Stability,* vol. 58, pp. 15-31, 1997.

[165] S. Ohno, M.-H. Lee, K. Y. Lin, and F. S. Ohuchi, "Thermal degradation of IM7/BMI5260 composite materials: characterization by X-ray photoelectron spectroscopy," *Materials Science and Engineering: A,* vol. 293, pp. 88-94, 2000.

[166] A. Chatterjee, "Thermal degradation analysis of thermoset resins," *Journal of applied polymer science,* vol. 114, pp. 1417-1425, 2009.

[167] P. Musto, E. Martuscelli, G. Ragosta, P. Russo, G. Scarinzi, and P. Villano, "FTIR spectroscopy and physical properties of an epoxy/bismaleimide IPN system," *Journal of materials science,* vol. 33, pp. 4595-4601, 1998.

[168] B. Yalçın, A. E. Özgür, and M. Koru, "The effects of various cooling strategies on surface roughness and tool wear during soft materials milling," *Materials & Design,* vol. 30, pp. 896-899, 2009.

[169] N. Bhatnagar, N. Ramakrishnan, N. K. Naik, and R. Komanduri, "On the machining of fiber reinforced plastic (FRP) composite laminates," *International Journal of Machine Tools and Manufacture,* vol. 35, pp. 701-716, 1995.

[170] S. Chandran M, M. Krishna, and K. Rai, "Preparation and characterization of chain-extended bismaleimide/carbon fibre composites," *International Journal of Polymer Science,* vol. 2010, 2010.

[171] B. Dao, J. Hodgkin, J. Krstina, J. Mardel, and W. Tian, "Accelerated ageing versus realistic ageing in aerospace composite materials. III. The chemistry of thermal ageing in bismaleimide based composites," *Journal of applied polymer science,* vol. 105, pp. 2062-2072, 2007.

[172] X.-H. Shen, J. Zhang, D. X. Xing, and Y. Zhao, "A study of surface roughness variation in ultrasonic vibration-assisted milling," *The International Journal of Advanced Manufacturing Technology,* vol. 58, pp. 553-561, 2012.

[173] C. Industries, "CYCOM 5250-4 Prepeg System : Technical Data Sheet," ed, 2011.

[174] T. Committee. Tool life testing in milling — Part 2: End milling [Online]. Available: https://www.iso.org/obp/ui/#iso:std:iso:8688:-2:ed-1:v1:en (Assessed 16 March 2016)

[175] A. Cooks, "Benchmarking of CFRP," N. F. H. A.H, Ed., ed, 2014.

[176] FLIR. FLIR T-Series specification [Online]. Available: http://www.flir.co.uk/cs/display/?id=41450 (Assessed 5 April 2017).

[177] J. Dionne, "Operation and Maintenance Manual : Coolant-Lubricant Spray System," C. C. Technologies, Ed., ed, 2012.

[178] (06/08). *InfiniteFocus*. Available: http://www.alicona.com/products/infinitefocus/ (Assessed 20 January 2017).

[179] M.-T. GmbH. (2016). *The Standard in Thermal Analysis*. Available: https://www.mt.com/dam/Analytical/ThermalAnalysi/TA-PDF /30326071_ V07.16_STARe_SW_V15_Brochure_en_LR.pdf (Assessed 5 December 2017).

[180] Anynomous. *Thermogravimetry for routine analysis*. Available: https://www.mt.com/dam/Analytical/ThermalAnalysi/TA-PDF/TGA2_Broch_EN_30247078_V04.15_Original_38299.pdf (Assessed 4 March 2016).

[181] M.-T. AG, "Differential Scanning Calorimetry for all Requirements," ed: Mettler-Toledo, 2011.

[182] O. Pecat and E. Brinksmeier, "Tool Wear Analyses in Low Frequency Vibration Assisted Drilling of CFRP/Ti6Al4V Stack Material," *Procedia CIRP,* vol. 14, pp. 142-147, 2014.

[183] R. Muhammad, N. Ahmed, A. Roy, and V. V. Silberschmidt, "Numerical Modelling of Vibration-Assisted Turning of Ti-15333," *Procedia CIRP,* vol. 1, pp. 347-352, 2012.

[184] S. Patil, S. Joshi, A. Tewari, and S. S. Joshi, "Modelling and simulation of effect of ultrasonic vibrations on machining of Ti6Al4V," *Ultrasonics,* vol. 54, pp. 694-705, 2014.

[185] A. I. Azmi, R. J. T. Lin, and D. Bhattacharyya, "Machinability study of glass fibre-reinforced polymer composites during end milling," *The International Journal of Advanced Manufacturing Technology,* vol. 64, pp. 247-261, 2013.

[186] K. Palanikumar and J. Paulo Davim, "Mathematical model to predict tool wear on the machining of glass fibre reinforced plastic composites," *Materials & Design,* vol. 28, pp. 2008-2014, 2007.

[187] S. Kumagai, T. Hosaka, T. Kameda, and T. Yoshioka, "Pyrolysis and hydrolysis behaviors during steam pyrolysis of polyimide," *Journal of Analytical and Applied Pyrolysis,* vol. 120, pp. 75-81, 2016.

[188] H. Hatori, Y. Yamada, M. Shiraishi, M. Yoshihara, and T. Kimura, "The mechanism of polyimide pyrolysis in the early stage," *Carbon,* vol. 34, pp. 201-208, 1996.

[189] A. Azmi, R. J. Lin, and D. Bhattacharyya, "Tool wear prediction models during end milling of glass fibre-reinforced polymer composites," *The International Journal of Advanced Manufacturing Technology,* pp. 1-18, 2013.

[190] F. Feucht, J. Ketelaer, A. Wolff, M. Mori, and M. Fujishima, "Latest Machining Technologies of Hard-to-cut Materials by Ultrasonic Machine Tool," *Procedia CIRP,* vol. 14, pp. 148-152, 2014.

[191] D. Wang, M. Ramulu, and D. Arola, "Orthogonal cutting mechanisms of graphite/epoxy composite. Part II: multi-directional laminate," *International Journal of Machine Tools and Manufacture,* vol. 35, pp. 1639-1648, 1995.

[192] M. R. Razfar and M. R. Z. Zadeh, "Optimum damage and surface roughness prediction in end milling glass fibre-reinforced plastics, using neural network and genetic algorithm," *Proceedings of the Institution of Mechanical Engineers, Part B: Journal of Engineering Manufacture,* vol. 223, pp. 653-664, 2009.

[193] P. Hu, J. M. Zhang, Z. J. Pei, and C. Treadwell, "Modeling of material removal rate in rotary ultrasonic machining: designed experiments," *Journal of Materials Processing Technology,* vol. 129, pp. 339-344, 2002.

[194] H. Gong, F. Z. Fang, and X. T. Hu, "Kinematic view of tool life in rotary ultrasonic side milling of hard and brittle materials," *International Journal of Machine Tools and Manufacture,* vol. 50, pp. 303-307, 2010.

Appendix A

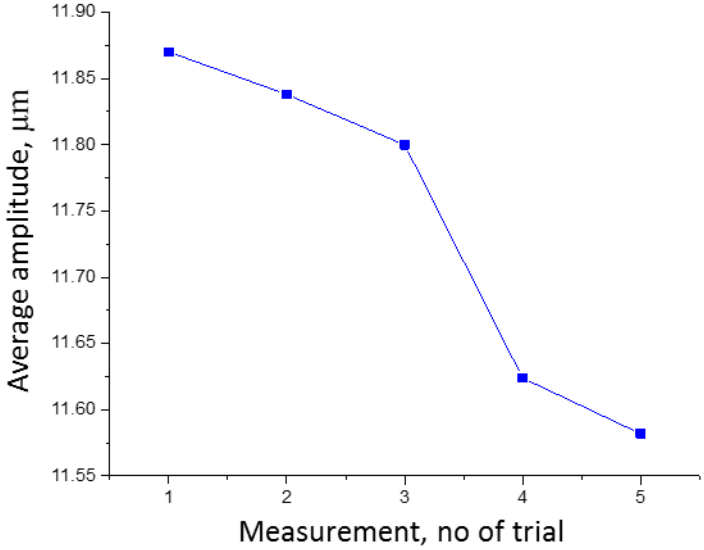

Figure A- 1: Average amplitude measured when aluminium strip was attached to the cutting tool. The graph indicates that the value of the average amplitude experienced sudden drop after three measurement trial due to the glue that attach the strip to the cutting tool start to melt down due to the heat produce by the ultrasonic vibration on the cutting tool.

Appendix B

KISTLER
measure. analyze. innovate.

Kalibrierschein
Calibration Certificate

Type **Kistler 9257B** Serial No. **1411822**

Kalibriert durch Calibration Technician	Datum Date
K. Ta	20. May. 2015

Referenzgeräte Reference Equipment	Typ Type	Serien-Nr. Serial No.
Gebrauchsnormal Working Standard	Kistler 9251A	329968
Ladungskalibrator Charge Calibrator	Kistler 5395A	988262

Umgebungstemperatur Ambient Temperature °C	Relative Feuchte Relative Humidity %
25	39

Messergebnisse Results of Measurement

Kalibrierter Bereich Calibrated Range kN		Empfindlichkeit Sensitivity pC / N	Linearität Linearity ≤ ± %FSO	Übersprechen Cross talk %	%
Fx	0 ... 5	-7,921	0,06	*Fx* → *Fy* 0,8	*Fx* → *Fz* 0,1
Fx	0 ... 0,5	-7,935	0,05	*Fx* → *Fy* 0,8	*Fx* → *Fz* 0,0
Fx	0 ... 0,05	-7,924	0,06		
Fy	0 ... 5	-7,910	0,05	*Fy* → *Fx* 0,3	*Fy* → *Fz* -0,2
Fy	0 ... 0,5	-7,917	0,09	*Fy* → *Fx* 0,3	*Fy* → *Fz* -0,1
Fy	0 ... 0,05	-7,922	0,05		
Fz	0 ... 10	-3,681	0,04	*Fz* → *Fx* 0,6	*Fz* → *Fy* 0,1
Fz	0 ... 1	-3,686	0,08	*Fz* → *Fx* 0,6	*Fz* → *Fy* 0,1
Fz	0 ... 0,1	-3,682	0,08		

Messverfahren **Kontinuierliche Kalibrierung, Vergleichsverfahren**
Measurement Procedure Continuous Calibration, Comparison Method

Bestätigung Confirmation

Das oben durch die Seriennummer identifizierte Gerät entspricht der Vereinbarung der Bestellung und hält die Herstelltoleranzen gemäss den Spezifikationen der Datenblätter ein, sofern nicht anders auf dem Kalibrierschein vermerkt. Das Kistler Qualitätsmanagement System ist nach ISO 9001 zertifiziert. Das Dokument erfüllt die Anforderungen von EN 10204 Abnahmeprüfzeugnis "3.1". Die aufgeführten Referenzgeräte sind auf nationale Normale rückgeführt. Das Dokument wurde elektronisch erstellt und ist daher ohne Unterschrift gültig.

The equipment identified by Serial No. complies with the agreement of the order and meets the manufacturing tolerances specified in the data sheets, unless otherwise specified on the calibration certificate. The Kistler Quality Management System is certified per ISO 9001. This document fulfils the requirements of EN 10204 Inspection Certificate "3.1". The reference equipment is traceable to national standards. The document was issued electronically and is therefore valid without signature.

Kistler Instrumente AG
Eulachstrasse 22
PO Box
CH-8408 Winterthur

Tel. +41 52 224 11 11
Fax +41 52 224 14 14
info@kistler.com

ZKB Winterthur BC 732
Swift: ZKBKCHZZ80A
Account: 1132-0374.628

IBAN: CH67 0070 0113 2003 7462 8
VAT: 229 713
ISO 9001 certified

www.kistler.com

Appendix C

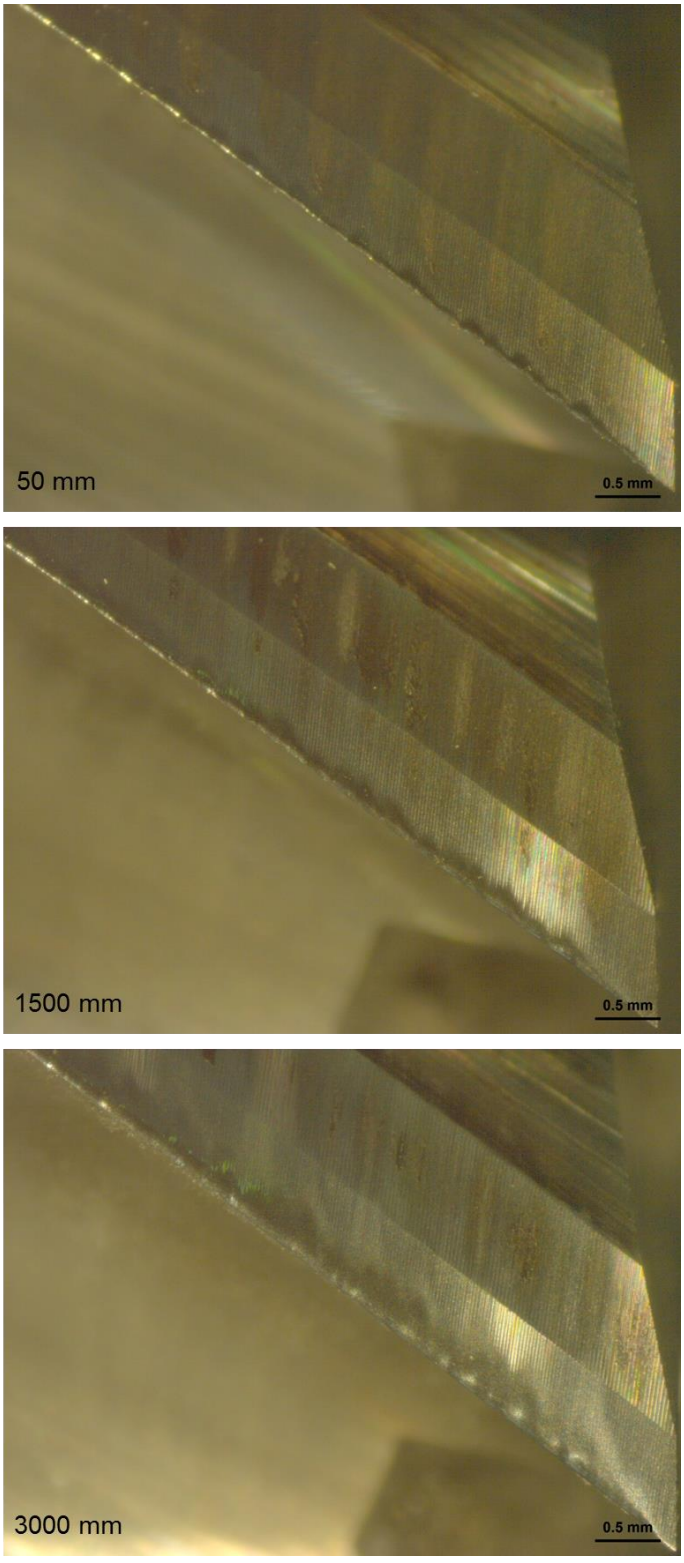

Figure C- 1 : Microscopy images of tungsten carbide end mill used in CM dry.

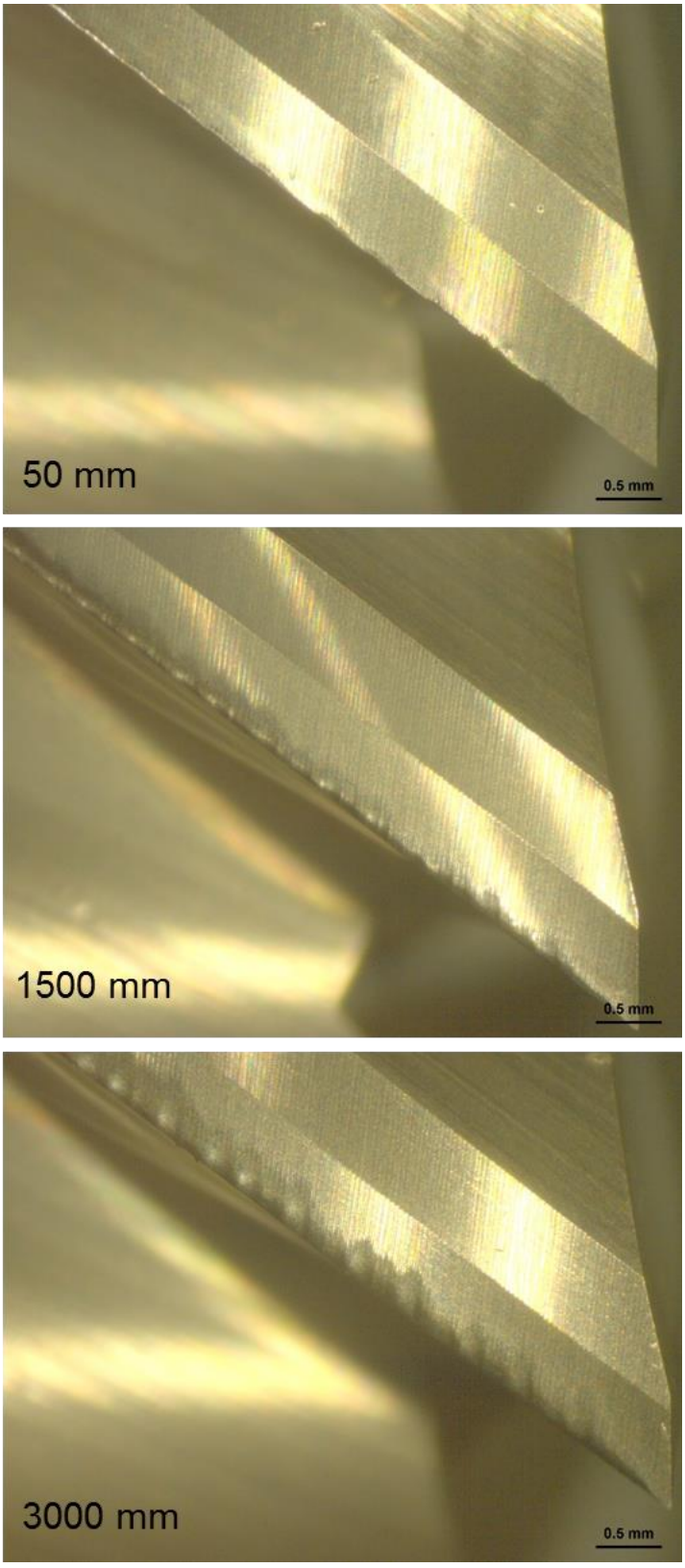

Figure C-2: Microscopy images of tungsten carbide end mill used in CM CCF.

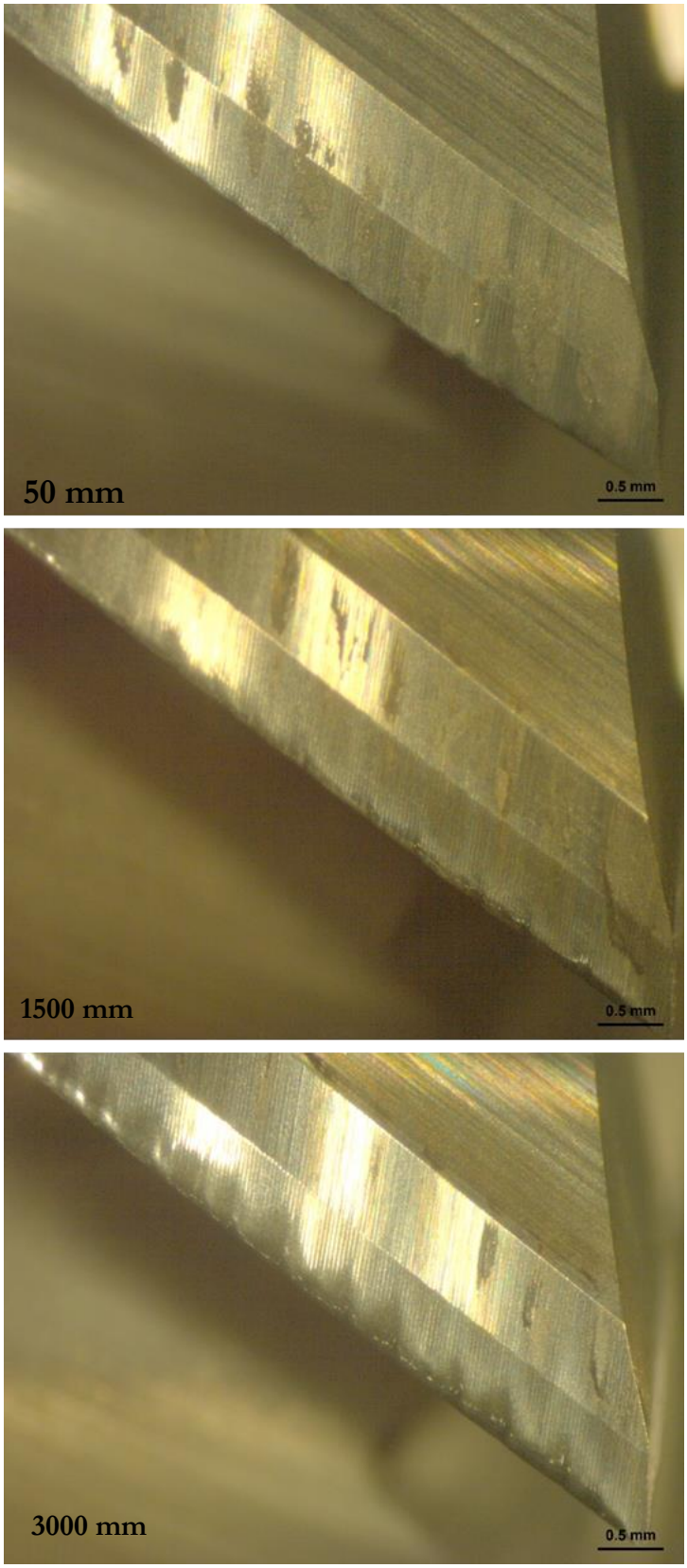

Figure C-3: Microscopy images of tungsten carbide end mill used in CM CO_2.

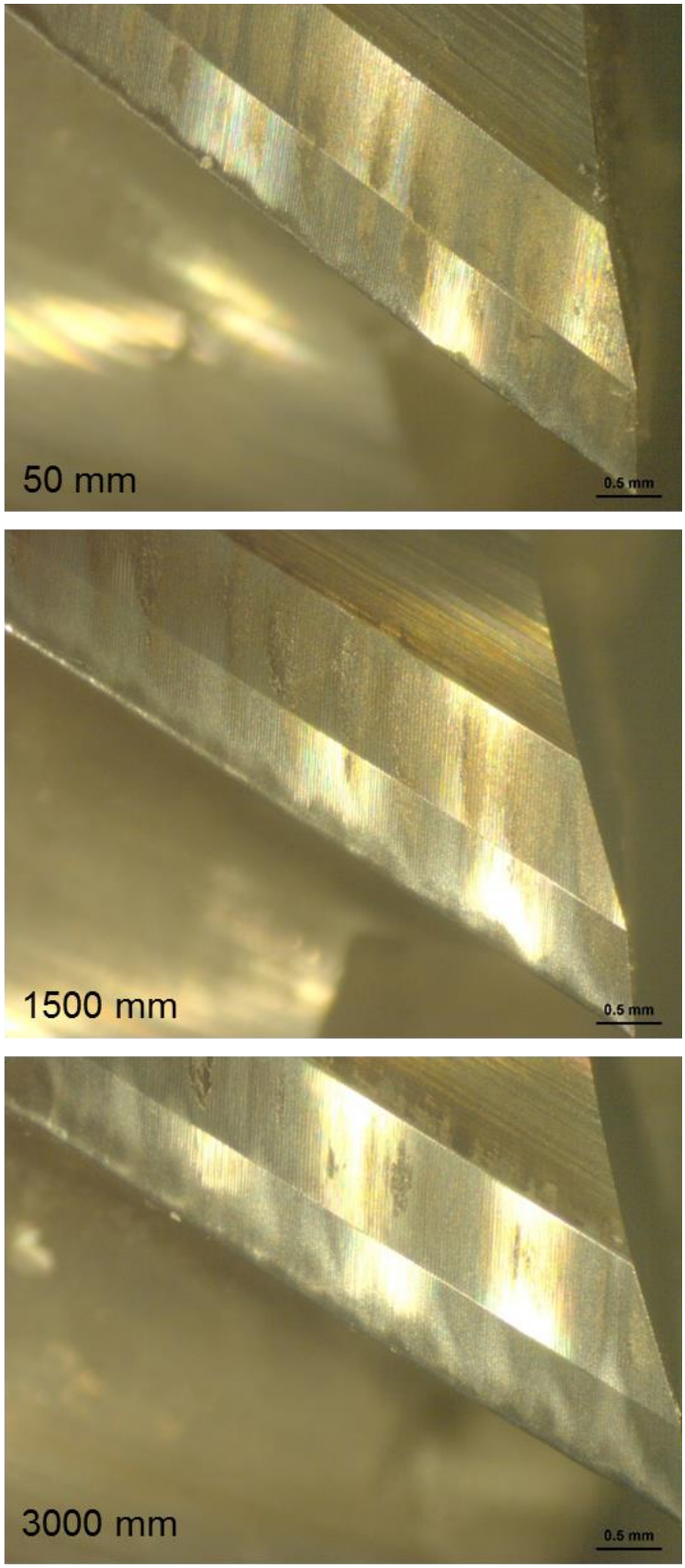

Figure C-4: Microscopy images of tungsten carbide end mill used in UAM dry.

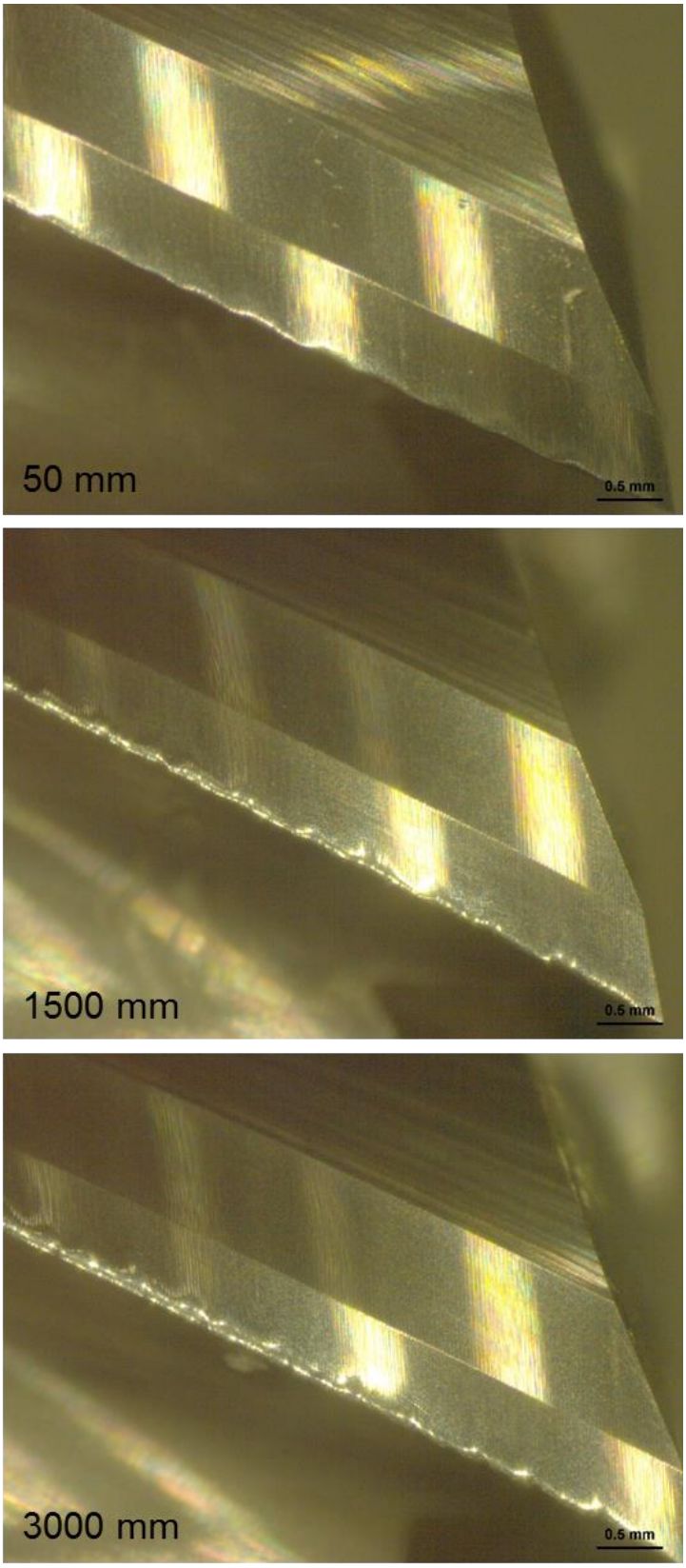

Figure C-5: Microscopy images of tungsten carbide end mill used in UAM CCF.

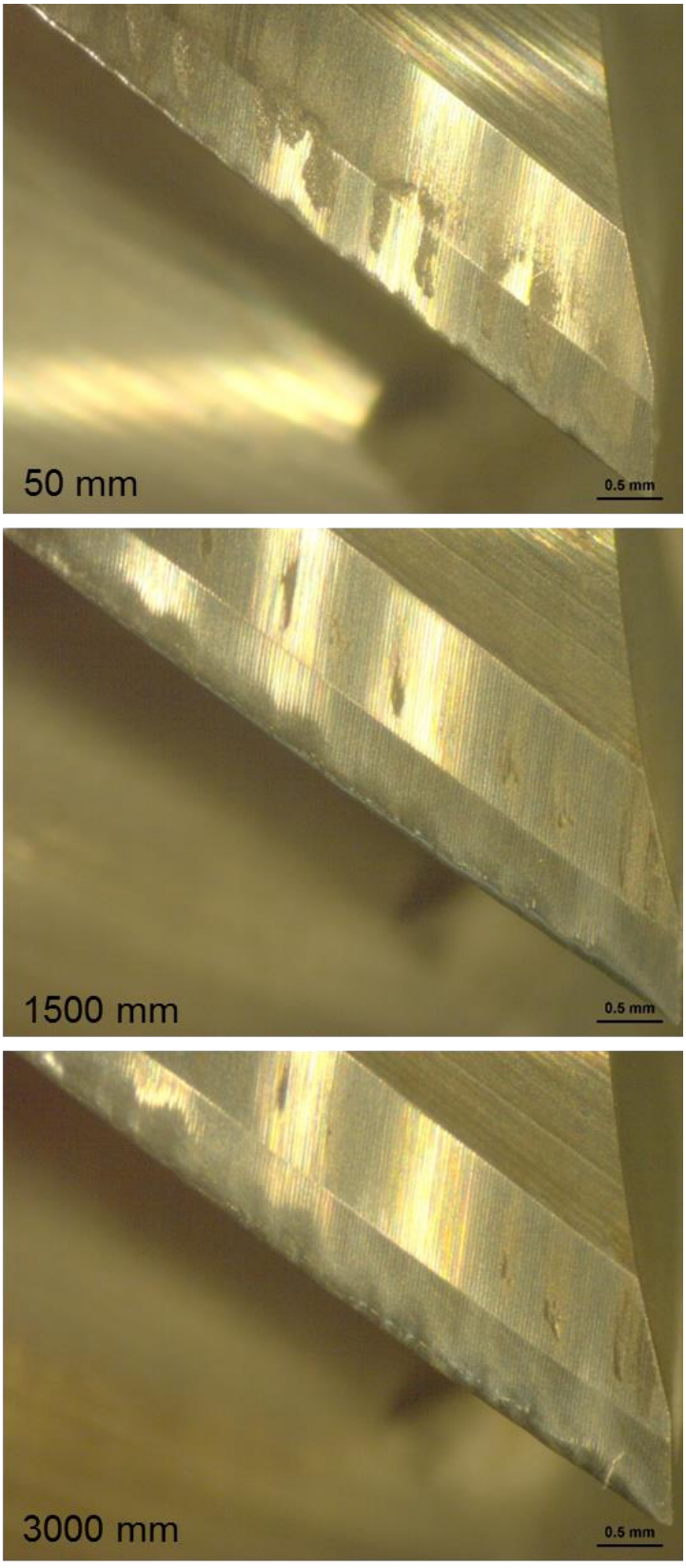

Figure C-6: Microscopy images of tungsten carbide end mill used in UAM CO_2.

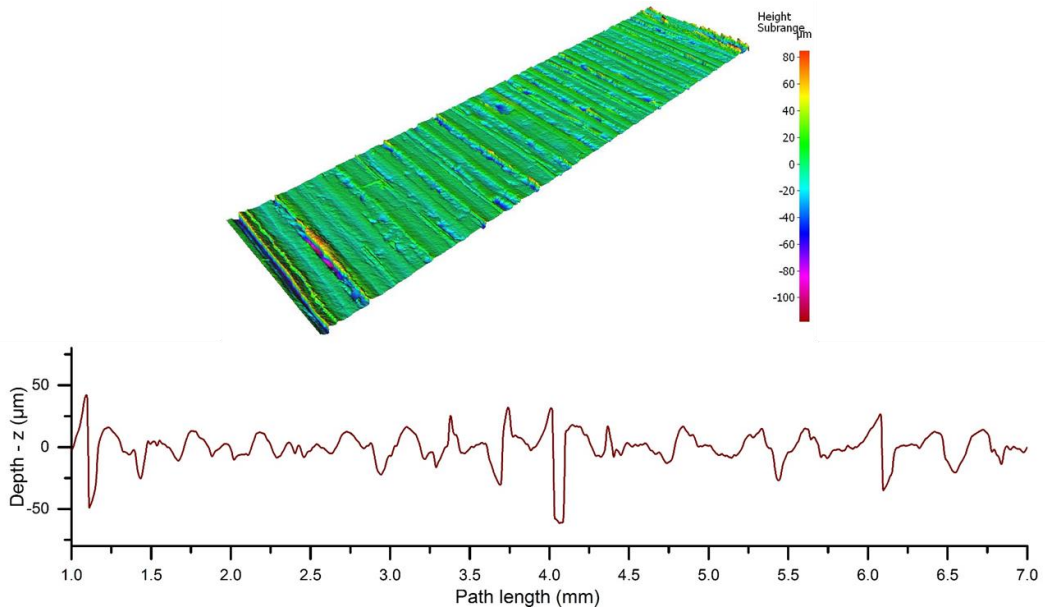

Figure C-7: Machined surface topography and roughness profile for CM in CCF environment machined surface taken in the Alicona with 5X magnification with Ra of 8.3 µm.

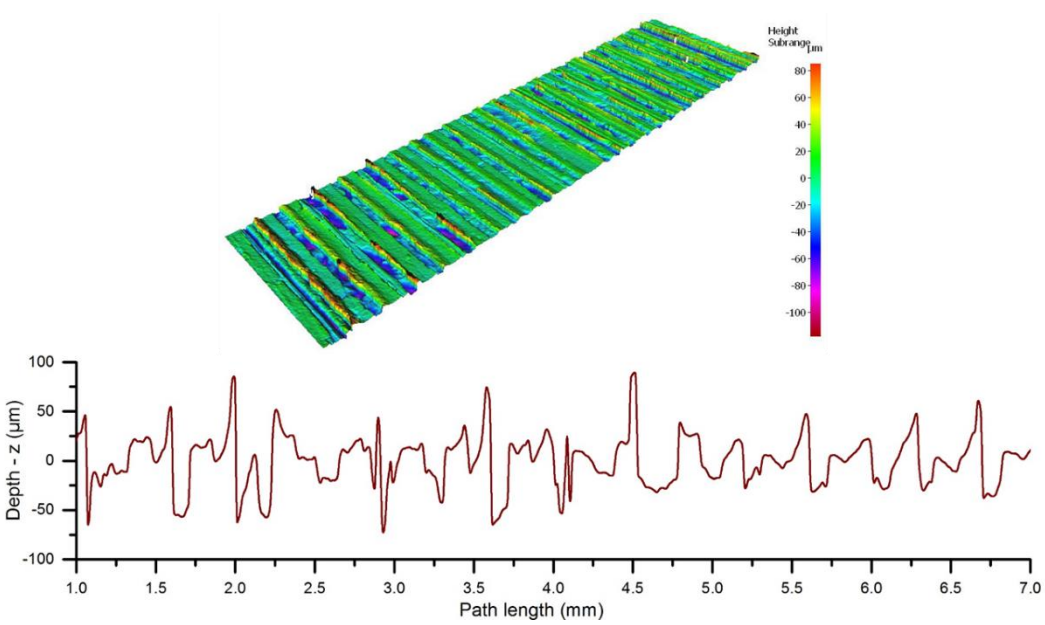

Figure C-8: Machined surface topography and roughness profile for CM in CO_2 environment machined surface taken in the Alicona with 5X magnification with Ra of 15.7 µm.

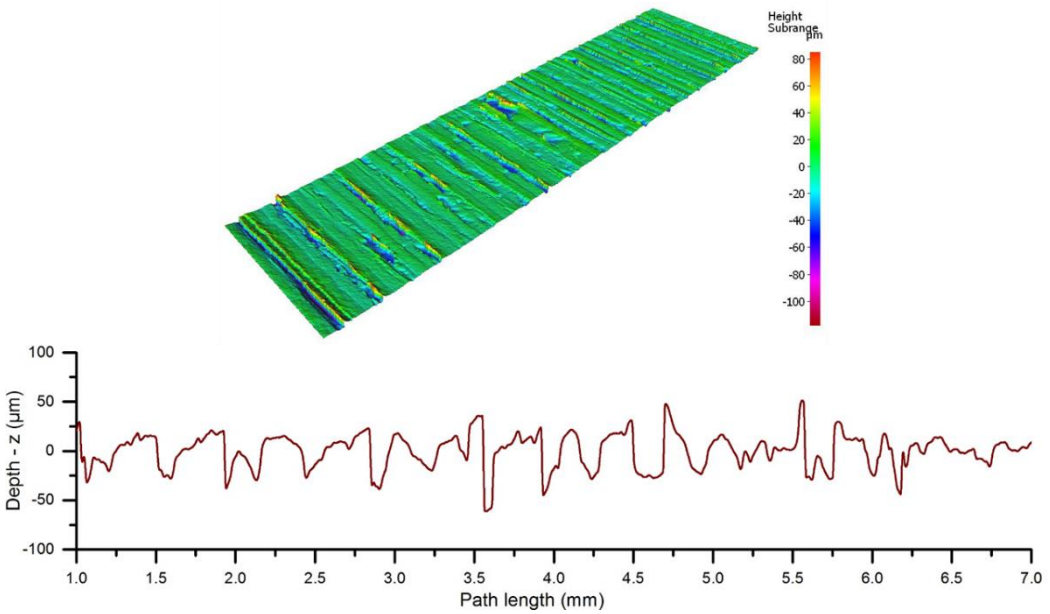

Figure C-9: Machined surface topography and surface roughness profile for UAM in CCF environment machined surface taken in the Alicona with 5X magnification with Ra of 13.3 µm.

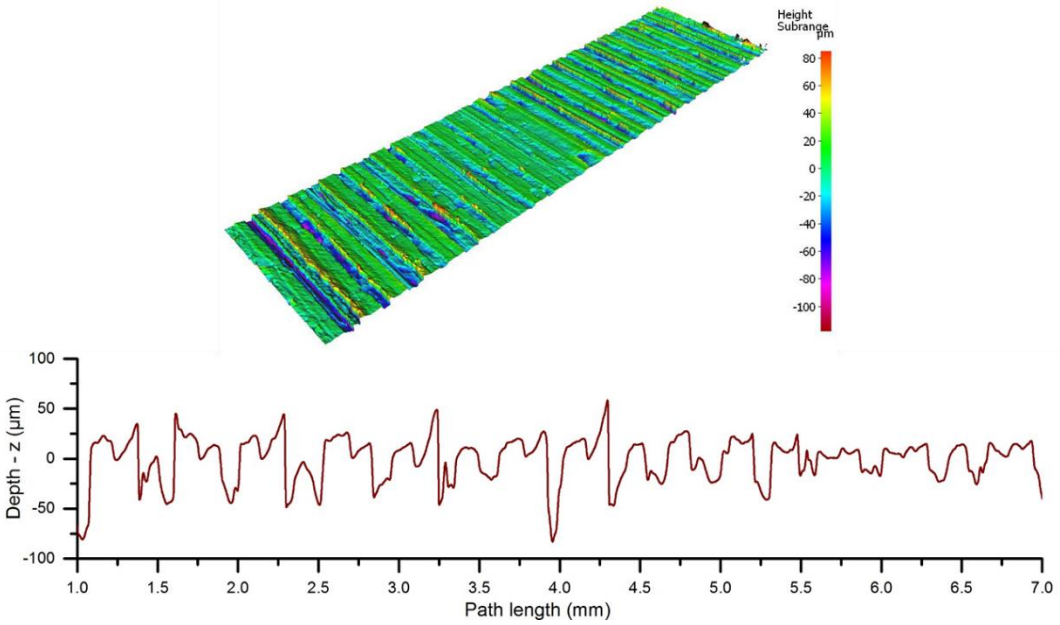

Figure C-10: Machined surface topography and roughness profile for UAM in CO_2 environment machined surface taken in the Alicona with 5X magnification with Ra of 15.5 µm.

Appendix D

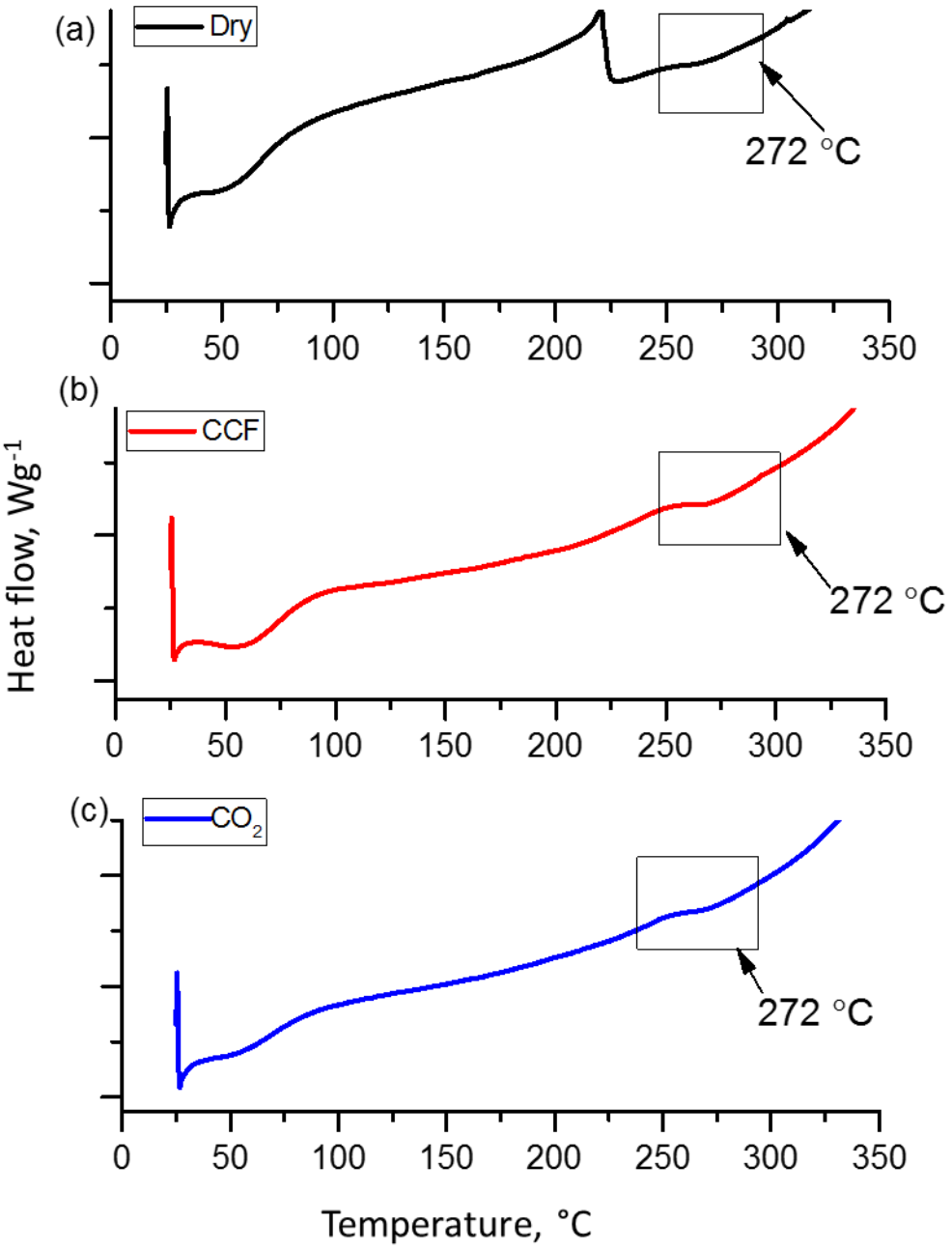

Figure D-1: DSC analysis of CM of CFRP in different machining environment (a) dry, (b) conventional cutting fluid and (c) CO_2. All sample was taken from 2000 mm machining length machined surface.

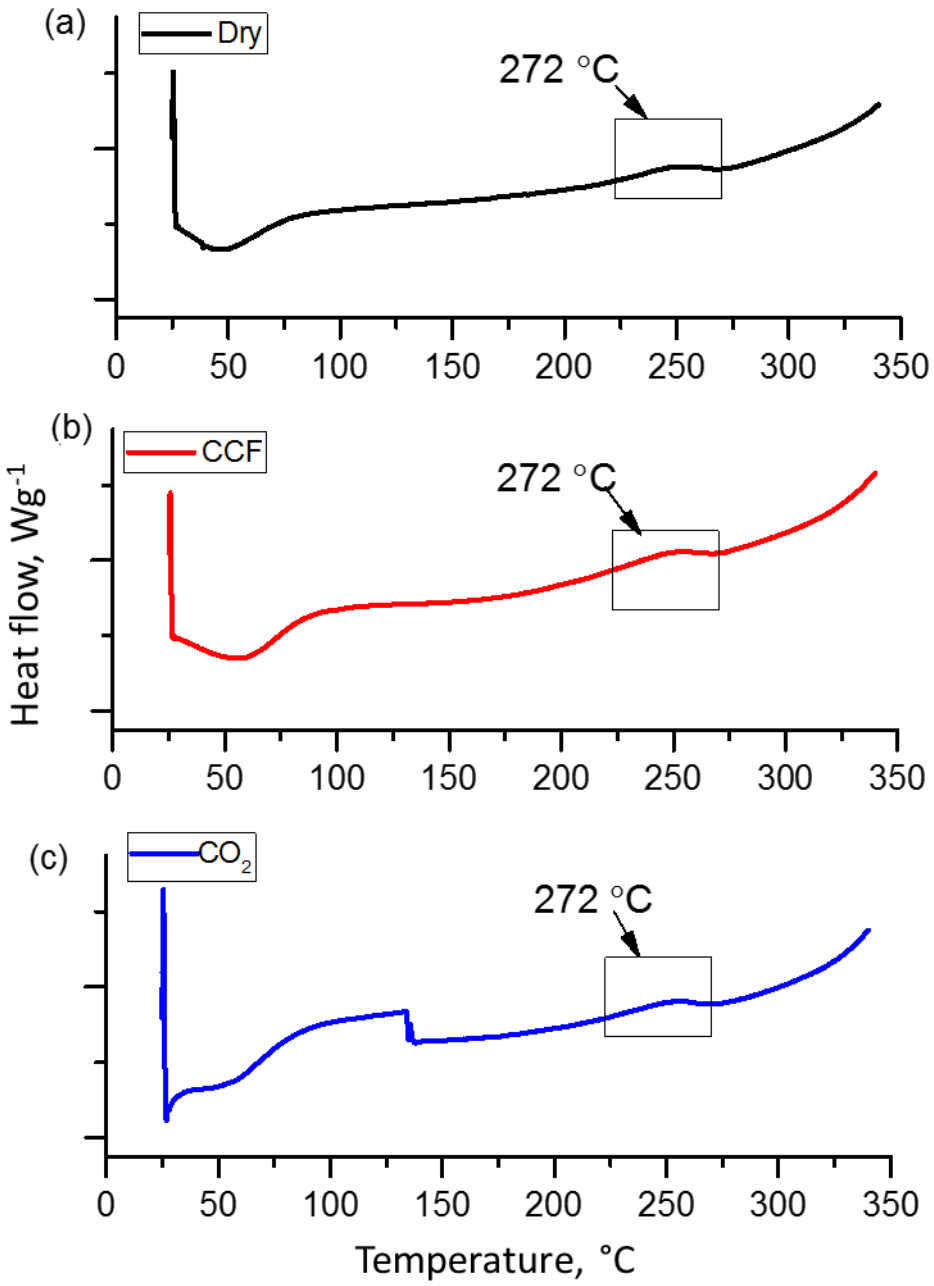

Figure D-2: DSC analysis of UAM of CFRP in different machining environment (a) dry, (b) Conventional cutting fluid and (c) CO_2. All sample was taken from 2000 mm machining length machined surface.

Appendix E

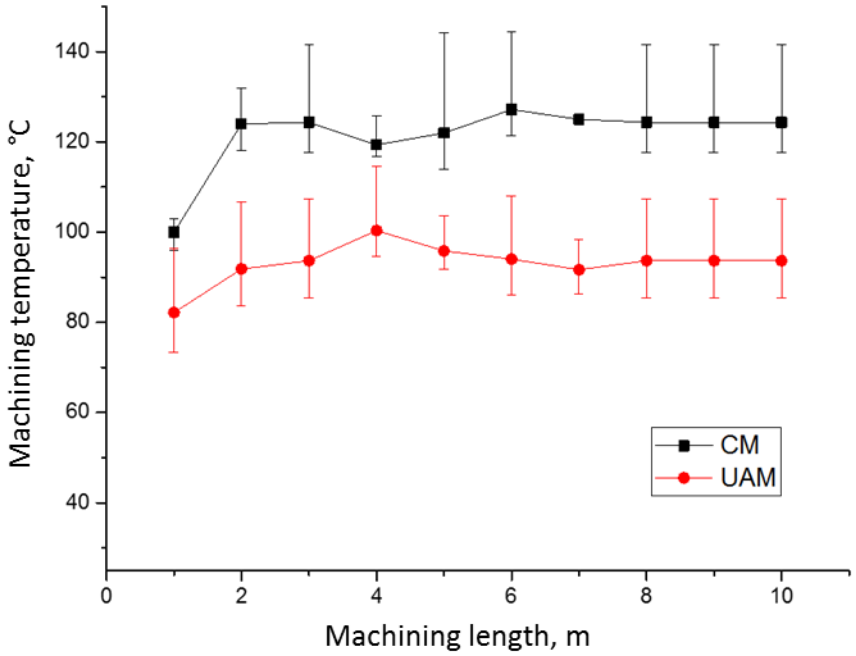

Figure E-1: Cutting temperature recorded by the FLIR thermal camera when milling CFRP with PCD end mill tool.

Appendix F

Table F-1: Total area covered by the broken fibre and degraded resin on abrasive diamond tool used for CM.

Part A	Area (μm²)
PG1	195312.7
PG2	474564.7
PG3	1993986
PG4	905075.6
PG5	2398425
PG6	429466.6
PG7	216321.8
PG8	508264.3
PG9	147135
PG10	163197.1
PG11	1127707
PG12	31575.7
PG13	634053.8
PG14	39903.26
PG15	102700.7
PG16	129187.8
PG17	118143.4
PG18	992501.7
PG19	2547295
PG20	801153.6
PG21	527246.9
PG22	1236948
PG23	239384.1
PG24	867305.1
PG25	296278.8
PG26	308814.6
PG27	165373.1
PG28	71032.57
PG29	178295.1
PG30	940920.4
PG31	111977.6
PG32	129933.3
PG33	443985.4
PG34	159944.4
PG35	208216.9
Total area	19841627

Part B	Area (μm²)
PG1	782811.1
PG2	327037.8
PG3	151814
PG4	138191.1
PG5	231601.4
PG6	125838.1
PG7	253883.3
PG8	179225.2
PG9	238852.7
PG10	2533391
PG11	738362
PG12	307308.4
PG13	363397.1
PG14	537294.9
PG15	186150.6
PG16	990913.4
PG17	407803.8
PG18	250784.3
PG19	378238.2
PG20	609629.2
PG21	432167.8
PG22	346687.7
Total area	10511383

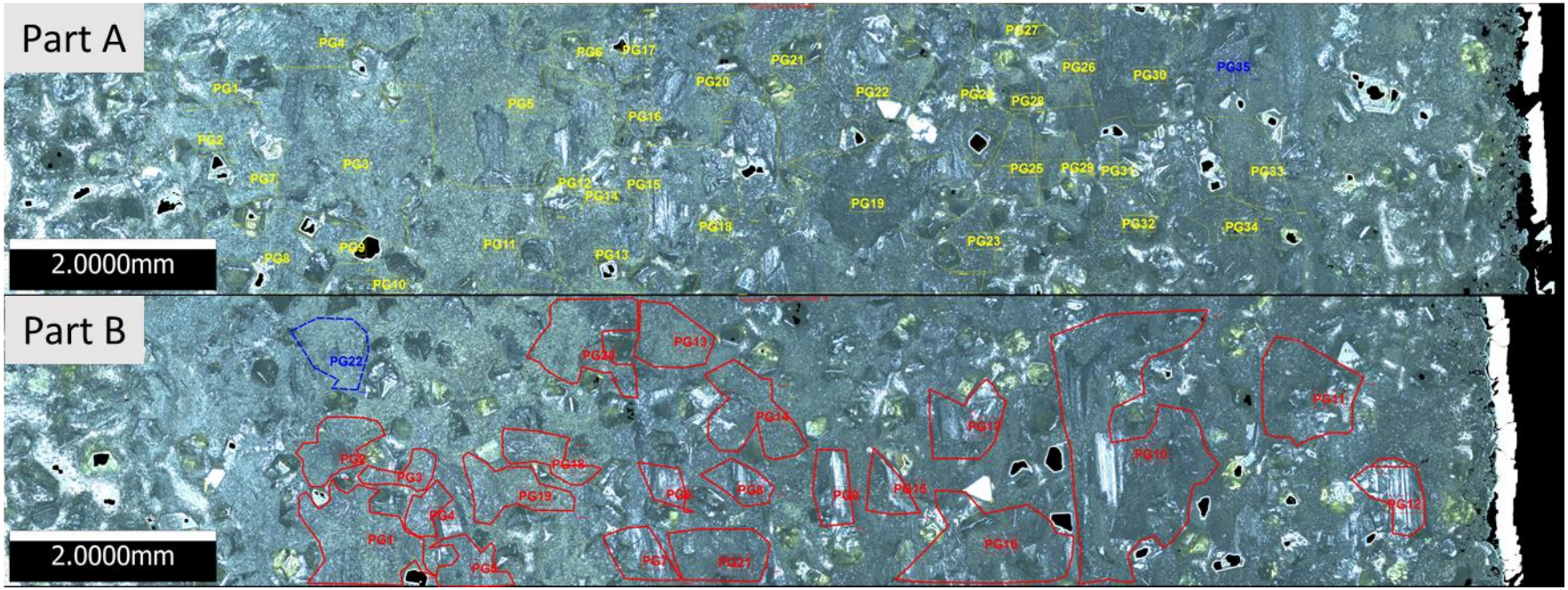

Figure F- 1: Total area covered by the broken fibre and degraded resin on abrasive diamond tool used for CM.

Table F-2: Total area covered by the broken fibre and degraded resin on abrasive diamond tool used for UAM.

Part A	Area [µm²]
PG1	1552738.41
PG2	222527.95
PG3	123306.634
PG4	150412.175
PG5	708248.532
PG6	1914948.46
PG7	274254.038
PG8	223738.588
PG9	373946.865
PG10	369431.951
PG11	402019.604
PG12	910402.786
PG13	280900.842
PG14	104312.054
PG15	315855.638
Total area	7927044.52

Part B	Area [µm²]
PG1	1044801
PG2	580049.8
PG3	1054008
PG4	568101.3
PG5	968701
PG6	1110391
PG7	274915
PG8	111459.5
PG9	187738.7
PG10	1055286
PG11	739307.9
PG12	441354.4
PG13	351842.3
PG14	144938.4
PG15	174522.5
PG16	377393.6
Total area	9184811

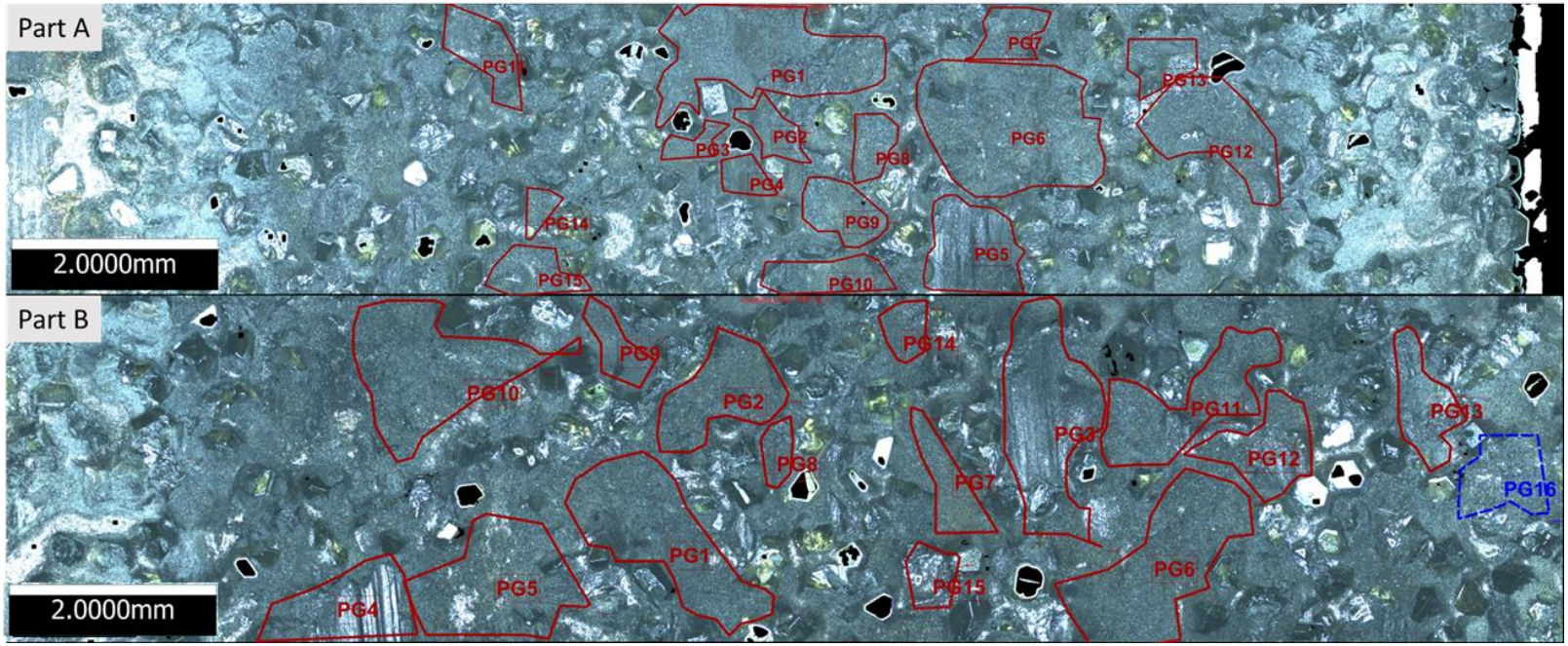

Figure F-2: Total area covered by the broken fibre and thermally degraded resin on abrasive diamond tool used for UAM.